Investigations of the role of myomegalin in the phosphorylation of cardiac myosin binding protein C

by
Gerrida Mathilda Uys

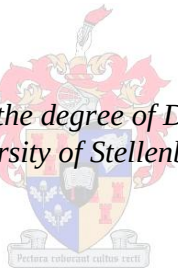

Dissertation presented for the degree of Doctor of Philosophy at the University of Stellenbosch

Promoter: Prof. Johanna Catharina Moolman-Smook
Faculty of Health Sciences
Department of Biomedical Sciences

December 2010

DECLARATION

By submitting this thesis/dissertation electronically, I declare that the entirety of the work contained therein is my own, original work, and that I have not previously in its entirety or in part submitted it for obtaining any qualification.

G.M. Uys

December 2010

ABSTRACT

Hypertrophic cardiomyopathy (HCM) is the most common inherited cardiac muscle disorder worldwide. The disease is characterized by extreme variability in the amount of hypertrophy that develops in different patients in response to sarcomeric protein-encoding gene mutations. The underlying defect in HCM is altered contractility of the sarcomere, primarily due to a defective sarcomere. Although numerous disease-causing genes have been identified for HCM, the factors that modify the amount of hypertrophy that develops in a given person are still unknown, it can be hypothesized that molecules that affect contractility can act as modifiers of the hypertrophic signal, and therefore influence the development of hypertrophy.

Cardiac contractility is regulated by dynamic phosphorylation of proteins within the sarcomere by kinases such as cAMP-activated protein kinase A (PKA). Because speed and energy efficiency of cardiac muscle contraction has to be regulated in order to match the body's needs, PKA is anchored close to its targets by A-kinase anchoring proteins (AKAPs) to enable spatio-temporal control of phosphorylation. Cardiac myosin binding protein-C (cMyBPC) and cardiac troponin I (cTNI) are HCM-causing sarcomeric proteins which regulate contractility in response to PKA phosphorylation. In a previous study, our laboratory identified a phosphodiesterase 4D-interacting protein as ligand of the N-terminal of cMyBPC via a yeast-two-hybrid (Y2H) cardiac library screen. This protein is also known in the literature as myomegalin (MMGL) isoform 4.

Because phosphodiesterases and PKA are sometimes anchored by the same anchoring protein (AKAP), we hypothesized that MMGL isoform 4 acts as an AKAP by anchoring PKA to the phosphorylatable N-terminal of cMyBPC, and tested this by direct protein-protein interaction analyses in a yeast-based system. The MMGL cDNA was cloned into a bait vector, which was directly assessed for interaction with two distinct PKA regulatory-subunit preys. We further investigated the function of MMGL itself by using the Y2H bait to screen a cardiac cDNA library for novel MMGL interactors. All the prey clones identified via these Y2H analyses were subsequently sequenced to determine their identity. Based on their identities and subcellular localization, all putative Y2H MMGL-prey interactions were further assessed by additional, separate biochemical techniques viz. *in vivo* co-immunoprecipitation and *in vivo* 3D co-localization. The interactions between MMGL and its known PKA-phosphorylatable sarcomeric ligands were also investigated under conditions of β-adrenergic stress, by quantitatively measuring levels of co-localization before and upon addition of the β-adrenergic agonist isoproterenol. Furthermore, in order to evaluate the role of MMGL in cMyBPC phosphorylation, we assessed the expression of the different phosphorylation isoforms of cMyBPC, with and without β-adrenergic stimulation, in the context of siRNA-mediated MMGL knockdown.

We further hypothesized that MMGL and PKA may serve as modifiers of the hypertrophic phenotype. This was tested by conducting a single nucleotide polymorphism (SNP) genotyping study of the genes encoding MMGL and the regulatory subunits of PKA viz. *PDE4DIP*, *PRKAR1A* and *PRKAR2A*, respectively, and comparing

genotypic data with clinical phenotypic traits in a family-based association study. A panel of 353 individuals, including genetically and clinically affected as well as unaffected HCM individuals, was identified. All these individuals were screened for the presence or absence of all three South African HCM founder mutations, and blood was collected and DNA extracted. Genotypes at multiple SNPs in each gene were determined by subjecting the DNA samples to TaqMan® allelic discrimination technology. Statistical analysis using quantitative transmission disequilibrium testing (QTDT) was done in order to establish whether the difference in genotype in these three genes might have an effect on HCM phenotype.

Our results showed that MMGL interacted with both PKA regulatory subunits as well as with other cardiac proteins that are PKA targets, including the sarcomeric protein cTNI. It was confirmed that two regulatory subunits of PKA (PRKAR1A and PRKAR2A), cardiac ankyrin repeat protein (CARP), copper metabolism gene *MURR1* domain 4 (COMMD4), α-enolase (ENO1), β-enolase (ENO3) and cTNI are novel interactors of MMGL. In order to classify a protein as an AKAP, interaction with one of PKA's regulatory subunits are prerequisite; MMGL showed interaction with both, confirming our hypothesis of MMGL being an AKAP, moreover, classifying it as a novel dual-specific sarcomeric AKAP. The identities of the AKAPs involved in the phosphorylation of cMyBPC and cTNI had been unknown; our results indicate that MMGL is the AKAP involved in the phosphorylation of both these PKA targets.

We also showed that quantitatively more interaction occurs between MMGL and its sarcomeric ligands cMyBPC and cTNI under β-adrenergic stress. This implicates that under elevated cAMP levels, PKA is dynamically recruited by MMGL to the PKA targets cMyBPC and cTNI, presumably to mediate cardiac stress responses and leading to increased cardiac contractility. Furthermore, siRNA-mediated knockdown of MMGL lead to a reduction of cMyBPC levels under conditions of β-adrenergic stress, indicating that MMGL-assisted phosphorylation is requisite for protection of cMyBPC against proteolytic cleavage.

The SNP modifier study indicated that one variant in *PDE4DIP* (rs1664005) showed strong association with numerous clinical hypertrophy traits, including maximal interventricular septum thickness, as well as a number of other composite score traits. Two variants in *PRKAR1A* (rs11651687 and rs3785906) also showed strong association with some of these clinical hypertrophy traits. These results therefore suggest that variants in these two genes may act as modifiers of the HCM phenotype.

In conclusion, this study ascribes a novel function to MMGL isoform 4: it meets all criteria for classification as an AKAP and appears to be involved in the phosphorylation of cMyBPC as well as cTNI; hence MMGL is likely to be an important component in the regulation of cardiac contractility, and by extension, in the development of hypertrophy. This has further implications for understanding the patho-aetiology of mutations in

cMyBPC and cTNI, and raises the question of whether MMGL might itself be considered a candidate HCM-causing factor.

OPSOMMING

Hipertrofiese kardiomiopatie (HKM) is die mees algemeenste oorerflike hartspier siekte wêreldwyd. Die siekte word gekenmerk deur die uiterste variasie in die hoeveelheid hipertrofie wat in verskillende pasiënte ontwikkel as gevolg van sarkomeriese proteïen-koderende mutasies. Die onderliggende gebrek in HKM is geaffekteerde kontraktiliteit van die sarkomeer, hoofsaaklik as gevolg van ‘n gebrekkige sarkomeer. Alhoewel daar verskeie siekte-veroorsakende gene vir HKM geïdentifiseer is, bly die faktore wat die hoeveelheid hipertrofie in ‘n gegewe persoon modifiseer, onbekend. Daar kan dus gehipotiseer word dat molekules wat kontraktiliteit beïnvloed as modifiseerders van die hipertrofiese sein kan optree, en dus die ontwikkeling van hipertrofie beïnvloed.

Hartspier kontraktiliteit word gereguleer deur die dinamiese fosforilasie van proteïene binne die sarkomeer deur kinases soos bv. cAMP-geaktiveerde proteïen kinase A (PKA). Die spoed en energie doeltreffendheid van hartspier kontraksie moet gereguleer word om by die liggaam se behoeftes aan te pas; dus word PKA naby sy teikens deur A-kinase anker proteïene (AKAPs) geanker om sodoende die beheer van fosforilasie beide in die korrekte area sowel as tydsduur te reguleer. Kardiale miosien-bindingsproteïen C (cMyBPC), asook kardiale troponien I (cTNI), is beide HKM-veroorsakende sarkomeriese proteïene wat kontraktiliteit beheer deur middel van fosforilasie deur PKA. In ‘n vorige studie in ons laboratorium is ‘n fosfodiesterase 4D-interaksie proteïen as bindingsgenoot van die N-terminaal van cMyBPC geïdentifiseer deur middel van ‘n gis-twee-hibried (G2H) kardiale biblioteek sifting. In die literatuur staan dié proteïen ook bekend as miomegalin (MMGL) isovorm 4.

Fosfodiesterases en PKA word soms deur dieselfde anker proteïen (AKAP) geanker, dus het ons hipotiseer dat MMGL isovorm 4 ook as AKAP kan optree deur PKA aan die fosforileerbare N-terminaal van cMyBPC te anker. Die hipotese is getoets deur middel van direkte proteïen-proteïen interaksie analises in ‘n gis-gebaseerde sisteem. Die MMGL cDNA was in ‘n jag-plasmied gekloneer, wat toe direk ge-evalueer is vir interaksie met twee verskillende PKA regulatoriese-subeenheid prooi-plasmiede. Die funksie van MMGL self is verder ondersoek deur die G2H jag-plasmied te gebruik om ‘n kardiale cDNA biblioteek te sif, sodoende om nuwe MMGL bindingsgenote te identifiseer. Alle prooi klone wat deur dié G2H analises geïdentifiseer is, was daarna onderworpe aan DNA-volgorde bepaling om hul identiteit vas te stel. Afhangende van hul identiteite en subsellulêre lokalisering, is alle moontlike G2H MMGL-prooi interaksies verder ge-evalueer deur bykomende, afsonderlike biochemiese tegnieke viz. *in vivo* ko-immunopresipitasie asook *in vivo* 3D ko-lokalisering. Die interaksie tussen MMGL en sy bekende PKA-gefosforileerde sarkomeriese bindingsgenote was ook ondersoek onder kondisies van β-adrenergiese stres, deur kwantitatief die vlakke van ko-lokalisering te meet voor en na byvoeging van die β-adrenergiese agonis isoproterenol. Om verder die rol van MMGL in cMyBPC fosforilasie te ondersoek, het ons die uitdrukking van die verskillende fosforilasie isovorms van cMyBPC, met en sonder β-adrenergiese stimulasie, in die konteks van siRNA-bemiddelde MMGL uitklop, bepaal.

Ons het verder hipotiseer dat MMGL en PKA as modifiseerders van die hipertrofiese fenotipe mag dien. Dit is getoets deur ‘n enkel nukleotied polimorfisme (SNP) genotiperings studie van die gene wat kodeer vir MMGL en die regulatoriese subeenhede van PKA, viz. *PDE4DIP*, *PRKAR1A* en *PRKAR2A*, en daarna dié genotipiese data met kliniese fenotipiese data te vergelyk in ‘n familie-gebaseerde assosiasie studie. ‘n Paneel van 353 individue wat genetiese en klinies geaffekteerde, sowel as ongeaffekteerde HKM individue insluit, was geidentifiseerd. Alle individue was ondersoek vir die aanwesigheid of afwesigheid van al drie Suid-Afrikaanse HKM stigter mutasies; bloedmonsters is gekollekteer en DNA uitgetrek. Die genotipes van veelvoudige SNPs in elke geen was bepaal deur die DNA monsters aan TaqMan® alleliese diskriminasie tegnologie met behulp van die ABI TaqMan® Validated SNP Genotyping Assays sisteem te analiseer. Statistiese analises deur middel van kwantitatiewe transmissie disekwilibrium toetse (QTDT) was gedoen om te bepaal of die verskil in genotipe in hierdie drie gene ‘n effek op HKM fenotipe het.

Ons resultate het gewys dat MMGL interaksie toon met beide PKA regulatoriese subeenhede, sowel as met ander kardiale proteïene wat ook PKA teikens is, insluitende die sarkomeriese proteïen cTNI. Dit is bevestig dat die twee regulatoriese subeenhede van PKA (PRKAR1A en PRKAR2A), kardiale ankyrin herhaal proteïen (CARP), koper metabolisme geen *MURR1* domein 4 (COMMD4), α-enolase (ENO1), β-enolase (ENO3) en cTNI almal nuwe bindingsgenote van MMGL is. ‘n Proteïen moet interaksie met een van die regulatoriese subeenhede van PKA toon om as AKAP geklassifiseer te word; MMGL het interaksie met beide getoon, wat ons hipotese bevestig dat MMGL ‘n AKAP is, asook dat MMGL as ‘n nuwe dubbel-spesifieke sarkomeriese AKAP geklassifiseer kan word. Die identiteite van die AKAPs wat betrokke is in die fosforilasie van cMyBPC en cTNI was onbekend tot nou; ons resultate wys dat MMGL die AKAP is wat betrokke is in die fosforilasie van beide hierdie PKA teikens.

Ons wys ook dat daar kwantitatief meer interaksie plaasvind tussen MMGL en sy sarkomeriese bindingsgenote cMyBPC en cTNI onder kondisies van β-adrenergiese stres. Dit impliseer dat PKA dinamies verwerf word deur MMGL, onder verhoogde vlakke van cAMP, tot by die PKA teikens cMyBPC en cTNI, moontlik om kardiale stres-response te bemiddel en dus te lei na verhoogde spierkontraksie. Verder het siRNA-bemiddelde uitklop van MMGL gelei na ‘n vermindering van cMyBPC vlakke onder kondisies van β-adrenergiese stres. Dit dui aan dat fosforilasie deur middel van MMGL-bystand ‘n voorvereiste is vir beskerming van cMyBPC teen proteolise.

Die SNP modifiseerder studie het gewys dat een variant in *PDE4DIP* (rs1664005) sterk assosiasie toon met verskeie kliniese hipertrofie kenmerke, insluitende maksimale interventrikulêre septum diktheid, sowel as ander van die saamgestelde telling kenmerke. Twee variante in *PRKAR1A* (rs11651687 en rs3785906) het ook sterk assosiasie getoon met verskeie van die kliniese hipertropfie kenmerke. Hierdie resultate dui dus daarop dat variante in hierdie twee gene as modifiseerders van die HKM fenotipe mag optree.

In samevatting skryf hierdie studie ‘n nuwe funksie aan MMGL isovorm 4 toe: dit voldoen aan alle vereistes om as AKAP geklassifiseer te word en dit blyk of dit betrokke is in die fosforilasie van cMyBPC en cTNI; dus is MMGL waarskynlik ‘n belangrike komponent in die regulasie van hartspier sametrekking, en dus met uitbreiding, in die ontwikkeling van hipertrofie. Dit hou verdere implikasies in om die siekte-oorsaak van mutasies in cMyBPC en cTNI te verstaan, en stel die vraag of MMGL self as ‘n kandidaat HKM-veroorsakende geen kan beskou word.

To my parents

“Success breeds success”

ACKNOWLEDGEMENTS

I would like to express my sincere gratitude to the following individuals. Without them, this project would have been impossible.

My promoter, Prof Hanlie Moolman-Smook. Thank you for giving me the opportunity to pursue this PhD. Thank you very much for your scientific input, vision, guidance and patience throughout this study. Thank you also for all the time you spent helping me compile this thesis. I would also like to thank you for your moral support and motivation. I have learned a great deal from you, and I am grateful and privileged to be your student.

Dr Craig Kinnear, Mrs Lundi Korkie and Dr Amsha Ramburan. Thank you for all your scientific and technical support and advice, and the time spent helping me no matter what problem I experienced. Also, for taking the time teaching me various techniques. All your input is invaluable to me.

Ms Carmen Swanepoel, for being with me on this journey from Day 1. Thank you for always providing me with a fresh perspective, no matter what the situation.

Ms Nadia Carstens. Thank you for assisting me with all statistical issues I experienced. Also, thank you for your sound advice regarding various aspects.

Dr Ben Loos, for the technical assistance you provided with the fluorescence microscope and co-localization assays.

Dr Johann Riedemann, for the technical input and assistance you provided with the RNAi and western blot experiments.

All members of the MAGIC Lab, past and present, for creating an enjoyable working environment.

To the Medical Research Council, the University of Stellenbosch and Prof Paul van Helden, for financial support.

INDEX PAGE

LIST OF ABBREVIATIONS

°C	degrees Celcius
α-MHC	alpha-myosin heavy chain
β-MHC	beta-myosin heavy chain
µl	microlitre
2-PGA	two-phospho-D-glycerate
3D	three-dimensional
5'-AMP	five prime adenosine monophosphate
a	adenine
aa	amino acid
Ade	adenine
ADP	adenosine diphosphate
aIVS	anterior interventricular septum
AKAP	A-kinase anchoring protein
AKAR	A-kinase anchoring reporter
AMP	adenosine monophosphate
ASREA	allele specific restriction enzyme analysis
ATP	adenosine triphosphate
AW	anterior wall
BAC	bacterial artificial chromosome
BLAST	Basic Local Alignment Search Tool
BLASTN	Basic Local Alignment Search Tool (nucleotide)
BLASTP	Basic Local Alignment Search Tool (protein)
bp	base pair
BSA	body surface area
BSA	bovine serum albumin
c	cytosine
Ca^{2+}	calcium
$CaCl_2$	calcium chloride

CaMK	calcium-calmodulin dependant kinase
CaMK II	calcium calmodulin dependant kinase type II
cAMP	cyclic adenosine monophosphate
CARP	cardiac ankyrin repeat protein
cDNA	complementary DNA
CEU	Central European
cfu	colony forming units
cGMP	cyclic guanosine monophosphate
CHF	chronic heart failure
CIP	calf intestinal alkaline phosphatase
cM	Centi-Morgan
cMyBPC	cardiac myosin binding protein C
Co-IP	co-immunoprecipitation
COMMD4	copper metabolism *MURR1* domain 4
cTNI	troponin I, cardiac isoform
CWT	cumulative wall thickness
DAP	dynein associated polypeptide
DBP	diastolic blood pressure
DCM	dilated cardiomyopathy
DMEM	Dulbecco's modified eagle media
DMSO	dimethyl suplhoxide
DNA	deoxyribonucleic acid
dNTP	deoxy-nucleotide triphosphate
DSCR3	Down syndrome critical region 3
DTT	1,4-dithiothreitol
E. coli	*Escherichia coli*
EDTA	ethylene-diamine-tetra-acetic acid
ENO1	α-enolase
ENO3	β-enolase
EPAC	guanine-nucleotide exchange protein

ERK5	extracellular signal-regulated kinase 5
EST	expressed sequence tag
FBXL10	F-Box and leucine-rich repeat protein 10
FISH	fluorescent *in situ* hybridization
Fn	fibronectin
FRET	fluorescence resonance energy transfer
g	guanine
GEF	guanine-nucleotide exchange factor
GFP	green fluorescent protein
GNG	cyclic nucleotide-gated
GPCR	G-protein coupled receptor
HCM	hypertrophic cardiomyopathy
HF	heart failure
His	histidine
HR	heart rate
HWE	Hardy-Weinberg equilibrium
I/R	ischaemia/reperfusion
IBD	identity by descent
IEF	isoelectric focusing
Ig	immunoglobulin
IP	immunoprecipitation
Isopro	isoproterenol
IW	inferior wall
kb	kilobase
K_m	Michaelis constant
kDa	kilo Dalton
KO	knockout
LB	Luria Bertani
LD	linkage disequilibrium
LDU	linkage disequilibrium unit

Leu	leucine
LGMN	legumain
LiAc	lithium acetate
LMM	light meromyosin
LQTS	long QT syndrome
LV	left ventricular
LVM	left ventricular mass
LW	lateral wall
M	molar
MAF	minor allele frequency
mAKAP	muscle-selective A-kinase anchoring protein
MAP	mitogen-activated protein kinase
MC	mutation carrier
MCS	multiple cloning site
mg	milligram
MGB	minor groove binder
MHC	myosin heavy chain
ml	millilitre
mLVWT	maximal left ventricular wall thickness
mM	millimolar
MMGL	myomegalin
MRC	Medical Research Council
MRI	magnetic resonance imaging
mRNA	messenger RNA
MTG	myeloid translocation gene
MyBPC	myosin binding protein C
NaCl	sodium chloride
NaOH	sodium hydroxide
NC	non carrier
NF-	nuclear factor kappa beta

OD	optical density
ORF	open reading frame
PAGE	polyacrylamide gel electrophoresis
PBS	phosphate buffered saline
PCI	phenol/chloroform/isoamyl alcohol
PCR	polymerase chain reaction
PDE4D	phosphodiesterase 4D
PDE4DIP	phosphodiesterase 4D interacting protein
PDEs	phosphodiesterases
PEG	polyethylene glycol
PEP	phosphoenolpyruvate
Pi	inorganic phosphate
PIPES	Piperazine-N,N-bis (2-ethanesulfonic acid) 1.5 Sodium
pIVS	posterior interventricular septum
PKA	protein kinase A
PKC	protein kinase C
PKD	protein kinase D
PKI	PKA inhibitor peptide
PLB	phospholamban
PMSF	phenylmethylsulphonyl fluoride
PP1	protein phosphatase 1
PP2A	protein phosphatase 2A
PP2B	protein phosphatase 2B
PRKAR1A	protein kinase regulatory type I alpha
PRKAR2A	protein kinase regulatory type II alpha
PVDF	polyvinylidene fluoride
PW	posterior wall
QDO	quadruple dropout
QTDT	quantitative transmission disequilibrium testing
RACK1	receptor for activated C kinase 1

RFP	red fluorescent protein
RIAD	RI-selective anchoring disrupter peptide
RISR	RI specifier region
RLC	regulatory light chain
RNA	ribonucleic acid
RNAi	RNA interference
rpm	revolutions per minute
RyR	ryanodine receptor
S1	myosin subfragment 1
S2	myosin subfragment 2
SBP	systolic blood pressure
SCD	sudden cardiac death
SD	synthetic dropout
SDS	sodium dodecyl sulphate
SDS-PAGE	sodium dodecyl sulphate polyacrylamide gel electrophoresis
Ser	serine
SERCA2	SR ATP-dependent Ca^{2+} pump
SHR	spontaneous hypertensive rat
siRNA	small interfering RNA
SNP	single nucleotide polymorphism
SNX3	sorting nexin 3
SR	sarcoplasmic reticulum
t	thymine
T_a	annealing temperature
TDO	triple dropout
TE	Tris-EDTA
TEMED	N,N,N’,N’-tetramethylethylenediamine
Thr	threonine
T_m	melting temperature
TM	tropomyosin

Tn	troponin
TNC	troponin C
TNT	troponin T
Trp	tryptophan
TUSC4	tumour suppressor candidate 4
Ub	Ubiquitin
UCR	upstream conserved region
UPS	ubiquitin proteasome system
UV	ultraviolet
V	Volts
V_{max}	maximal shortening velocity
V_o	unloaded shortening velocity
w/v	weight per volume
WB	western blot
WKY	Wistar Kyoto
WT	wild type
www	world wide web
X-α-Gal	X-alpha-galactosidase
Y2H	yeast-two-hybrid
YFP	yellow fluorescent protein
YPDA	yeast peptone dextrose adenine
YRI	Yoruba

LIST OF FIGURES

Figure 1.9. Schematic representation of an AKAP. The PKA heterotetramer (yellow) anchors to an AKAP via an amphipathic helix. When cAMP binds to the regulatory (R) subunit of PKA, the catalytic (C) subunits are activated and released to phosphorylate various nearby substrates. An AKAP may also serve as a scaffold protein for various other signaling proteins (A, B and C) (McConnachie *et al.*, 2006)

Figure 1.10. A representation of the mAKAP complex, showing how PDE4D3 and PKA are tethered to the nuclear membrane via mAKAP, thereby regulating the local cAMP flux. PDE4D3 also acts as a scaffold protein for ERK5. PDE4D3 activity will eventually reduce cAMP levels back to basal levels, which in turn will shut down the kinase (Donelson Smith *et al.*, 2006)

Figure 1.11. Myomegalin interacts with PDE4D (Verde *et al.*, 2001), and with trisphosphorylated cMyBPC (A. Ramburan, PhD thesis), opening the possibility that it might act as AKAP anchoring PKA to the MyBPC motif

Figure 1.12. MMGL isoform and conserved domain structure in *Homo sapiens*. Exons not drawn to scale in relation to nucleotide size. Image produced from http://www.ensembl.org and http://www.ncbi.nlm.nih.gov

Figure 2.1. Graphical representative example of the heart showing the 3 levels at which measurements of wall thickness were made. A) Long-axis view of left ventricle, taken at level of mitral valve, papillary muscles as well as just above apex (levels indicated by dotted lines). B) An example of a 2D echocardiographic ultrasound of the left ventricle. Abbreviations: AV- aortic valve, LA-left atrium, LV-left ventricle, LVOT-left ventricular outflow tract, MV- mitral valve, RVOT-right ventricular outflow tract. Taken from http://www.med.yale.edu/.../aortic_regurgitation.html with minor modifications by JC Moolman-Smook

Figure 2.2. Overview of TaqMan® allelic discrimination technology. Selective annealing of the TaqMan® probes plus exonuclease cleavage of a 5' allele-specific dye label generates the assay signal, enabling allelic discrimination (taken from TaqMan® SNP Genotyping Assays Product Bulletin, Applied Biosystems)

Figure 3.1. Activation of nutritional reporter genes by PKA-MMGL interaction during direct protein-protein interaction assays. Small-scale Y2H matings between pGBKT7-MMGL and pACT2-PRKAR1A (i) and pACT2-PRKAR2A (ii) on solid medium lacking Leu, Trp, His and Ade (QDO). Both subunits show interaction with MMGL, but that of PRKAR2A with MMGL appears to be stronger than that of PRKAR1A, as judged by the number and colour of colonies arising

Figure 3.6. Western blots of *in vivo* co-immunoprecipitations of MMGL and putative interactors. **A:** Endogenous CARP (i), ENO1 (ii), ENO3 (iii) and cTNI (iv) immunoprecipitated exogenous dsRed-/YFP-MMGL *in vivo* in lysates of ds-Red-/YFP-MMGL transfected, differentiated H9C2 cardiomyocytes. (v) indicates that GFP-COMMD4 immunoprecipitates dsRed-MMGL in differentiated H9C2 cardiomyocytes transfected with both GFP-COMMD4 and dsRed-MMGL **B:** Reciprocal immunoprecipitations indicate that dsRed-/YFP-MMGL immunoprecipitated endogenous CARP (i), ENO1 (ii), ENO3 (iii) and cTNI (iv) in lysates of ds-Red-/YFP-MMGL transfected, differentiated H9C2 cardiomyocytes. (v) indicates that dsRed-MMGL immunoprecipitates GFP-COMMD4. The dsRed antibody is directed against the dsRed-MMGL fusion protein, while the JL-8 antibody is directed against the YFP/GFP fusion proteins. The clear protein G control lanes show that these precipitations are not spurious, but are the result of physical association between the relevant proteins. *Abbreviations:* IP-immunoprecipitate; Prot G-protein G control; WB-western blot

Figure 3.7. Live cell fluorescence imaging showing that co-localization of MMGL isoform 4 and cMyBPC increases under adrenergic stress. Each panel represents a single frame of the 25 images that were captured for the Z-stack. Each of the first three columns shows a single colour channel, while the image in the last column shows an overlay of the four colour channels used. **A:** Colocalization (yellow) between dsRed-MMGL and GFP-cMyBPC in the absence (-isopro) and presence (+isopro) of the beta-adrenergic agonist, isoproterenol. Co-localization levels have increased ten minutes after the addition of isoproterenol. **B:** Quantification of co-localization shown in A shows that co-localization increases but does not reach statistical significance

Figure 3.8. Live cell fluorescence imaging showing that co-localization of MMGL isoform 4 and cTNI increases under adrenergic stress. Each panel represents a single frame of the 25 images that were captured for the Z-stack. Each of the first three columns shows a single colour channel, while the image in the last column shows an overlay of the four colour channels used. **A:** Colocalization (yellow) between dsRed-MMGL and GFP-cTNI in the absence (-isopro) and presence (+isopro) of the beta-adrenergic agonist, isoproterenol. Co-localization levels have increased ten minutes after the addition of isoproterenol. **B:** Quantification of co-localization shown in A shows that co-localization increases but does not reach statistical significance

Figure 3.9. Real-time quantification of *PDE4DIP* cDNA transcribed from RNA extracted from cells transfected with either a non-silencing control or a particular *PDE4DIP* siRNA. *Pde4dip* Rn_RGD:708410_3_HP (MMGL 3) resulted in optimal knockdown of *PDE4DIP* (80%)

LIST OF TABLES

CHAPTER ONE: INTRODUCTION

INDEX **PAGE**

CHAPTER 1: INTRODUCTION

Life-giving oxygen and nutrients reaches all parts of the body by the continuous circulation of blood pumped by the heart. Cardiomyocytes, specialized heart muscle cells adapted to contract and respond swiftly to physiological stimuli, maintain this cycle by contracting in response to action potentials, originating from the pacemaker of the heart, the sinoatrial node. The rate of action potentials fired by the sinoatrial node is mediated by two opposing nerve systems, the sympathetic nervous system, using noradrenaline and adrenaline to increase the rate, and the parasympathetic nervous system, releasing acetylcholine to reduce the action potentials fired. This stimulus-response coupling ensures that the cardiac output is matched by the body's physiological needs (Scott and Santana, 2010).

On a molecular level, the arrival of hormones and neurotransmitters to cardiomyocyte receptors results in numerous signal-tranduction cascades. One of the most prominent cardiac signal-transduction pathways is the G-protein-coupled receptor pathway, involving effector molecules such as adenylyl cyclase, which regulates the production of second messengers (Oldham *et al.*, 2008). Ca^{2+} and cyclic AMP (cAMP) are the two most common second messengers in cardiac signaling pathways, acting at defined sites and, through signaling, these second messengers control contraction, excitability and gene expression of respective target proteins.

One such target protein that regulates cardiac contractility through the cAMP signaling pathway during times of physiological stress is cardiac myosin binding protein C (cMyBPC). Since its discovery in 1973, this still very enigmatic protein has been the focus of numerous studies, especially when it became known that mutations in the gene encoding for cMyBPC is a leading cause of hypertrophic cardiomyopathy (HCM) (Watkins *et al.*, 1995, Bonne *et al.*, 1995).

This chapter will briefly describe HCM and the disease's association with cMyBPC, followed by an overview of cMyBPC itself. A more detailed overview of cAMP signaling and regulation of contractility in the heart will follow, as will a summary of previous studies in this laboratory, all of which will provide context for the current study.

1.1. HYPERTROPHIC CARDIOMYOPATHY

1.1.1. HCM – a sarcomeric disease characterized by the extreme variability in the amount of cardiac hypertrophy that develops

Hypertrophic cardiomyopathy (HCM) is one of the most common inherited cardiac diseases, affecting one in every five hundred people (Maron *et al.*, 1995). This autosomal dominantly inherited disease is the most common cause of sudden cardiac death (SCD) in young people (Maron *et al.*, 1996). Myocyte disarray, interstitial fibrosis and left ventricular hypertrophy characterize HCM, as shown in Figure 1.1 (Wynne *et al.*,

2001). The underlying defect in HCM is altered contractility of the sarcomere, primarily due to a defective sarcomere caused by mutations in the genes encoding sarcomeric proteins (Thierfelder *et al.*, 1994). One of the hallmarks of HCM is the extreme variability in the amount of cardiac hypertrophy that develops in different patients in response to sarcomeric protein-encoding mutations (Moolman *et al.*, 1997, Maron *et al.*, 1987). Although numerous disease-causing genes have been identified, the factors that modify the amount of hypertrophy that develops in a given person are still unknown (Marian 2002).

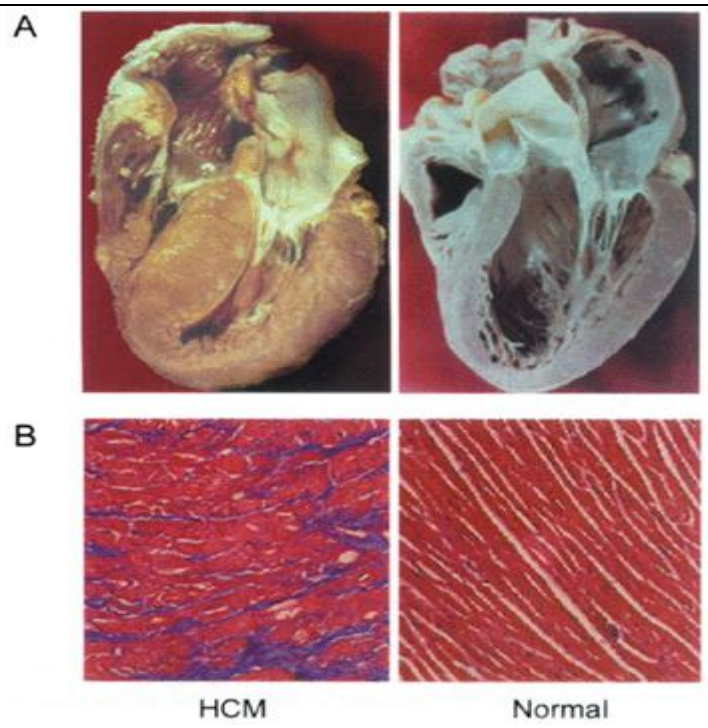

Figure 1.1. Pathology of hypertrophic cardiomyopathy. A. Post-mortem examination of heart showing left ventricular hypertrophy with reduced left ventricular cavity size, as compared to a normal heart. B. Histopathology section of HCM heart showing myofibre disarray and interstitial fibrosis, as compared to a non-diseased section (Chung *et al.*, 2003)

HCM mutations have been described predominantly in the genes encoding β-myosin heavy chain, cardiac troponin T, and cardiac myosin binding protein C (cMyBPC) (Crilley *et al.*, 2003). In 2003, a study by Richard *et al.* suggested that mutations in the gene encoding for cMyBPC (*MYBPC3*) are the most common HCM-causing mutations. The impact of this gene had been underestimated primarily due to the fact that the mutations in this gene is typically associated with benign phenotypes that do not present clinically, and cases are often identified incidentally and/or only at a later age (Richard *et al.*, 2003). It was suggested that mutations in *MYBPC3* are responsible for a very important clinical subclass of HCM (Watkins *et al.*, 1995). Presently, *MYBPC3* mutations are considered the second most frequent gene associated with HCM worldwide, with only *MYH7* (encoding the β-cardiac myosin heavy chain) mutations exceeding *MYBPC3* mutations (Barefield and

Sadayappan, 2010) Together, these two genes account for 79% of all sarcomeric mutations associated with HCM (http://cardiogenomics.med.harvard.edu/genes/gene-list).

Interestingly, some of these mutations are associated with a normal life expectancy, whereas other mutations are associated with a high SCD risk (Moolman-Smook *et al.*, 2003). For example, mutations in cardiac troponin T generally cause minimal hypertrophy, but a high risk of SCD, whereas some mutations in β-myosin heavy chain and cMyBPC cause severe hypertrophy, but patients may still have a long life expectancy (Moolman-Smook *et al.*, 2003). However, even within families, individuals carrying the same mutation often present very different clinical pictures. Thus, penetrance is variable, and hypertrophy and the risk for SCD are not necessarily dependent only on the disease-causing mutation, but appear to be modified by additional environmental or genetic factors; these are the reason why some patients, who appear to have a mild phenotype, can suffer lethal complications (Crilley *et al.*, 2003).

The mechanism by which HCM-causing mutations result in hypertrophy is not completely clear. In short, it has been speculated that the mechanism could involve mutant proteins being incorporated into the sarcomere, thereby resulting in a dominant negative effect. Such incorporated "poison peptides" may disrupt normal aspects of sarcomeric function (Flavigny *et al.*, 1999, Sato *et al.*, 2003). Contrasting findings suggest that mutant alleles cause haploinsufficiency of sarcomeric proteins by effectively acting as null alleles (see Section 1.1.2) (Rottbauer *et al.*, 1997, Van Dijk *et al.*, 2009, Marston *et al.*, 2009). However, it is clear that altered contractility in the sarcomere is the first trigger for the development of hypertrophy. Thus, it could be hypothesized that molecules that affect contractility can act as modifiers of the hypertrophic signal, and therefore influence the development of hypertrophy. Interestingly, cMyBPC is also one of the primary proteins by which contractility is regulated in the cardiac sarcomere.

1.1.2. *MYBPC3* – one of the two most commonly implicated genes in HCM

Since 1995, up to 150 HCM-causing *MYBPC3* mutations have been described (Barefield and Sadayappan, 2010). Seventy percent of these *MYBPC3* mutations are predicted to cause truncated proteins, with the C-termini lacking myosin and/or titin binding sites (Figure 1.2; for further detail about the structure of cMyBPC, see Section 1.2) (Watkins *et al.*, 1995, Bonne *et al.*, 1995, Carrier *et al.*, 1997). These mutations are usually associated with incomplete disease penetrance and late onset of disease (Niimura *et al.*, 1998, Moolman *et al.*, 2000).

Interestingly, early studies indicated that cardiac tissue from affected HCM patients with *MYBPC3* mutations did not contain mutant peptides or normal levels of cMyBPC, which made it extremely difficult to characterize the functional outcome of *MYBPC3* mutations (Rottbauer *et al.*, 1997). Several studies have since shown that

patients with C-terminal truncation mutations demonstrate a lower level of total cMyBPC than individuals with no *MYBPC3* mutations, suggesting that haploinsufficiency might be the pathological mechanism (Moolman *et al.*, 2000, Van Dijk *et al.*, 2009, Marston *et al.*, 2009). The ubiquitin-proteasome system targets the truncated cMyBPC for degradation, which could explain the absence of mutant cMyBPC protein (Sarikas *et al.*, 2005). This also provides evidence that the mutant *MYBPC3* allele causes haploinsufficiency of cMyBPC in the sarcomere by effectively acting as a null allele (Van Dijk *et al.*, 2009). Moreover, the study by Marston *et al.* showed that not only patients with truncation mutations, but also patients with missense *MYBPC3* mutations, had reduced levels of cMyBPC, which further supports haploinsufficiency as a disease mechanism for MyBPC-related HCM (Marston *et al.*, 2009). However, contrasting findings have also been reported, suggesting that at least some *MYBPC3* mutations may have a dominant-negative effect on sarcomere organization due to a poison polypeptide effect (Flavigny *et al.*, 1999, Sato *et al.*, 2003).

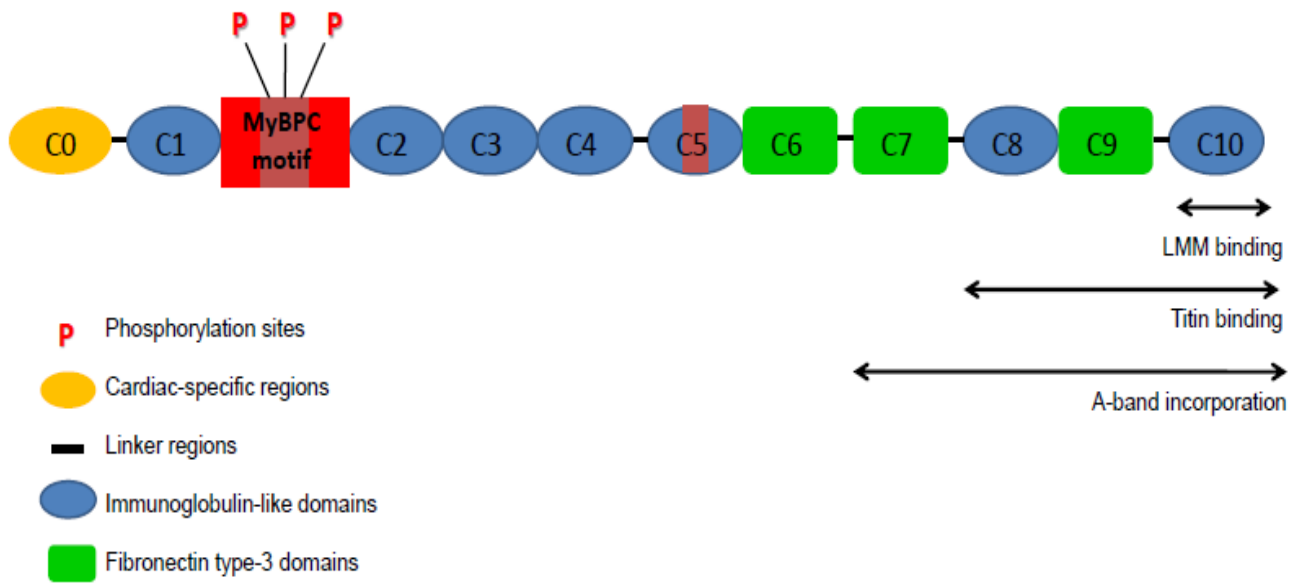

Figure 1.2. Schematic representation of cardiac myosin binding protein C (cMyBPC), indicating domains of known function and cardiac-specific regions (Moolman-Smook *et al.*, 2002)

In the N-terminal, several mutations, which cause HCM with varying penetrance, have been reported to occur in the C1-C2 domains, a region which includes the phosphorylatable MyBPC motif, emphasizing the importance of this region (Barefield and Sadayappan, 2010). Two specific mutations have been identified which occur within the cardiac-specific LAGGGRRIS sequence within the cMyBPC motif, close to two of the phosphorylation sites; this suggested that cMyBPC phosphorylation may be critical to normal function (Richard *et al.*, 2003). Moreover, patients exhibiting end-stage heart failure showed decreased cMyBPC phosphorylation at Ser-282

(El-Armouche *et al*, 2007). Furthermore, HCM patients showed diminished cMyBPC phosphorylation levels at Ser-282 in both end-stage heart failure and HCM (Jacques *et al.*, 2008).

It is well known that MyBPC forms an integral part of vertebrate striated muscle; however, its precise roles and quaternary arrangement in the sarcomere are not yet completely understood, while functional studies of MyBPC have been limited because of the highly modular nature of this protein. However, as this protein is one of the principle effectors in the regulation of cardiac contractility, it is relevant to briefly place this protein within the context of the sarcomere, and to discuss the known functional domains and interactions of this protein that are likely to be important for maintenance of sarcomeric structure and regulation of cardiac contractility. Moreover, it is relevant to this thesis to discuss cMyBPC phosphorylation and the regulation of cardiac contractility, both in health and disease.

1.2. CARDIAC MYOSIN BINDING PROTEIN C (cMyBPC)

1.2.1. MyBPC is a regulatory protein found in the sarcomere

The sarcomere is the smallest contractile unit of muscle. It consists of thick and thin filaments, which generate force in striated and cardiac muscle. The major protein constituting the thick filaments is myosin, with filamentous actin being the major constituent of thin filaments. These two proteins interact together to form a molecular motor, generating a contractile force (Vander *et al.*, 2001). Figure 1.3 illustrates a simplified version of the sarcomere.

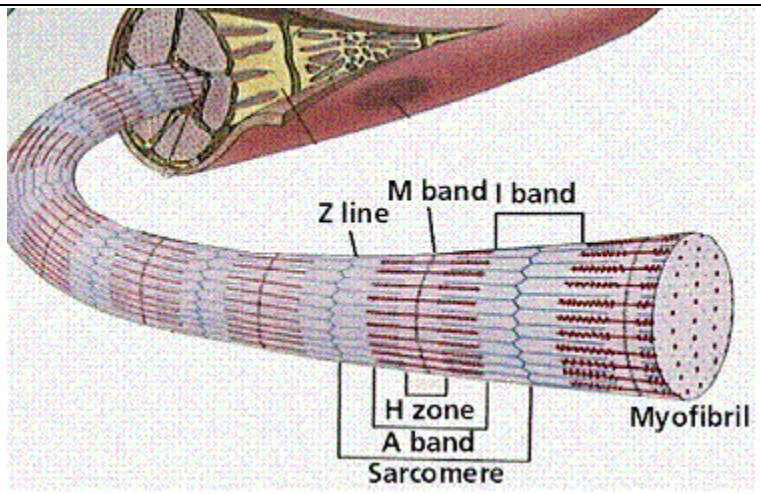

Figure 1.3. The sarcomere, the smallest contractile unit of muscle (http://circulatory-system.org/muscule/im4.gif)

However, the fundamental contractile properties of muscle cannot be generated by actin and myosin alone. A system consisting only of actin and myosin lacks the calcium-dependent switch crucial for controlling the

transition between the resting and contractile states of muscle. Control is provided by additional regulatory proteins of the thick and thin filaments, which are involved in assembly, maintenance of structural integrity, and regulation of contractile activity (Flashman *et al.*, 2004). In the thin filament, control is achieved by tropomyosin and the three subunits of troponin (TNI), which block the access of the myosin head to its binding site on actin in the absence of calcium (Winegrad 1999). The thick filament also contains regulatory proteins viz. myosin binding protein C, -H and –X (MyBPC-C, -H, and –X) (Offer *et al.*, 1973). The focus will now turn to cMyBPC, because of its above-mentioned role in HCM, as well as its role in sarcomeric structure and regulation of cardiac contractility.

Offer *et al.* identified MyBPC as a novel protein that interacts with myosin, and it is localized to the C zone of the A band of the sarcomere, as shown in Figure 1.4 (Offer *et al.*, 1973, Craig *et al.*, 1976). Three isoforms of MyBPC exist, viz. fast skeletal, slow skeletal, and cardiac (Weber *et al.*, 1993, Yasuda *et al.*, 1995) and separate genes encode the three isoforms, the different isoforms are not produced by alternative splicing. The genes encoding the human fast (*MYBPC2*) and slow skeletal (*MYBPC1*) isoforms are situated on chromosomes 19 and 12, respectively (Weber *et al.*, 1993), with the gene encoding for the cardiac isoform (*MYBPC3*) situated on chromosome 11 (Gautel *et al.*, 1995). The two skeletal isoforms can occur together, even in the same sarcomere, in some muscle types, but never in the human heart (Reinach *et al.*, 1983). The cardiac isoform is found only in the heart (Weber *et al.*, 1993).

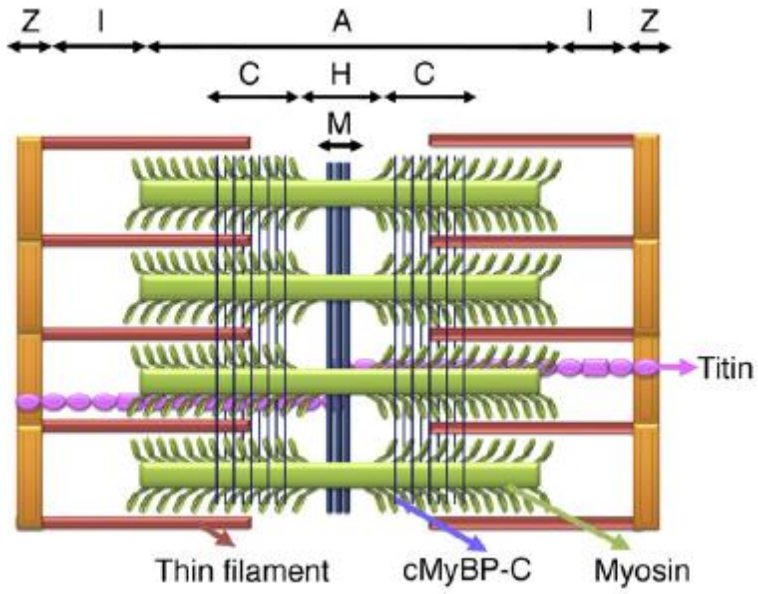

Figure 1.4. Schematic diagram showing the location of cardiac myosin binding protein C (cMyBPC) in the C-zone of the sarcomere (Barefield and Sadayappan, 2010)

Both the skeletal isoforms consist of ten globular domains (C1-C10) (Figure 1.2); seven of these are immunoglobulin (Ig) domains and three are fibronectin (Fn) type III domains, and these domains are always arranged in the same order (Okagaki *et al.*, 1993). The MyBPC motif, which is a conserved 105-residue linker region, occurs between domains C1 and C2 (Gautel *et al.*, 1995).

The 140kDa cardiac isoform of MyBPC differs from the two skeletal isoforms in three important ways. Firstly, cardiac MyBPC (cMyBPC) contains an additional immunoglobulin module with 101 residues at the N terminus (C0). Secondly, a 28-residue loop is inserted into the C5 immunoglobulin domain. Thirdly, nine additional residues with the amino acid sequence LAGGGRRIS plus three phosphorylation sites occur in the MyBPC motif and are unique to cMyBPC (Gautel *et al.*, 1995). Figure 1.2 shows the arrangement of the domains, as well as the differences between the skeletal and cardiac isoforms.

1.2.2. The role of MyBPC in thick filament formation and its arrangement in the sarcomere

Studies showed that MyBPC binds to myosin via interaction with the light meromyosin (LMM) portion of the myosin rod, the myosin region that forms the backbone of the thick filament (Moos *et al.*, 1975). All three MyBPC isoforms bind LMM via their C-terminal domain C10 (Okagaki *et al.*, 1993), contributing to the formation of the thick filament backbone (Figure 1.2). MyBPC also binds to titin, another component of the thick filament (Furst *et al.*, 1992), via the C-terminal domains C8 to C10 of MyBPC (Figure 1.2) (Freiburg and Gautel, 1996). Titin has a region that also lies in the C zone of the A band, like MyBPC, and which is also made up of IgI-like and Fn3 domains; this region consists of a series of eleven 11-domain superrepeats (Labeit *et al.*, 1992). Trinick proposed that the position that MyBPC attains in the thick filament may be due to the titin Ig domains, because MyBPC, like the 11-domain superrepeats of titin, is confined to the C zone (Trinick 1996). It was therefore concluded that the interaction between MyBPC, myosin and titin is crucial for attaining the ordered arrangement of the sarcomere (Freiburg and Gautel, 1996). The interaction between MyBPC and titin alone is actually quite weak, but combining all three molecules, viz. myosin, titin and MyBPC at the MyBPC C-terminus forms a complex binding which is a surprisingly stable structure.

Given these findings, the question that resulted was: Is MyBPC truly necessary for the formation of filament assembly, and if it was not present, what would the effect be? Studies done by co-expressing MyBPC and myosin heavy chain (MHC) in mammalian non-muscle cells partly answered the question. Co-expression of MyBPC and MHC resulted in the formation of long, compact filaments encircling the nucleus. In the absence of MyBPC, dysfunctional, diffuse, spindle-shaped structures formed (Seiler *et al.*, 1996, Welikson and Fischman, 2002). It was also found that myosin filaments can form *in vitro* in the absence of MyBPC, but the addition of physiological ratios of MyBPC caused the filaments to increase in length with improved structure and filament

compactness (Koretz 1979, Davis 1988). Truncated MyBPC expression also yielded results that further led to the suggestion that the C10 domain is crucial in filament formation (Welikson and Fischman, 2002).
Knockout mouse model studies by Harris *et al.* yielded surprising results in the light of these *in vitro* studies. Homozygous-null mice were still viable, and regular sarcomere striations were seen, including features such as the Z line, A band and M line. The striations and Z line, A band and M line were, however, frequently misaligned (Harris *et al.*, 2002). In a study by McConnell *et al.*, mice expressing homozygous C-terminal truncated cMyBPC incorporated very low levels of the mutant protein into the sarcomere, and had an abnormal, yet intact, sarcomere structure (McConnell *et al.*, 1999). However, in both these models, mice developed contractile dysfunction and cardiomyopathies after three months, which shows that cMyBPC is not necessary for sarcomeric development during embryogenesis and basal cardiac function, but it is essential for proper sarcomeric organization and function. On the other hand, heterozygous mice with either C-terminal truncation or cMyBPC knockout displayed normal cardiac function together with regular sarcomere organization, and survived into adulthood (Harris *et al.*, 2002, McConnell *et al.*, 1999).

Flashman *et al.* concluded that MyBPC does play a role in the formation of the thick filament and its stability, however, it is not essential for sarcomere formation (Flashman *et al*., 2004), probably as other factors besides MyBPC exist that contribute to sarcomere assembly in the native filament. Winegrad noted: "Although MyBPC is not necessary for the formation of thick filaments, it is necessary for the formation of normal thick filaments" (Winegrad 1999).

There are currently two models that describe the arrangement of cMyBPC at the C-terminus with myosin and titin, viz. the collar model and the strut model as shown in Figure 1.5. The collar model proposes that three cMyBPC molecules form a trimeric collar around the thick filament, with domains C5-C10 of each molecule wrapping around the width of the thick filament backbone in such a way that domains C5-C8 and C7-C10 of parallel-arranged, sequential cMyBPC molecules interact (Moolman-Smook *et al.*, 2002, Flashman *et al.*, 2004, Flashman *et al.*, 2007). Support for this model came from experiments that revealed interactions between domains C5-C8 and domains C7-C10 in cardiac and fast skeletal MyBPC (Moolman-Smook *et al.*, 2002), but not slow skeletal MyBPC (Flashman *et al.*, 2008). The strut model proposed that three or more cMyBPC molecules are arranged axially along the thick filament as support rods, as was suggested by image analysis of electron micrographs (Squire *et al.*, 2003, Zoghbi *et al.*, 2008, Al-Khayat *et al.*, 2009); however the study by Al-Khayat *et al.* also found evidence of structures which are not incompatible with the collar model closer to the thick filament backbone (Al-Khayat *et al.*, 2009). The arrangement of the N-terminal domains (C0-C4) is not predicted by either of the two models, but both models propose that the N-terminal domains extend into the interfilamental space where they can reach and interact with the thin filament (Squire *et al.*, 2003, Winegrad 1999).

1.2.3. The effects of sarcomeric protein phosphorylation

β-adrenergic stimulation results in the phosphorylation of three sarcomeric components, viz. phospholamban, troponin I and cMyBPC. The phosphorylation of these proteins is mediated via cyclic adenosine monophosphate (cAMP)-dependent protein kinase A (PKA) (Jeacocke and England, 1980, Wolska *et al.*, 2002, Garvey *et al.*, 1988). In the case of cMyBPC, phosphorylation also takes place via an endogenous calcium/calmodulin kinase (CaMK) tightly associated with cMyBPC (Schlender and Bean, 1991); furthermore, it was found that cMyBPC is also phosphorylated by protein kinase C (PKC) (Venema and Kuo., 1993) and protein kinase D (PKD) (Haworth *et al.*, 2004), although not through the β-adrenergic pathway. Phosphorylation of sarcomeric proteins ultimately results in changes in contractile function and cardioprotection (Montgomery *et al.*, 2002).

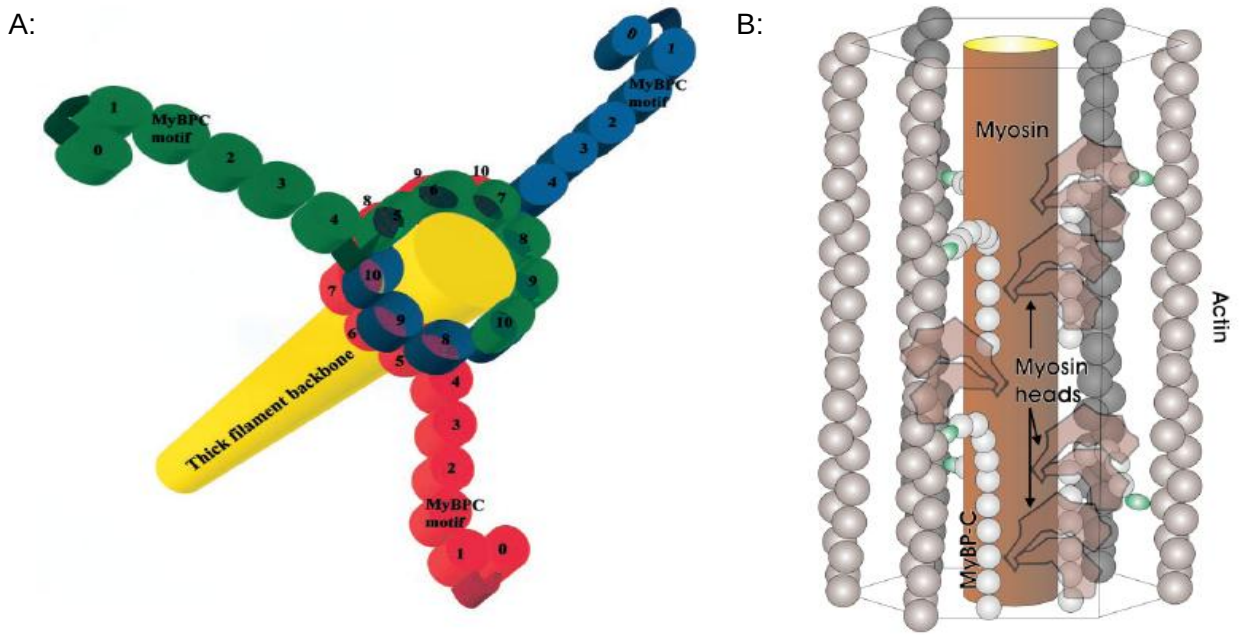

Figure 1.5. Two independent models predicting the arrangement of cMyBPC with myosin at the C-terminus. A: the collar model (Moolman-Smook *et al.*, 2002) B: the strut model (Squire *et al.*, 2003) see text for details

What happens when phosphorylation of these proteins occur? It was found that in the heart, contractility is significantly enhanced by the dynamic phosphorylation of phospholamban, troponin I and cMyBPC (Garvey *et al.*, 1988, Gautel *et al.*, 1995). Gautel *et al.* investigated the importance of PKA-dependent cMyBPC phosphorylation, and described the presence of four phosphorylation sites (termed A-D) in the MyBPC motif. However, steric constraints from domain C2 causes Ser-360 (site D) to not be phosphorylated, leaving only three N-terminal phosphorylation sites at Ser-273 (site A), Ser-282 (site B) and Ser-302 (site C). It was found that CaMK could phosphorylate cMyBPC to ~1 mol Pi per molecule, but PKA could phosphorylate the protein to ~3 mol Pi per molecule (Schlender and Bean, 1991). It appears that site B on the cardiac LAGGGRRIS insertion

can be phosphorylated by both PKA and CaMK, hence facilitating the phosphorylation of sites A and C by PKA by abolishing steric constraints (McClellan *et al.*, 2001). However, it was found that a critical level of calcium is necessary for CaMK-mediated phosphorylation of cMyBPC at site B, before the other sites could be phosphorylated. The critical calcium concentration required for this monophosphorylation is less than that required for activation of contraction, and thus it is not clear whether cMyBPC is ever unphosphorylated under normal physiological circumstances in the sarcomere. However, at activating calcium concentrations, with cMyBPC being fully phosphorylated, increased contraction force can be observed (McClellan *et al.*, 2001). The skeletal isoforms of MyBPC do not contain the LAGGGRRIS insertion, and are therefore not phosphorylated by PKA or CaMK (Lim and Walsh, 1986).

It was also found that, of these three phosphorylation sites, two can be phosphorylated by PKC (Ser-273 and Ser-302) (Mohamed *et al.*, 1998). A new PKA phosphorylation site was also identified *in vitro* in murine cMyBPC at Ser-307 (Shaffer *et al.*, 2008).

cMyBPC is dephosphorylated in response to cholinergic agonists, eg. acetylcholine, and this process occurs predominantly via protein phosphatase 2A (PP2A) (Hartzell and Titus, 1982, Schlender *et al.*, 1987).

How does phosphorylation of cMyBPC lead to increased cardiac contraction? Myosin subfragment-2 (S2) is the portion of the rod joining the myosin head to the thick filament backbone, and it was shown *in vitro* that a weak interaction occurs between this myosin region and MyBPC (Starr and Offer, 1978). This binding is mediated by domains C1-C2 of MyBPC, which includes the MyBPC motif (Gruen *et al.*, 1999). This interaction was found in both cardiac and skeletal isoforms of MyBPC and myosin. However, it was found that the interaction between the cardiac isoform and myosin S2 was abolished by phosphorylation of the MyBPC motif and this suggested a possible functional, rather than just structural, role for the cardiac isoform (Gruen *et al.*, 1999). It was suggested that when cMyBPC is phosphorylated and the S2 binding is abolished, the myosin crossbridges assumes a more favourable position for actin binding (Weisberg and Winegrad, 1999).

However, in a much more recent study, it was shown that two binding domains in cMyBPC viz. C1 and the MyBPC motif can also bind to actin (Shaffer *et al.*, 2009). The C1 binding occurs irrespective of the phosphorylation state of the MyBPC motif, whereas the binding of actin to the motif only occurs during the unphosphorylated state. Thus, when the MyBPC motif is phosphorylated, its binding with actin is abolished. It has therefore been suggested that in the unphosphorylated state, the MyBPC motif binds to actin, blocking myosin head binding and limiting cross-bridge attachment to the thin filament (Shaffer *et al.*, 2009).When the motif is phosphorylated, its binding to actin is abolished, rendering actin free to interact with other ligands like myosin S1 or S2, myosin light chains or thin filament regulatory proteins. Cross-bridge kinetics will therefore be

affected by the position and docking of myosin heads onto the unbound actin (Galinska-Rakoczy *et al.*, 2008, Shaffer *et al.*, 2009), and increased cardiac contractility will likely occur, as shown in Figure 1.6.

It can be concluded that cMyBPC N-terminal phosphorylation is mainly regulated by β-adrenergic stimulation that activates PKA, and intracellular levels of calcium that activates CaMK. The level of phosphorylation of the MyBPC motif then determines the state of interaction between cMyBPC and myosin S2, which affects the potential for binding of the myosin heads with actin. Alternatively, the phosphorylation level will determine whether actin is freed from binding to the MyBPC motif to interact with myosin. Thus, either way, the phosphorylation of cMyBPC acts as a sarcomeric regulator of cardiac contractility.

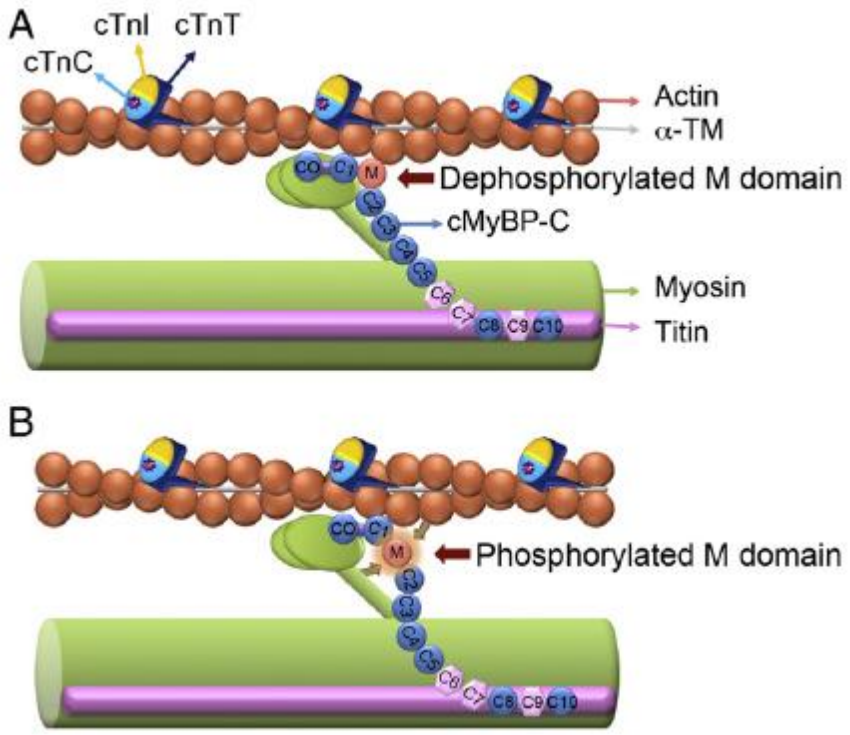

Figure 1.6. Proposed mechanism of how dynamic phosphorylation of the MyBPC motif (indicated as the M domain in this figure) may influence cross-bridge kinetics. A: During the unphosphorylated state, the C1 and M domain binds to actin. B: Upon phosphorylation of the M domain, the binding between the M domain and actin is abolished, and actin is free to bind to myosin, enabling increased cardiac contraction (Shaffer *et al.*, 2009, Barefield and Sadayappan, 2010)

1.2.4. cMyBPC phosphorylation is cardioprotective

The level of cMyBPC phosphorylation decreases during heart failure development, ischemic-reperfusion (I/R) injury and pathological hypertrophy (Sadayappan *et al.*, 2005). In cMyBPC- transgenic mice which expressed a non-phosphorylatable version of cMyBPC (in which the phosphorylatable serines in N-terminal cMyBPC had

been mutated to non-phosphorylatable alanines) on a cMyBPC-null background, depressed cardiac function was observed, along with altered sarcomeric structure. It was deduced that the mutant, unphosphorylatable protein was unable to rescue the original cMyBPC-null phenotype, causing functional deficits. However, overexpression of normal, wild-type cMyBPC on this background rescued the null phenotype. This suggested that phosphorylation of cMyBPC is necessary for normal cardiac function (Sadayappan *et al.*, 2005, Sadayappan *et al.*, 2006). The importance of phosphorylation was emphasized in similar cMyBPC-null transgenic mice where the knock-in cMyBPC was mutated to a constant trisphosphorylated state. These mice developed protection against I/R injury together with reduced cellular damage and attained fairly normal cardiac function (Sadayappan *et al.*, 2006, Sadayappan *et al.*, 2005).

The dephosphorylation of cMyBPC is associated with degradation by proteases like calpain I (Decker *et al.*, 2005, Sadayappan *et al.*, 2006). Following I/R injury, the total levels of phosphorylated cMyBPC is reduced, especially the trisphosphorylated form, a phenomenon which appears to be caused by increased cleavage of unphosphorylated cMyBPC by proteases. This cleavage is coupled to disruption of the thick filament, a reduced level of actin-myosin cross-bridges and dysfunctional contractility (Decker *et al.*, 2005, Sadayappan *et al.*, 2006). This inversely proportional ratio of cMyBPC phosphorylation to proteolytic degradation suggests that phosphorylated cMyBPC is protected against proteolytic cleavage, preserving normal cardiac function, whereas absence of phosphorylation results in reduced levels of cMyBPC as a result of increased degradation of the protein (Decker *et al.*, 2005, Sadayappan *et al.*, 2006)

In summary, the dynamic phosphorylation of the N-terminal of cMyBPC, mainly by β-adrenergic-activated PKA, significantly enhances cardiac contraction by causing rearrangement of the myosin crossbridges and thin filament structure (Gautel *et al.*, 1995, Levine *et al.*, 2001, Weisberg and Winegrad, 1996) and renders the protein resistant to degradation, contributing to a cardioprotective effect (Decker *et al.*, 2005, Sadayappan *et al.*, 2006). The N-terminal region of the protein appears to be crucial for this role of regulating cardiac contractility, together with its structural role. However, PKA activation affects a number of cellular pathways, not only cMyBPC, and thus it is relevant to discuss the manner in which particular cellular responses to PKA activation are targeted.

1.3. COMPARTMENTALIZATION OF cAMP- SIGNALING PATHWAY EFFECTORS

1.3.1. Kinases need to be compartmentalized for effective second-messsenger signaling

As mentioned in the previous section, cardiac contractility is significantly enhanced by the dynamic phosphorylation of cMyBPC via cAMP-activated PKA, PKC and CaMK (Garvey *et al.*, 1988, Gautel *et al.*, 1995). Since these kinases regulate a broad range of cellular responses, their compartmentalization in close proximity to their targets, including their sarcomeric targets, would facilitate control over which proteins are

phosphorylated in response to signaling via ubiquitous second messengers, such as cAMP, cyclic-guanosine-monophosphate (cGMP) and Ca^{2+} (Pawson and Scott, 1997, Wong and Scott, 2004). Similarly, co-compartmentalization of enzymes or proteins that generate or terminate these second messenger metabolites, such as the phosphodiesterases which degrade cAMP and cGMP, along with the relevant responsive kinases, helps to optimise the precision and speed of response to second messenger signaling (Pawson and Nash, 2000).

Compartmentalization of kinases in general is achieved by either direct docking of the kinase on the target protein, or by anchoring the kinase to, or close to, the target via an adaptor protein (Colledge and Scott, 1999). A number of adaptor proteins that anchor PKA, PKC, or CaMKs near their particular substrates and away from others have been described in various tissues. These anchoring proteins are highly varied in sequence, and are not necessarily functionally equivalent. Moreover, in some cases, the same adaptor protein has also been shown to anchor both the kinase and the relevant phosphodiesterase, viz. PKA and phosphodiesterase 4D (the latter is responsible for hydrolysing the cAMP that activates PKA) close to the PKA target (Dodge *et al.*, 2001). In muscle, such co-compartmentalization is crucial for maintaining contractility, as was shown by Fink *et al.*: disruption of A-kinase anchoring protein (AKAP)-mediated PKA-anchoring has significant detrimental effects on the contractility of cardiomyocytes, which is particularly noticeable upon β-adrenergic stimulation (Fink *et al*., 2001). Interestingly, in the absence of β-adrenergic stimulation, such disruption did not cause significant effects on cardiac contractility (Fink *et al*., 2001). The increase in phosphorylation of particularly cMyBPC and cTNI upon β-adrenergic stimulation was significantly reduced in cells where AKAP/PKA anchoring were disrupted, compared to controls where no disruption took place. The increase in phosphorylation of other phosphorylatable proteins such as phospholamban was not affected by this disruption, and it was therefore speculated that an unidentified myofibril-associated AKAP might function to anchor PKA to cMyBPC and cTNI (Fink *et al.*, 2001).

It is therefore important to further investigate the role that adaptor proteins play, especially in cMyBPC phosphorylation, because this process is so intricately involved in normal and enhanced levels of cardiac contractility.

1.3.2. Scaffolding and adaptor proteins create new signaling pathways

In complex metazoans, a point is reached where evolution is not driven by the creation of new genes, but by shuffling modular protein-protein domains to create new signaling pathways (Bhattacharyya *et al.*, 2006). Excellent examples of this strategy are scaffolding and adaptor proteins that play an important role in the assembly of multi-protein signaling complexes (Pawson and Scott, 1997, Pawson and Nash, 2000). These signaling scaffolds serve as central platforms that integrate, and at the same time, disseminate, multiple cellular signals. Signaling scaffolds ensure that enzymes are kept near their relevant targets by sequestering a signaling

enzyme to a specific subcellular environment. In this way, scaffolds are an essential means by which a common signaling pathway can serve many diverse functions, and play a role in the spatiotemporal resolution of cellular signaling (Beene and Scott, 2007).

As mentioned earlier, PKA is a cAMP-dependent kinase and is particularly important in the heart, because cAMP signaling regulates calcium dynamics as well as the rate and force of contraction. Several studies over the years have, however, demonstrated that not all agonists that lead to an increased cAMP concentration elicit similar PKA-mediated responses. This begged the question: How can signaling-specificity be achieved by such a broad-action kinase like PKA? (Hayes and Brunton, 1982). It is now known that scaffolding, anchoring and adaptor proteins function to direct signaling enzymes to discrete subcellular compartments to maintain localized pools of kinase activity (Pawson and Nash, 2000). In the cAMP pathway, AKAPs are responsible for clustering PKA into discrete intracellular compartments (Colledge and Scott, 1999). Figure 1.7 shows a representation of various cardiac AKAPs throughout the cell that targets PKA to specific compartments.

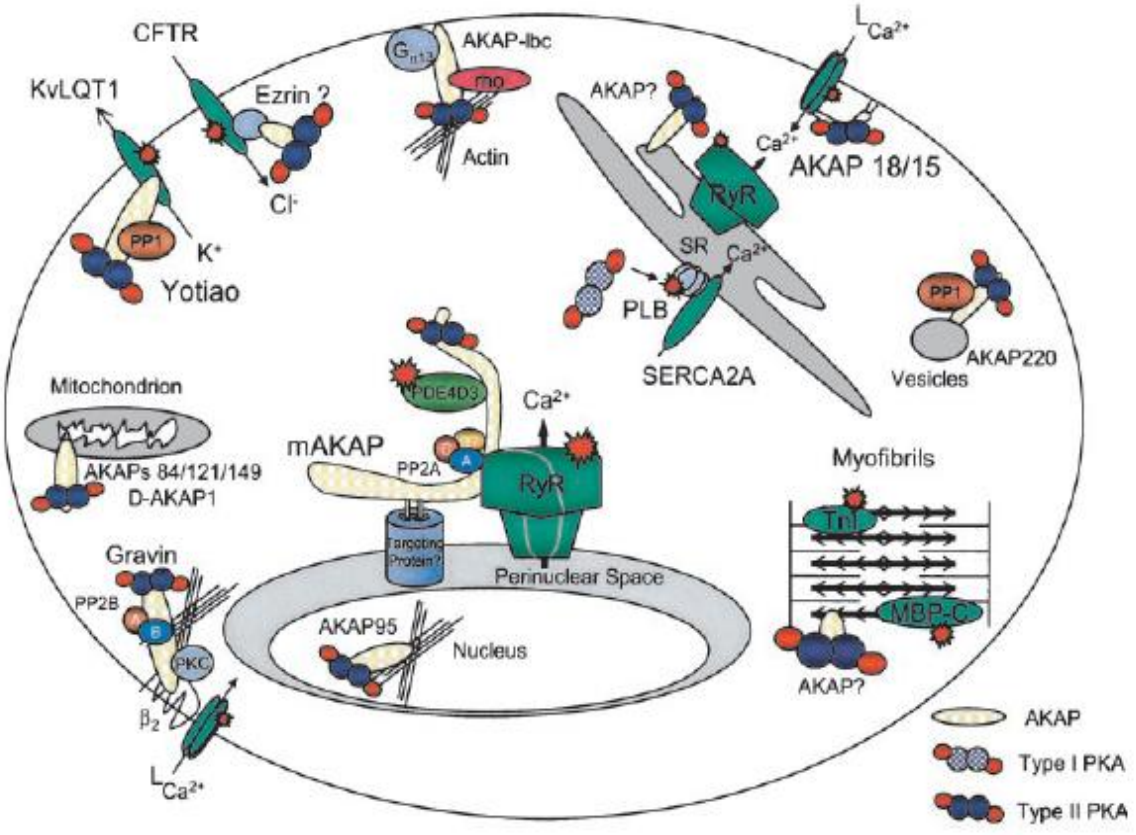

Figure 1.7. An illustration demonstrating cardiac A-kinase anchoring proteins (AKAPs) clustering PKA, and sometimes other kinases and enzymes, to discrete subcellular compartments throughout the cell, allowing for maintained localized pools of kinase activity (Kapiloff 2002)

1.3.3. AKAPs play a role in the dynamics of cAMP gradients

Imaging studies have shown that cAMP levels are unevenly distributed throughout the cell, within dynamic pools (Zaccolo and Pozzan, 2002, Rich *et al.*, 2001). cAMP flux is determined by two enzyme sets: Firstly G-protein-activated adenylyl cyclases, which synthesize cAMP from adenosine triphosphate (ATP), and secondly phosphodiesterases (PDEs) that terminate cAMP signaling by hydrolyzing it to 5'-adenosine monophosphate (5'-AMP). When cAMP is synthesized, it diffuses into the cytosol to activate downstream effector proteins such as cyclic-nucleotide-gated (CNG) channels, guanine-nucleotide exchange proteins (EPACs) and the serine-threonine kinase, PKA. In this way, a mechanism is therefore provided whereby extracellular stimuli can influence biological processes. After the processes take place, members of the PDE superfamily degrades the cAMP to 5'-AMP, thereby terminating the signal. AKAPs target PKA to substrates in the proximity of cAMP gradients generated by the counterbalancing actions of adenylyl cyclases and PDEs, and thereby contribute to the specificity of cAMP signaling. AKAPs therefore provide a mechanism of cAMP regulation in response to external stimuli within specialized subcellular regions and for particular time intervals (Tasken and Aandahl, 2004, Wong and Scott, 2004).

Some PDEs are also tethered to specific cellular sites via various PDE-binding proteins, thereby also contributing to generating local cAMP gradients. Moreover, it was found that some AKAPs can act as anchoring protein for PDEs, in addition to anchoring PKA (Dodge *et al.*, 2001, Asirvatham *et al.*, 2004). Anchoring PKA and PDEs together via the same AKAP would ensure tight regulation of cAMP signaling, as shown in Figure 1.8.

Several studies indicated that cAMP, which is freely diffusible, is actually compartmentalized in the heart, and therefore ensures localized cardiac cAMP action. Whole-cell patch recordings demonstrated localized activation of calcium channels in frog hearts by localized stimulation of β-adrenergic receptors (Jurevicius and Fischmeister, 1996). Zaccolo and Pozzan performed live cell imaging studies which monitored the activation of PKA in rat neonatal cardiac myocytes; this study clearly indicated that β-adrenergic stimulation activated a specific subpopulation of PKA moieties (Zaccolo and Pozzan, 2002). This localized action is a due to a direct association between PKA and AKAPs.

1.3.4. The AKAP/PKA complex

Protein phosphorylation, achieved by protein kinases, has been proclaimed as a principal means of reversibly controlling biochemical events. The kinase superfamily, consisting of ~518 members, participates in all aspects of cellular regulation (Manning *et al.*, 2002). Kinase research now focuses on how kinases are organized in relation to their effectors and substrates within the three dimensions of the cell, and research has shown that AKAPs have emerged as important signal-organizing components for PKA and other kinases (Donelson Smith

et al. 2006). The AKAP group of proteins is a structurally diverse group, and is defined by their ability to bind and target PKA (Tasken and Aandahl, 2004) Figure 1.9 illustrates a diagram of a prototypic AKAP, which anchors PKA, together with other signaling proteins, to a specific targeting domain.

PKA is a heterotetramer that consists of a regulatory (R)-subunit dimer, plus a catalytic (C)-subunit dimer, with each R-subunit bound to a C-subunit dimer (Scott 1991). The genes encoding the C-subunits have been characterized and are identified as Cα, Cβ and Cγ (Scott 1991). Cα and Cβ are ubiquitously expressed and are 93% identical. Cγ is only 80% identical to the other subunits and is expressed exclusively in the testis (Beebe and Corbin, 1986). For the R-subunits, four genes have been identified viz. RIα, RIIα, RIβ and RIIβ (Scott 1991). The RIα and RIIα-subunits are the most predominant, and are expressed in most tissues. RIβ and RIIβ are expressed mostly in reproductive tissues and in the central nervous system (Scott 1991, Cadd and McKnight., 1989).

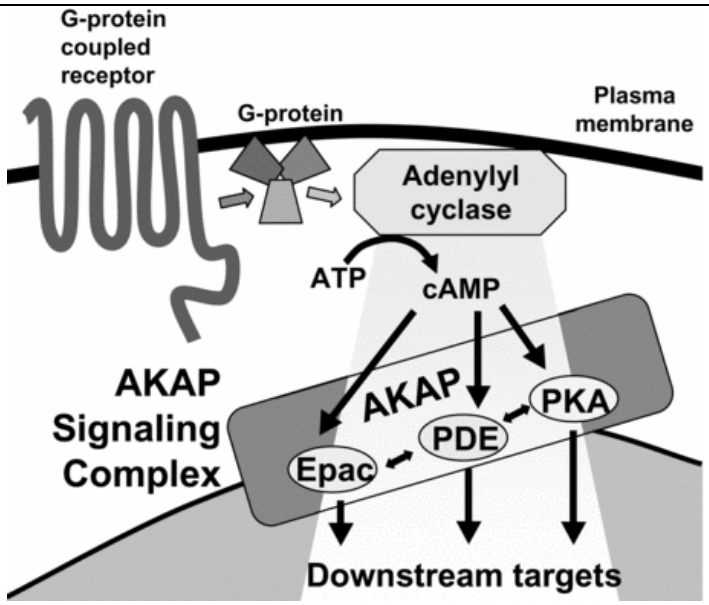

Figure 1.8. A simplified diagram of an AKAP signaling complex indicating that, in addition to PKA, an AKAP may also bind other cAMP effectors such as EPACs or PDEs. This ensures the appropriate subcellular response to cAMP signaling (Scott 2006)

It has been observed that RI associates only with other RI-subunits, and RII only with other RII-subunits (Scott 1991). The type-I PKA holoenzyme therefore consists of RI-subunits (RIα/RIβ) and is found in the cytosol, while the type-II holoenzyme consists of RII-subunits (RIIα/RIIβ) and is particulate bound (Scott 1991). When cAMP binds to PKA R subunits, the active C subunit (Cα, Cβ or Cγ) is released to phosphorylate nearby substrates (Dell'Acqua and Scott., 1997). Studies using various animal hearts determined that 50% of the cAMP-dependent protein kinase activity was associated with the particulate fraction i.e. the RII-subunits (Corbin *et al.*,

1977). Binding of individual hormones to their receptors also tend to preferentially activate a particular R-subunit. An example in cardiomyocytes is the activation of PKA-RII, which is particulate bound, by isoproterenol, an adrenergic agonist, while prostaglandin E_2, a vasodilator and noradrenalin-release inhibitor, activates PKA-RI, which is found in the cytosol (Keely 1979, Hayes and Brunton., 1982). Thus, in the cell, PKA acts globally through the cytosolic RI, and locally through the particulate bound RII.

The localization of PKA-RII to specific sites in the cell is mediated through the association with AKAPs. Most AKAPs that have been characterized bind the RII subunit, although several AKAPs have been reported that binds the RI subunit (Angelo and Rubin., 1998). However, the binding affinity of RII for AKAPs is typically higher than that of RI, and this allows for subcellular placement of the PKA-RII holoenzyme (Carr *et al.*, 1992, Alto *et al.*, 2003). Each AKAP has a distinct binding affinity for RII because of limited sequence conservation of the RII binding domain on individual AKAPs (Alto *et al.*, 2003). The binding affinity for RII/AKAP interaction further increases with the PKA-induced phosphorylation of the RII-subunit (Zakhary *et al.*, 2000). These binding affinities and kinetics become important in heart failure, where β-adrenergic signal desensitization occurs. In tissue isolated from failing hearts, RII phosphorylation is decreased and suggests a decrease or redistribution of anchored PKA signaling (Zakhary *et al.*, 2000). Dual-specific AKAPs have also been described, e.g. D-AKAP1 and D-AKAP2; these AKAPs can anchor both types of PKA R-subunit (Huang *et al.*, 1997, Wang *et al.*, 2001); it was also shown that some dual-specific AKAPs have a higher binding affinity for RII (Miki and Eddy, 1999).

The N-terminal domain of the PKA R-subunit binds to AKAPs via an amphipathic helix, which is found on most AKAPs (Carr *et al.*, 1992), see Figure 1.9. The Ht31 peptide is a partial protein fragment that has been developed to interrupt the RII/AKAP interaction. This peptide also contains the amphipathic α-helical region of an AKAP, but does not contain a targeting domain, and therefore binds RII with the same nanomolar affinity as a full-length AKAP, competing for RII binding, thereby disrupting AKAP/PKA interactions when overexpressed (Carr *et al.*, 1992, Rosenmund *et al.*, 1994, Lester and Scott, 1997).

Fink *et al.* demonstrated that PKA binding to AKAPs in cardiomyocytes was disrupted after adenovirus-mediated expression of the Ht31 peptide, as described in Section 1.3.1. The results of Fink *et al.* clearly demonstrate that PKA, when anchored to an AKAP, regulates specific, localized phosphorylation events without interrupting global cAMP signaling, and leads to normal cardiac contraction (Fink *et al.*, 2001).

Using a genetically encoded PKA-activity reporter known as A-kinase activity reporter (AKAR), Zhang *et al.* demonstrated that the rate of phosphorylation was enhanced three- to four-fold when PKA was bound to the same complex as its substrate (Zhang *et al.*, 2001). The results of Zhang *et al.* provided evidence that the release of the PKA C-subunit from an AKAP complex in response to cAMP, would preferentially lead to

phosphorylation of a specific, localized pool of substrate (Zhang *et al.*, 2001). Taking the results of Fink and Zhang *et al.* into account, it can clearly be seen that AKAPs play a crucial role in the PKA-mediated phosphorylation of specific, localized substrates, and in the case of cardiomyocytes, normal cardiac contractility.

For a protein to be classified as an AKAP, it has to meet four criteria. Firstly, a protein has to interact with the R-subunit of PKA inside a cell. Secondly, the unique targeting domains that are contained within an AKAP must participate in either protein/protein or lipid/protein interactions; this will dictate the subcellular localization of the relevant PKA. Thirdly, an AKAP must be able to coordinate multiple signaling pathways by anchoring additional signaling enzymes e.g. phosphatases, PDEs and other kinases (Colledge and Scott, 1999, Dodge and Scott, 2000). Lastly, an AKAP must be able to form larger, multiprotein units through the interaction with other scaffolding or adaptor proteins (Colledge *et al.*, 2000). If a protein meets these four criteria, it can be classified as an AKAP, and it will have the ability of functioning as a signal processing unit that can link upstream activators with their downstream targets. This allows for specificity of signaling and the integration of multiple signaling events (Dodge-Kafka *et al.*, 2006)

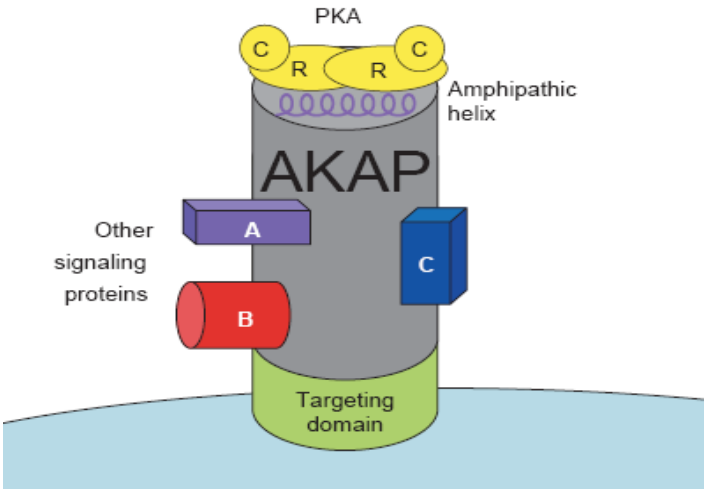

Figure 1.9. Schematic representation of an AKAP. The PKA heterotetramer (yellow) anchors to an AKAP via an amphipathic helix. When cAMP binds to the regulatory (R) subunit of PKA, the catalytic (C) subunits are activated and released to phosphorylate various nearby substrates. An AKAP may also serve as a scaffold protein for various other signaling proteins (A, B and C) (McConnachie *et al.*, 2006)

1.3.5. AKAP signaling complexes

The biological role of AKAPs coordinating multiple signaling pathways by anchoring additional signaling enzymes became apparent when Coghlan *et al.* discovered that AKAP79 not only anchored PKA, but also protein phosphatase PP2B (Coghlan *et al.*, 1995). Their finding suggested for the first time that signals controlling the phosphorylation and dephosphorylation of a substrate can pass through a single AKAP signaling

complex. Studies that followed the one by Coghlan *et al.* showed that AKAP79 also interacts with PKC, creating a way of integrating cAMP signals with Ca^{2+} and phospholipid signals at the same subcellular locus (Klauck *et al.*, 1996). It then became apparent that AKAPs not only bind PKA, but fulfill the crucial task of acting as signaling complexes, by binding other kinases, protein phosphatases as well as other signaling transduction enzymes.

As already mentioned, cAMP flux needs to be spatio-temporally controlled, and this requires the concerted action of two enzyme classes viz. adenylyl cyclases which synthesize cAMP, and PDEs which hydrolyze cAMP into 5'-AMP. Houslay and Adams, as well as Conti *et al.*, identified several proteins that bind PDEs, and target them to distinct microenvironments (Houslay and Adams, 2003, Conti et al., 1995). A good example of such PDE is PDE4D3. This enzyme is differentially localized via interactions with scaffolding proteins e.g. β-arrestin and myomegalin (Perry *et al.*, 2002, Verde *et al.*, 2001). Just as scaffolding proteins anchor PDEs, many AKAPs group PKA together with PDEs to stop cAMP signals as they diffuse into the cell (Dodge *et al.*, 2001).

1.3.5.1. Muscle-Selective AKAP illustrates how AKAP signaling complexes modulates contractility

An important example of an AKAP that functions as part of a multienzyme complex is muscle-selective AKAP (mAKAP). mAKAP, with a size of 255-kDa, is localized to the nuclear envelope and sarcoplasmic reticulum (SR) in the heart and skeletal muscle, and is also expressed in the brain (Kapiloff *et al.*, 1999). The enzymes that form part of the mAKAP complex are involved in the regulation of cardiac function, and include PKA, phosphodiesterase 4D3 (PDE4D3), the calcium-activated calcium channel or ryanodine receptor (RyR), phosphatases PP2A, PP1 and PP2B, nesprin-1α, the GTP exchange protein Epac and the extracellular signal-regulated kinase 5 (ERK5) (Dodge *et al.*, 2001, Dodge-Kafka *et al.*, 2005).

The localization of mAKAP to the nuclear envelope and SR has been determined by immunohistochemical studies of cardiac tissue (Kapiloff *et al.*, 1999, Ruehr *et al.*, 2004, Marx *et al.*, 2000). mAKAP is targeted to the nuclear envelope by the direct association of the spectrin-repeat domain on mAKAP to the nuclear-associated Nesprin-1α (Pare *et al.*, 2005). Overexpression of the mAKAP spectrin-repeat domain causes disruption of the mAKAP/Nesprin binding. This suggests that the localization of mAKAP to the nuclear envelope is saturable (Zhang *et al.*, 2001). It is currently still unclear how mAKAP anchors to the SR, but it is speculated that a direct association between mAKAP and the RyR through a conserved leucine zipper motif on the RyR may be responsible (Marx *et al.*, 2001).

Dodge *et al.* found that PDE4D3 co-purified with both mAKAP and the RII subunit of PKA in immunoprecipitation studies using rat heart extracts (Dodge *et al.*, 2001). They also showed that the PDE4D3 isoform directly interacts with mAKAP, and that PDE4D3 and mAKAP co-localized at the nuclear membrane of

cardiac myocytes (Dodge *et al.*, 2001). On discovering that both PDE4D3 and PKA interact with mAKAP, the possibility was raised that this complex might be closely involved with regulating local cAMP concentrations as well as mAKAP-associated PKA activity. By inhibiting mAKAP-associated PDE4 activity, the activity of the anchored PKA was enhanced, as expected (Dodge *et al*., 2001). PDE4D3 contains two PKA-phosphorylation sites, at Ser13 and Ser54. When Ser54 is phosphorylated, a 2-3 fold enhancement of PDE activity is observed (Sette and Conti, 1996). Not surprisingly then, mAKAP-associated PKA phosphorylation of PDE4D3 was found to cause a two-fold increase of PDE4D3 activity (Dodge *et al*., 2001).

From these above-mentioned findings, it was suggested that mAKAP forms a cAMP signaling complex by anchoring both PKA and PDE4D3. The complex operates by means of a negative-feedback loop, in which PKA's activity is attenuated by PDE4D3. Under basal conditions, mAKAP-bound PDE4D3 maintains local cAMP levels below the threshold value needed to activate mAKAP-anchored PKA. When a hormonal signal, e.g. β-adrenergic stimulation, activates adenylyl cyclase via G-coupled protein receptors, the cAMP level increases. The increased cAMP level overrides the PDE activity, and causes the C-subunit of PKA to be released. This leads to the phosphorylation of the Ser54 site on PDE4D3, which increases the local PDE (PDE4D3) activity. The increased PDE activity causes increased cAMP hydrolysis, and so cAMP levels return to basal. When basal cAMP levels are reached, the PKA holoenzyme reforms, and the process can start again (McConnachie *et al.*, 2006). Figure 1.10 summarizes these findings.

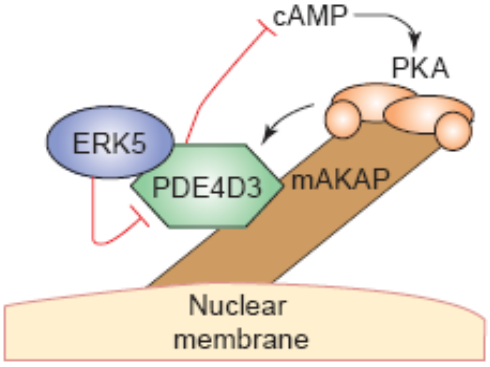

Figure 1.10. A representation of the mAKAP complex, showing how PDE4D3 and PKA are tethered to the nuclear membrane via mAKAP, thereby regulating the local cAMP flux. PDE4D3 also acts as a scaffold protein for ERK5. PDE4D3 activity will eventually reduce cAMP levels back to basal levels, which in turn will shut down the kinase (Donelson Smith *et al.*, 2006).

Interestingly, phosphorylation of the Ser13 site only enhances the affinity of PDE4D3 for mAKAP, but does not affect PDE activity. By enhancing the affinity of PDE4D3 for mAKAP, the negative-feedback loop is also enhanced (Carlisle Michel *et al.*, 2004). PKA phosphorylation has also been shown to modulate protein-protein

interactions within several other AKAP complexes (Tao *et al.*, 2003). The consequences of such type of regulation are as follows: In the case of mAKAP, PKA may phosphorylate PDE4D3 at Ser54 and Ser13 in response to hormonal stimulation, which means that PDE will be drawn into the AKAP complex with increased activity. This will decrease the local cAMP level back to basal levels. Dodge-Kafka *et al.* speculated that this arrangement of PKA and PDE may generate local cAMP fluctuations and pulses of compartmentalized PKA activity. These authors therefore determined the dynamics of the negative-feedback loop by using live cell imaging techniques to monitor the temporal activation of PKA, by using modified versions of the A-kinase activity reporter 2 (AKAR2)-PKA reporter. In addition to PKA activity, the AKAR2-PKA activity reporter is sensitive to PDE and can therefore monitor both the activation and termination of PKA signaling (Zhang *et al.*, 2005). The modified versions of AKAR2-PKA used by Dodge-Kafka *et al.* could either bind PKA alone (AKAR-PKA) or PKA and PDE4D3 (AKAR-PKA-PDE). Cells that expressed the AKAR-PKA reporter showed sustained elevation of fluorescence resonance energy transfer (FRET), upon cAMP stimulation. This indicated that PKA that was associated with AKAR2 was activated. In cells that expressed the AKAR-PKA-PDE reporter, the FRET response was short-lived, most likely due to a drop in cAMP levels because the AKAR-PKA-associated PDE activity increased (Dodge-Kafka *et al.*, 2005). The interaction of PDE4D3 and PKA to the same complex therefore resulted in variable periodical levels of PKA activity, ranging from basal to high and back to basal, in cells expressing AKAR-PKA-PDE. This suggested that the co-localization of PKA and PDE is a critical component for attenuating PKA signaling. This reporter study of Dodge-Kafka *et al.* serves as a model for the recruitment of PKA and PDE into a single complex to control local cAMP gradients, and demonstrates that cAMP compartmentalization by the mAKAP complex controls the timing of PKA activation as well as regulating the spatial location of PKA.

Moreover, the study by Dodge-Kafka *et al.* also revealed that PDE4D3 itself acts as a scaffolding protein, and recruits ERK5 to the mAKAP complex. PDE4D3 contains two ERK5-binding domains which mediates direct interactions between these two enzymes. Mutated forms of either domain inhibit the association between ERK5 and the mAKAP complex. ERK5 is similar to PKA in that it also regulates PDE4D3 catalytic activity (Hoffman *et al.*, 1999). When Ser579 is phosphorylated by ERK5, cAMP hydrolysis is decreased by 40% (Dodge-Kafka *et al.*, 2005). Phosphorylation of PDE4D3 at Ser579 by ERK2 also inhibits PDE activity, and causes an increased level of cAMP concentration. The resultant relative increase in cAMP levels, in return, stimulates the release of the PKA C-subunit. This demonstrates an alternative feedback system where ERK-signaling pathways lead to the inhibition of PDE activity, and consequently, increased cAMP levels (Hoffman *et al.*, 1999). On the other hand, these results show that mAKAP can assist in the bi-directional regulation of PKA activity by binding PDE4D3, ERK5 and PKA to the same anchoring protein. This is another example of how the mAKAP complex dictates local cAMP concentrations.

The GTP exchange protein Epac is another cAMP effector that was shown to mediate the cAMP inhibitory effect. Epac is also associated with the mAKAP complex via a direct binding to PDE4D3. Epac acts as a guanine nucleotide exchange factor for the small G-protein Rap1, and is stimulated by cAMP (Kawasaki *et al.*, 1998). When Epac was activated with specific cAMP analogs, ERK5 stimulation was attenuated. This demonstrates, yet again, the importance of PDEs as anchoring proteins (Dodge-Kafka *et al.*, 2005).

The theory of compartmentalization suggested that cellular cAMP-mediated events, although reactive to different durations and concentrations of cAMP, can still originate from the same microdomain. The mAKAP complex illustrates this theory as follows: When a stimulus arrives, and cAMP concentrations are in the nanomolar range, PKA is activated. As the stimulus continues, the cAMP concentration reaches the micromolar range, causing PDE4D3 and Epac to be sequentially activated (Beavo and Brunton, 2002). When the cAMP signal reaches its maximum, PDE4D3 is phosphorylated by PKA and results in the increase of cAMP hydrolysis. The resulting decrease of cAMP levels starts to shut off the stimulus, and terminates the actions of PDE4D3 and Epac. Lastly, PKA's activity is attenuated (Sette and Conti, 1996, Hoffmann *et al.*, 1999). This is a perfect example where three distinct cAMP-binding proteins co-exist within a complex and thus in a particular microdomain, with their own different ranges of activation (Dodge-Kafka *et al.*, 2005).

Tasken *et al.* suggested that another AKAP, AKAP450 is involved in an analogous function to mAKAP, but at centrosomal locations rather than at the nuclear membrane. AKAP450 tethers the enzymes PKA and PDE4D3 as well as the phosphatases PP1 and PP2A together to form a signaling complex, just like mAKAP does (Tasken *et al.*, 2001). Similarly, Bajpai *et al.* showed that yet another AKAP, AKAP110, binds the PDE4A isoform to the acrosome of spermatozoa, whereas Asirvatham *et al.* did similar work on AKAP149 and AKAP121, as well the Nervy and myeloid translocation gene (MTG) anchoring proteins, and found that these proteins target and bind the PDE4A and PDE7A isoforms to various subcellular regions (Bajpai *et al.*, 2006, Asirvatham *et al.*, 2004). This illustrates more examples of AKAP-PKA-PDE clusters functioning as signaling units that respond to upstream signals deriving from adenylyl cyclase and G-protein-coupled receptor (GPCR) networks. These signaling complexes continually change the signaling environment in which cAMP levels are distributed unevenly in the cell.

The findings mentioned in this section highlight the central role that AKAPs play in the customized regulation of cAMP signaling, and emphasize the pleiotropic nature of the second messenger cAMP (Donelson Smith *et al.*, 2006).

1.3.5.2. The mAKAP complex may play a vital role in cardiac function

As previously mentioned, the mAKAP complex is localized at both the SR and nuclear envelope. Because this large complex is found at both locations, diverse roles are suggested for the complex at these respective locations (Dodge-Kafka *et al.*, 2006). The mAKAP complex at the SR location plays a role in calcium dynamics in the heart, which is mediated through the regulation of the ryanodine receptor (RyR). A function of mAKAP is to link PKA to the RyR so that the RyR can be phosphorylated, and it has been shown that mAKAP-tethered PKA phosphorylates both cardiac and skeletal isoforms of the RyR (Kapiloff *et al.*, 1999, Ruehr *et al.*, 2004).When the RyR is phosphorylated at Ser2808 via PKA, the probability of an open channel, as well as the sensitivity of the RyR to calcium-dependent activation, is increased (Marx *et al.*, 2000). Marx *et al.* demonstrated that in failing hearts, PKA-mediated RyR hyperphosphorylation is observed, which leads to exhaustion of the SR calcium stores and an increased diastolic SR calcium leak. The physiological importance of the PKA negative-feedback loop is verified here, because RyR hyperphosphorylation is attributable to a decreased PDE4D3 level (Lehnart *et al.*, 2005). Lehnart *et al.* also showed that deletion of the PDE4D gene in mice leads to progressive cardiomyopathy, as well as cardiac arrhythmias and accelerated heart failure after myocardial infarction. Taking these data into consideration, it can clearly be seen that regulation of RyR phosphorylation by the mAKAP complex has noteworthy impact on SR calcium dynamics. Moreover, the disruption of cAMP dynamics may result in the development of cardiac disease.

The understanding of the function of the mAKAP complex at the nuclear envelope is still unclear, but studies suggest that it may play a role in the regulation of cardiac hypertrophy (Dodge-Kafka *et al.*, 2005, Pare *et al.*, 2005). When mAKAP expression in rat neonatal ventriculocytes was knocked down via RNA interference, the ability of prohypertrophic agonists to stimulate an increase in myocyte size and the fetal gene expression typically seen in hypertrophy, was blocked. The mechanism that the complex uses to induce hypertrophy is still unknown. It was, however, speculated that, by localizing the kinases ERK5 and PKA close to nuclear targets such as transcription factors, mAKAP may assist the increase in fetal gene expression essential for hypertrophy induction (Dodge-Kafka *et al.*, 2005, Pare *et al.*, 2005).

1.3.5.3. The AKAP Yotiao is also linked to cardiac function

Long-QT syndrome (LQTS) is an inherited cardiac disease, which is characterized by arrhythmias that often leads to sudden cardiac death, normally during increased sympathetic stimulation (Watanabe *et al.*, 2005). Mutations in the gene *KCNQ1*, amongst others, leads to LQTS. This gene encodes the ion channel subunit KCNQ1 that occurs in the K^+ channel (Kassand Moss, 2003). The K^+ channels are responsible for delayed rectifier K^+ currents (I_{KS}) which shape the duration of cardiac action potentials in response to β-adrenergic signaling (Westphal *et al.*, 1999). PKA phosphorylates KCNQ1 at Ser27, which leads to a significant increase in channel currents (Marx *et al.*, 2002).

Potet *et al.* found that the K^+ channel is associated with and is regulated by AKAP-bound PKA, and it was determined that Yotiao is the particular AKAP that binds this channel to PKA (Potet *et al.*, 2001, Marx *et al.*, 2002). Yotiao is a 210-kDa protein and was first found to associate with the *N*-methyl-*D*-aspartate receptor in neurons. It serves the function of tethering a kinase/phosphatase signaling complex to the ion channel at the *N*-methyl-*D*-aspartate receptor in neurons (Westphal *et al.*, 1999).

Yotiao is the AKAP responsible for tethering both PP1 and PKA to the K^+ channel. Although the effect of Yotiao-anchored PP1 on KCNQ1 is still unknown, this AKAP-bound phosphatase is the predominant enzyme that regulates the K^+ ion channel under basal conditions. It limits the effect of PKA until a cAMP increase leads to overpowering of the phosphatase action, and hence PKA activation (Westphal *et al.*, 1999). Marx *et al.* showed that the disruption of the K^+ ion channel association with Yotiao resulted in decreased cAMP enhancement of the channel's activity. KCNQ1 binding to Yotiao is mediated via a conserved leucine zipper coiled-coiled motif; Yotiao/K^+ channel disruption can be caused by a single amino acid mutation (G589D) in this leucine zipper coiled-coiled motif. This mutation was found in 508 out of 939 Finnish LQTS patients (Fodstad *et al.*, 2004). This clearly suggests that specific PKA anchoring to the K^+ channel is necessary for normal channel function *in vivo* (Marx *et al.*, 2002), and that lack of such anchoring triggers disease. This finding was thus the first genetic evidence proving that PKA targeting to particular sub-cellular regions is physiologically essential. The finding also gave considerable weight to the anchoring hypothesis (Dodge-Kafka *et al.*, 2006).

1.3.5.4. AKAP-Lbc

As described in section 1.3.4, the peptide Ht31 interrupts the interaction between an AKAP and the PKA RII subunit. The Ht31 peptide is a partial protein fragment, derived from a protein first identified in human thyroid that binds the PKA RII subunit with high affinity, competing with full-length AKAPs to bind PKA. Ht31 has been widely used as a molecular tool to investigate the molecular mechanisms of PKA anchoring, as well as to determine the biological importance that anchored PKA has on physiological proceedings (Carr *et al.*, 1992, Rosenmund *et al.*, 1994, Fink *et al.*, 2001).

By performing a database search that exposed similarities between full-length Ht31 and the guanine nucleotide exchange factor Lbc, Diviani *et al.* showed that full-length Ht31 functions as a Rho-selective guanine nucleotide exchange factor, revealing the function of full-length Ht31. Full-length Ht31 differs from the partial Ht31 used as molecular tool in that it contains, in addition to an amphipathic α helix, a domain that targets it to its phosphorylation target (Diviani *et al.*, 2001). Full-length Ht31 proved to be an AKAP and is now known as AKAP-Lbc, a large 320-kDa protein. Diviani *et al.* showed that AKAP-Lbc contains several domains that are involved in the activation of the small G-protein RhoA, including consecutive Dbl and Pleckstrin-homology

domains. It was also showed that $G\alpha_{12}$, which is the upstream activator of Rho, also associates with AKAP-Lbc. This suggests that this AKAP may function by coupling G-protein activation with Rho signaling (Diviani *et al.*, 2001).

Studies by Lang *et al.* and Ellerbroek *et al.* have found that PKA has an antagonistic effect on Rho signaling. It is now known that PKA, when bound to AKAP-Lbc, decreases the activation of Rho (Lang *et al.*, 1996, Ellerbroek *et al.*, 2003). This is mediated by blocking the Rho-guanine nucleotide exchange factor (GEF) activity of the scaffolding protein (Diviani *et al.*, 2004, Jin *et al.*, 2004). When Ser1565 on AKAP-Lbc is phosphorylated by PKA, the recruitment of the protein 14-3-3 to the complex is stimulated, which inhibits Rho activation. To have an inhibitory effect on Rho, PKA must be anchored to the AKAP-Lbc complex, and AKAP-Lbc must also be oligomerized for 14-3-3 (Diviani *et al.*, 2004, Baisamy *et al.*, 2005). This shows that AKAP-Lbc is involved in the integration of two effector pathways, coupling cAMP signaling with the small G-protein Rho. This allows for coordinated G-protein functional regulation.

Studies have shown that Rho signaling is closely linked with the generation of cardiac hypertrophy. However, the physiological role that AKAP-Lbc Rho-GEF activity plays in cardiac function is still unknown. Because Rho signaling is involved in hypertrophy induction, it can be speculated that AKAP-Lbc acts as an adaptor protein, facilitating G-protein activation of Rho. This may lead to the enhancement cardiotrophic effects of this small G-protein (Clerk and Sugden, 2000).

A study by Carnegie *et al.* has shown that the AKAP-Lbc complex also tethers PKC and PKD, and plays an important role in the activation of PKD (Carnegie *et al.*, 2004). Activation of PKD by the AKAP-Lbc complex is mediated by recruiting both PKD and PKDη, which is the upstream activator of PKD. This allows for the linear transduction of signals from one kinase to the next, and demonstrates a common way in which scaffolding proteins are arranged molecularly (Carnegie *et al.*, 2004, Pawsonand Nash, 2000). When PKA phosphorylates Ser2737 on AKAP-Lbc, the release of active PKD into the cytoplasm is mediated by AKAP-Lbc. This demonstrates that AKAP-Lbc facilitates specific activation of PKD, as well as amplifying the PKD signal by processing multiple PKD enzymes in a short time span (Carnegie *et al.*, 2004).

AKAP-Lbc is yet another example of an AKAP that acts as a multi-enzyme complex, illustrating the importance of cyclic nucleotide signaling compartmentalization, and that might well be involved in cardiac function.

1.3.5.5. AKAP15/18

A low molecular weight (81 amino acids) AKAP has been cloned in two unrelated laboratories, and was named AKAP15 or AKAP18 depending on the laboratory (Fraser *et al.*, 1998, Gray *et al.*, 1997) This AKAP is now

referred to as AKAP15/18, and is expressed exclusively in the plasma membrane of cardiomyocytes. AKAP15/18 is anchored to the plasma membrane by covalently attached lipid moieties, and this molecular configuration allows for the regulation of plasma membrane substrates.

The first identified target of AKAP15/18 was the L-type calcium channel, the major voltage-gated calcium channel in the heart that is responsible for the action potential's plateau phase (Bers 2002 , Fraser *et al.*, 1998, Gray *et al.*, 1997). Gao *et al.* showed that AKAP-anchored PKA phosphorylation is accountable for the increased probability of an open L-type channel that allows the potentiation of the inward calcium channel (Gao *et al.*, 1997). It was determined, through the works of Fraser *et al.* and Gray *et al.*, that AKAP15/18 is the AKAP responsible for facilitating this effect. AKAP15/18-anchored PKA phosphorylates Ser1928 on the α_{1C}-subunit as well as on multiple sites on the β_2-subunit (Gray *et al.*, 1997, Fraser et al., 1998). The AKAP is anchored to the L-type calcium channel via a leucine zipper motif at the C-terminus of the α_{1C}-subunit. Inhibition of the voltage-dependent potentiation of the channel occurred when a synthetic peptide was introduced that mimics channel binding (Hulme *et al.*, 2002). β-adrenergic regulation blockage of the channel was also observed when the binding between AKAP15/18 and the L-type calcium channel was disrupted (Hulme *et al.*, 2002, Hulme *et al.*, 2003). This demonstrates that PKA anchoring to the channel via AKAP15/18 is necessary for specific and rapid responses to small, localized cAMP concentrations that are mediated by adrenergic stimulation, in order to achieve normal channel functioning.

Protein phosphatase 2B (PP2B) and the β_2-adrenergic receptor have been identified as partners in the L-type calcium channel complex, although it is not clear whether the interactions are direct or AKAP-mediated (Sacchetto *et al.*, 2001). In the brain, direct association of the β_2-adrenergic receptor with the channel has been shown, and this strongly suggests that the L-type calcium channel, together with the β_2-adrenergic receptor, PP2B and AKAP15/18 may form a multiprotein complex in the heart (Davare *et al.*, 2001). It is therefore clear that AKAP15/18 plays a crucial role in cardiac calcium dynamics, as well as the facilitation of the inotropic actions of the β_2-adrenergic receptor.

1.3.6. Summary of the relevance of AKAPs

The main AKAPs already mentioned, viz. mAKAP, Yotiao, AKAP-Lbc and AKAP15/18, all play an important role in cardiac function, where they function by coordinating signal transduction complexes. Signal transduction is coordinated by the AKAPs via the recruitment of multiple signaling enzymes (the most important being PKA) close to their respective substrates. This allows upstream effectors to be joined with specific downstream targets within a single signaling complex, allowing specific compartmentalization as well as optimal signaling precision and speed. It can therefore be concluded that the most important function of AKAPs is to allow biological signal transduction to take place quickly and precisely, amplifying specific responses and maintaining the fidelity of

signal transduction networks, with the end-goal of eliciting the appropriate and correctly timed physiological response.

Since the discovery of the first AKAPs, viz. MAP2 and AKAP75 in 1982 and 1984, respectively, this family of proteins has grown and currently more than 70 members have been identified (Theurkauf and Vallee, 1982, Sarkar *et al.*, 1984), 13 of which are found in cardiac tissue (Ruehr *et al.* 2004). However, although the molecular composition of AKAP-bound signal transduction units have been greatly dissected and discovered, the understanding of the biological functions that they mediate is still only in its infancy. The next challenge, in addition to identifying novel AKAPs, will be the investigation of the specific functional roles of all those AKAPs in physiological processes (Carlisle Michel *et al.*, 2002).

1.4. A PREVIOUS STUDY REVEALED A POSSIBLE NEW AKAP

While investigating the interactions of cMyBPC, our laboratory identified a potential new AKAP. As the interactions of the N-terminal region of cMyBPC under its various phosphorylation states appear to be integral to the regulatory role of cMyBPC in contractility, a series of yeast-two-hybrid (Y2H) library screens using various phosphorylation-mimics of the C1-C2 region of this protein as bait has been performed in our laboratory. In particular, to gain further insight into the interactions of the trisphosphorylated form of the N-terminal region of cMyBPC, a construct of domains C1-C2 was used as bait in a Y2H cardiac library screen in which the serines in the three phosphorylation sites of the MyBPC motif had been replaced by glutamic acids (PPP). As a result of this screen, three of 19 putative interactors of PPP were identified as isoform 4 of phosphodiesterase 4D interacting protein (PDE4DIP), also known as myomegalin (Verde *et al.*, 2001, A.Ramburan, PhD thesis). The same study also identified myomegalin isoform 4 as an interactor of unphosphorylated cMyBPC (A.Ramburan, PhD thesis).

As mentioned previously (Section 1.3.5), PDE4D is a phosphodiesterase specifically responsible for hydrolyzing cAMP, the second messenger molecule which activates PKA (Beltman *et al.*, 1993). The fact that in some cases, an AKAP anchors both PKA and a phosphodiesterase to the PKA-target (Fink *et al.*, 2001), made the finding of interaction between cMyBPC, a PKA-target, and an isoform of a phosphodiesterase-interacting protein particularly intriguing. Although it is known that myomegalin anchors PDE4D (Verde *et al.*, 2001), it is not known whether myomegalin is also an AKAP, nor whether it binds to other PKA-targets. Although a CaMK has been found to co-purify with cMyBPC (Gautel *et al.*, 1995, Schlender and Bean, 1991), the mechanism of PKA anchoring to cMyBPC has never been described; yet it is plausible that close compartmentalization of PKA to the sarcomere would be crucial to regulate phosphorylation of this protein and cTNI in the control of the response of cardiac contractility to adrenergic stimulation. Furthermore, it has also been shown that co-compartmentalization of both PKA and PDE4D is crucial for maintaining contractility in muscle, because the

disruption of AKAP-mediated PKA anchoring had detrimental effects on cardiomyocyte contractility following adrenergic stimulation (Fink *et al.*, 2001).

The findings related above led us to question whether myomegalin is an AKAP, and if so, whether it targets PKA specifically to cMyBPC in cardiomyocytes, or to other PKA-targets as well. Furthermore, because of the role of cMyBPC phosphorylation in the regulation of cardiac contractility, and because of the effect of disruption of AKAP-mediated PKA on contractility, we speculated that myomegalin may be involved in regulating cardiac contractility, as schematically indicated in Figure 1.11.

The focus will now turn to PDE4D, the protein with which myomegalin (also known as phosphodiesterase 4D interacting protein/ PDE4DIP) is known to directly interact. A literature study of myomegalin itself will then follow.

1.4.1. Myocardial phosphodiesterases

As mentioned previously (Section 1.3.3), in the heart, two main mechanisms contribute to the increase of the local level of cAMP. Firstly, the membrane-bound enzyme adenylyl cyclase stimulates cAMP production by converting ATP to cAMP. Secondly, cAMP degradation by myocardial phosphodiesterases is slowed down by inhibition through enzymes that eliminate cAMP by its conversion to 5'AMP. Both of these processes result in an increase in intracellular cAMP concentration, which stimulates myocardial effects such as increased cardiac contraction. In contrast, the function of phosphodiesterases (PDEs) is to hydrolyze cAMP, lowering the intracellular concentration.

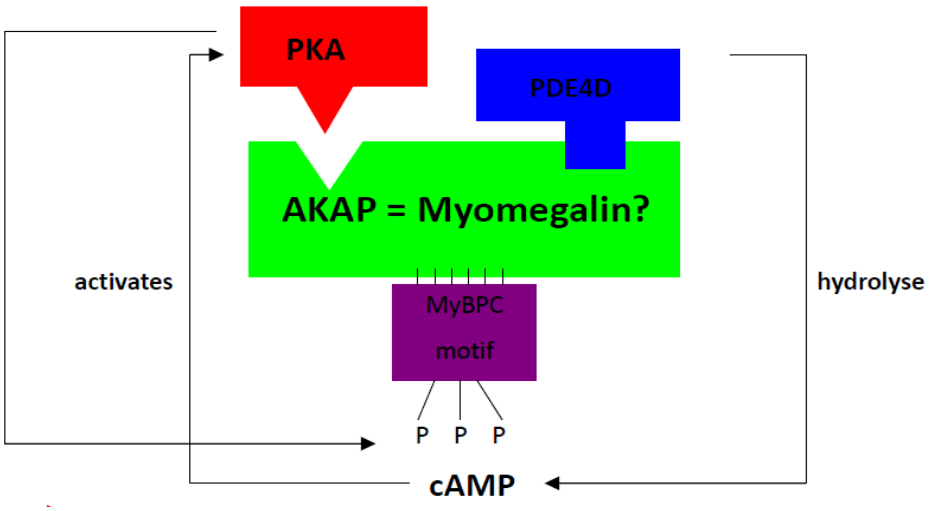

Figure 1.11. Myomegalin interacts with PDE4D (Verde *et al.*, 2001), and with un- and trisphosphorylated cMyBPC (A. Ramburan, PhD thesis), opening the possibility that it might act as AKAP anchoring PKA to the MyBPC motif.

Currently, at least eleven PDE subfamilies are known, which includes 20 genes and approximately 50 enzyme isoforms. These isoforms are all identified based on primary amino acid sequence as well as regulatory and kinetic properties (Beavo 1995, Conti *et al.*, 1995). PDEs are polypeptides that contain C-terminal catalytic domains of approximately 270 amino acid residues. These C-terminal catalytic domains are indistinguishable in about 20-25% of the isozymes belonging to different subfamilies. The N-terminal regulatory domains are, however, unique in amino acid sequence in each PDE subfamily. This domain contains binding sites for specific regulators of isoenzyme activity such as Ca^{2+}/calmodulin, cGMP and synthetic PDE inhibitors, plus phosphorylation sites that are targeted by protein kinases, as well as membrane-associated domains that anchors PDE isoenzymes to particular subcellular compartments (Osadchii 2007).

In human myocardial tissue, four different PDE isoforms are present viz. PDE1, PDE2, PDE3 and PDE4. Although most PDE cAMP-hydrolyzing activity (69%) is present in the cytosol, activity has also been found in the microsomal fractions (i.e. membrane-bound PDEs attached to sarcolemma, T tubule, mitochondria and sarcoplasmic reticulum) and cardiac myocyte nuclei (Ahluwalia *et al.*, 1984, Lugnier *et al.*, 1999). All four isoforms were found to be present in the cytosolic fraction, with only PDE3 and PDE4 present in the microsomal fraction. Lugnier *et al.* suggested different subcellular localizations for cardiac microsomal PDE3 and PDE4, with PDE3 associated with T tubule and sarcoplasmic reticulum areas, and PDE4 targeted to the sarcolemma (Lugnier *et al.*, 1993).

When the N-terminal serine amino acid residues (usually Ser54) in PDEs are phosphorylated by various protein kinases, the cAMP-hydrolyzing activity of myocardial PDEs is increased by two to three times (Harrison *et al.*, 1986, Beltman *et al.*, 1993, Sette and Conti 1996). The aforementioned negative feedback loop (Section 1.3.5.1) between cAMP-dependent PKA that activates PDE, which again hydrolyzes cAMP, aims to limit subsarcolemmal cAMP accumulation in cardiomyocytes after β-adrenergic stimulation. In a study by Rochais *et al.*, cAMP-gated channels was used as cAMP sensors; the study showed that an increase in PDE3 and PDE4 activity occurs through cAMP-dependent PKA phosphorylation of the PDEs following β-adrenergic stimulation or via direct adenylyl cyclase activation by the drug forskolin (Rochais *et al.*, 2004). The study also showed that the inhibition of PKA results in an increased β-adrenergic-mediated cAMP accumulation in rat cardiomyocytes. This effect is due to the lack of PKA-mediated phosphorylation of PDE3 and PDE4 (Rochais *et al.*, 2004).

1.4.2. Phosphodiesterase 4 (PDE4)

PDE4 is a cAMP-specific, cGMP-independent isoenzyme, with a cAMP K_m value of about 25 times lower than cGMP K_m values in human ventricular tissue (Reeves *et al.*, 1987). Furthermore, Fougier *et al.* showed that, in rat cardiomyocytes, the value for soluble PDE4 cAMP V_{max} was 5 to 10 times higher than cGMP V_{max} (Fougier *et al.*, 1986). Thus, it is clear that PDE4 has a very high cAMP substrate-specificity.

Although 90% of the total cAMP-hydrolyzing activity is provided by the PDE3 and PDE4 isoenzymes (Kostic *et al.*, 1997), it is still not agreed upon which of these myocardial enzymes plays the most important role in cAMP hydrolysis and therefore, in regulation of cardiac contractility. Recent studies, however, showed that PDE4, rather than PDE3, plays a more pivotal role in cardiomyocyte contraction. Specifically, the duration and amplitude of the cAMP transient in heart cells was shown to be more efficiently increased by PDE4 inhibitors than PDE3 inhibitors, both under resting conditions and after β-adrenergic agonist exposure (Mongillo *et al.*, 2004, Nikolaev *et al.*, 2006). Moreover, in a study using rat hearts, it was found that the selective PDE4 inhibitors rolipram and Ro 20-1724 were more effective than IBMX, a non-selective inhibitor of all four PDE isoenzymes, in increasing isoproterenol-induced cAMP accumulation in ventricular myocytes (Katano and Endo, 1992). Furthermore, immunocytochemical studies by Mongillo *et al.* showed that PDE3A and PDE4D have discrete subcellular localizations in rat heart cells. It was found that PDE3A was targeted to internal membranes, whereas PDE4D was generally anchored to sarcomeric structures.

The PDE4 subfamily is made up of four genes viz. *PDE4A*, *PDE4B*, *PDE4*C and *PDE4D*. These genes encode eighteen different isoforms of the PDE4 enzyme. In rat cardiac myocytes, PDE4D and PDE4B provide 90% of the total cAMP-hydrolyzing activity, while PDE4A and PDE4C only provide 10%. The cAMP-hydrolyzing activity of PDE4D is also double that of PDE4B (Kostic *et al.*, 1997).

PDE4 activity is regulated by PKA-mediated phosphorylation. In the case of the splice variant PDE4D3, PKA phosphorylation on Ser54 contributes to a considerable increase of the enzyme's cAMP-hydrolyzing activity. Interestingly, PKA-mediated phosphorylation of Ser13 on PDE4D3 promotes binding of the phosphodiesterase to mAKAP (Section 1.3.5.1), which, as already mentioned, is a scaffolding and adaptor protein that anchors PDE4D to distinct subcellular compartments (Carlisle Michel *et al.*, 2004). Thus, PKA-mediated phosphorylation of two different serine sites in the same phosphodiesterase cause two distinct effects, the first being increased hydrolysis of cAMP, and the second being facilitation of the binding of the PDE to an anchoring protein. This latter effect causes localized PDE activity, and mediates the more rapid attenuation of local intracellular cAMP signals, induced by β-adrenergic stimulation.

PDE4D proved to be the most commonly expressed isoenzyme in rat (Richter *et al.*, 2005) and mice (Lehnart *et al.*, 2005) myocardial tissue. While Okruhlicova *et al.* showed that much of PDE4 is localized to the sarcolemma of cardiac myocytes in rats (Okruhlicova *et al.*, 1996), the PDE4D isoenzyme is localized to the Z-line of the sarcomere (Mongillo *et al.*, 2004). This strongly suggests that PDE4D is involved in the regulation of cardiac muscle contraction.

Splice variants of PDE4D that occurs in the heart was found to be PDE4D3, PDE4D8 and PDE4D9 (Lehnart *et al.*, 2005), with the PDE4D3 splice variant identified as an integral part of the ryanodine receptor macromolecular complex in murine and human hearts. Rat myomegalin, which shares domain structure with myomegalin isoform 4 (Section 1.4), was shown to interact with PDE4D3 (Verde *et al.*, 2001).

Studies have shown that variants that are derived from the *PDE4D* gene may be particulate or soluble, depending on the amino terminus that is present in the protein (Bolger *et al.*, 1997, Jin *et al.*, 1998). Immunofluorescence studies have also shown that PDE4D variants are located in different subcellular compartments. In a study by Jin *et al.*, two PDE variants (PDE4D3 and PDE4D4) with long amino termini were found to be co-localized to a perinuclear region which corresponds to centrosomal inner or Golgi structures, as well as to the membrane cortical region. In contrast, PDE4D2, whose expression is cAMP dependent, is recovered mostly in soluble fraction (Jin *et al.*, 1998). PDE4D has also displayed localization in discrete subcellular structures in macrophages (Pryzwansky *et al.*, 1998). All of these findings suggested that the subcellular localization of PDE4D is delicately controlled, and that this localization may be dynamically regulated during cAMP signaling (Verde *et al.*, 2001).

In animal models of cardiac disease, cardiac contractility is significantly attenuated in response to PDE inhibitors. This may be related to the fact that PDE inhibitors cause a noteworthy decreased cAMP elevation. This results in reduced cAMP-PKA-mediated phosphorylation of the proteins troponin I, phospholamban and cMyBPC in failing hearts (Bartel *et al.*, 1996, Gilbert *et al.*, 1995).

As already mentioned in Section 1.3.4, in cardiac myocytes, scaffolding proteins such as myomegalin (Verde *et al.*, 2001), mAKAP (Dodge-Kafka *et al.*, 2005) and β-arrestins (Baillie *et al.*, 2003) facilitate targeting of PDEs to specific subcellular locations, and hence, compartmentalized cAMP degradation. By targeting PDEs to particular subcellular locations and structures, the state of cAMP-dependent activation of local PKA pools can be controlled. Modification of the extent of PKA-mediated phosphorylation of various substrate proteins can therefore take place. Myomegalin or phosphodiesterase 4D-interacting protein is a scaffolding protein highly expressed in heart and skeletal cells. When cardiac cells were double stained with myomegalin-specific and PDE4D-specific antibodies, a co-localization was revealed between the two proteins in the sarcoplasmic reticulum region as well as the Z region of the sarcomere (Verde *et al.*, 2001). Furthermore, myomegalin was identified as a ligand of the un- and trisphosphorylated mimic of cMyBPC, a C-zone sarcomeric protein, in the study that led up to the present study, and will now be discussed further.

1.4.3. Myomegalin (aka phosphodiesterase 4D interacting protein/PDE4DIP)

Only recently has it been realized that scaffold proteins play a necessary and often indispensable role in signal transduction. Scaffold proteins normally have no enzymatic activity, and function solely by bringing together different signaling molecules. Several PDE isoforms have been recovered in the particulate bound fraction of homogenates, and some have been immunolocalized to various cellular compartments (Conti *et al.*, 1995, Houslay and Adams, 2003), suggesting interactions with scaffolding proteins.

Verde *et al.* set off to understand the mechanism of PDE4 subcellular targeting (see previous section) by identifying proteins that interact with PDE4D variants and anchor it to various organelles. They identified a novel protein, called myomegalin, that interacts with PDE4D, thereby targeting PDE4D to particulate structures (Verde *et al.* in 2001).

The official name of this protein in *Homo sapiens* is phosphodiesterase 4D interacting protein (PDE4DIP), with aliases myomegalin (MMGL) and cardiomyopathy-associated protein 2 (CMYA2) (http://www.ncbi.nlm.nih.gov/gene/9659). The protein is encoded by the gene *PDE4DIP* (GeneID 9659) and results in five protein isoforms due to alternative splicing, designated MMGL isoforms 1- 5. As mentioned in Section 1.4, a previous study identified MMGL isoform 4 as an interactor of un- and trisphosphorylated cMyBPC (A. Ramburan, PhD thesis). This isoform encodes a protein of 173 amino acids and is the smallest MMGL isoform in humans, and shares a conserved microtubule-associated domain with isoforms 1, 2 and 3, but not 5 (http://www.ncbi.nlm.nih.gov/). Figure 1.12 shows the exonic structure and conserved domains of the five different MMGL isoforms in relation to each other.

MMGL is expressed predominantly in heart and skeletal muscle cells; however, human MMGL has not been extensively studied; most studies to date were done on rat myomegalin, the first ortholog of this protein to be found.

Verde *et al.* found that there are at least four different transcripts of rat myomegalin; it was suggested, after RT-PCR analyses, that the presence of the four different transcripts is the result of alternative splicing of the mRNA derived from the rat *Pde4dip* gene (Verde *et al.*, 2001). Abundant transcripts of 7.5 - 8 kb were found in the heart and skeletal muscle which contained the entire open reading frame (ORF) of rat myomegalin. These transcripts were also detected in small amounts in the lung, liver and brain. Two shorter transcripts were also detected: a 5.9 kb transcript in the heart, and a 2.5 kb transcript in the testis. Another transcript of about 4.3 kb was detected in skeletal muscle only.

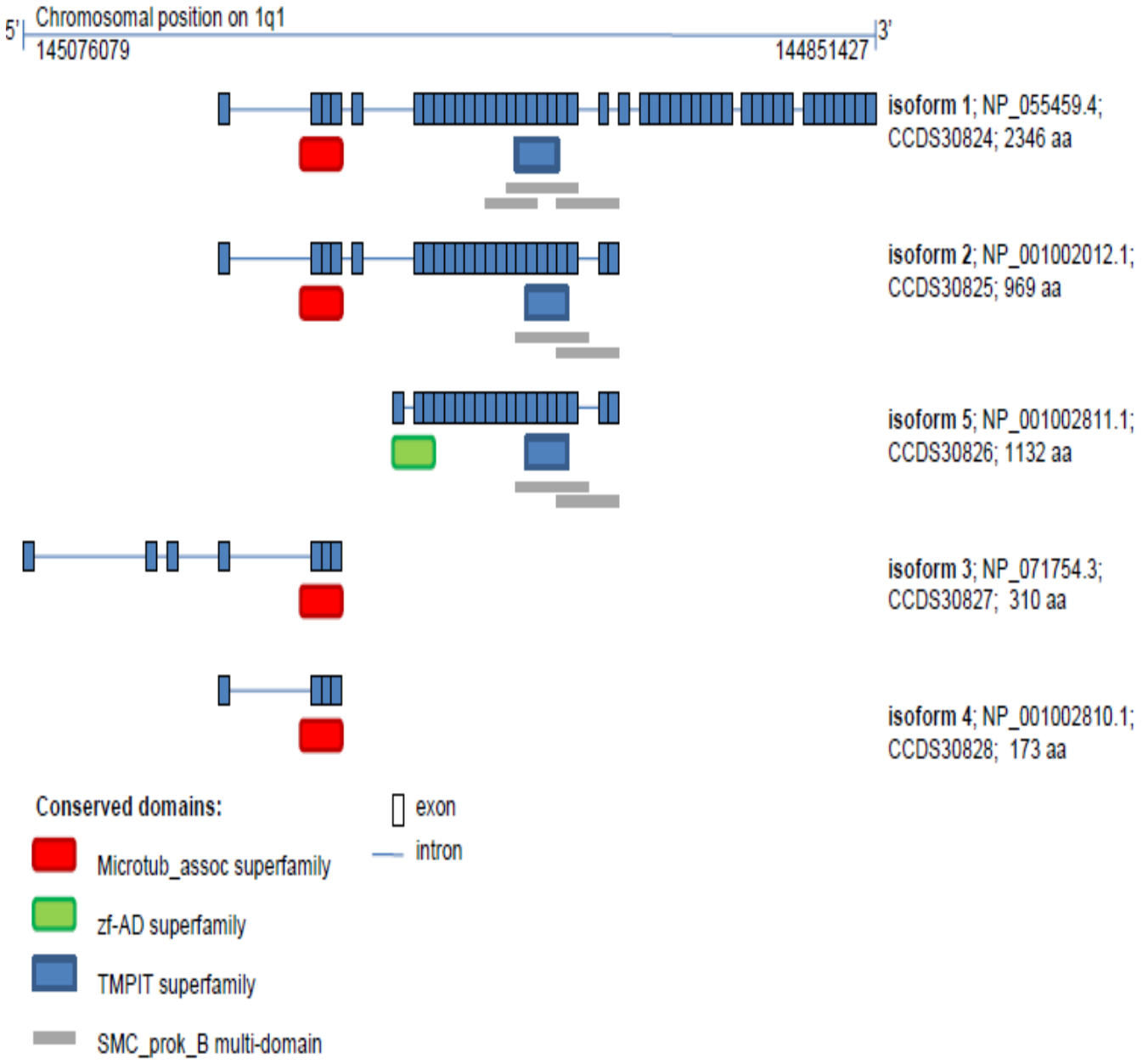

Figure 1.12. MMGL isoform and conserved domain structure in *Homo sapiens*. Exons not drawn to scale in relation to nucleotide size. Image produced from http://www.ensembl.org and http://www.ncbi.nlm.nih.gov

Full length rat myomegalin consists of 2324 amino acids with a calculated molecular mass of 262 kDa, whereas in humans, the biggest isoform, viz. MMGL isoform 1 consists out of 2346 amino acids. This isoform shares 77% homology with rat myomegalin, including conservation of domains (Verde *et al.*, 2001, http://www.ncbi.nlm.nih.gov/BLAST). Using computer-assisted predictions, the secondary structure was found to consist mainly of coiled-coil and α-helical domains, as well as a 20% identity to MHC, although no ATP-binding domain sequences similar to MHC could be identified. Full-length rat myomegalin, which is very similar to human MMGL isoform 1, contains a putative leucine zipper at the amino terminus between residues 8

and 31, as well as domains that are shared with microtubule-associated proteins, and an uncharged proline rich region at the COOH-terminal region. Rat myomegalin also contains a helix-loop-helix domain between amino acids 1079 and 1094. This domain is homologous to regions found in a human cytoplasmic linker protein called CLIP-170, as well as rat dynein associated polypeptide (DAP)-150. CLIP-170 functions by binding microtubules and is involved in the processes of endocytosis and organelle transport, whereas the function of DAP-150 is still widely unknown (Pierre *et al.*, 1992, Holzbaur *et al.*, 1991).

It was found that rat myomegalin binds tightly to particulate structures, and immunocytochemistry was used to further establish the localization of the protein in transfected COS-7 cells. It was determined that rat myomegalin is localized to an inner Golgi/centrosome region, as had also been shown for PDE4D (Jin *et al.*, 1998). Furthermore, in skeletal muscle and heart cells, these two proteins were found to co-localize in the same myofiber region, viz. either to the Z band region between sarcomeres, or the sarcoplasmic reticulum. Interestingly, numerous other cAMP-signal transduction proteins also localized to these regions (i.e. Z region and sarcoplasmic reticulum) speculated for rat myomegalin: these proteins include L channels, adenylyl cyclase and the regulatory subunit of PKA (Gao *et al.*, 1997, Yang *et al.*, 1998). Verde *et al.* therefore concluded that it is possible for myomegalin, in rats and humans, to function by anchoring PDE4D to a specific site where signaling cascades takes place in muscle cells. cAMP-regulated phosphorylations, as well as the control of PKA-activation state may be mediated through PDE4D localization via myomegalin (Verde *et al.*, 2001).

PDE4D deletion mutagenesis studies further showed that rat myomegalin and PDE4D interact via a domain that corresponds to the amino terminus of an upstream conserved region 2 (UCR2) of PDE4D, however the region of myomegalin involved in this interaction was not defined. This UCR2 domain of PDE4 consists of a region of α-helical structure with charges being amphipathically distributed. Myomegalin's C-terminus also contains α-helical domains, and this may mediate its interaction with PDEs. However, the UCR2 domain is conserved in all forms of PDE4, raising the possibility that other PDE4s could also interact with myomegalin. However, co-immunoprecipitation studies showed that not all PDE variants interact with myomegalin: although PDE4D1 and PDE4D3 interact with myomegalin, PDE4D2 does not (Verde *et al.*, 2001).

It is still unknown whether interaction with myomegalin alters the PDE's catalytic activity. The N-terminal domain of PDE4D is involved in intramolecular interactions and functions as an autoinhibitory domain which regulates the catalytic activity of PDE4D, and it has been reported that phosphorylation alters the interaction of this PDE4D domain with its N-terminus, at least in PDE4D3 (Lim *et al.*, 1999). It is therefore possible that phosphorylation, which involves the N-terminus of PDE4D may affect its ability to bind to myomegalin via this domain. Furthermore, studies have indicated that PDE4D3 may translocate when activated by the mitogen

activated protein kinase pathway (Liu *et al.*, 1999). It is therefore possible that the PDE4D-myomegalin interaction may be a dynamic process, and that, during signaling, translocation may occur (Verde *et al.*, 2001).

Both rat and human myomegalin have an extensive coiled-coil composition, and this makes it very likely that it either oligomerizes with itself, or binds to other proteins. Also consistent with this conclusion is the fact that it contains a leucine zipper domain, which is known to facilitate protein-protein interactions. Verde *et al.* therefore concluded that myomegalin may interact with other proteins as well, in addition to PDE4D. MMGL isoform 4, of particular interest to this study, also contains a leucine zipper domain and has a coiled-coil composition, making the possibility of this isoform interacting with other proteins very likely.

In an independent study by Soejima *et al.*, the BodyMap database, a human and mouse gene expression database, was used to establish that the gene encoding myomegalin in humans consists of 8 exons within a genomic sequence of over 70 kB. They named this gene myomegalin-like (*MMGL*), and found that it resulted in four alternatively spliced transcripts (Soejima *et al.*, 2001). The gene was strongly expressed in skeletal muscle and the heart, and with faint expression in the brain and placenta. *MMGL* was mapped to chromosome position 1q1 by radiation hybrid mapping as well as FISH with BAC clones, which placed in within dilated cardiomyopathy (DCM) candidate loci (Soejima *et al.*, 2001).The study showed that the subcellular localization for *MMGL*-expressed protein is in the cytoplasm and nucleus. A high level of homology (~80%) was showed between *MMGL* and rat myomegalin proteins (Soejima *et al.*, 2001). Interestingly, MMGL isoform 4 consists of 173 aa and is identical to the first 173 aa of transcript variant 1 described by Soejima et al. Because rat myomegalin is predicted to be a cyclic nucleotide phosphodiesterase interacting protein (Verde *et al.*, 2001), it was suggested that in humans, *MMGL* may play a role in PDE signal transduction, as well as cardiac development (Soejima *et al.*, 2001).

It is now recognized that human MMGL/PDE4DIP is encoded by *PDE4DIP*, located on chromosome 1q1, and results in five different isoforms due to alternative spicing, as shown in Figure 1.12.

1.5. STUDY HYPOTHESIS AND AIM

As described in Section 1.4, MMGL isoform 4 was identified as a ligand of the un- and trisphosphorylated mimic of cMyBPC, a protein which is one of the two most commonly implicated in HCM when its corresponding gene is mutated. As can be concluded from the above literature study on MMGL, not much light has been shed on MMGL's function in the cell. Because of MMGL's evident interaction with cMyBPC, a regulator of sarcomeric contractility, it was important to elucidate the function of this rather unfamiliar protein.

The interaction between cMyBPC, a PKA target, and a phosphodiesterase-interacting protein is particularly intriguing in light of the fact that in some cases an AKAP anchors both PKA and PDE4D (Dodge-Kafka *et al.*, 2005). The mechanism of PKA anchoring to cMyBPC has not been elucidated, and although it is known that MMGL anchors PDE4D (Verde *et al.*, 2001), it was also not known whether MMGL acts as an AKAP, nor whether it binds to other PKA-targets. Moreover, it remained unknown which AKAPs are responsible for the phosphorylation of sarcomeric proteins (Dodge-Kafka *et al.*, 2006). Furthermore, it has also been shown that co-compartmentalization of both PKA and PDE4D is crucial for maintaining contractility in muscle, because the disruption of AKAP-mediated PKA anchoring had detrimental effects on cardiomyocyte contractility following adrenergic stimulation (Fink *et al.*, 2001).

The findings related above led us to hypothesize that MMGL is an AKAP, and that it might also target PKA to other sarcomeric proteins. Furthermore, because of the role of cMyBPC phosphorylation in the regulation of cardiac contractility, and because of the effect of disruption of AKAP-mediated PKA on contractility, we speculated that MMGL may be involved in regulating cardiac contractility, and as such may influence cardiac hypertrophy development.

We therefore proposed to determine whether MMGL isoform 4 acts as an anchoring protein for the regulatory subunits of PKA, thereby establishing whether MMGL acts as an AKAP. Secondly, we proposed to discover other ligands of MMGL by means of Y2H library screening, and to establish whether these are also known PKA-targets. Additionaly, we proposed to investigate the effect of adrenergic stimulation of the binding of MMGL to particular sarcomeric proteins, including cMyBPC and other sarcomeric proteins, should they be identified. We also aimed to investigate the effect of siRNA-mediated knockdown of MMGL on expression of the different phosphorylation isoforms of cMyBPC in the context of adrenergic stimulation. Lastly, because of the crucial role of dynamic phosphorylation of cMyBPC in normal cardiac contractility, and the fact that mutations in the corresponding gene leads to HCM, we aimed to assess whether variants in the genes encoding MMGL and both of the PKA regulatory subunits may act as genetic modifiers of hypertrophy.

1.6. RESULTS FROM THE PRESENT STUDY

1.6.1. MMGL binds to PKA regulatory subunits

As the primary characteristic of an AKAP is the ability to bind at least PKA regulatory subunit, we investigated the possibility that MMGL functions as an AKAP by using Y2H direct protein-protein interaction assays to determine binding between MMGL and the two cardiac-expressed regulatory subunits of PKA. Both regulatory subunits (PRKAR1A and PRKAR2A) interacted with MMGL, as assessed by growth and light colour of the colonies on quadruple dropout nutritional selection medium, compared to relevant controls. Using *in vivo* colocalization with 3D-fluorescence microscopy, we also demonstrated that MMGL isoform 4 occurs in the

same 3D-subcellular region as the two PKA regulatory isoforms in H9C2 cardiomyocytes. To further verify physical interaction between MMGL and these PKA isoforms in a cellular context and in the absence of GAL4 domains, we performed pull-down assays in diffentiated H9C2 cardiomyocytes. As commercial antibodies against MMGL/PDE4DIP did not detect isoform 4, which is the smallest isoform of this protein, we used an antibody directed against the fluorescent protein dsRed to detect a dsRed-fusion of MMGL isoform 4. In this way, endogenous PRKAR1A and PRKAR2A were shown to immunoprecipitate dsRed-MMGL, and *vice versa*.

1.6.2. MMGL binds to additional PKA targets

We also further investigated the function of MMGL isoform 4 by using it as Y2H bait to screen a cardiac cDNA library in order to identify its additional binding partners. Thirteen in-frame putative MMGL-interactors that activated all three nutritional reporter genes in the presence of the MMGL bait, but not in the presence of heterologous baits were, identified. Proteins with defined vesicular localizations were not considered of primary interest for follow-up in this study; these included the mitochondrial protein COX5A, the proteosome 26S subunit and sorting nexin 3. Of the remaining ten putative MMGL interactors, six encoded the sarcomeric protein, cardiac troponin I (cTNI). Further support for the validity of these interactions was provided by finding that MMGL occurs in the same 3D-subcellular region as all five of the putative interactors identified in the Y2H library screen, viz. CARP, COMMD4, ENO1, ENO3 and cTNI, in differentiated cardiomyocytes.

Moreover, in pull-down assays, exogenous fluorescently-tagged MMGL and endogenous ENO1, ENO3, CARP, and cTNI reciprocally co-precipitated each other. As COMMD4 had a similar mobility to antibody light chains, which interfered with detection of these proteins in Western blots, a GFP-tagged fusion of this protein was expressed in H9C2 cells for pull-down assays. In these assays, exogenous GFP-COMMD4 immunoprecipiated exogenous dsRed-MMGL, and *vice versa*.

1.6.3. Colocalization between MMGL and sarcomeric proteins cTNI and cMyBPC increases upon adrenergic stress

cTNI is a known PKA target (Patel *et al.*, 2001), while the remaining four putative interactors were shown to be likely PKA targets using Phosphomotif Finder (www.hprd.org/PhosphoMotif_finder); we therefore investigated the effect of isoproterenol stimulation of the H9C2 cells on colocalization, using the most frequent, and clearly sarcomeric, interactor, viz. cTNI, as example. Treating H9C2 cells transfected with dsRed-MMGL/GFP-cTNI with isoproterenol resulted in an increase in 3D colocalization between these two proteins, compared to non-treated cells. Similar results were obtained with GFP-cMyBPC and dsRed-MMGL colocalization, implicating that PKA is dynamically recruited by MMGL to distinct sarcomeric locations to mediate cardiac stress responses, leading to increased cardiac contraction.

1.6.4. Effect of MMGL knockdown

In order to evaluate the role of MMGL in cMyBPC phosphorylation, we assessed the expression of the different phosphorylation isoforms of cMyBPC, in the presence of adrenergic stimulation, in the context of siRNA-mediated MMGL knockdown.

Using Western blots of 2-dimensional isoelectric focusing (IEF) gels, we found that similar amounts of the mono- and diphosphorylated forms of cMyBPC are expressed in untreated H9C2 cells, while lesser amounts of the un- and trisphosphorylated forms, relative to the other isoforms, were present. When these cells were exposed to increased $CaCl_2$ and isoproterenol, to activate CaMK and PKA such that maximum phosphorylation of the MyBPC-motif is likely (McClellan *et al.*, 2001), the relative amount of the trisphosphorylated form increased markedly, while the relative amount of unphosphorylated cMyBPC decreased. However, similar adrenergic stimulation in the presence of MMGL knockdown resulted in markedly reduced expression of all isoforms.

1.7. SNP MODIFIER GENOTYPING STUDY

It is observed that in many single gene disorders, particularly autosomal dominant disorders, the phenotype is affected by genetic factors other than the causal mutations (Marian 2002). This "genetic background" is often referred to as modifier genes. Modifier genes differ between individuals due to polymorphisms in the DNA. The modifier genes are neither necessary nor sufficient to cause the disease, but will affect the severity of the final phenotype (Alcalai *et al*., 2008). It can therefore be said that the final phenotype will be the result of interactions between the causal mutations, the modifier genes and the environment. (Marian 2002).

In HCM, the primary mutation genotype is clearly not the only reason for the variability of the hypertrophic phenotype. Through genotype-phenotype correlations, it is commonly seen that in any given family, individuals who carry the same HCM mutations have different amounts of hypertrophy, with some patients severely affected (i.e. showed marked ventricular hypertrophy) whereas others are more mildly affected, and yet others showed normal gross heart structure (Fananapazir and Epstein, 1994, Epstein *et al*., 1992, Solomon *et al*., 1993, Marian *et al.*, 1995). These differences in hypertrophy are not consistently explained by differences in other factors which can also influence hypertrophy, such as age, sex, blood pressure or sporting activity. In HCM it is now recognized that although the hypertrophic phenotype is determined to some extent by the causal mutations, it is also markedly influenced by the effect of other modifier genes and the environment (Marian 2002). HCM, previously considered as a classic example of a "monogenic" cardiac disorder, is therefore, in a sense, not purely monogenic, because its phenotype is affected by the expression of multiple genes (Marian 2001).

Concluding from our results that MMGL acts as the AKAP anchoring PKA to the MyBPC motif, which leads to phosphorylation of cMyBPC and hence, increased cardiac contractility, we hypothesized that MMGL and the two regulatory PKA subunits may be involved in the regulation of cardiac contractility, and that variation in the genes which encode these proteins, viz. *PDE4DIP*, *PRKAR1A* and *PRKAR2A*, may influence hypertrophy development together with the causal mutations. We therefore assessed SNP variants in the genes encoding for MMGL and the two cardiac-expressed regulatory subunits of PKA as modifiers of hypertrophy, because of their direct involvement in cMyBPC phosphorylation, and, ultimately, cardiac contractility.

PDE4DIP, *PRKAR1A* and *PRKAR2A* were prioritised as candidate hypertrophy modifier genes, based on their role in altered sarcomeric contractility. In these three genes, intragenic SNP polymorphisms spread throughout the genes were selected for use in association studies in order to capture the spectrum of genetic variation within these candidate genes. Informative SNPs deposited in public domain databases (NCBI, Genecards and HAPMAP) were selected and prioritised according to high heterozygosity values in the CEU and YRI populations, validation status and potential functional significance of the variant. Validated ABI TaqMan® genotyping assays were subsequently used to perform high throughput genotyping in three cohorts of comprehensively phenotyped South African HCM families in which one of three founder mutations segregate.

Quantitative measures of the hypertrophic phenotype, viz left ventricular mass, maximal interventricular septum thickness and maximal posterior wall thickness were then analyzed with a family-based statistical method using quantitative transmission disequilibrium testing (QTDT) to assess association of these gene variants with hypertrophy development.

It was found that one SNP in *PDE4DIP* (rs1664005), which was in LD with other SNPs in the study population, showed significant association with most of the hypertrophy traits that were analysed. Two SNPs in *PRKAR1A* (rs11651687 and rs3785906) also showed association with some hypertrophy traits. This study therefore suggests that *PDE4DIP* and *PRKAR1A* may modulate the extent of cardiac hypertrophy, and therefore act as modifier genes because of their role in regulation of cardiac contractility.

CHAPTER TWO: MATERIALS AND METHODS

INDEX **PAGE**

CHAPTER 2: MATERIALS AND METHODS
PART ONE: PROTEIN INTERACTION STUDY

2.1. DNA EXTRACTION

2.1.1. Bacterial plasmid purification using Fermentas Plasmid Preparation kit

Escherichia coli (*E. coli*) colonies containing plasmids of interest were picked from the appropriate selection plates, and, together with the correct antibiotic, inoculated in 10ml of Luria-Bertani (LB) media (Appendix I) in a 50ml polypropylene tube. The culture was subsequently incubated at 37°C shaking at 250rpm overnight in a YIH DER model LM-530 shaking incubator (SCILAB Instrument Co. Ltd., Taipei, Taiwan).

Following the incubation period, the culture was centrifuged for 10min at 3000rpm in a Beckman model TJ-6 centrifuge (Beckman Coulter, Scotland, U.K.), after which the supernatant was discarded. The plasmid DNA was subsequently extracted using the Fermentas Plasmid Preparation kit (Fermentas Life Sciences, USA) as per manufacturer's instructions. Afterwards, 3µl of this purified plasmid was resolved on a 1% SB agarose gel (Appendix I) for verification (Section 2.3.1).

2.1.2. Bacterial plasmid purification using Wizard® Purefection Midi Plasmid DNA purification kit

In order to isolate plasmid DNA free of endotoxins, which was subsequently used to transfect H9C2 cells for *in vivo* co-localization (Section 2.17) and *in vivo* co-immunoprecipitation assays (Section 2.15), the Wizard® Purefection Midi Plasmid DNA purification kit (Wizard® Purefection Midi Plasmid DNA purification kit, Promega Corp. Madison Wisconsin, USA) was used.

Using 50ml polypropylene tubes, 20µl of a bacterial glycerol stock, of the appropriate vector, was inoculated into 10ml LB media (containing the appropriate antibiotic) and incubated at 37°C shaking at 250rpm overnight in a YIH DER model LM-530 shaking incubator. Following this incubation period, the cultures were centrifuged for 10min at 3000rpm in a Beckman model TJ-6 centrifuge (Beckman Coulter, Scotland, U.K.), after which the supernatant was discarded and the plasmid DNA extracted using the Wizard® kit, according to the manufacturer's instructions. The DNA was resuspended in 50µl sterile water after extraction and the concentration visually determined by resolving an aliquot of the DNA on a 1% SB agarose gel (Appendix I) (Section 2.3.1).

2.1.3. Yeast plasmid purification

Yeast cells containing the plasmid of interest were inoculated in 1ml synthetic dropout (SD) medium containing the correct dropout supplement (BD Bioscience, Clontech, Paulo Alto, CA, U.S.A.). The cells were then incubated overnight at 30°C in a shaking incubator, shaking at 250rpm. After this inoculation period, 4ml YPDA

media (a blend of yeast extract, peptone and dextrose supplemented with adenine) (Appendix I) was added to the cell culture. An additional incubation period of 4h at 30°C, shaking at 250rpm, then followed. Thereafter, the cell culture was centrifuged at 3000rpm for 5min in a Beckman model TJ-6 centrifuge (Beckman Coulter, Scotland, U.K.) after which the supernatant was discarded by decanting. The pellet was then resuspended in the remaining supernatant, and transferred to a 2ml Eppendorf microfuge tube. To the pellet was then added 200µl yeast lysis buffer (Appendix I), 200µl PCI and 0.3µg sterile 450-600µm glass beads. The yeast cells were milled by vortexing this mixture for 2.5min using a Snijders model 34524 press-to-mix vortex (Snijders Scientific, Tilburg, Holland). Centrifugation followed at 14000rpm for 10min at room temperature in an Eppendorf model 5417C centrifuge (Eppendorf AG, Hamburg, Germany) for phase separation. The aqueous phase was transferred to a clean 1.5ml microfuge tube. Purification followed by taking 100µl of the aqueous phase and cleaning it using the GFX™ PCR DNA Purification kit (Section 2.1.4). Following purification, the DNA was eluted in 30µl sterile water. The eluted product was afterward used to transform DH5α *E. coli* cells (Section 2.12.1).

2.1.4. DNA purification using the Wizard® Purefection Mini Plasmid DNA purification kit

The Wizard® Purefection Mini Plasmid DNA purification kit (Wizard® Purefection Mini Plasmid DNA purification kit, Promega Corp. Madison Wisconsin, USA) was used to purify yeast plasmid preparations (Section 2.1.3) as well as PCR-amplified DNA products (Section 2.2) according to manufacturer's instructions. The purified products were subsequently used for nucleotide sequencing (Section 2.4) and cloning reactions (Section 2.8).

2.2. POLYMERASE CHAIN REACTION

2.2.1. Oligonucleotide primer design and synthesis

Oligonucleotide primers were designed using sequence data available from either the Ensembl database (http://www.ensembl.org) or the Genbank database (http://www.ncbi.nlm.nih.gov/Entrez). Each set of primer sequences were analyzed for self-complimentarity and primer-primer complimentarity, as well as compatibility of melting temperatures before synthesis, using DNAMAN™ version 4 software (Lynnion Biosoft Corp©). Oligonucleotide primers were synthesized according to standard phosphoramidite methodology at the Department of Molecular and Cell Biology, University of Cape Town (UCT), Cape Town, South Africa.

2.2.1.1. Primers for generation of inserts for yeast-two-hybrid cloning

A primer set was designed to amplify the *PDE4DIP* cDNA sequence for cloning into the appropriate bait vector, containing the appropriate restriction enzyme sites as well as a universal "seat" sequence, to facilitate restriction digestion of end fragments. Primers were also designed to amplify the *PRKAR1A* and *PRKAR2A* cDNA sequences for cloning into the appropriate prey vector, containing restriction enzyme sites as well as universal seat sequences. The sequences of the primers used for this part of the study are shown in Table 2.1.

Table 2.1. Primer sequences used for generation of inserts for Y2H cloning

Gene	Primer name	Primer sequence	T_a (°C)
PDE4DIP	MMGL F	ATCGTATCG CATATG ATGTCTAATGGATATCGCAC	51
	MMGL R	ATCGTATCG GAATTC CTACTTGTCCCTCTGGGC	54
PRKAR1A	R1A F	ATCGTATCG GGATCC ATGGAGTCTGGCAGTACC	52
	R1A R	ATCGTATCG CTCGAG TCAGACAGACAGTGACAC	45
PRKAR2A	R2A F	ATCGTATCG CCATGG ATGAGCCACATCCAGATC	52
	R2A R	ATCGTATCG GGATCC TGTGGCACACCTACTGCCC	62

Abbreviations: *PDE4DIP*, phoshodiesterase 4D interacting protein; *PRKAR1A*, protein kinase regulatory type I alpha; *PRKAR2A*, protein kinase regulatory type II alpha; T_a, annealing temperature used in PCR; °C, degrees Celcius

Sequences in black font represents the sequence of the primer that anneals to the DNA in the PCR reaction. The sequence in coloured fonts represents sites for cloning: Blue, universal enzyme seat; red, *Nde*I restriction site; green, *Eco*RI restriction site; orange, *Bam*HI restriction site; pink, *Xho*I restriction site; brown, *Nco*I restriction site.

2.2.1.2. Primers for yeast-two-hybrid insert screening

In order to amplify inserts cloned into Y2H cloning vectors, primers were designed to match vector-specific sequences flanking the multiple cloning site (MCS) of pGBKT7 (BD Bioscience, Clontech, Palo Alto, CA, U.S.A.) and pACT2 (BD Bioscience, Clontech, Palo Alto, CA, U.S.A.) Y2H cloning vectors. The specific vector sequences used in the design of these primers were obtained from the Clontech™ Matchmaker™ vector handbook (www.clontech.com). The sequences of these primers are shown in Table 2.2.

Table 2.2. Primer sequences and annealing temperatures used for the amplification of inserts from cloning vectors

Primer name	Primer sequence	T_a (°C)
pGBKT7 F	TCATCGGAAGAGAGTAG	45
pGBKT7 R	TCACTTTAAAATTTGTATACA	45
pACT2 F	CTATTCGATGATGAAGATACCCCACCAAACC	57
pACT2 R	GTGAACTTGCGGGGTTTTTCAGTATCTACGA	57

Abbreviations: °C, degrees Celcius; T_a, annealing temperature

2.2.1.3. Primers for generation of inserts for *in vivo* 3D co-localization cloning

Primer sets were designed to amplify the *ANKRD1*, *COMMD4*, *ENO1*, *ENO3*, *PRKAR1A* and *PRKAR2A* cDNA sequences, respectively, for cloning into the $pGFP^2$-C1 fluorescent vector (BD Bioscience, Clontech, Palo Alto, CA, U.S.A.). A primer set was also designed to amplify the *PDE4DIP* cDNA sequence for cloning into the pDs-

Red-C1 fluorescent cloning vector (BD Bioscience, Clontech, Palo Alto, CA, U.S.A.). All primers were designed to contain appropriate restriction enzyme sites, as well as universal seat sequences. The sequences of the primers used for this part of the study are shown in Table 2.3. In a previous study done in our laboratory, the full-length cDNA sequence of *TNNI3* and *MYBPC3* was cloned into the pGFP^2-C1 vector, and these constructs were used again for the present study.

2.2.2. PCR conditions

The following PCR conditions were used to amplify the *PDE4DIP* cDNA sequence from genomic DNA, as well as to amplify the *PRKAR1A* and *PRKAR2A* cDNA sequences. The resulting MMGL fragment was subsequently cloned into the pGBKT7 Y2H cloning vector as well as the pDs-Red-C1 fluorescent vector, and the PRKA fragments were cloned into the pACT2 Y2H cloning vector.

For the amplification of the above-mentioned cDNA sequences, 100ng of normal human genomic DNA was used as a template in the reaction performed in a 50µl volume containing 150ng of each primer (Table 2.1 and 2.3), 1.5µl of an equimolar dNTP (2.5mM of each, dATP, dCTP, dGTP, dTTP) solution, 5µl Taq DNA polymerase 10X reaction buffer (Bioline UK Ltd, London, UK), 1.5µl of a 1.5mM $MgCl_2$ solution (Bioline UK Ltd, London, UK), 2.5µl DMSO, 1µl Taq DNA polymerase (Bioline UK Ltd, London, UK) and ddH_2O to a final volume of 50µl. Amplification was performed in a GeneAmp® PCR system 9700 thermal cycler (Perkin-Elmer, Applied Biosystems Inc, Foster City CA, U.S.A.) and the conditions are summarized in Table 2.4.

2.2.3. High fidelity PCR

High fidelity PCR was used to amplify the *ANKRD1, COMMD4, ENO1, ENO3, PRKAR1A* and *PRKAR2A* cDNA sequences from genomic DNA. The resulting fragments were cloned into the pGFP-C1 fluorescent cloning vector.

For amplification, 100ng of normal human genomic DNA was used as a template in the reaction performed in a 50µl volume containing, 150ng of each primer (Table 2.3), 1.5µl of an equimolar dNTP (2.5mM of each, dATP, dCTP, dGTP, dTTP) solution supplied by the manufacturer (TaKaRa Shuzo Co.Ltd, Shiga, Japan), 5µl Ex Taq™ Mg^{2+}-containing 10X reaction buffer supplied by the manufacturer (TaKaRa Shuzo Co.Ltd, Shiga, Japan), 2U Ex Taq™ (TaKaRa Shuzo Co.Ltd, Shiga, Japan), and ddH_2O to a final volume of 50µl. Amplification was performed in a GeneAmp® PCR system 9700 thermal cycler (Perkin-Elmer, Applied Biosystems Inc, Foster City CA, U.S.A.) and the conditions summarized in Table 2.5.

Table 2.3. Primer sequences used for generation of inserts for *in vivo* 3D co-localization cloning

Gene	Primer name	Primer sequence	T_a (°C)
ANKRD1	CARP F	ATCGTATCG CTCGAG ATGATGGTACTGAAAGTAG AGGAACTGG	62
	CARP R	ATCGTATCG GGATCC TCAGAATGTAGCTATGCGAG AGGTC	62
COMMD4	COMMD4 F	ATCGTATCG CTCGAG ATGAGGTTCCGGTTCTGTGG	61
	COMMD4 R	ATCGTATCG GGATCC TCAGCCCAGG GAGCTCATCAGGG	74
ENO1	ENO1 F	ATCGTATCGGATATCATGTCTATTCTCAAGATCCATGCC	48
	ENO1 R	ATCGTATCGCCGCGGTTGCTTGGCCAAGGGGTTTCTG	48
ENO3	ENO3 F	ATCGTATCG CTCGAG ATGGCCATGCAGAAAATCTT TGCCC	83
	ENO3 R	ATCGTATCG GGATCC TCACTTGGCCTTCGGGTTAC GG	76
PDE4DIP	dsRed MMGL F	ATCGTATCG GTCGAC ATGTCTAATGGATATCGCAC	51
	dsRed MMGL R	ATCGTATCG GGATCC CTACTTGTCCCTCTGGGC	54
PRKAR1A	R1A F	ATCGTATCG CTCGAG ATGGAGTCTGGCAGTACC	62
	R1A R	ATCGTATCG GGATCC TCAGACAGACAGTGACAG	60
PRKAR2A	R2A F	ATCGTATCG CTCGAG ATGAGCCACATCCAGATCCCG CCG	90
	R2A R	ATCGTATCG GGATCC TGTGGCACACCTA CTGCCCGAG	87

Abbreviations: *ANKRD1*, ankyrin repeat domain 1; *COMMD4*, COMM domain containing 4; *ENO1*, Enolase 1 (alpha) *ENO3*, Enolase 3 (beta, muscle), *PDE4DIP*, phosphodiesterase 4D interacting protein; *PRKAR1A*, protein kinase regulatory type I alpha; *PRKAR2A*, protein kinase regulatory type II alpha; T_a, annealing temperature; °C, degrees Celcius. Sequences in black font represents the sequence of the primer that anneals to the DNA in the PCR reaction. The sequence in coloured fonts represents sites for cloning: Blue, universal enzyme seat; red, *Xho*I restriction site; green, *Bam*HI restriction site; brown, *Sal*I restriction site yellow, *Eco*RV restriction site; orange, *Sac*II restriction site; purple, *Bgl*II restriction site

Table 2.4. PCR conditions used to amplify the cDNA sequence of *PDE4DIP*, *PRKAR1A* and *PRKAR2A* from genomic DNA

Primer set	[$MgCl_2$] mM	T_D °C	Time sec	T_a °C	Time sec	T_E °C	Time Sec
MMGL F/R	1.5	94	30	52	30	72	30
dsRed-MMGL F/R	1.5	94	30	52	30	72	30
PRKAR1A F/R	1.5	94	30	46	30	72	120
PRKAR2A F/R	1.5	94	30	47	30	72	120

Abbreviations: °C, degrees Celcius; mM, millimolar; sec, seconds; T_a, annealing temperature; T_D, denaturing temperature; T_E, extension temperatute

2.2.4. Bacterial colony PCR

Bacterial colony PCRs were performed in order to rapidly identify bacterial colonies containing the appropriate recombinant plasmid with desired insert. The primers used for generation of inserts for Y2H cloning and vector cloning (see Tables 2.1 and 2.3) was then used in conjunction with PCR conditions identical as described in Section 2.2.3. An amount of an individual *E. coli* colony was picked from an agar plate, containing the correct selective antibiotic, and used as DNA template, instead of using 100ng of human genomic DNA.

Amplification was performed in a GeneAmp® PCR system 9700 thermal cycler (Perkin-Elmer, Applied Biosystems Inc, Foster City CA, U.S.A.). The cycling parameters consisted of a single denaturing cycle of 94°C for 5min followed by 30 cycles of 94°C for 30sec, T_a for 30sec and 72°C for 1min. The amplified products were subsequently electrophoresed on a 1% agarose gel for verification.

2.3. GEL ELECTROPHORESIS

2.3.1. Agarose gel electrophoresis

In the study, agarose gel electrophoresis was used to visualize PCR-amplified fragments or plasmid preparations for verification. In order to verify that the PCR amplifications (or plasmid preparations) were successful, the products were electrophoresed as follows: 6µl PCR product or plasmid preparation was loaded together with 1µl bromophenol blue (Appendix I) loading dye into separate wells of a 1-2% (depending on the size of the product) agarose gel. The agarose gel contained 1µg/ml ethidium bromide and 1X SB buffer (Appendix I). A 100bp size marker (Promega, Madison WI, U.S.A.) was co-electrophoresed with all amplified PCR products. Electrophoresis was performed at 10V/cm for 10min in 1X SB running buffer. After electrophoresis, the DNA fragments were visualized on a long wave 3UV trans-illuminator (UVP, Inc. Upland, CA, U.S.A.) and photographs were taken using an ITC Polaroid camera and Sony videographic printer (Sony Corporation, Shinagawa-ku, Tokyo, Japan).

Table 2.5. High fidelity PCR conditions used to amplify the cDNA sequences of the Y2H preys from genomic DNA for cloning into the pGFP-C1 vector for co-localization

Primer set	[$MgCl_2$] mM	T_D °C	Time sec	T_a °C	Time sec	T_E °C	Time Sec
ANKRD F/R	1.5	94	30	62	30	72	30
COMMD4 F/R	1.5	94	30	65	30	72	30
ENO1 F/R	1.5	94	30		30	72	30
ENO3 F/R	1.5	94	30	77	30	72	30
PRKAR1A F/R	1.5	94	30	61	30	72	30
PRKAR2A F/R	1.5	94	30	88	30	72	30

Abbreviations: °C, degrees Celcius; mM, millimolar; sec, seconds; T_a, annealing temperature; T_D, denaturing temperature; T_E, extension temperatute

2.3.2. Sodium dodecyl sulphate polyacrylamide gel electrophoresis (SDS-PAGE)

Sodium dodecyl sulphate polyacrylamide gel electrophoresis (SDS-PAGE) was used to electrophorese protein products, derived from *in vivo* co-immunoprecipitation (Co-IP) reactions (Section 2.15).

For *in vivo* Co-IPs, the protein products were electrophoresed in 100x80x3mm, 15-20% polyacrylamide gels containing 10% SDS (Appendix I). After mixing with 6% SDS loading dye (Appendix I), the samples were incubated at 95°C for 5min, and subsequently loaded onto the gels. Electrophoresis followed at 100 V for 1 – 1.5h in 1X SDS running buffer (Appendix I). Afterwards, the protein samples in the gel were transferred to a polyvinylidene fluoride (PVDF) membrane for visualization via Western blotting (Section 2.16).

2.3.3. Transfer of protein from SDS polyacrylamide gels to PVDF membrane

In order to visualise protein bands of *in vivo* co-immunoprecipitation assays, western blotting was done by transferring the protein samples seperated via SDS-PAGE to a polyvinylidene fluoride (PVDF) membrane (GE Healthcare Limited, Amersham Place, Little Chalfont, Buckinghamshire, UK) as follows: Following electrophoresis, the gel apparatus was dismantled and the gel rinsed in ddH_2O by shaking it for 5min on ice. Afterwards, the ddH2O was removed and ice-cold transfer buffer (Appendix I) was added to the gel and the gel agitated for 20min. During this period, the PVDF membrane was prepared for transfer by incubating it for 15sec in undiluted methanol, followed by a rinse in ddH_2O for 5min. After removal of the water, ice-cold transfer

buffer was added to the membrane, together with cut pieces of Whatman paper and western blot sponges, and shaked for 10min.

The blotting apparatus was then stacked forming a sandwich, with western blot sponges on the outside, followed by cut pieces of Whatman paper on the inside, with the gel (on the anode side) and the membrane (on the cathode side) in the middle. During stacking, everything was kept soaked with transfer buffer. The sandwiches were closed and inserted into the transfer apparatus filled with transfer buffer, together with an ice pack and magnet, and placed on a magnetic stirrer and electrophoresed at 100V for 1h.

2.4. AUTOMATED DNA SEQUENCING

Automated DNA sequencing of cloned inserts was performed at the Core Sequencing Facility of the Department of Genetics at the University of Stellenbosch, R.S.A. on an ABI Prism™ 3100 automated sequencer (P.E. Applied Biosystems, Forster City, CA, U.S.A.). Vector specific primers (see Table 2.2) as well as primers used for the generation of cloning inserts (Tables 2.3 and 2.4) were used for these sequencing reactions.

2.5. DNA SEQUENCING ANALYSIS

ChromasPro software (Techelysium Pty Lmt, Helensvale, Queensland, Australia) was used for sequence analysis. Sequence analysis consisted of verification of the sequence integrity (reading frame and cloning sites) of inserts cloned into the respective cloning vectors (Section 2.8), identification of putative interactor prey clones isolated during the Y2H library screen (Section 2.14), as well as verification of the integrity of the inserts cloned for *in vivo* co-localisation (Section 2.17) and *in vivo* co-immunoprecipitation (Section 2.15). The nucleotide sequences of the bait and prey inserts as determined by automated sequencing (Section 2.4) were compared to the appropriate cDNA and mRNA sequences obtained from the Genbank database (www.ncbi.nlm.nih.gov/Entrez) and the Ensembl database (www.ensembl.org). The sequences obtained for the Y2H prey constructs through automated sequencing were entered into BLAST and analysed against the Genbank database using BLASTN (www.ncbi.nlm.nih.gov/BLAST). To determine whether the prey insert encoded for an in-frame protein, the nucleotide sequence of the prey insert sequence in the absence of vector or GAL4 domain sequences were translated in DNAMAN and a BLASTP search followed of the translated sequence against public protein databases in order to assign identity to them.

2.6. BRADFORD PROTEIN CONCENTRATION DETERMINATION

The protein concentration of all cell lysates was determined prior to starting *in vivo* co-immunoprecipitations or western blots via Bradford protein concentration determination. In order to calculate a standard curve of protein concentrations, 10µl of a dilution range of bovine serum albumin (BSA) standards ranging from 0 – 1000µg/µl was loaded into the wells of a luminometer plate, together with cell lysate samples, in duplicate. Two hundred

microlitres of Bradford solution (Appendix I) was then added to each standard sample as well as lysate sample. A Synergy HT luminometer (BioTek Instruments Inc., Vermont, USA) was then used to determine the protein concentration of each well, and the KC4™ v 3.4 program (BioTek Instruments Inc.,Vermont, USA) used to calculate and set up the standard curve, as well as each sample's protein concentration.

2.7. RESTRICTION ENZYME DIGESTION FOR CLONING

For cloning, the PCR-generated inserts viz. *PDE4DIP*, *PRKAR1A*, *PRKAR2A*, *ANKRD1*, *COMMD4*, *ENO1* and *ENO3* (Section 2.2.2 and 2.2.3) as well as the respective cloning vectors viz. pGBKT7, pACT2, pGFP-C1 and pDs-Red were double-digested with their appropriate restriction enzymes (see Tables 2.1 and 2.3), as indicated in Table 2.6. The digests were prepared in a 100µl reaction volume as follows: 40µl insert DNA or 20µl pGBKT7 vector DNA was mixed with 5µl restriction enzyme, 10µl restriction enzyme buffer D (Promega, Madison WI, U.S.A.) and the appropriate volume of ddH_2O. These mixtures were then incubated at 37°C for 3h. After incubation, the samples were purified using the Wizard® Purefection Mini Plasmid DNA purification kit (Wizard® Purefection Mini Plasmid DNA purification kit, Promega Corp. Madison Wisconsin, USA), as discussed in Section 2.1.4.

The samples were eluted in 50µl ddH_2O and subsequently mixed with 5µl of the second restriction enzyme, 10µl restriction buffer H (Promega, Madison WI, U.S.A.) and the appropriate volume of ddH_2O. Incubation at 37°C for 3h followed, after which the samples were again purified using the Wizard® Purefection Mini Plasmid DNA purification kit. To prevent the double-digested vectors from annealing to itself in ligation reactions, it was treated with calf intestinal alkaline phosphatase (CIP) (Section 2.8.3) prior to ligation reactions. The double-digested inserts were not CIP treated and used directly in ligation reactions.

2.8. GENERATION OF CONSTRUCTS

2.8.1 Generation of Y2H constructs

The Y2H bait-insert was cloned into the pGBKT7 bait-vector (Appendix IV) and, after automated sequencing to verify integrity of the sequence and conservation of the GAL4 DNA-BD reading frame, transformed into the yeast strain AH109. This construct (pGBKT7-MMGL:AH109) was used to screen a CLONTECH MATCHMAKER™ pre-transformed cardiac cDNA library, comprised of cardiac cDNAs cloned into the pACT2 prey-vector (Appendix IV) and transformed into the yeast strain Y187.

Table 2.6. Restriction enzymes used to digest cDNA inserts and vectors subsequently used in Y2H, colocalization and *in vivo* co-immunoprecipitation analyses

cDNA insert	Vector	Restriction enzymes	Application
PDE4DIP	pGBKT7(1), pDs-Red-C1(2)	*Nde*I, *Eco*RI (1) *Sal*I, *Bam*HI (2)	Y2H analysis (1), colocalization, *in vivo* co-immunoprecipitation (2)
PRKAR1A	pACT2 (1), pGFP-C1 (2)	*Xho*I, *Bam*HI	Y2H analysis (1), colocalization (2)
PRKAR2A	pACT2 (1), pGFP-C1 (2)	*Nco*I, *Bam*HI (1), *Xho*I, *Bam*HI (2)	Y2H analysis (1), colocalization (2)
ANKRD1	pGFP-C1	*Xho*I, *Bam*HI	colocalization
COMMD4	pGFP-C1	*Xho*I, *Bam*HI	colocalization, *in vivo* co-immunoprecipitation
ENO1	pGFP-C1	*Eco*RV, *Sac*II	colocalization
ENO3	pGFP-C1	*Xho*I, *Bam*HI	colocalization

The Y2H prey-inserts viz. PRKAR1A and PRKAR2A, were cloned into the pACT2 prey-vector and, after automated sequencing to verify integrity of the sequence and conservation of the GAL4 DNA-AD reading frame, transformed into the yeast strain Y187. These constructs (pACT2-R1A:Y187 and pACT2-R2A:Y187) were used to perform a direct Y2H protein-protein interaction test on pGBKT7-MMGL:AH109.

2.8.2. Generation of co-localization and *in vivo* co-immunoprecipitation constructs

For *in vivo* co-localisation, the PCR fragments representing *ANKRD1*, *COMMD4*, *ENO1*, *ENO3*, *PRKAR1A* and *PRKAR2A* were cloned into the pGFP^2-C1 fluorescent vector and the integrity of the insert sequence and reading frame verified by automated sequencing (Section 2.4). The PCR fragment representing *PDE4DIP* was cloned into the pDs-Red-C1 fluorescent vector and subjected to the same verifications as the prey sequences, and was used in subsequent colocalization and *in vivo* co-immunoprecipitation experiments. *TNNI3* and *MYBPC3* cloned into the pGFP^2-C1 vector was already available in our laboratory, and used again for this study.

2.8.3. Alkaline phosphatase treatment of vector

The ends of the linearised plasmid were CIP-treated to remove phosphate groups. This prevents the linearised vector from re-circularising by self-ligation (Section 2.7). Alkaline phosphatase treatment was accomplished by mixing 50µl of the digested vector with 1µl CIP (Promega, Madison WI, USA), 10µl CIP buffer (Promega, Madison WI, USA) and 38µl ddH_2O. Incubation of the sample then followed at 37°C for 30 min, after which another 2µl CIP was added and the mixture incubated for a further 30 min. After this, 2µl 0.5M EDTA was

added to the mixture and the sample incubated at 65°C for 20 min to inactivate the enzyme. The vector was then purified by using the Wizard® Purefection Mini Plasmid DNA purification kit (Wizard® Purefection Mini Plasmid DNA purification kit, Promega Corp. Madison Wisconsin, USA) (Section 2.1.4).

2.8.4 DNA ligation

DNA ligations were performed in order to generate the various constructs described in Sections 2.8.1 and 2.8.2. For ligation, 2µl of the double-digested insert (Section 2.7) was added to 1µl of CIP-treated, double-digested vector (Sections 2.8.1 and 2.8.3). To this mixture, 5µl 2X T4 DNA ligase buffer (Promega, Madison WI, USA), 5U T4 DNA ligase (Promega, Madison WI, U.S.A.) and ddH_2O to a final volume of 10µl, was added. The sample was then incubated at 4°C overnight. After this incubation period, 5µl of the sample was transformed into the bacterial strain DH5α (Section 2.12.1) and plated onto appropriate selective LB agar plates. Following overnight incubation at 37°C, successful ligation reactions were confirmed by bacterial colony PCRs (Section 2.2.4).

2.9. BACTERIAL STRAINS, YEAST STRAINS AND CELL LINES

2.9.1. Bacterial strains

To facilitate selection and purification of vector constructs, ligation reactions were transformed into the *E.coli* DH5α strain. The transformed colonies were then selected on the basis of their ability to grow on LB agar plates (Appendix I) containing selection antibiotics. Recombinant plasmids were thereafter identified by colony PCR (Section 2.2.4). When selecting for pGBKT7 or pDs-Red-C1, kanamycin was used as selection antibiotic, whereas ampicillin was used when selecting for pACT2 and zeocin was used when selecting for $pGFP^2$-C1.

2.9.2. Yeast strains

The pGBKT7 bait construct was transformed into the yeast strain AH109, and the pACT2 prey constructs were transformed into the yeast strain Y187. The clones present in the pre-transformed CLONTECH cDNA library used in the Y2H library screen had been transformed into the yeast strain Y187 by the manufacturer. Details of yeast phenotypes are given in Appendix III.

2.9.3. Cell lines

Suitable combinations of vectors were co-transfected into the rat atrial myocyte cell line H9C2 for the *in viv*o 3D co-localization (Section 2.17) assays. For *in vivo* co-immunoprecipitations, the pDs-Red-MMGL construct (Section 2.8.2) was also transfected into the H9C2 cell line.

2.10. GENERATION OF *E.coli* DH5α COMPETENT CELLS

An amount (50µl) of an *E.coli* DH5α frozen (-80°C) glycerol stock was inoculated in 10ml LB media (Appendix I) and incubated overnight at 37°C at 200rpm in a YIH DER model LM-530 shaking incubator. After the inoculation period, a 1ml aliquot of the culture was added to 200ml LB media contained in a 2 L Erlenmeyer flask. Incubation of this culture at room temperature, while shaking at 200rpm, then followed for an overnight period, until the culture reached a mid log phase (OD_{600}=0.6). Shaking took place on a Labcon orbital shaker (Labcon Pty Ltd Maraisburg, R.S.A.). When the culture reached the mid-log phase, it was decanted into 4X 50ml polypropylene tubes and centrifuged at 3000rpm for 15min at 4°C in a Multitex centrifuge (MSE instruments, England). After discarding the supernatant, the pellet was resuspended in 4ml ice-cold CAP buffer (Appendix I). The suspended cells were then transferred to 1.5ml microfuge tubes in 500µl aliquots. Storage at -80°C of the cells followed until needed.

2.11. CULTURING OF CELL LINES

2.11.1 Culture of cells from frozen stocks

2.11.1.1 Thawing the cells

Rattus norvegicus (rat) cardiac (atrial) myocytes, H9C2, were purchased from the American Type Culture Collection (ATCC, Manassas, VA, USA). Thawing of the frozen stock was done by rapidly immersing the vials in a 37°C water bath for 10min. Immediately after thawing, the outside of the vials were sterilized with 70% ethanol.

2.11.1.2 Removing Dimethyl sulphoxide (DMSO) from stocks and culturing cells

It is necessary to remove DMSO from the frozen stock in order to ensure maximum viability of the cells upon plating. The DMSO was removed as follows: 1ml of complete growth media (Appendix I), pre-heated to 37°C, was added to the frozen stock and mixed by gentle pipetting. Afterwards, this mixture was transferred to a 12ml Greiner tube (Greiner Bio-one, Frickenhausen, Germany) and another 5ml of growth media was added. Centrifugation at 1000rpm followed for 3min using a Sorval® GLC-4 General Laboratory centrifuge (Separations Scientific, Johannesburg, RSA) after which the supernatant was removed. The pellet was subsequently resuspended in another 5ml of growth media and centrifugation repeated at 1000rpm for 3min. Afterwards, the cells were resuspended in 10ml growth media and transferred into a T25 culture flask. The cells were distributed evenly over the growth surface of the flask by swirling the flask gently, and incubated at 37°C in a Farma-thermosteri-cycle 5% carbon dioxide humidified incubator (Farma International, Miami, Florida, USA).

2.11.1.3 Splitting of cell cultures

Splitting of pre-confluent cultures (approximately 70-80% confluency) was done every 2-4 days, by removing the growth media from the flask, after which washing with sterile phosphate buffered saline (PBS) containing no calcium or magnesium (Cambrex, Walkersville, MD, USA) followed. In order to loosen the cells from the growth surface of the flask, 2ml of trypsin (Highveld Biological, Lyndhurst, RSA) was added. After 5min, 5ml growth media was added and the cells gently resuspended, after which it was transferred to a 12ml Greiner tube and pelleted by centrifugation at 1000rpm for 3min in a Sorval® GLC-4 General Laboratory centrifuge. After centrifuging, the cells were resuspended in 10ml growth media and transferred to 4 flasks each containing 10ml growth media.

2.11.2. Cell lysis

Both untransfected as well as transfected H9C2 cell lysates were used in subsequent *in vivo* co-immunoprecipitation and Western blot analyses (Section 2.15 and 2.16). Lysis of cells was accomplished as follows: Cells were scraped off the bottom of 6-well plates or 135mm petri dishes (depending on the amount of cells cultured) using a cell scraper, and, in the case of 6-well plates, the cells from three wells containing similarly transfected cells pooled together in a 50 ml polypropylene tube to obtain sufficient cells for subsequent assays. The samples were centrifuged for 10min at 3000rpm in a Beckman model TJ-6 centrifuge (Beckman Coulter, Scotland, U.K.) after which the supernatant was discarded, leaving a small amount of media behind. The samples were transferred to 1.5ml microcentrifuge tubes; 200µl of PBS (Appendix I) was added and mixed with the samples. Centrifugation for 1min at 3000rpm followed in an Eppendorf model 5417 C centrifuge (Eppendorf, Germany), after which the supernatant was discarded. Two hundred microlitres of passive lysis buffer (Appendix I) was then added and the samples incubated on ice for 30min. Centrifugation at 4°C for 10min at 14000rpm followed, after which the supernatant was transferred and frozen at -80°C until required.

2.12. TRANSFORMATIONS AND TRANSFECTION OF PLASMIDS INTO PROKARYOTIC AND EUKARYOTIC CELLS

2.12.1. Bacterial plasmid transformation

The appropriate aliquot of competent *E.coli* DH5α cells was removed from a -80°C freezer and thawed on ice for 20-30min. After thawing, 1µl plasmid preparation (Section 2.1.4) or 3-5µl of the ligation reaction (Section 2.8.4) was added to the competent *E.coli* DH5α cells. Incubation on ice followed for 20min. Transformation was then performed by placing the mixture in a Lasec 102 circulating water bath at 42°C for exactly 45sec (Lasec Laboratory and Scientific Company Pty Ltd, Cape Town, R.S.A.). The sample was then incubated at room temperature for 2min after which 1ml LB media was added to the mixture and the sample incubated for 1h at 37°C, shaking at 200rpm in a YIH DER model LM-530 shaking incubator. Following incubation, 200µl of the sample was plated onto LB agar plates containing the appropriate selection antibiotic (Appendix I). The

remaining transformation mixture was then centrifuged for 1min at 14000rpm in an Eppendorf model 5417C centrifuge (Eppendorf AG, Hamburg, Germany) and the supernatant was discarded. The pellet was then resuspended in 200µl LB media and also plated on LB agar plates containing the appropriate antibiotic. The plates were inverted and incubated for 16h at 37°C in a model 329 stationary CO_2 incubator (Former Scientific, Marieta, Ohio, U.S.A.)

2.12.2. Yeast plasmid transformation

Yeast strains to be transformed were streaked from frozen glycerol stocks onto YPDA agar plates (Appendix I) and incubated at 30°C for 2-3 days in a Sanyo MIR262 stationary ventilated incubator (Sanyo Electronic Company, Ora-Gun, Japan). After the incubation period, a volume representing 20-50µl yeast cells was picked and resuspended in 1ml sterile ddH_2O in a sterile 2ml tube. The cells were then centrifuged at 13000rpm for 30sec in a Beckman Microfuge Lite (Beckman Instruments Inc., CA, U.S.A.) to form a pellet. The supernatant was discarded and the pellet was resuspended in 1ml 100 mM lithium acetate (LiAc) and incubated for 5min at 30°C in a MIR262 stationary ventilated incubator. The cells were pelleted again by centrifugation at 13000rpm for 30sec after which all the LiAc was removed from the tube. After removal of the LiAc, the following was added to the pellet in this order: 240 µl of 50% polyethylene glycol (PEG), 36µl 1M LiAc, 25µl of 2 mg/ml heat denatured and snap-cooled sonicated herring sperm DNA (Promega, Madison WI, U.S.A.), 10-20µl plasmid preparation and ddH_2O, to a final volume of 350µl. The sample was then vortexed by using a Snijders model 34524 press-to-mix vortex (Snijders Scientific, Tilburg, Holland) for at least 1min and incubated at 42°C for 20-30min in a Lasec 102 circulating water bath (Lasec Laboratory and Scientific Company Pty Ltd, Cape Town, R.S.A.). After the incubation period, the cells were pelleted by centrifugation at 13000rpm for 1min, after which all the supernatant was removed. Resuspension of the pellet in 250µl sterile Millipore ddH_2O followed, and 150µl of this resuspension was then plated onto the appropriate selection plates (Appendix I). The plates were incubated inverted at 30°C for 2-5 days in a Sanyo MIR262 stationary ventilated incubator (Sanyo Electronic Company, Ora-Gun, Japan).

2.12.3. Transfection of H9C2 cells for use in co-localization and *in vivo* co-immunoprecipitation assays

For the co-localization assays, approximately 20000-30000 cells/well were seeded in complete growth medium, $DMEM^{10\%FBS+1\%PS}$, (Lonza, Walkersville, MD, USA) in borosilicate coverglass chambers (Nunc, New York, USA) and incubated at 37°C in a Farma-thermosteri-cycle 5% carbon dioxide humified incubator. To determine the confluency level, the cells were visualized after 48h using a Nikon TMS light microscope (housed at the Department of Physiology, University of Stellenbosch). Once the cells reached approximately 70-80% confluency, transfection was performed. For each transfection, 100µl serum-free medium ($DMEM^{1\%PS}$) (Lonza, Walkersville, MD, USA) was aliquoted into sterile 1.5ml microcentrifuge tubes and 6µl of Genejuice® (Novagen, Madison, WI, USA) added to the tube. Vortexing of the mixture followed using a Snijders model

34524 press-to-mix vortex after which the mixture was incubated at room temperature for 5min. One microgram of vector DNA (pGFP^2-C1:pDs-Red-C1 1:1) (Table 2.8) was then added to the mixture and mixed by gentle pipetting. Incubation of this Genejuice/DNA/medium mixture followed at room temperature for 30mins. Afterwards, the mixture was added drop-wise to the cells in the growth media while the chambers were carefully rocked back and forth in order to distribute the drops evenly across the chamber surface. The cells were then incubated at 37°C in a Farma-thermosteri-cycle 5% carbon dioxide humified incubator for 48h. Afterwards, the cells were differentiated into cardiac myotubes (Section 2.12.4).

For *in vivo* co-immunoprecipitation assays, cells were cotransfected with the appropriate vector construct combinations in the same manner and conditions as described above, except for seeding approximately 1x10^4 cells in 135mm petri dishes to yield larger protein concentrations. For each transfection, 1152µl serum-free DMEM was aliquoted into sterile 2 ml microcentrifuge tubes together with 26µl Genejuice® and vortexed, followed by a 5min incubation at room temperature. After incubation, 8.64µg vector DNA (pDs-Red-C1:pGFP 1:1) was added and mixed by gentle pipetting, followed by incubation at room temperature for 15min. Drop-wise addition of this mixture to the cells in DMEM$^{10\%FBS+1\%PS}$ followed. Following the 48h incubation period at 37°C, cells were lysed (Section 2.11.2).

2.12.4. Differentiation of transfected H9C2 cells used for *in vivo* co-localization

The growth medium was changed 48hrs after transfection in order to differentiate cardiac myocytes into myotubes. After the growth media was removed, the cells were washed with sterile PBS (containing no calcium or magnesium) and 3µl of differentiating growth medium (DMEM$^{1\%horse\ serum\ +\ 1\%PS}$) (Lonza, Walkersville, MD, USA) was added. Incubation then followed at 37°C in a Farma-thermosteri-cycle 5% carbon dioxide humidified incubator for seven days, with the cells being washed again and fresh differentiating media added on day four. On day seven, the cells were visualized using an Olympus IX 81 motorised inverted microscope (Olympus, Hamburg, Germany) to confirm differentiation. Following this, the cells were photographed for co-localization (Section 2.17).

Table 2.7. Transfection experiment layout for the *in vivo* co-localization assay

Transfection (1:1)*	pDs-Red construct	pGFP^2 construct
Test 1	MMGL	ANKRD1
Test 2	MMGL	COMMD4
Test 3	MMGL	ENO1
Test 4	MMGL	ENO3
Test 5	MMGL	PRKAR1A
Test 6	MMGL	PRKAR2A
Test 7	MMGL	TNNI3
Genejuice® control	-	-
Untransfected control	-	-

*****Ratio to a total of 1µg

2.13. ASSESSMENT OF Y2H CONSTRUCTS

2.13.1. Phenotypic assessment of yeast strains

Before transformation, each of the yeast strains used in the Y2H analysis was phenotypically assessed. Assessment were achieved by plating strains AH109 and Y187 onto selective agar plates lacking essential amino acids, i.e. agar plates SD^{-Ade}, SD^{-Trp}, SD^{-His}, SD^{-Leu}, SD^{-Ura} . Non-transformed yeast cells that were able to grow on SD^{-Ura} and unable to grow on SD^{-Ade}, SD^{-Trp}, SD^{-His} and SD^{-Leu} were used for transformation and subsequent Y2H analysis.

2.13.2. Toxicity tests of transformed cells

It was important to establish whether the bait construct (Section 2.8.1) had any noticeable toxic effect on the host yeast strain, AH109 (Section 2.9.2), before proceeding with the Y2H assay. To establish if the constructs were toxic to the host cells, a growth curve of AH109 transformed with pGBKT7-MMGL was generated and afterwards compared to a growth curve of AH109 transformed with non-recombinant pGBKT7. These two growth curves were set up in tandem and under the same experimental conditions.

To generate the two growth curves, each of the transformed yeast strains was grown to stationary phase in SD^{-W} media in a 50ml polypropylene tube at 30°C in a YIH DER model LM-530 shaking incubator shaking at 200rpm. After this incubation, a 1:10 dilution of each primary culture was made in SD^{-W} and incubated for an extra 24h. During this incubation, over a period of 8h, a 1ml aliquot of the culture was taken every 2h and its OD_{600nm} was measured. An overnight (24h) reading was also measured. A linearised graph of the log of these OD_{600nm} readings versus time was drawn and the slopes of the graphs generated for the recombinant and non-recombinant transformants were compared.

2.13.3. Testing the mating efficiency

To determine whether the bait construct had any significant effect on the mating efficiency of the AH109 yeast cells, small scale yeast matings were performed. The AH109 transformed with pGBKT7-MMGL bait construct was mated with the prey host strain, Y187 transformed with the non-recombinant prey vector pACT2 or the control prey vector pTD1.1, supplied by the manufacturer (BD Bioscience, Clontech, Palo Alto, CA, U.S.A.). At the same time, control matings were also performed in which the yeast strain AH109 transformed with non-recombinant pGBKT7 or the control pGKT7-53 vector supplied by the manufacturer was mated with the prey host strain, Y187 transformed with the non-recombinant prey vectors pACT2 or the pTD1.1 control vector. The experiment was performed as follows:

Each of the yeast strains used in the mating efficiency tests was plated onto the appropriate nutritional selection plates as follows: AH109 pGBKT7-MMGL, AH109 pGBKT7 and AH109 pGBKT7-53 on SD^{-W} plates and Y187 pACT2 and Y187 pTD1.1 on SD^{-L} plates. Incubation of the plates followed for 2-5 days in a Sanyo MIR262 stationary ventilated incubator (Sanyo Electronic Company Ltd, Ora-Gun, Japan). From these plates, a single colony was used for each of the test mating experiments. The test matings were performed in 1ml YPDA media (Appendix I) in a 2 ml microfuge tube. The matings were incubated overnight at 30°C, shaking at 200rpm in a YIH DER model LM-530 shaking incubator. After the incubation period, serial dilutions (1:10, 1:100, 1:1000 and 1:10000) of the mating cultures were plated onto SD^{-L}, SD^{-W} and SD^{-L-W} agar plates. The plates were incubated for 4-5 days at 30°C in a Sanyo MIR262 stationary ventilated incubator. Following this period, the colonies on each plate were counted and used to calculate the mating efficiency (Appendix II).

2.14. Y2H ANALYSIS

2.14.1. The cardiac cDNA library

The library used for the Y2H library screen was a pre-transformed human MATCHMAKER™ cardiac cDNA library (BD Bioscience, Clontech, Palo Alto, CA, U.S.A.) consisting of *S.cerevisciae* Y187 transformed with a cardiac cDNA library constructed in pACT2. The library consisted of normal, whole hearts pooled from three Caucasian males between the ages of 28 and 47 years. The library was *Xho*I-$(dT)_{15}$ primed, and contained approximately $3.5x10^6$ independent clones that was inserted into the pACT2 vector between the *Xho*I and *Eco*RI sites. The library had an average insert size of 2.0kb, with a range of between 0.4 and 4.0kb.

2.14.2. Establishment of bait culture

An AH109 colony transformed with pGBKT7-MMGL was streaked out on SD^{-W} plates, after which four of the resultant colonies were inoculated into four separate 500ml Erlenmeyer flasks containing 50ml SD^{-W} media each. Four bait cultures were produced in order to facilitate pooling of the initial cultures, allowing the generation of a final bait culture with a titer of at least $1X10^{10}$. This translated into a 100-fold excess of bait to prey to ensure a

high mating efficiency. The four cultures were incubated at 30°C overnight, shaking at 200rpm in a YIH DER model LM-530 shaking incubator. After incubation, the cultures were transferred to four separate 50ml polypropylene tubes and centrifuged at 3000rpm for 10min at room temperature to pellet the cells in a Beckman Microfuge Lite centrifuge (Beckman Instruments Inc., CA, U.S.A.). After centrifugation, the supernatants were discarded and the four pellets resuspended together in 50ml SD^{-W} media, followed by transfer of this suspension to a single 500ml Erlenmeyer flask. The culture was then incubated for 16h in a YIH DER model LM-530 shaking incubator, shaking at 200rpm. Following incubation, the titer of the bait culture was estimated by measuring the OD_{600nm} of a 1ml aliquot of this culture. Haemocytometric cell count was then used to confirm this estimation.

Subsequently, the cells were pelleted again by centrifugation at 3000rpm at room temperature for 10min. Discarding of the supernatant followed and the pellet was resuspended in 50ml SD^{-W} media. Aliquots of 10µl of this culture were taken for control mating experiments.

2.14.3. Library mating

An aliquot of 1ml of the pre-transformed cardiac cDNA library was taken from -80°C and thawed at room temperature (BD Biosciences, Clontech, Palo Alto, CA, U.S.A.). After thawing, the aliquot was mixed by vortexing using a Snijders model 34524 press-to-mix vortex (Snijders Scientific, Tilburg, Holland). An aliquot of 10µl was then transferred to a sterile 1.5ml microfuge tube to be used for library titering. The pGBKT7-MMGL transformed AH109 pellet (Section 2.8) was then resuspended in 45ml 2X YPDA media (Appendix I) supplemented with 10µg/ml kanamycin (Kan) in a 2L Erlenmeyer flask. The remaining 990µl of the library culture was then added , after which the mating culture was incubated overnight at 30°C, shaking at 200rpm in a YIH DER model LM-530 shaking incubator (SCILAB instrument Co. Ltd, Taipei, Taiwan).

After this overnight incubation period, the entire mating culture was transferred into a sterile 50ml polypropylene centrifuge tube. The culture was then centrifuged at 3000rpm for 5min in a Beckman Microfuge Lite centrifuge (Beckman Instruments Inc., CA, U.S.A.) to pellet the cells. The supernatant was subsequently removed. The Erlenmeyer flask in which the mating was performed was then rinsed twice with 40ml 2X YPDA containing 10µg/ml Kan. With each rinsing, the 2X YPDA medium was used to resuspend the cell pellet and the cells then re-pelleted by centrifugation for 10min at 3000rpm. After the final centrifugation step, the supernatant was removed and the pellet resuspended in 15ml 0.5X YPDA containing 10µg/ml Kan.

To determine mating efficiency, serial dilutions of 100µl aliquots (1:10; 1:100; 1:1000 and 1:10000) of this cell suspension were plated onto 90mm SD^{-L}, SD^{-W} and SD^{-L-W} agar plates. The rest of the library maiting culture was plated directly onto 60 140mm triple dropout (TDO) (media lacking leucine, tryptophan and histidine)

(Appendix I) agar plates in 250µl aliquots. The TDO plates were subsequently incubated inverted at 30°C for 2 weeks in a Sanyo MIR262 stationary ventilated incubator. Growth was monitored and colonies were picked and restreaked onto quadruple dropout (QDO) (media lacking leucine, trypthophan, histidine and adenine) plates to test for activation of both the *HIS3* and *ADE2* nutritional reporter genes. Incubation of these plates followed for 3-6 days at 30°C. Colonies that grew on the QDO plates were picked and plated onto QDO plates containing X-α-galactose, in order to assess activation of the *MEL1* reporter gene, and incubated at 30°C for a further 3-5 days.

2.14.4. Establishing a library titer

The serial dilutions plated onto 90 mm SD^{-L}, SD^{-W} and SD^{-L-W} agar plates (Section 2.13.3) were incubated for 4 days in a Sanyo MIR262 stationary ventilated incubator (Sanyo Electronic Company Ltd, Ora-Gun, Japan). Colony counts were then performed on the different plates in order to calculate the mating efficiency of the library mating and the number of library plasmids screened (Appendix II)

2.14.5. Control matings

In order to determine whether the recombinant pGBKT7-MMGL:AH109 construct had any negative effects on the ability of the transformed AH109 strain to mate with the library strain (Y187), control matings were set up. An aliquot of 10µl of pGBKT7-MMGL:AH109 culture and a single test prey colony (yeast strain Y187 transformed with pTD 1.1 control vector) (BD Biosciences, Clontech, Palo Alto, CA, U.S.A.). were co-inoculated in 1ml 0.5X YPDA containing 10µg/ml Kan in a 2ml microfuge tube. Incubation of this mixture followed at 30°C, with shaking at 200rpm, overnight in a YIH DER model LM-530 shaking incubator (SCILAB instrument Co. Ltd. Taipei, Taiwan). After this incubation period, serial dilutions (1:10; 1:100; 1:1000; 1:10000) of the mating mixture were plated onto SD^{-L}, SD^{-W} and SD^{-L-W} agar plates. These plates were subsequently incubated at 30°C for 4 days in a Sanyo MIR262 stationary ventilated incubator (Sanyo Electronic Company Ltd, Ora-Gun, Japan). Afterwards, colony counts were performed and the mating efficiency was calculated as described in Section 2.14.3.

2.14.6. Detection of activation of nutritional reporter genes

2.14.6.1. Selection of transformant yeast colonies

The pGBKT7-MMGL:AH109 bait construct to be used for the Y2H analysis was plated onto SD^{-L}, SD^{-W} and SD^{-L-W} agar plates and incubated for 4-6 days at 30°C in a Sanyo MIR262 stationary ventilated incubator (Sanyo Electronic Company Ltd, Ora-Gun, Japan). Growth on SD^{-W} plates indicated transformation of the yeast with the pGBKT7-MMGL bait plasmid, growth on SD^{-L} plates indicated transformation of the yeast with a prey plasmid and growth on SD^{-L-W} plates indicated the presence of both bait and prey plasmids. These transformant yeast colonies were subsequently picked and used in direct Y2H screens and a library screen (Section 2.14).

2.14.6.2. Selection of diploid yeast colonies containing putative interactor peptides

Diploid yeast colonies containing both bait and prey plasmids were plated onto TDO plates (Appendix I) as well as QDO plates (Appendix I) in order to identify colonies in which an interaction between the bait- and prey-fusion peptides had taken place. Growth on TDO plates indicated transcriptional activation of the *HIS3* nutritional reporter gene, whereas growth on QDO plates indicated transcriptional activation of both *HIS3* and the *ADE2* reporter genes. The activation of these genes in diploid yeast cells is an indication of interaction between bait and prey peptides.

2.14.7. Detection of activation of colourimetric reporter genes via X-α-Galactosidase assay

X-α-Galactosidase assays were conducted to establish the activation of the *MEL1* reporter gene by the specific interaction between specific bait and prey peptides. Yeast colonies that had *HIS3* and *ADE2* activation, as determined via their growth on QDO plates, were replicated from QDO plates onto Hybond N^+ nylon membranes. The membranes were then placed colony-side up onto a QDO plate containing 20mg/ml X-α-Gal solution (BD Biosciences, Clontech, Palo Alto, CA, U.S.A.). Incubation followed at 30°C for 3-5 days, after which the intensity of the blue colour of the colonies which activated the *MEL1* reporter gene, was visually assessed.

2.14.8. Rescuing prey plasmids from diploid colonies

Yeast colonies that grew on QDO and produced blue colour on X-α-galactosidase assays contained putative MMGL interactors. In order to further assess the specificity of this putative interaction, as well as to facilitate identification of the interactor proteins, the individual preys needed to be isolated from the diploid colonies. Plasmid DNA was isolated from each of the diploid cells as described in Section 2.1.3 and then transformed into the *E.coli* strain DH5α as described in Section 2.13.1. The transformants were plated onto LB amp plates which allows only for the growth of cells containing the prey constructs. Subsequently, these prey constructs were purified from the *E.coli* (Section 2.1.1) and transformed into the yeast strain Y187.

2.14.9. Interaction specificity test

Interaction specificity tests were performed to determine whether the interactions detected by the Y2H analysis were specific between the pGBKT7-MMGL bait and a particular prey peptide. Each Y187 colonies expressing a particular prey peptide was individually mated with the yeast strain AH109 transformed with the pGBKT7-MMGL construct, AH109 transformed with non-recombinant pGBKT7, AH109 transformed with the pGBKT7-53 control bait-plasmid, encoding murine p53, supplied by the manufacturer (BD Biosciences, Clontech, Palo Alto, CA, U.S.A.) and AH109 transformed with a heterologous bait, encoding a reelin domain from the brain protein reeler. After selection for expression of both bait and prey proteins, these diploid clones were streaked

out onto TDO and QDO plates to test for activation of nutritional reporter genes. This tested whether the prey-peptides interacted with the heterologous baits or only with the MMGL bait.

Clones that specifically interacted with the MMGL bait only were considered as putative true interactors. The inserts of these putative interactors were subsequently sequenced to determine their identities.

2.14.10 Direct Y2H protein-protein interaction assays

Small scale yeast matings were performed to determine whether the regulatory subunits of PKA, viz.. PRKAR1A and PRKAR2A, interacted directly with MMGL. The pGBKT7-MMGL:AH109 bait construct was mated with both pACT2-PRKAR1A:Y187 and -PRKAR2A:Y187 prey constructs as follows:

Each of the yeast strains were plated onto suitable nutritional selection plates (pGBKT7-MMGL:AH109 bait on SD^{-W} plates; pACT2-PRKAR1A/R2A:Y187 preys on SD^{-L} plates) and incubated for 2-5 days at 30°C in a Sanyo MIR262 stationary ventilated incubator. A single colony from each of these selection plates was used for each test mating experiment: a bait and a prey colony were resuspended together to 1ml YPDA media in a 2ml microcentrifuge tube. The matings were incubated overnight at 30°C, shaking at 200rpm, in a YIH DER model LM-530 shaking incubator. Afterwards, 100µl of the mating cultures were plated onto SD^{-L-W} agar plates and incubated for 4-5 days at 30°C in a Sanyo MIR262 stationary ventilated incubator. Following this incubation period, the colonies on each plate were plated onto TDO agar plates, and incubated for four days at 30°C. After this, the mating mix was transferred to QDO agar plates and incubated at 30°C for seven days. Growth of the yeast on the respective plates was assessed on days 4 and 7.

2.15. *IN VIVO* CO-IMMUNOPRECIPITATION (Co-IP)

Prior to immunoprecipitation, the appropriate pre-prepared cell lysates (Section 2.11.2) were thawed on ice, and the concentration of the lysates determined via a Bradford assay (Section 2.6). The appropriate amount of lysate was then transferred to a clean microcentrifuge tube and the volume equalized to 200µl by adding passive lysis buffer (PLB) containing protease inhibitors and phenylmethylsulfonyl fluoride (PMSF) (Appendix I), with a final protein concentration of 200µg/µl. The lysates were then precleared by adding 20µl of Protein G agarose beads (KPL, Gaithersburg, MD, USA) to each sample and incubating it at 4°C on a rotating wheel for 2h. Following incubation, the supernatant was collected after centrifugation at 7000rpm for 30sec at room temperature. Depending on the optimum amount determined by optimization (Section 2.16), 1-2µg of the appropriate primary antibody was then added to each lysate sample, followed by incubation at 4°C on a rotating wheel overnight.

After the overnight incubation period, 60µl of Protein G agarose beads was added to each sample and incubated at 4°C on a rotating wheel for 2h. Afterwards, the beads were collected by centrifugation at 7000rpm for 30sec,

and the supernatant collected and transferred to separate tubes kept on ice serving as controls in subsequent Western blot experiments (Section 2.16). The beads were then washed five times with ice cold PLB containing all protease inhibitors by adding PLB to the beads, mixing it, and collecting the beads again via centrifugation at 7000rpm for 30sec.

Following the washing steps, 40µl of 6X SDS loading dye (Appendix I) was added to each sample and boiled for 5min at 95°C. Afterwards, the beads were pelleted by centrifugation at 14000rpm for 3min, and the supernatant loaded onto a SDS polyacrylamide gel (Section 2.3.2).

2.16. WESTERN BLOTTING

In order to visualize precipitated protein bands obtained from *in vivo* co-immunoprecipitation and isoelectric focusing (IEF) assays (Section 2.15.2 and 2.18.3), Western blots were done. The ratios of primary and secondary antibodies used to detect the various putative interactors of MMGL, as well as the antibody against the pDs-Red-MMGL and pGFP-MyBPC constructs were first optimized. Together with each Western blot to determine protein interactions, a Western blot for β-actin was also done to serve as a control. Table 2.8 shows the respective optimal antibody as well as secondary antibody concentration ratios from a 1mg/ml stock determined for use in Western blotting.

2.16.1. Membrane blocking

Following the transfer of proteins from the SDS polyacrylamide gel (Section 2.3.2) onto the PVDF membrane (Section 2.3.3), the membranes were removed from the transfer apparatus and rinsed with ddH_2O for 5min with shaking. The membranes were then blocked with 5% fat free powder milk (Weigh-Less) dissolved in TBST (Appendix I) for 1h, with shaking, to eliminate non-specific binding of the antibodies.

2.16.2. Addition of primary antibody

The PVDF membranes were briefly rinsed twice with TBST (Appendix I) following membrane blocking with 5% fat free powder milk dissolved in TBST. Afterwards, the appropriate ratio of primary antibody:5% milk in TBST (as shown in Table 2.8) was added to each membrane followed by an overnight incubation shaking at 4°C. Following this incubation period, the membranes were briefly rinsed twice with TBST, followed by washing each membrane for 15min shaking in TBST at room temperature, followed by three additional wash steps of 5min each, with fresh changes of TBST in between.

2.16.3. Addition of secondary antibody

After all excess primary antibody was washed off the PVDF membrane, the appropriate ratio of secondary antibody: 5% milk in TBST (as shown in Table 2.8) was added to each membrane, followed by a 1h incubation step shaking at room temperature. Following this incubation period, the membranes were briefly rinsed twice with TBST, followed by washing each membrane for 15min shaking in TBST at room temperature, followed by three additional wash steps of 5min each, with fresh changes of TBST in between.

2.16.4. Chemiluminescent visualization of membrane proteins using the SuperSignal® West Pico Chemiluminescent Substrate kit

After all excess secondary antibody was removed from the PVDF membrane, the two substrate components of the SuperSignal® West Pico Chemiluminescent Substrate kit (Thermo Scientific, Pierce Biotechnology, Rockford, IL, USA), viz. the SuperSignal West Pico Luminol/Enhancer solution and the SuperSignal West Pico Stable Peroxide solution, was mixed in a 1:1 ratio to prepare the substrate Working Solution. The membrane was subsequently incubated for 5min in the Working Solution. After removing excess Working Solution by light tapping on a paper towel, the membrane was placed inside an autoradiography cassette and covered with a transparent plastic sheath, and exposed to autoradiography film (Eastman Kodak Company, Rochester, New York, USA). A glow-in-the-dark sticker was placed in the left hand corner of the cassette next to the membrane for orientation. Exposure time varied from 10sec to overnight exposure, depending on the strength of the signal. Following sufficient exposure time, the film was processed in a Hyperprocessor™ automatic autoradiography film processor (Amersham Pharmacia Biotech UK Ltd., Little Chalfont, Bucks, UK).

2.17. *IN VIVO* CO-LOCALIZATION

To assess the proposed protein-protein interactions in a realistic cellular environment, the *in vivo* co-localization assay was the method of choice. The putative interactors were expressed in mammalian cells as fusion proteins with different fluorescent tags and were subsequently viewed via fluorescence microscopy at the Central Analytical Facility (CAF) (Central Analytical Facility, Department of Physiology, University of Stellenbosch). After viewing, the images were processed for co-localization. For this study, the dsRed (red fluorescent protein) and GFP (green fluorescent protein) tags were utilized.

2.17.1. Co-localization assay

H9C2 rat cardiomyocytes were co-transfected with the suitable combination of vectors (Section 2.12.3) and afterwards, allowed to differentiate for 7-10 days (Section 2.12.4). Prior to image acquisition, the culture media was removed and replaced with culture media containing a 1:200 dilution of the nucleic acid stain Hoechst H-33342 (Sigma). The purpose of the dye is to stain the nuclear material blue in order for orientation purposes during the acquisition of Z-stacked images. Immediately after the addition of the nuclear dye, the cells were

photographed using an Olympus IX 81 motorised inverted microscope (Olympus) and afterwards, the CellR software was used to perform image analysis. Table 2.9 shows the excitation and emission spectra, as well as filter requirements.

Z-stacks were used to co-localize the tagged proteins in three dimensions. Double-labeled images, utilizing the co-transfected samples, were obtained at different focal planes; images were processed by the CellR software to determine co-localization. Z-stacking was performed by first taking a GFP image at the lowest stack level, and then taking a dsRed image at the same level. The camera was then adjusted to the second lowest image and the process repeated. This sequence was repeated for each layer until the last image was taken. To determine the highest and lowest stack position, the camera was first focused on the nucleus of the cell to be imaged and then the image was taken out of focus by moving the objective up (to the top of the cell) and then down (to the bottom of the cell). These top and bottom co-ordinates were recorded by the software. A 60X oil immersion objective was used to collect image stacks at 0.26µm intervals in the plane. Subsequently, each co-localized image was created from the average of 25 frames.

Chambers containing cells co-transfected with pDsRed-MMGL and pGFP-TNNI3 or pGFP-MyBPC were treated with 0.1µM isoproterenol and Z-stacks of the same cells taken again after 10min as described above in order to monitor changes in co-localization upon β-adrenergic stimulation.

2.18. RNA-INTERFERENCE-MEDIATED *PDE4DIP* KNOCKDOWN

To investigate the effect of RNA interference (RNAi) -mediated *PDE4DIP* knockdown in H9C2 cardiomyocytes on cMyBPC phosphorylation, pGFP-cMyBPC (Section 2.2.1.3) was immunoprecipitated from cells with and without *PDE4DIP* knockdown, under different adrenergic-stimulation conditions. These immunoprecipitates were then electrophoresed on IEF gels to separate the four phosphorylation states of cMyBPC. Western blots of these gels were then probed with the JL-8 antibody (Section 2.16) to detect pGFP-cMyBPC. The relative amount of the four phosphorylation states were subsequently compared between cells with and without *PDE4DIP* knockdown, with varying β-adrenergic stimulated conditions.

Table 2.8. Antibodies and antibody concentrations optimised for use in *in vivo* co-immunoprecipitation as well as Western blot assays

Antigen	Primary antibody and manufacturer	Optimum ratio	Secondary antibody	Optimum ratio
ANKRD	CARP (Santa Cruz Biotechnologies)	1:1000	Donkey anti-goat	1:5000
β-actin	β-actin (Cell Signaling Technology)	1:5000	Donkey anti-rabbit	1:5000
dsRed	Living Colors™ DsRed (Clontech)	1:1000	Goat anti-mouse	1:5000
ENO1	ENO1 (Abnova)	1:1000		1:5000
ENO3	ENO3 (Abnova)	1:1000	Goat anti-mouse	1:5000
PRKAR1A	PRKAR1A (Abnova)		Goat anti-mouse	1:5000
PRKAR2A	PRKAR2A (Abnova)	1:1000	Goat anti-mouse	1:5000
TNNI3	TNNI3 (Abnova)	1:500	Goat anti-mouse	1:5000
GFP/YFP	Living Colors™ JL-8 (Clontech)	1:1000	Goat anti-mouse	1:5000

Table 2.9. Excitation and emission spectra and filter requirements of fluorescent proteins used in *in vivo* co-localization

Fluorescent protein	Excitation	Emission	Filter set
Ds-Red	556nm	586nm	TxRED
GFP[2]	395nm	510nm	GFP
Hoechst H-33342[*]	351nm	460nm	DAPI

*Nuclear stain, not a fluorescent protein tag

2.18.1. siRNA preparation, transfection and optimization

Four different rat siRNAs (Qiagen, Hilden, Germany) designed to achieve knockdown of *PDE4DIP* were optimized to establish which siRNA resulted in optimal knockdown of the targeted gene; the most effective of these was used in subsequent knockdown experiments. Table 2.10 summarizes these siRNA sequences as well as respective catalog numbers. For optimizing the four *PDE4DIP* siRNAs, H9C2 cells were cultured until confluent (Section 2.11), and subsequently transfected with the appropriate siRNAs. H9C2 cells ($2x10^5$ cells) were seeded

in 6-well plates (Costar®, Corning Incorporated, Corning, NY, USA) and cultured till 80% confluent. Stock siRNAs of 20µM was prepared prior to transfection by the addition of 250µl siRNA suspension buffer to a 5nmol synthesis. The tubes were heated at 90°C for 1min, followed by an incubation period of 1h at 37°C. The stocks were then either used for subsequent experiments or frozen at -20°C.

Table 2.10. *PDE4DIP* predicted siRNA sequences from the *species*, Rat

Product name	siRNA sequences	Catalog no.
Pde4dip_Rn_RGD:708410_1_HP siRNA	Sense: r(CAU UCG AAA GAU ACG UCA A)dTdT Antisense: r(UUG ACG UAU CUU UCG AAU G)dTdT	S102012843
Pde4dip_Rn_RGD:708410_2_HP siRNA	Sense: r(GCA AGA UAC GAC AAU CCA A)dTdT Antisense: r(UUG GAU UGU CGU AUC UUG C)dTdT	S102012850
Pde4dip_Rn_RGD:708410_3_HP siRNA	Sense: r(GGU GUU ACG CAG UCG ACU A)dTdT Antisense: r(UAG UCG ACU GCG UAA CAC C)dTdT	S102012857
Pde4dip_Rn_RGD:708410_4_HP siRNA	Sense: r(CGG GAA CAA CUU AGU UCA A)dTdT Antisense: r(UUG AAC UAA GUU GUU CCC G)dTdT	S102012864
NCS	Sense: UUC UCC GAA CGU GUC ACG UdT Antisense: ACG UGA CAC GUU AGA AdTdT	1022076

Abbreviations: NCS-non-silencing control; siRNA-small interfering RNA

For siRNA transfection, 12µl of the 20µM siRNA stock was added to 88µl serum free medium followed by addition of 7µl HiPerFect® transfection agent (Qiagen, Hilden, Germany) to each tube to achieve a final siRNA concentration of 100nM. The samples were incubated at room temperature for 5min to allow the formation of complexes during which the culture media in the 6-well plates were replaced with 2.3ml fresh $DMEM^{10\%FBS+1\%PS}$ (Lonza, Walkersville, MD, USA). Afterwards, the complexes were added dropwise to each well, and rocked gently to enable uniform distribution. The cells were then incubated for 24h at 37°C in a Farma-thermosteri-cycle 5% carbon dioxide humified incubator.

Total RNA extraction followed after 24h using the RNeasy Plus Mini kit (Qiagen) as per manufacturer's instructions. The effect of siRNA transfection on MMGL mRNA expression using the four different *PDE4DIP* siRNAs was then determined by a 2-step Q-RT-PCR using the Corbett Rotorgene system. cDNA was transcribed from the extracted RNA using the Quantitect Reverse Transcription kit (Qiagen) as per manufacturer's instructions. The Quantifast SYBR green PCR kit (Qiagen) was then used to perform a real-time quantification of cDNA transcribed from the extracted RNA with or without non-silencing control (NSC) or *PDE4DIP* siRNAs. *PDE4DIP* levels were quantified with reference to three rodent reference genes (transferring receptor –

TRFR, glyceraldehydes-3-phosphate dehydrogenase – *GAPDH* and heat shock protein 1β - *Hsp1β*) selected from a panel of 6 commonly used housekeeping genes.

2.18.2. MMGL knockdown

Rn_RGD:708410_3_HP siRNA (Qiagen) resulted in the lowest *PDE4DIP* gene expression quantification levels, and was used in subsequent experiments. Confluent H9C2 cells were transfected with pGFP-cMyBPC using Genejuice® (Novagen)(Section 2.12.3). These cells were then either transfected after 24h with 10nM *PDE4DIP* Rn_RGD:708410_3_HP siRNA using HiPerFect® Transfection Reagent (Qiagen), or no siRNA transfection. Treatment with 65mM $CaCl_2$ followed after 24h for 10min, followed by a 0.1µM isoproterenol treatment for another 10min, or no treatment. All cells were then lysed (Section 2.11.2) and concentrations determined via Bradford assays (Section 2.6), and all volumes equalized to 200µl by adding PLB containing protease inhibitors and PMSF with a final concentration of 200µg/µl. A non-denaturing immunoprecipitation of pGFP-cMyBPC from the lysate followed using 1µg of the JL-8 antibody (directed against GFP) with the Dynabeads® Protein G and DynaMag™-2 system (Invitrogen) as per manufacturer's instructions. Isoelectric focusing of the GFP-cMyBPC immunoprecipitates followed to separate the four possible phosphorylated forms of cMyBPC.

2.18.3. Isoelectric focusing

For the first dimension separation, the pGFP-cMyBPC immunoprecipitates were suspended in ReadyPrep 2-D Rehydration buffer 1 (Bio-Rad) containing Bio-lite pH 3-10 buffer (Bio-Rad) to a final volume of 200µl. The protein/rehydration buffer mix was then applied to a pH 4-7 (11cm) immobilized pH gradient (IPG) strip (Bio-Rad). Rehydration of the strip followed for 12h at room temperature. Afterwards, IEF was done under the following conditions: 8000V for 20min, 8000V for 2h and 8000V for 40 000 V hours at 21°C (Protean IEF Cell, Bio-Rad). Strips were stored at -80°C after IEF until required.

For 2-dimensional gel electrophoresis (2-DE), equilibration of the IPG strips was done by incubating the strips in equilibration buffer (0.375M tris-HCl, 6M urea, 20% glycerol, 2%, SDS) containing DTT (Sigma-Aldrich) for 15min and then in equilibration buffer containing iodoacetamide (Sigma-Aldrich) for 15min shaking at room temperature. Following equilibration, the IPG strips were placed on top of a Criterion XT 12% bis-tris precast gel (Bio-Rad) and sealed with 0.5% agarose (Bio-Rad). Electrophoresis of the second dimension separation was done under constant voltage (200V) for 1-2h in 5% XT-MOPS running buffer (Bio-Rad). Transfer of the gel to a nitrocellulose membrane and subsequent western blotting (Sections 2.3.3 and 2.16) with the JL-8 antibody followed.

PART 2: MODIFIER STUDY

2.19. STUDY SUBJECTS AND BLOOD COLLECTION

Approval was granted for the present study by the University of Stellenbosch (US) Ethics Committee (N04/03/062). Written informed consent was given by the subjects entered for the study, and blood samples were collected from each subject for molecular genetic testing. During the process, 22 consecutively referred index cases were identified that carried one of three South African founder mutations i.e. R92W in *TNNT2*, R403W in *MYH7* and A797T in *MYH7*. Moolman-Smook *et al.* (1999) previously described these mutations within a South African population. Pedigree tracing was done for these index individuals and their family members were asked to participate in the modifier genotyping study. The families were either of South African Caucasian or of Mixed Ancestry descent, as shown in Table 2.11. A panel of 353 individuals including genetically and clinically affected as well as unaffected individuals was identified. All these individuals were screened for the presence or absence of all three founder mutations.

2.19.1. Clinical evaluation

Study subjects 18 years or older were used in the present study and were clinically characterized by a cardiologist, Dr Miriam Revera of Pavia University, Italy. A two-dimensional (2D) echocardiography was done on each subject, with the clinician being unaware of each subject's mutation status. A 2.5Hz transducer was used in standard parasternal long-axis and short-axis, apical four- and two-chamber views using a GE Healthcare Vivid7 cardiovascular ultrasound system, and analysis included echocardiographic recordings in M-mode, 2D and Doppler blood-flow imaging. Maximal left ventricular wall thickness (mLVWT) was determined at three levels viz. mitral valve, papillary muscle and supra-apex level as shown in Figure 2.1. 2D-echocardiographic measurements were done in six segments of the left ventricular wall at the mitral valve and papillary muscle levels, and in four segments at the smaller supra-apex level. A total of 16 segments were therefore measured.

The six segments measured at the mitral valve and papillary muscle levels consisted of the anterior interventricular septum (aIVS), posterior interventricular septum (pIVS) and the anterior wall (AW), lateral wall (LW), inferior wall (IW) and posterior wall (PW) of the left ventricle. Evaluation of the supra-apex level of the left ventricle consisted of segments IVS, AW, LW and PW as per four chamber view. All variables were measured according to the recommendation of the American Society of Echocardiography (http://www.asecho.org/guidelines.php). The biplane area-length method was used to measure atrium volumes (Schiller *et al.*, 1989). For each subject, covariates of cardiac structure were noted which includes systolic blood pressure (BP) (SBP), diastolic BP (DBP), age, sex, body surface area (BSA) and heart rate (HR).

Table 2.11. South African HCM-affected families of Caucasian and Mixed Ancestry descent that were analysed in the present study

	Pedigree	Ethnic group	n	Gene	Mutation	Location
1	131	Caucasian	25	*MYH7*	A797T	exon 21
2	101	Caucasian	22	*MYH7*	A797T	exon 21
3	104	Mixed Ancestry	14	*MYH7*	A797T	exon 21
4	124	Caucasian	4	*MYH7*	A797T	exon 21
5	123	Mixed Ancestry	16	*MYH7*	A797T	exon 21
6	138	Caucasian	32	*MYH7*	A797T	exon 21
7	145	Mixed Ancestry	4	*MYH7*	A797T	exon 21
8	147	Mixed Ancestry	10	*MYH7*	A797T	exon 21
9	158	Caucasian	5	*MYH7*	A797T	exon 21
10	159	Mixed Ancestry	11	*MYH7*	A797T	exon 21
11	163	Caucasian	9	*MYH7*	A797T	exon 21
12	172	Caucasian	8	*MYH7*	A797T	exon 21
13	106	Mixed Ancestry	69	*MYH7*	R403W	exon 13
14	134	Mixed Ancestry	9	*MYH7*	R403W	exon 13
15	157	Mixed Ancestry	4	*MYH7*	R403W	exon 13
16	100	Mixed Ancestry	43	*TNNT2*	R92W	exon 9
17	103	Mixed Ancestry	5	*TNNT2*	R92W	exon 9
18	109	Mixed Ancestry	8	*TNNT2*	R92W	exon 9
19	139	Mixed Ancestry	41	*TNNT2*	R92W	exon 9
20	137	Mixed Ancestry	7	*TNNT2*	R92W	exon 9
21	149	Mixed Ancestry	10	*TNNT2*	R92W	exon 9
22	173	Mixed Ancestry	2	*TNNT2*	R92W	exon 9

Abbreviations: n = number of individuals screened for SNPs in the present study includes mutation and non-mutation carriers, *MYH7* - myosin heavy chain gene 7; *TNNT2* - troponin T gene

In order to better describe the extent of hypertrophy in each subject, additional hypertrophy parameters were calculated. These parameters included left ventricular mass (LVM). LVM was calculated by using the formula for the estimation of LVM from 2-D LV linear dimensions, as recommended by the American Society of Echocardiography:

$LVM = 0.8 \times (1.04[\ (LVIDd + PWTd + SWTd)^3 - (LVIDd)^3\ ] + 0.6g$

Additionally, principle component analysis was performed to statistically define composite scores that best reflect the variability in left ventricle-wide hypertrophy. Each wall thickness measurement was transformed to approximate normality using quantile normalization prior to this analysis (Pilia *et al*., 2006).

2.20. BLOOD COLLECTION AND DNA EXTRACTION

2.20.1. Blood collection

The subjects' blood was collected in 2x 5ml ethylene-diamine-tetra-acetic acid (EDTA) tubes (Vacutainer, RSA) for DNA extraction. Blood was also collected in 1x 10ml heparin tubes (Vacutainer, RSA) to establish

permanent lymphoblastoid cell lines using the method described by Neitzel (1986). Blood samples collected from subjects at other South African centres were couriered to the research laboratory within 24h of sampling.

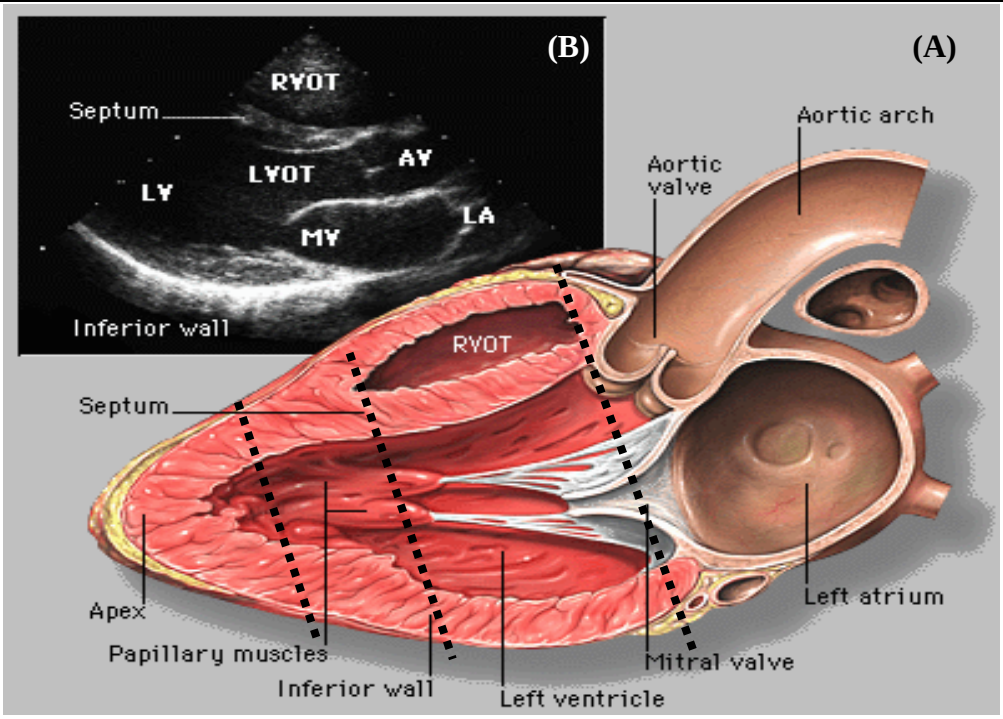

Figure 2.1. Graphical representative example of the heart showing the 3 levels at which measurements of wall thickness were made. A) Long-axis view of left ventricle, taken at level of mitral valve, papillary muscles as well as just above apex (levels indicated by dotted lines). B) An example of a 2D echocardiographic ultrasound of the left ventricle. Abbreviations: AV - aortic valve, LA - left atrium, LV - left ventricle, LVOT - left ventricular outflow tract, MV - mitral valve, RVOT - right ventricular outflow tract. Taken from http://www.med.yale.edu/.../aortic_regurgitation.html with minor modifications by JC Moolman-Smook.

2.20.2. Extraction of nuclei from whole blood

DNA was extracted from nucleated blood cells according to the method described by Corfield *et al.* (1993) with slight modifications. All DNA extractions, cell transformations and maintenance were performed by Mrs. Ina le Roux, with a list of all solutions used for DNA extractions provided in Appendix I.

2.21. BIOINFORMATICS

2.21.1. Selection of Candidate Genes

The genes encoding MMGL (*PDE4DIP*) as well as two regulatory subunits of PKA (*PRKAR1A* and *PRKAR2A*) were chosen as candidate genes for the modifier study. Variants in these three genes may influence cardiac contractility, and hence hypertrophy development, because of the involvement of PKA in the phosphorylation of cMyBPC, which plays a crucial role in optimal cardiac contractility and therefore possibly hypertrophy

development in mutant individuals. Of the four PKA R-subunit genes (*PRKAR1A*, *PRKAR2A*, *PRKAR1B* and *PRKAR2B*), *PRKAR1A* and *PRKAR2A* were chosen because *PRKAR1A* is known to interact with PDE4D (Dodge *et al.*, 2001) while it has been shown that *PRKAR2A* has a high cardiac expression (www.genecards.org). Table 2.12 shows the candidate genes chosen for investigation as well as their respective protein functions.

Table 2.12. Candidate genes chosen for SNP variant genotyping study

Gene	Location on chromosome	Size (bp)	Protein function
PDE4DIP	1q12	1604	Acts as structural/scaffolding protein to localize components of the cAMP dependent pathway
PRKAR1A	17q23	3653	Forms part of the regulatory-subunit dimer of the PKA heterodimer, which phosphorylates various substrates
PRKAR2A	3p21	2381	Forms part of the regulatory-subunit dimer of the PKA heterodimer, which phosphorylates various substrates

Abbreviations: *PDE4DIP* - phosphodiesterase 4D interacting protein, *PRKAR1A* - Protein kinase cAMP-dependant regulatory, type 1, alpha, *PRKAR2A* - Protein kinase cAMP-dependant, regulatory, type 2, alpha, cAMP-3'5'-cyclic adenosine monophosphate, PKA - protein kinase A, SNP - single nucleotide polymorphism

2.21.2. SNP selection

Genetic map distance was defined in terms of linkage disequilibrium units (LDUs) by Maniatis *et al.* (2002). According to Maniatis *et al.*, LDUs define a metric coordinate system where locations are additive and distances are proportional to the allelic association between markers. Linkage disequilibrium (LD) maps can be efficiently used to position markers for population-based disease association studies, and are analogous to genetic maps expressed in centi-Morgans (cM) (Collins *et al.*, 2004).

For *PRKAR1A* and *PRKAR2A*, SNPbrowser v 3.5.3 software was used to select SNPs for the present study to achieve an even spacing of 0.5 LDUs on the metric LD map for the Central European (CEU) and Yoruba (YRI) populations, using default parameters set on the software (De La Vega, 2007). The software utilizes a set of metric LD maps constructed from the HapMap NCBI b36 assembly using the LDMAP software (Kuo *et al.*, 2007). Using the LDMAP software, SNPs that are in perfect LD have zero distance between them, whereas SNPs without significant correlation are separated by more than three LDUs (De La Vega *et al.*, 2006).

Only SNPs for which validated TaqMan® SNP genotyping assays were available were chosen. For *PDE4DIP*, such SNPs were selected manually based on a criterion of a minor allele frequency (MAF) of 0.2 or more for the CEU or YRI population. By means of its chromosomal position obtained from Genecards, the various SNPs were spread out approximately evenly across the gene, aiming to cover more or less the whole gene. A list of SNPs chosen for investigation is given in Table 2.13.

2.22. TaqMan® SNP GENOTYPING

Genotypes were deteremined for all the subjects by subjecting the DNA samples to TaqMan® allelic discrimination technology using the ABI TaqMan® Validated SNP Genotyping Assays (Applied Biosystems, Foster City CA, USA).

Each ABI TaqMan® Validated SNP Genotyping Assay consists of two primers to amplify the sequence of interest, as well as two TaqMan® MGB probes for allele detection. Each probe contains a reporter dye at the 5' end of each allele-specific probe (the allele 1 probe contains the VIC reporter dye, and the allele 2 probe contains the FAM reporter dye). The probes also contain a minor groove binder (MGB) and a non-fluorescent quencher (NFQ) at the 3' end of each probe. The function of the MGB is to increase the probe's melting temperature (T_m) without increasing the probe length, which results in greater differences in T_m values between matched and mismatched probes, giving more accurate allelic discrimination (Kutyavin *et al.*, 2000). Figure 2.2 explains how detection is achieved with proven 5' nuclease chemistry by means of exonuclease cleavage of a 5' allele-specific dye label, generating a permanent assay signal by removing the effect of the 3' non-fluorescent quencher.

2.22.1. Real-time PCR amplification conditions

Amplification of each SNP was done by polymerase chain reaction (PCR) in a single reaction tube on a thermostable 384-well plate on an ABI Prism 7900HT Sequence Detection System (Applied Biosystems Inc, Foster City CA, USA) following manufacturer's instructions. An EpMotion® liquid handling robot was used to dispense the PCR reagents and samples into the 384-well plates (Eppendorf, Hamburg Germany). Each PCR reaction consisted of 2.5µl ABI TaqMan® Universal PCR Master Mix, 10ng genomic DNA, 0.25µl ABI TaqMan® primer and probe dye mix and 1.25µl Dnase-free sterile filtered water, totaling a 5µl reaction mix. Each thermostable 384-well plate consisted of 330 PCR amplifications and 54 non-template controls which lacked genomic DNA in the sample, to serve as a test for contamination. Each reaction was subsequently subjected to PCR conditions as follows: 2min at 50°C, 10min at 95°C, followed by 40 cycles of 15sec at 92°C and 1.5min at 60°C each.

Table 2.13. SNPs chosen for investigation as well as the respective TaqMan® assays used for genotyping each variant

Gene	SNP ID	Chromosome	Chromosomal position (bp)	Nucleotide change	ABI TaqMan® Assay
PDE4DIP	rs1628172	1	143623510	a/g	C_42456720_10
	rs12409452	1	143640607	a/g	C_42456764_10
	rs2798892	1	143643577	a/c	C_42456794_10
	rs2798880	1	143659232	a/g	C_42456918_10
	rs1664005	1	143699625	a/g	C_42457524_10
	rs7516133	1	143726347	c/t	C_42457945_10
	rs771114	1	143745154	c/t	C_42458222_10
	rs7548981	1	143749946	c/g	C_42458295_10
	rs674143	1	143772125	a/g	C_42458629_10
PRKAR2A	rs3774628	3	48776844	a/g	C_27499285_10
	rs3923913	3	48817868	c/t	C_26008486_10
	rs9755490	3	48846668	a/c	C_26861278_10
PRKAR1A	rs4265886	17	64021487	c/t	C_221617_10
	rs11651687	17	64029901	a/g	C_11630616_10
	rs3785906	17	64035235	a/g	C_341301_10
	rs6958	17	64040373	c/g	C_7461387_10

Abbreviations: *PDE4DIP* - phosphodiesterase 4D interacting protein, *PRKAR1A* - Protein kinase cAMP-dependant,regulatory, type 1, alpha, *PRKAR2A* - Protein kinase cAMP-dependant,regulatory, type 2, alpha, SNP - single nucleotide polymorphism, bp - base pairs

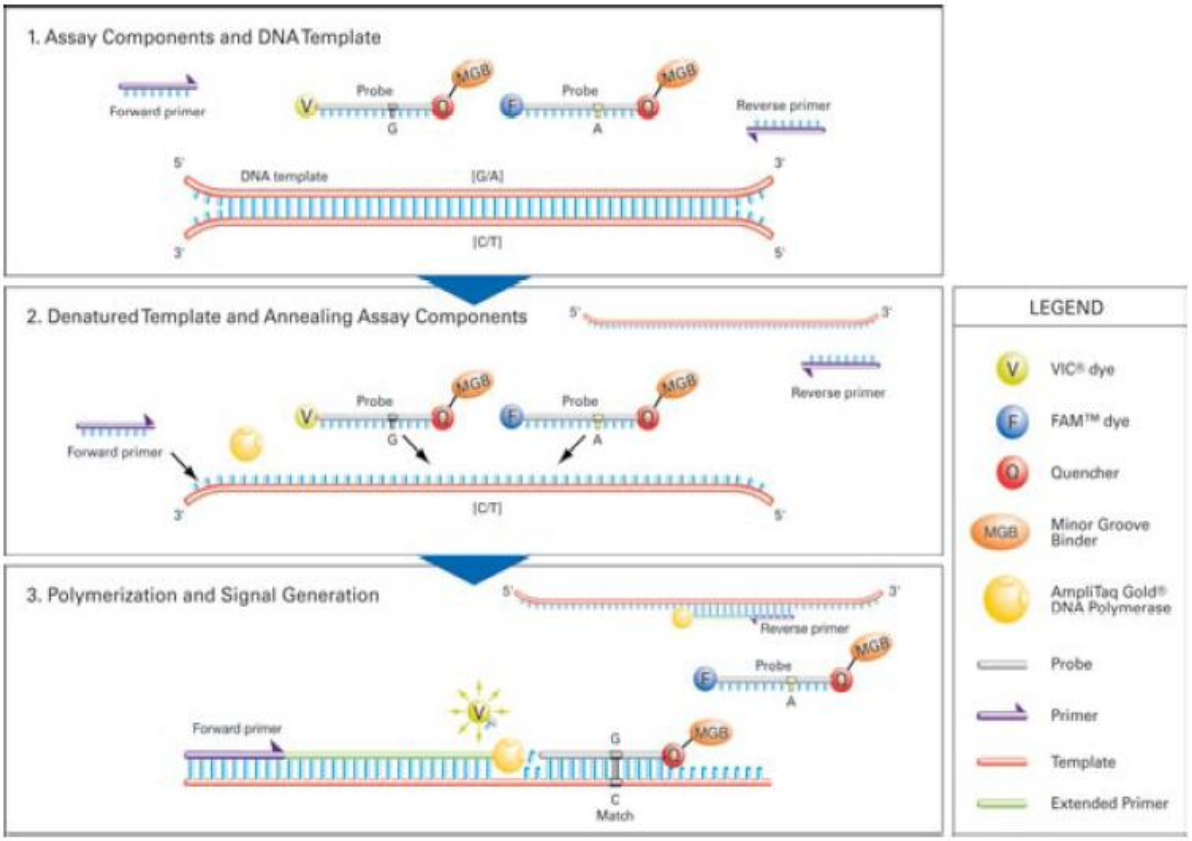

Figure 2.2. Overview of TaqMan® allelic discrimination technology. Selective annealing of the TaqMan® probes plus exonuclease cleavage of a 5' allele-specific dye label generates the assay signal, enabling allelic discrimination (taken from TaqMan® SNP Genotyping Assays Product Bulletin, Applied Biosystems).

2.22.2. Allelic discrimination

Allelic discrimination was achieved by running end point detection using ABI Prism 7900HT and Sequence Detection System (SDS) 2.3 software (autocaller confidence level 95%). The software allows for reading of fluorescence and does automatic allele calling by generating allelic discrimination plots. Subsequently, a text file was generated and directly incorporated into a database. The results obtained were additionaly confirmed by visual inspection of the real-time PCR multicomponent analysis plots.

2.23. STATISTICAL ANALYSIS

The Cyrillic 2.1 (Cherwell Scientific, UK) program was used to enter genotypic and phenotypic data of patients onto family trees. This program was then used to export pedigree and genotypic data in MLINK format; this data was then collated with the appropriate echocardiographic and covariate data in an Excel spreadsheet, to create a pedigree file for statistical analysis.

In order to investigate the association between polymorphisms and hypertrophic traits, family-based tests for association were used, employing the QTDT (quantitative transmission disequilibrium test) program developed by Abecasis *et al*. (2002). The advantage of using family-based association tests is that it allows tracing of the transmission of alleles associated with hypertrophic phenotypes from parent to offspring in multiple generations. In order to adjust for various known confounding variables, as well as for specific relatedness between family members in estimating the various variance components (viz. environment, polygenic and specific genes), linear mixed-effect models were used within the QTDT program. QTDT allows for the assessment of linkage, population stratification and association of quantitative traits, depending on the model implemented in the program. In this study, after performing a population stratification test, both the orthogonal and total model of the QTDT program were used assess particular phenotype-genotype associations.

2.23.1. Descriptive statistics and trait distribution

Pedstats v. 6.11 (Wigginton and Abecasis, 2005) was used to verify the validation of input files and Mendelian inheritance within families. It was also used to test conformance of genotypes with Hardy-Weinberg equilibrium (HWE). Graphical summaries were generated of allele and genotype frequencies, as well as the distribution and familial correlations of quantitive traits and covariates. Pedstats selected unrelated individuals from families for Hardy-Weinberg testing and frequency estimation.

2.23.2. Linkage disequilibrium (LD) determination

Utilizing the genotype data generated in this study, pairwise LD statistics for the study cohort was generated using Haploview v. 4.1 (Barrett *et al*., 2005). Pairwise LD was analysed in terms of D' values, and each SNP variant was classified as being in strong, uncertain or no LD. The program also enables haplotype analysis by constructing haplotypes using a common block definition (Gabriel *et al*., 2002). In the case of a D' value indicating strong LD, a haplotype block is created.

2.23.3. Quantitative transmission disequilibrium test

A pedigree and data file was created as specified by the QTDT tutorial (http://www.sph.umich.edu/csg/abecasis/QTDT/) for all subsequent analyses of all the quantititive hypertrophic traits. Simwalk2 was used to estimate the specific relationship between family members by integrating the analyses using identity-by-descent (IBD) probalities (Sobel *et al*., 2001). The following covariates were also included: systolic BP, diastolic BP, age, sex, BSA and HR. The three founder groups (A797T, R403W and R92W) were also included to adjust for ancestral relatedness within each founder group and to correct for the possible influence of the distinct HCM causal mutation on variability of the hypertrophic phenotype.

Two different QTDT models were used viz. the total model and the orthogonal model. The total model allows for more statistical power, but does not compensate for population stratification. The orthogonal model is robust to population stratification, but has less power as only certain matings are included in the test. A test for population stratification was therefore done, and the orthogonal mode used for SNPs where stratification was detected, and the total model where no stratification was observed. For the orthogonal model, exact p-values for all QTDT significant associations were determined using Monte-Carlo permutation tests (McIntyre *et al.*, 2000).

CHAPTER THREE: RESULTS

INDEX **PAGE**

CHAPTER 3: RESULTS

3.1. INTERACTION OF TRISPHOSPHO-cMyBPC WITH MYOMEGALIN

As the interactions of the N-terminal region of cMyBPC under its various phosphorylation states appear to be integral to the regulatory role of cMyBPC in contracility, a series of Y2H library screens using various phosphorylation-mimics of the C1-C2 region of the protein as bait have been performed in our laboratory. Of particular relevance to this study, was the library screen in which a construct of C1-C2 was used in which the serines in the three phosphorylation sites of the MyBPC motif had been replaced by glutamic acids (PPP) was used as bait to gain further insight into the interactions of the trisphosphorylated form of the N-terminal region of cMyBPC (A. Ramburan, PhD thesis).

During successive rounds of nutritional and colorimetric selection, 19 putative interactors of the trisphosphorylated mimic of cMyBPC were identified, which were able to activate the *HIS3*, *ADE2* and *MEL1* reporter genes in the presence of the PPP bait, but not in the presence of heterologous baits. Of these, three in-frame prey plasmids encoded isoform 4 of PDE4D-interacting protein, also known as myomegalin (MMGL). In order to verify that it is the C1-C2 region of cMyBPC that interacts with MMGL, and not the GAL4 regions of the Y2H bait protein, and to assess whether trisphosphorylation of the MyBPC motif was crucial to the putative interaction, the native C1-C2 as well as a trisphospho-mimic were used in *in vitro* co-immunoprecipitation assays. The results indicated that MMGL interacts with the native as well as the trisphospho-mimic of C1-C2 in the absence of the Y2H GAL4 domains (A. Ramburan, PhD thesis).

This interaction between MMGL and the N-terminal of cMyBPC was intriguing, as the former protein is known to anchor PDE4D to particulate structures; PDE4D, in turn, is known to hydrolyze cAMP and thus to attenuate PKA-driven phosphorylation (Verde *et al*., 2001). Furthermore, it has been shown that some adaptor proteins can anchor both PKA and PDE4D (Dodge *et al*., 2001), raising the possibility that MMGL may be anchoring PKA to at least cMyBPC in the sarcomere as an AKAP; hence this interaction was prioritized for further investigation in the present study.

3.2. MYOMEGALIN BINDS TO PKA REGULATORY SUBUNITS

3.2.1. Direct Y2H protein-protein interaction assays

One of the prerequisites for a protein to be classified as an AKAP is the ability to bind to a regulatory subunit of PKA (Colledge *et al*., 1999, Dodge *et al*., 2000). The possibility that MMGL isoform 4 functions as an AKAP was therefore investigated by using direct Y2H protein-protein interaction assays to determine binding between MMGL and two regulatory subunits of PKA, viz. PRKAR1A and PRKAR2A. PRKAR1A was prioritized as potential subunit based on its known interaction with PDE4D (Dodge *et al*., 2001), whereas PRKAR2A is highly expressed in the heart (www.genecards.org).

The PKA regulatory subunits PRKAR1A and PRKAR2A were cloned into the pACT2 vector, which expresses the PKA subunits fused to the GAL4 DNA activation domain, and transformed into the yeast strain Y187. Subsequently, small scale yeast matings (Section 2.14.10) were performed by mating the PKA regulatory subunit clones with pGBKT7-MMGL in AH109, expressing the MMGL isoform 4 fused to the GAL4 DNA binding domain. Control matings were also carried out by mating pGBKT7-MMGL with empty pACT2 and pACT2-TUSC4, which encodes a heterologous protein viz. tumour suppressor candidate 4.. The interaction observed between pGBKT7-MMGL and pACT2-cTNI, one of the strongest bait-prey interactions observed in the Y2H library screen (see section 3.3.2.), was used as a positive control to compare PKA-MMGL interaction.

Positive interaction was observed between both the PKA regulatory subunits and MMGL. However, PRKAR2A appeared to show a stronger interaction with MMGL than PRKAR1A, as judged by the number and colour of colonies arising as result of activation of nutritional reporter genes by PKA subunit-MMGL interaction, as shown in Figure 3.1.

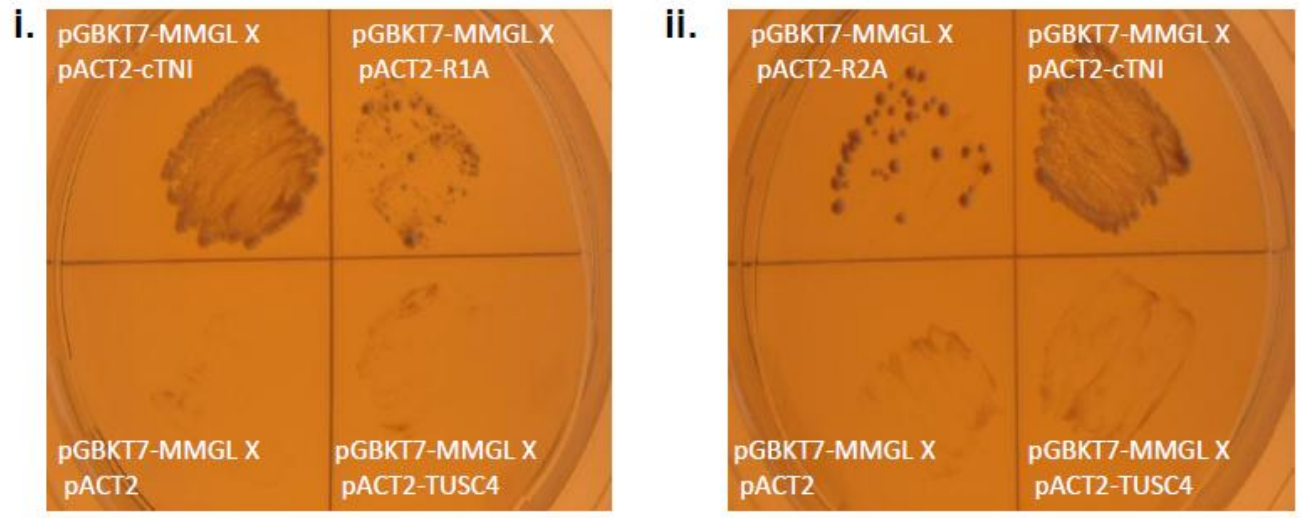

Figure 3.1. Activation of nutritional reporter genes by PKA-MMGL interaction during direct protein-protein interaction assays. Small-scale Y2H matings between pGBKT7-MMGL and pACT2-PRKAR1A (i) and pACT2-PRKAR2A (ii) on solid medium lacking Leu, Trp, His and Ade (QDO). Both subunits show interaction with MMGL, but that of PRKAR2A with MMGL appears to be stronger than that of PRKAR1A, as judged by the number and colour of colonies arising. n=2

3.2.2. Three dimensional *in vivo* co-localization of MMGL and PKA regulatory subunits

To assess the interactions of the PKA regulatory subunits with MMGL identified by Y2H in a cellular environment, *in vivo* co-localization, using fluorescence microscopy, was used. In the images presented below and in all similar images that follows, a panel represents a single frame of the 25 images that were captured for

the Z-stack. In the following figure, images i-iii shows a single colour channel, while image iv shows an overlay of the four colour channels used.

According to the results obtained via this technique, MMGL was shown to exist in the same three dimensional subcellular space as both PKA regulatory subunits viz. PRKAR1A and PRKAR2A in H9C2 cardiomyocytes (Figure 3.2). This supports the hypothesis that MMGL acts as an AKAP because of its ability to anchor PKA regulatory subunits; furthermore, it suggests that MMGL might act as a dual-specific AKAP because of its ability to anchor not only one, but two types of PKA regulatory subunits (Colledge and Scott, 1999; Wang *et al*., 2001).

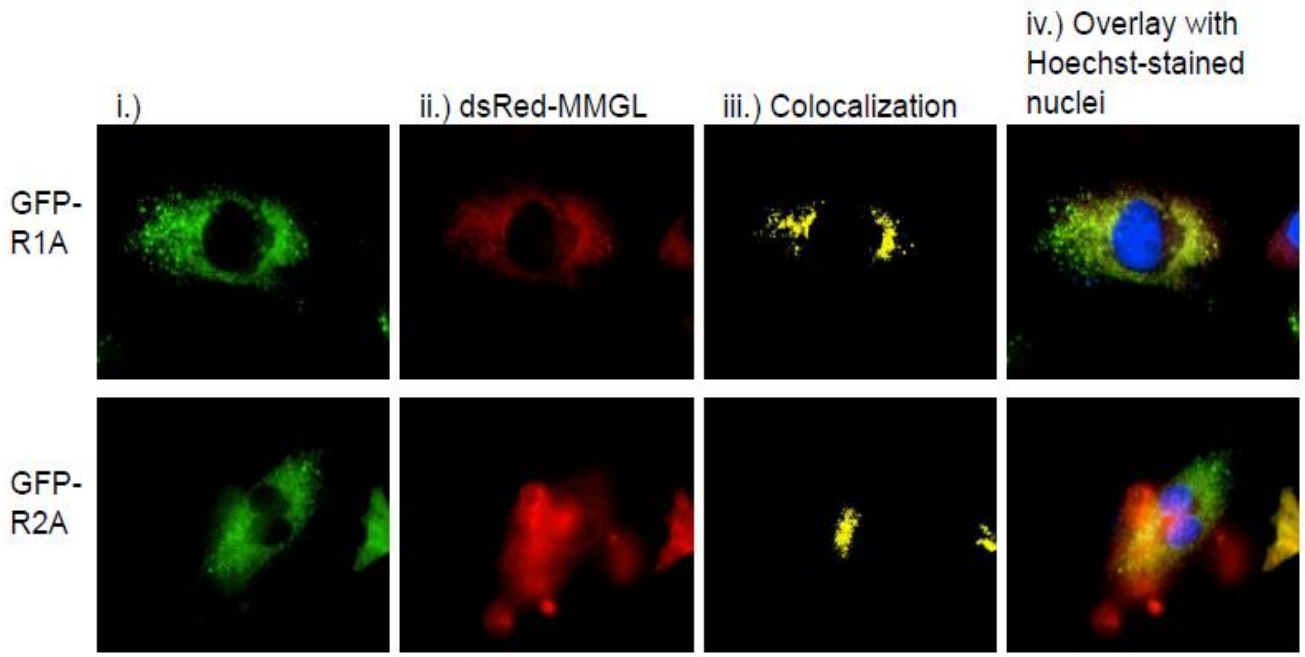

Figure 3.2. Live cell fluorescence imaging of co-localization of MMGL with PRKAR1A and PRKAR2A in differentiated H9C2 cardiomyocytes. (i) GFP-tagged PRKAR1A and PRKAR2A (green). (ii) dsRed-tagged MMGL (red). (iii) Co-localization of PRKAR1A and PRKAR2A with MMGL (yellow). (iv) Overlay of images A-C with Hoechst H-33342 labeling of the nuclei (blue). Magnification: 60X oil immersion before 70% reduction

3.2.3. *In vivo* co-immunoprecipitation of MMGL and PKA regulatory isoforms

To further verify physical interaction between MMGL and these PKA regulatory isoforms in a cellular context and in the absence of GAL4 domains, pull-down assays in differentiated H9C2 cardiomyocytes were performed. As commercial antibodies against MMGL did not detect isoform 4, which is the smallest isoform of this protein and the one identified in the original Y2H screen, an antibody directed against dsRed fluorescent protein was used in a pull-down assay to detect a dsRed-fusion of MMGL isoform 4 (dsRed-MMGL) (Section 2.8.2). In this

way, endogenous PRKAR1A and PRKAR2A were shown to immunoprecipitate dsRed-MMGL, and *vice versa* (Figure 3.3).

Figure 3.3. Western blots of *in vivo* co-immunoprecipitations of PKA regulatory subunits and MMGL. (i) Endogenous PRKAR1A and PRKAR2A immunoprecipitate exogenous dsRed-MMGL in lysates of pDs-Red/MMGL-transfected, differentiated H9C2 cardiomyocytes. Conversely, (ii) PRKAR1A and (iii) PRKAR2A also immunoprecipitate exogenous dsRed-MMGL in these lysates. The clear protein G control lanes show that these precipitations are not spurious, but are the result of physical association between the relevant proteins. Additional lanes in (ii) have been removed for cosmetic effect. *Abbreviations:* IP-immunoprecipitate; Prot G-protein G control; WB-western blot

Taken together, the direct protein-protein Y2H assays, the fluorescent co-localization images as well as the pull-down assays all supports the hypothesis that MMGL acts as an AKAP because of its interactions with both PKA regulatory subunits. Moreover, considering that only one such interaction is already sufficient to classify a protein as an AKAP, MMGL can therefore be described as a dual-specific AKAP.

3.3. MYOMEGALIN BINDS TO ADDITIONAL PKA TARGETS

The function of MMGL isoform 4 was further investigated by using it as a Y2H bait to screen a pretransformed cardiac cDNA library in order to identify any additional binding partners, other than cMyBPC and the PKA regulatory isoforms.

3.3.1. Y2H analysis of MMGL

3.3.1.1. Sequence analysis of the bait construct

After the generation of the pGBKT7-MMGL bait construct, DNA sequence analysis was done to verify the integrity of the sequence and that the reading frame had been retained. The results of this analysis showed that the bait was in the correct reading frame, and that the integrity of the nucleotide sequence had been retained throughout the construction process.

3.3.1.2. Phenotype test

The transformed yeast strain AH109 containing the bait construct was able to grow on appropriate selection media (SD^{-W} and SD^{-U}) but unable to grow on selection media lacking other essential amino acids (SD^{-A}, SD^{-L}, SD^{-H}) (Section 2.13.1). This confirmed that the phenotype of the AH109 strain was retained after transformation with the pGBKT7-MMGL construct.

3.3.1.3. Toxicity test

A growth curve (Section 2.13.2) was generated in order to establish whether the pGBKT7-MMGL construct was toxic to the yeast strain AH109 in which the growth of the AH109 yeast strain transformed with pGBKT7-MMGL was compared to the growth of AH109 transformed with non-recombinant pGBKT7. It was concluded that the pGBKT7-MMGL construct had no toxic effect on the growth of the AH109 yeast strain, because the slope of the linearized test curve proved to be similar to the slope of AH109 transformed with non-recombinant pGBKT7 (Figure 3.4).

3.3.1.4. Mating efficiency of AH109 transformed with pGBKT7-MMGL bait construct

A small-scale yeast mating (Section 2.13.3) was done in order to determine whether the transformation of the pGBKT7-MMGL bait had significantly affected the mating ability of the AH09 host strain. The mating efficiency of pGBKT7-MMGL (in host strain AH109) and pACT2 (in host strain Y187) was compared to the mating efficiency of pGBKT7-53 and pACT2. The results of this mating efficiency test showed that the pGBKT7-MMGL bait construct did not affect the mating efficiency of AH109, seeing that the mating efficiency of the MMGL test was higher than the minimum of 2% that is suggested by the manufacturer of the MATCHMAKER Y2H system (Table 3.1).

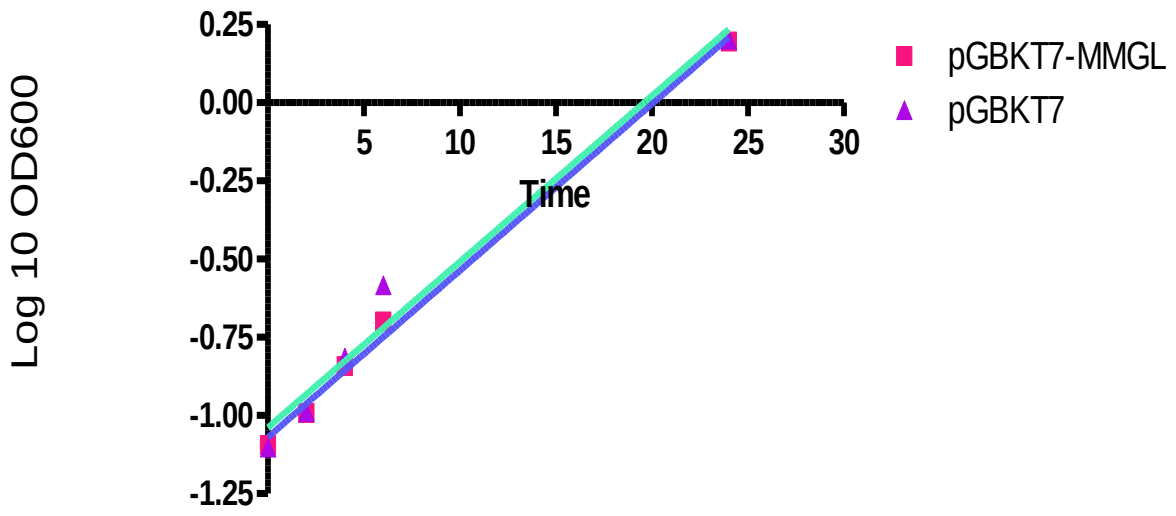

Figure 3.4. Linear growth curve of yeast strain AH109 transformed with either non-recombinant pGBKT7 or pGBKT7-MMGL bait constructs. The growth rate of the pGBKT7-MMGL bait transformant were compared to the non-recombinant pGBKT7 transformant in order to determine whether the bait constructs had toxic effects on the AH109 strain. The growth rate was determined by calculating the slope of the curve, and, seeing that the slopes were comparable, indicated that the bait construct had no toxic effect on the growth of the host yeast strain.

Table 3.1. Effect of the pGBKT7-MMGL bait construct on AH109 mating efficiency

Mating tests	**Mating efficiency (%)**
pGBKT7-53:AH109 x pACT2:Y187	2.33
pGBKT7-MMGL:AH109 x pACT2:Y187	8.33

3.3.2. Y2H screening of pretransformed cardiac cDNA library with the pGBKT7-MMGL bait

After meeting the quality control criteria discussed above, the pGBKT7-MMGL bait was used to screen a cardiac cDNA library, and it was calculated that approximately 7 x 10^6 cardiac cDNA clones were screened. Judging from the growth of the colonies on TDO plates (Table 3.2), 1130 clones were able to activate the *HIS3* reporter gene. From these 1130 clones, 872 clones were able to activate the *ADE2* reporter gene, judged by the growth on the QDO plates (Table 3.2). After the X-α-galactosidase assay, a further 612 clones that were unable to activate the *MEL1* reporter gene were eliminated (Table 3.2). The 260 clones that were able to activate the *MEL1* reporter gene were grouped into 93 primary clones, and 167 secondary clones, based on colour intensity in the X-α-galactosidase assay, as well as robustness of growth on the QDO plates. Heterologous bait matings

were subsequently performed on all primary and secondary prey colonies, to assess the specificity of interactions of these prey clones in pACT2 with the pGBKT7-MMGL bait (Table 3.3)

The preys that showed specific interaction with the pGBKT7-MMGL bait in the heterologous bait matings were nucleotide sequenced and identity was determined by utilizing online nucleotide and protein sequence databases as described in Section 2.5. Only the preys whose nucleotide sequence was in the appropriate reading frame as dictated by the upstream GAL4 sequence were considered as putative positive interactors of pGBKT7-MMGL and are shown in Table 3.4.

3.3.3. Y2H library screen in summary

From the 1130 clones that were able to activate the *HIS3* reporter gene, 872 clones were able to activate the *ADE2* reporter gene. Following this test, a further 612 clones were eliminated which left 260 clones that could activate the *MEL1* reporter gene, and these 260 clones were subsequently tested for interaction specificity via heterologous bait matings. As seen in Table 3.3, only 13 clones passed the stringent bait-specificity (heterologous bait mating) test, and were sequenced to determine their identities. Table 3.4 shows the identities of these putative interactors. Because we were particularly interested in the role that MMGL may play in the phosphorylation of cMyBPC, and hence cardiac contractility, only identified interactors with known roles in this particular area of the sarcomere were prioritized for further investigation in the present study. The mitochondrial protein COX5A, proteasome 26S subunit and sorting nexin 3 (SNX3) were therefore eliminated as putative interactors of myomegalin for the purposes of this study. The putative interactors of myomegalin identified via the Y2H library screen were therefore as follows: troponin (cTNI), cardiac ankyrin repeat protein (CARP), COMM domain containing 4 (COMMD4), enolase 1 (ENO1) and enolase 3 (ENO3).

cTNI is a well-known thin filament protein and was identified six times in the library screen. Moreover, it is a known PKA target (Patel *et al.*, 2001), which further supports the hypothesis that MMGL acts as an AKAP. The remaining preys had been identified in one or more of the cMyBPC-related library screens, indicating that they may well occur in the vicinity of the sarcomere. Using Phosphomotif Finder (www.hprd.org/Phosphomotif_finder), the remaining putative interactors were also shown to be likely PKA targets.

Table 3.2. Activation of nutritional and colourimetric reporter genes by prey-MMGL interaction. Tabulated are a representative subset of the scoring of the 1130 clones that activated the *HIS3* reporter gene, 872 clones that activated the *ADE2* reporter gene and 260 clones that activated the *MEL1* reporter gene.

Clone #	A Growth on TDO (*HIS3* activation)	B Growth on QDO (*ADE2* activation)	C X-α-galactosidase assay (colour) (*MEL1* activation)
1	+++	+++	++ (medium blue)
11	++++	+++	++ (medium blue)
76	++++	++++	+++ (dark blue)
163	+++	++	+ (no blue)
192	+++	+++	+++ (dark blue)
258	++++	+++	++ (medium blue)
329	+++	+	+ (light blue)
495	++++	++++	+++ (dark blue)
550	+++	++	++ (no blue)
618	++	++	+ (light blue)
715	++++	++++	+++ (dark blue)
744	++	+	+ (no blue)
885	++++	+++	++ (medium blue)
992	+++	+++	+ (light blue)
1108	++	++	+ (no blue)

Colonies in blue font activated *HIS3*, *ADE2* and *MEL1* reporter genes. TDO = solid media lacking Leu, Trp and His; QDO = solid media lacking Leu, Trp, His and Ade. Growth of colonies on solid media: ++++=very good, +++=good, ++=weak, +=very weak, -=no growth

Table 3.3 Interaction of the preys with heterologous baits in specificity tests. Tabulated is a representative subset of the scoring of the clones that were subjected to heterologous bait mating; all the clones considered as putative interactors are highlighted in red

Clone #	pGBKT7-MMGL	pGBKT7-53	pGBKT7-C5	Reelin	pGBKT7
11	++++	+	++++	-	+
24	++++	++++	++++	++++	++++
73	++++	+	++++	-	+
128	+++	++	+	-	-
130	++++	-	-	-	-
137	+++	-	-	-	-
148	++	+	-	+	-
149	+++	-	-	+	-
160	+++	+	+	-	-
192	+++	++	+	-	-
200	++	-	-	+	-
203	+++	-	-	+	-
287	+++	++++	++++	+	+
495	+++	++++	++++	++++	++++
583	++++	++	++++	-	-
695	++++	++++	++++	++++	++++
715	+++	-	++	+	-

Colonies were scored after 7 days on QDO. QDO = solid media lacking Leu, Trp, His and Ade. Growth of colonies on solid media: ++++ = very good, +++ = good, ++ = weak, + = very weak, - = no growth

Table 3.4 Identification of MMGL putative interactor clones from the Y2H cardiac cDNA library screen.

	Genomic hit **BLASTN**			**In-frame protein hit** **BLASTP**		
Clone #	**Identity**	**Accession # E-value**	**Accession # E-value**	**Size of peptide encoded by insert (amino acids)**	**Cellular localisation**	**Domains**
128	*Homo sapiens* troponin I type 3 (cardiac) (TNNI3)	NM 000363, 0.0	NP 000354.3, 2e-82	237	Thin filament	Troponin
160	*Homo sapiens* troponin I type 3 (cardiac) (TNNI3)	NM 000363, 0.0	NP 000354.3, 2e-65	263	Thin filament	Troponin
137	*Homo sapiens* troponin I type 3 (cardiac) (TNNI3)	NM 000363, 0.0	P 19429, 3e-63	273	Thin filament	Troponin
148	*Homo sapiens* troponin I type 3 (cardiac) (TNNI3)	NM 000363, 0.0	P 19429, 1e-62	237	Thin filament	Troponin
149	*Homo sapiens* troponin I type 3 (cardiac) (TNNI3)	NM 000363, 0.0	P 19429, 5e-42	243	Thin filament	Troponin
200	*Homo sapiens* troponin I type 3 (cardiac) (TNNI3)	NM 000363, 0.0	P 19429, 3e-55	244	Thin filament	Troponin

	Genomic hit BLASTN		In-frame protein hit BLASTP			
Clone #	**Identity**	**Accession # E-value**	**Accession # E-value**	**Size of peptide encoded by insert (amino acids)**	**Cellular localisation**	**Domains**
192	*Homo sapiens* Cardiac ankyrin repeat protein (CARP)	NM 014391, 0.0	NP 055206, 2e-121	383	Cytosol, nucleus	Ankyrin repeat
583	*Homo sapiens* COX5A	NM 004255, 0.0	NP 004246.1, 8e-67	204	COX5A	Mitochondrion
715	*Homo sapiens* COMM domain containing 4 (COMMD4)	NM 017828, 0.0	NP 060298.2, 3e-97	203	COMMD4	Cytoplasm
73	*Homo sapiens* proteosome (prosome, macropain) 26S subunit	NM 002812, 0.0	NP 002803.1, 5e-113	277	Nin 1 C	Cytosol
130	*Homo sapiens* Enolase 1 (alpha) (ENO1)	NM 001428, 0.0	NP 001419, 4e-116	280	Enolase	Cytoplasm
203	*Homo sapiens* Enolase 3 (beta, muscle) (ENO3)	NM 053013, 0.0	NP 001967,1, 0.001	362	None	Cytoplasm, localised to Z-line

	Genomic hit BLASTN		In-frame protein hit BLASTP			
Clone #	**Identity**	**Accession # E-value**	**Accession # E-value**	**Size of peptide encoded by insert (amino acids)**	**Cellular localisation**	**Domains**
11	*Homo sapiens* Sorting nexin 3 (SNX3)	NM 003795, 0.0	NP 003786.1, 8e-62	185	Phox (PX)	Cytosol

3.3.4. 3D *in vivo* co-localization of MMGL and putative interactors identified in the Y2H library screen

To assess the interactions of the putative ligands identified by Y2H with MMGL in a cellular environment, *in vivo* co-localization, using fluorescence microscopy, was used. It was shown that MMGL occurs in the same three dimensional subcellular space as all five putative interactors identified in the Y2H library screen viz. CARP, COMMD4, ENO1, ENO3 and cTNI (Figure 3.5). No nuclear expression was observed with any of the proteins. In the images presented, a panel represents a single frame of the 25 images that were captured for the Z-stack. In Figure 3.5, images (i-iii) shows a single colour channel, while image (iv) shows an overlay of the four colour channels used.

3.3.5. *In vivo* co-immunoprecipitation of MMGL and putative Y2H interactors

To further verify physical interaction between MMGL and these ligands in a cellular context and in the absence of GAL4 domains, pull-down assays in diffentiated H9C2 cardiomyocytes were performed. As commercial antibodies against MMGL did not detect isoform 4, which is the smallest isoform of this protein, antibodies directed against pDs-Red/pYFP was used to detect dsRed-/YFP-fusions of MMGL isoform 4 (dsRed-MMGL/YFP-MMGL) (Section 2.8.2). Exogenous, fluorescently-tagged YFP-MMGL and endogenous CARP reciprocally co-precipitated each other (Figure 3.6 i), with dsRed-MMGL reciprocally co-precipitating endogenous ENO1, ENO3, and cTNI, as shown in Figure 3.6 (ii-iv). As COMMD4 had a similar mobility to antibody light chains, which interfered with detection of the protein in western blots, a GFP-tagged fusion of COMMD4 was expressed in H9C2 cells for pull-down assays. Figure 3.6 (v) shows that in the assay, exogenous GFP-COMMD4 immunoprecipiated exogenous dsRed-MMGL, and *vice versa*.

It is not immediately clear why the dsRed-MMGL fusion protein appeared to have migrated slower during electrophoresis, which occurred during repeat experiments under different gel conditions. However, in other independent experiments conducted in our laboratory using dsRed fusions of different proteins, the same occurrence was observed.

The results presented thus far therefore strongly suggests that MMGL interacts with both PKA regulatory isoforms, as well as with each of the prioritized five putative prey interactors identified in the Y2H screen, in a cellular milieu, and in the absence of the GAL4 domains.

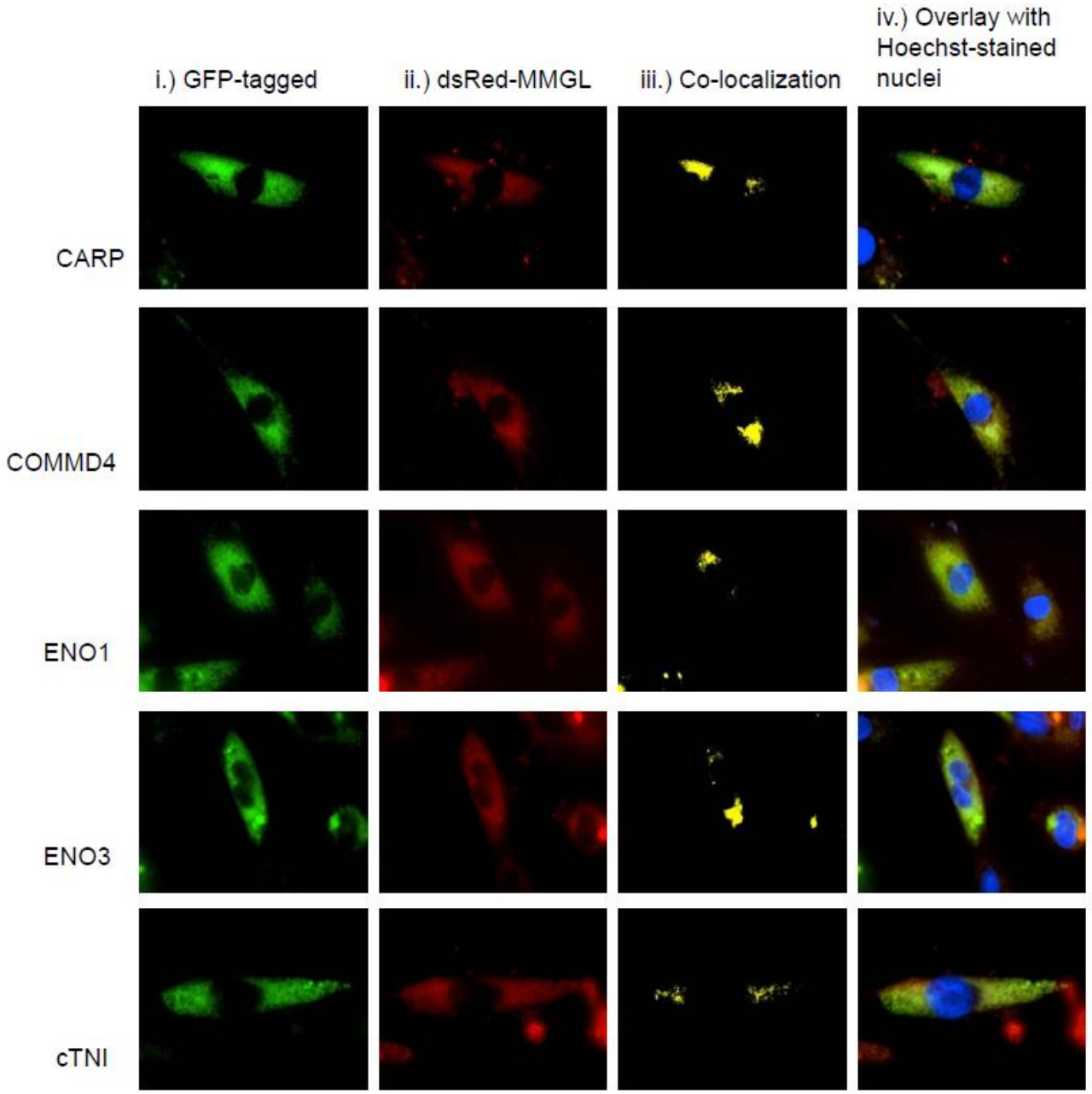

Figure 3.5. Live cell fluorescence imaging of co-localization of MMGL and the putative interactors identified in the Y2H library screen in differentiated H9C2 cardiac myocytes. (i) GFP-tagged putative library screen interactors (green), as indicated to the left of the row. (ii) dsRed-tagged MMGL in the same cell(s) (red). (iii) Co-localization of interactors and MMGL within these cell(s) generated from Z-stack images (yellow). (iv) Overlay of images A-C with Hoechst H-33342 labelling of the nuclei (blue). Magnification: 60X oil immersion before 70% reduction. The presence of yellow staining in each of the images in Column C indicates that each of the respective preys co-localize with MMGL in differentiated H9C2 cardiomyocytes.

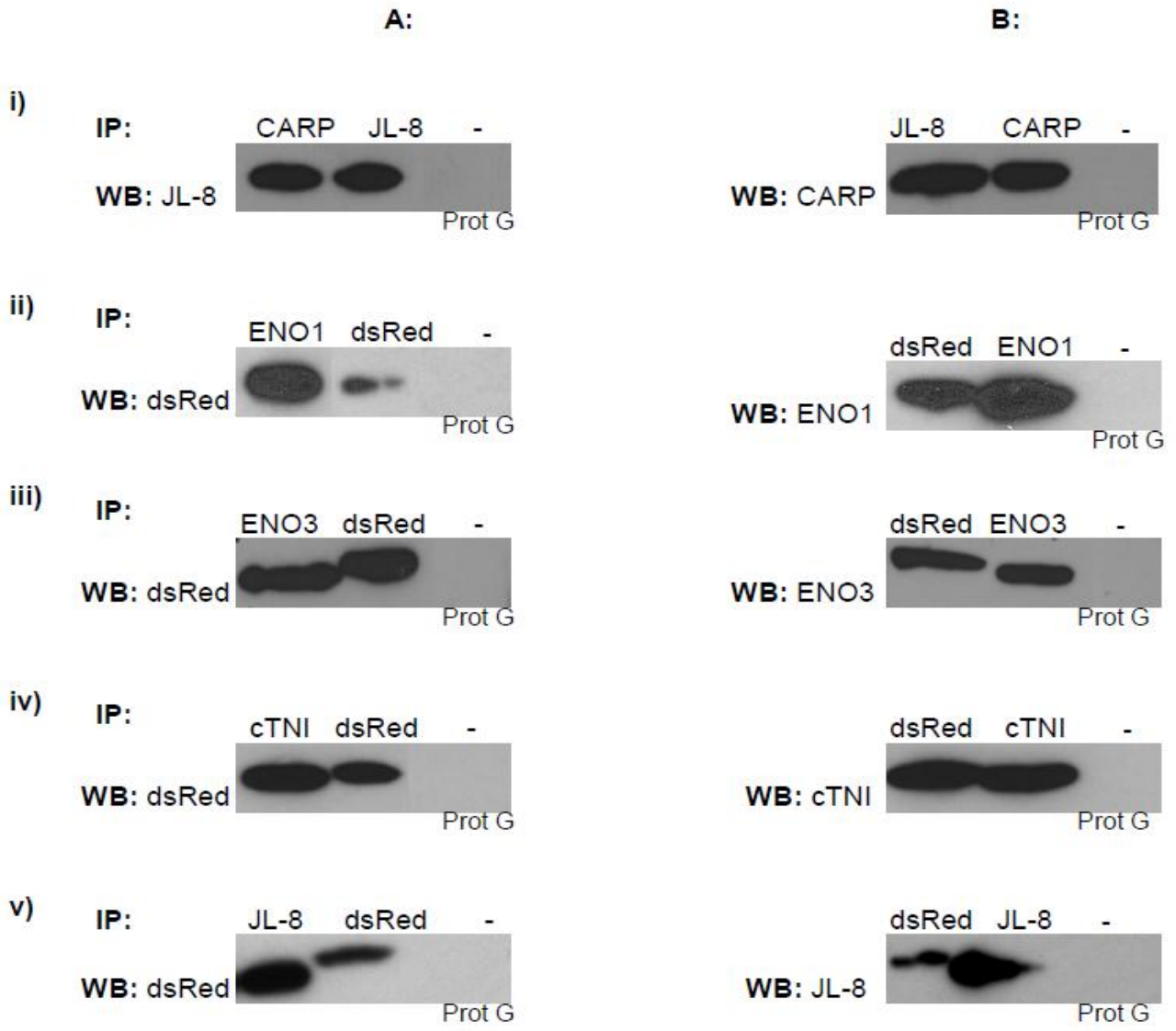

Figure 3.6. Western blots of *in vivo* co-immunoprecipitations of MMGL and putative interactors. **A:** Endogenous CARP (i), ENO1 (ii), ENO3 (iii) and cTNI (iv) immunoprecipitated exogenous dsRed-/YFP-MMGL *in vivo* in lysates of ds-Red-/YFP-MMGL transfected, differentiated H9C2 cardiomyocytes. (v) indicates that GFP-COMMD4 immunoprecipitates dsRed-MMGL in differentiated H9C2 cardiomyocytes transfected with both GFP-COMMD4 and dsRed-MMGL **B:** Reciprocal immunoprecipitations indicate that dsRed-/YFP-MMGL immunoprecipitated endogenous CARP (i), ENO1 (ii), ENO3 (iii) and cTNI (iv) in lysates of ds-Red-/YFP-MMGL transfected, differentiated H9C2 cardiomyocytes. (v) indicates that dsRed-MMGL immunoprecipitates GFP-COMMD4. The dsRed antibody is directed against the dsRed-MMGL fusion protein, while the JL-8 antibody is directed against the YFP/GFP fusion proteins. The clear protein G control lanes show that these precipitations are not spurious, but are the result of physical association between the relevant proteins. Additional lanes in (A) have been removed for cosmetic effect. *Abbreviations:* IP-immunoprecipitate; Prot G-protein G control; WB-western blot

3.4. CO-LOCALIZATION INCREASES BETWEEN MMGL AND PKA TARGETS UPON β-ADRENERGIC STIMULATION

As mentioned earlier, cMyBPC and cTNI are known PKA targets (Mohamed *et al.*, 1998; Patel *et al.*, 2001), while the remaining five putative interactors were shown to be likely targets using Phosphomotif Finder (www.hprd.org/PhosphoMotif_finder), and hence adrenergic stimulation would be expected to affect interaction between MMGL and these preys. The effect of adrenergic stimulation on co-localization between MMGL and cMyBPC, as well as cTNI, being the most frequent Y2H putative interactor, was therefore investigated.

Z-stacked fluorescent microscopy images showing co-localization of MMGL and cMyBPC as well as cTNI in H9C2 cardiomyocytes were obtained, as shown in Figure 3.7 and 3.8. These same cells were then treated with 0.1µM isoproterenol, a β-adrenergic agonist, and incubated for 10min at 37°C, after which they were imaged again. Treating H9C2 cells co-transfected with dsRed-MMGL and either GFP-cMyBPC or GFP-cTNI with isoproterenol resulted in an increase in 3D co-localization between the respective protein pairs, as shown in Figure 3.7 and 3.8, compared to non-treated cells. This suggests that under adrenergic stimulation, and consequential increased intracellular levels of cAMP, PKA is dynamically recruited by MMGL to the PKA targets cMyBPC and cTNI, presumably to mediate cardiac stress responses and leading to increased cardiac contractility.

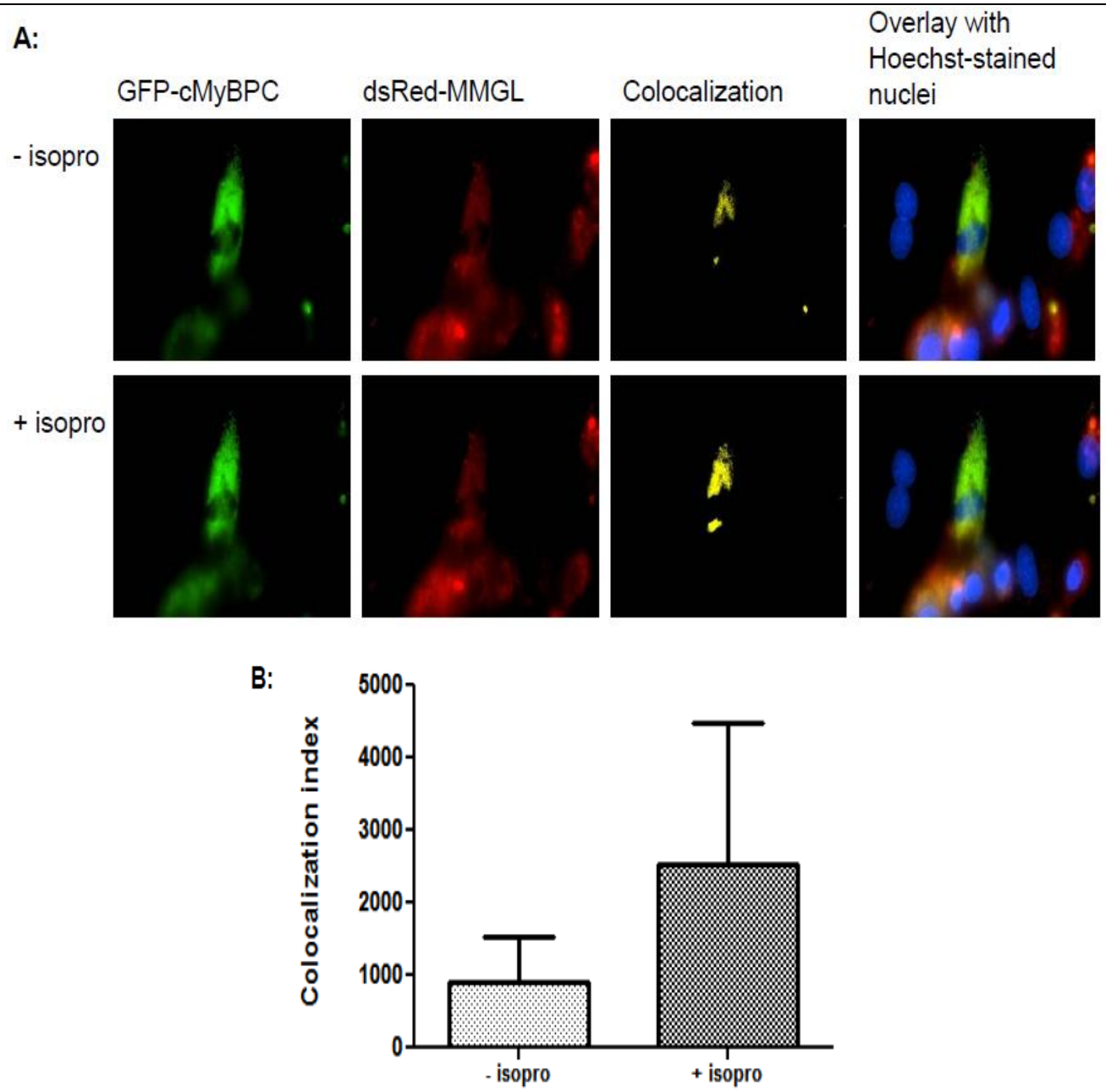

Figure 3.7. Live cell fluorescence imaging showing that co-localization of MMGL isoform 4 and cMyBPC increases under adrenergic stress. Each panel represents a single frame of the 25 images that were captured for the Z-stack. Each of the first three columns shows a single colour channel, while the image in the last column shows an overlay of the four colour channels used. **A:** Colocalization (yellow) between dsRed-MMGL and GFP-cMyBPC in the absence (-isopro) and presence (+isopro) of the beta-adrenergic agonist, isoproterenol. Co-localization levels have increased ten minutes after the addition of isoproterenol. **B:** Quantification of co-localization shown in A shows that co-localization increases but does not reach statistical significance. Data presented as mean ±SEM; n=3

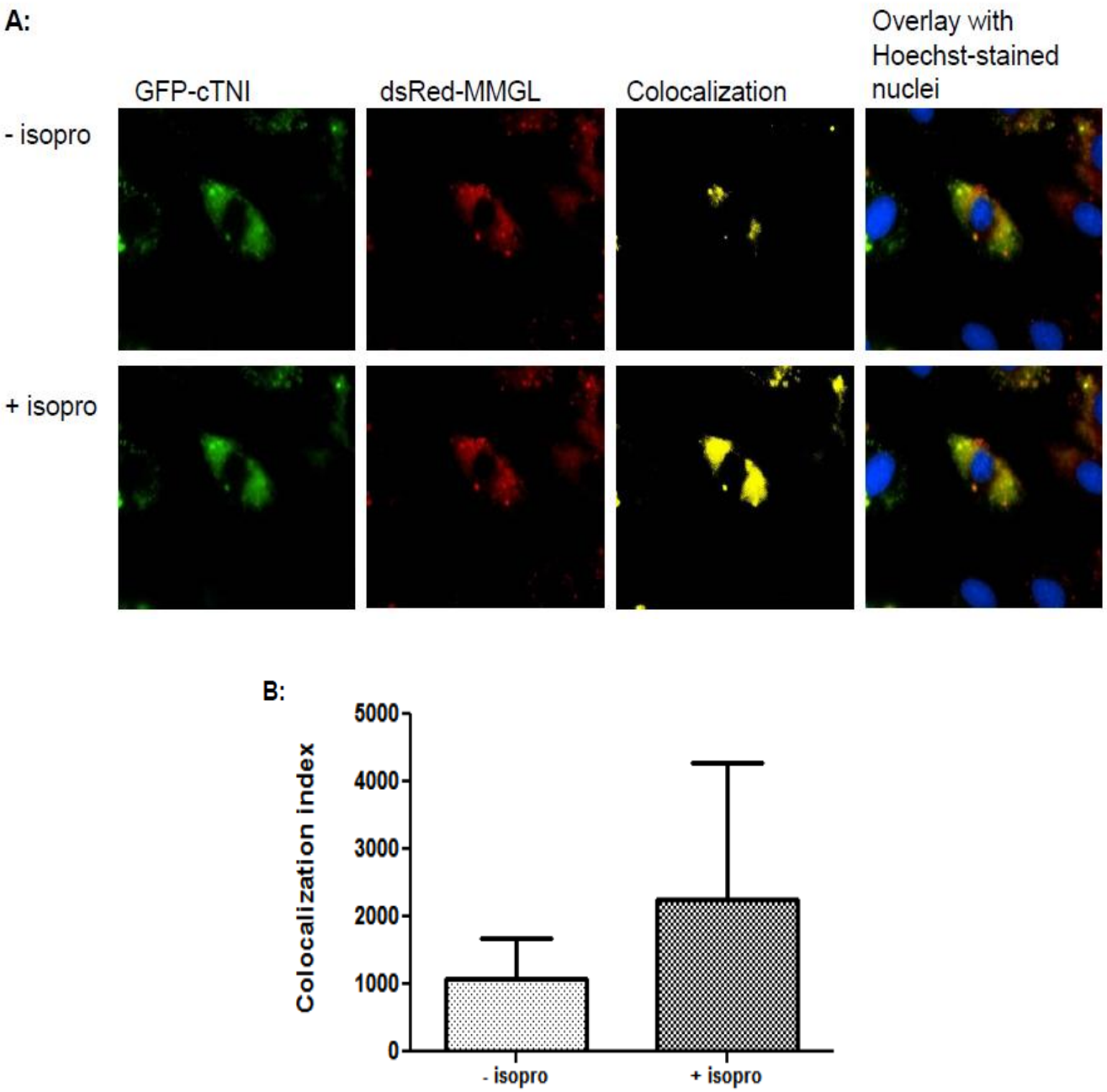

Figure 3.8. Live cell fluorescence imaging showing that co-localization of MMGL isoform 4 and cTNI increases under adrenergic stress. Each panel represents a single frame of the 25 images that were captured for the Z-stack. Each of the first three columns shows a single colour channel, while the image in the last column shows an overlay of the four colour channels used. **A:** Colocalization (yellow) between dsRed-MMGL and GFP-cTNI in the absence (-isopro) and presence (+isopro) of the beta-adrenergic agonist, isoproterenol. Co-localization levels have increased ten minutes after the addition of isoproterenol. **B:** Quantification of co-localization shown in A shows that co-localization increases but does not reach statistical significance. Data presented as mean ±SEM; n=3

3.5. RNAi-MEDIATED MMGL KNOCKDOWN

3.5.1. Optimizing *PDE4DIP* siRNAs

Having accumulated evidence that MMGL isoform 4 acts as an AKAP, the role of MMGL in cMyBPC phosphorylation was evaluated by assessing the expression of the different phosphorylation isoforms of cMyBPC, with and without adrenergic stimulation in the context of siRNA-mediated MMGL knockdown.

Of four siRNAs tested (Section 2.18.1), *Pde4dip* Rn_RGD:708410_3_HP siRNA (MMGL 3) (Qiagen, Hilden, Germany) was found to provide optimal knockdown of *PDE4DIP* (80%) in H9C2 cells (Figure 3.9); thus this MMGL (MMGL3) siRNA was used in subsequent experiments to silence *PDE4DIP* gene expression.

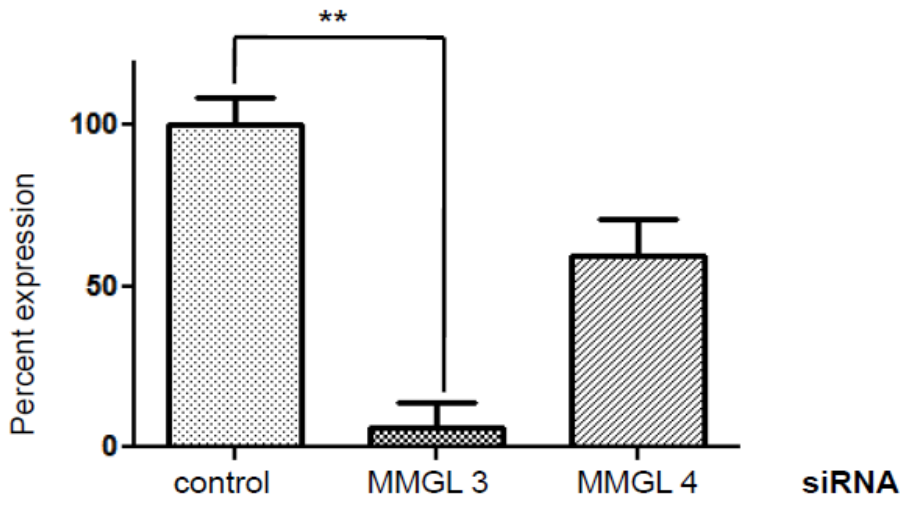

Figure 3.9. Real-time quantification of *PDE4DIP* cDNA transcribed from RNA extracted from cells transfected with either a non-silencing control or a particular *PDE4DIP* siRNA. *Pde4dip* Rn_RGD:708410_3_HP (MMGL 3) resulted in optimal knockdown of *PDE4DIP* (80%) $p = 0.0016$.

3.4.2. Effect of MMGL knockdown

To assess the effect of MMGL on cMyBPC phosphorylation, MMGL was knocked down by a siRNA approach, and the levels of the different cMyBPC phophorylation isoforms compared in lysates of cells that had been exposed to adrenergic stimulation via isoproterenol or not. To detect the different phosphorylation forms of cMyBPC, 2-dimensional IEF gels were run and western blotted.

Results showed that similar amounts of the mono- and diphosphorylated forms of cMyBPC are expressed in H9C2 cells not treated with isoproterenol, while lesser amounts of the un- and trisphosphorylated forms, relative to the other isoforms, are present (Figure 3.10 i).

When these cells are exposed to increased $CaCl_2$ and isoproterenol, to activate CaMK and PKA such that maximum phosphorylation of the MyBPC-motif is likely (McClellan *et al.*, 2001), the relative amount of the trisphosphorylated form increases markedly, while the relative amount of unphosphorylated cMyBPC decreases (Figure 3.10 ii). However, under adrenergic stimulation, MMGL knockdown results in very low expression of all isoforms (Figure 3.10 iii).

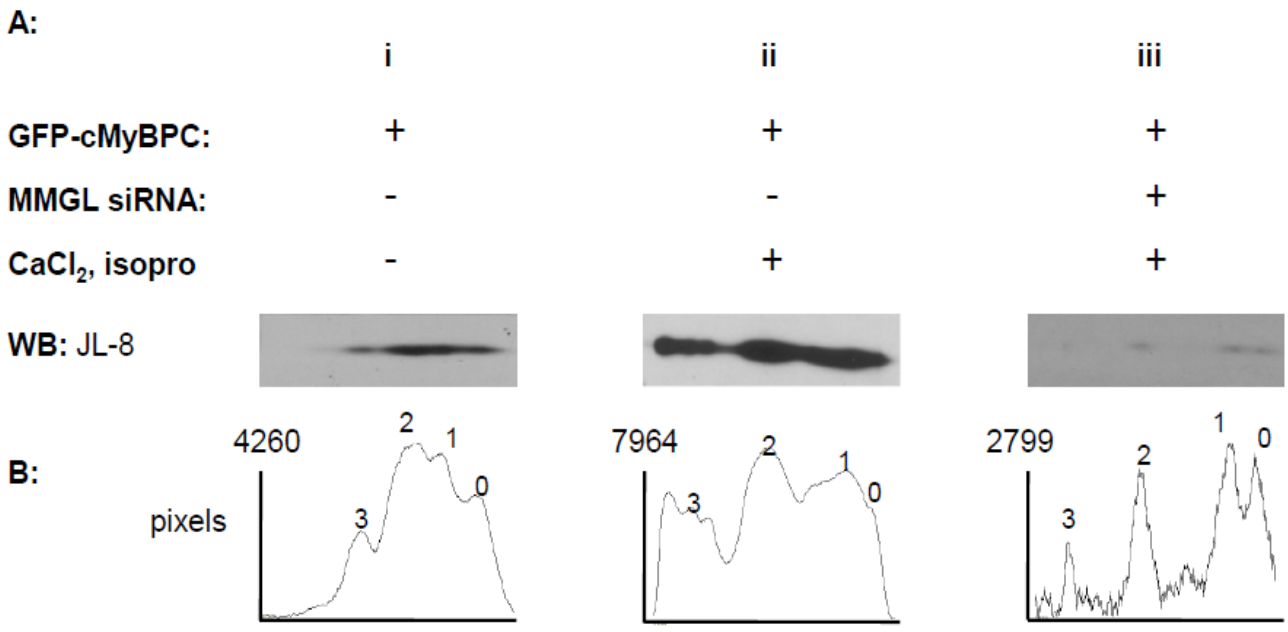

Figure 3.10. Effect of knockdown on the level of the different phosphorylated forms of cMyBPC in cells either exposed to adrenergic stimulation or not. **A:** Western blots of 2-dimensional IEF gels showing the expression of the four phosphorylation isoforms of GFP-cMyBPC in H9C2 cells (i) under non-stimulated conditions; (ii) under adrenergic stimulation, and (iii) under adrenergic stimulation in the absence of MMGL (i.e. with MMGL knock-down). **B:** Quantification of cMyBPC isoforms in the autoradiographs of the 2-dimensional IEF gels shown in (A), graphing the levels of the four phosphorylation isoforms (0=unphosphorylated; 1=monophosphorylated, 2=diphosphorylated, 3=trisphosphorylated). (i) Under non-stimulated conditions, levels of the mono- and diphosphorylated forms are similar and increased compared to the trisphosphorylated form. (ii) Under adrenergic stress, there is a relative increase in the trisphosphorylated form of cMyBPC and reduction of the non-phosphorylated form. (iii) Upon MMGL knock-down, adrenergic stress leads to a reduction in the levels of all cMyBPC phosphorylation forms.

3.6. MODIFIER STUDY

As discussed in Chapter 1, myomegalin and the two regulatory subunits of PKA were considered as potential modifier genes of the highly variable HCM hypertrophy phenotype. Single nucleotide polymorphisms (SNPs) representing variation within these three genes (*PDE4DIP, PRKAR1A* and *PRKAR2A*) and a SNP genotyping modifier study, comparing clinical HCM traits with the various genotypes obtained for the SNPs in these genes, was done with the following results:

3.6.1. Baseline statistics for the study cohort

Table 3.5 depicts the baseline clinical characteristics of the study cohort used for the study of *PDE4DIP*, *PRKAR1A* and *PRKAR2A* as potential modifiers of hypertrophic cardiomyopathy. The study population is stratified into mutation carrier (MC) and non-carrier (NC) groups for the three HCM causal mutations present in the cohort. In this population, 127 individuals were identified with HCM causal mutations.

3.6.2. Prioritising SNPs for investigation

SNPs were prioritized according to a density-selection strategy, rather than a tag-SNP strategy as the LD structure within the study population is not known. Additionally, SNPs were only selected if the SNP could be genotyped by means of validated Taqman® SNP genotyping assays. Validated Taqman® SNPs with a minor allele frequency (MAF) of 0.2 or more for the CEU or YRI population were selected such that a spread of SNPs across the genes was achieved. The CEU population consists of 30 parent-offspring trios with north and western European ancestry, whereas the YRI population sample consist of 30 parent-offspring trios from the Yoruba population in Ibadan, Nigeria (obtained from Centre d'Etude du Polymorphisme Humain). These two populations were deemed the HAPMAP populations closest to the study population. Table 3.6 depicts the MAF of each SNP covered in the present study for these two HAPMAP groups.

The average physical distances between SNPS were 59531, 520025 and 323923kb for the MMGL, PRKAR1A and PRKAR2A genes, respectively (Figs 3.11 and 3.12). For PRKAR1A and PRKAR2A, the spacing of these SNPs amounted to a spacing of 0.5 linkage disequilibrium units (LDUs) on the metric linkage disequilibrium (LD) map for the HapMap CEU and YRI populations.

Table 3.5. Basic characteristics of the study cohort stratified into mutation carrier (MC) and non-carrier (NC) groups according to HCM mutation status

	A797T		**R92W**		**R403W**	
	MC	**NC**	**MC**	**NC**	**MC**	**NC**
Total:	56	50	41	29	30	21
Males (%)	32 (57)	27 (54)	18 (44)	11 (38)	19 (63)	8 (38)
Age	43.5 (14-81)	36.5 (14-68)	37 (14-78)	33 (17-60)	39.5 (18-72)	35 (16-58)
BSA (m^2)	1.9 (1.3-2.5)	1.9 (1.5-2.3)	1.7 (1.3-2.2)	1.8 (1.3-2.1)	1.8 (1.3-2.3)	2.0 (1.5-2.3)
SBP (mm Hg)	120 (100-180)	120 (90-180)	120 (90-200)	120 (90-160)	122.5 (100-170)	125 (100-230)
DBP (mm Hg)	80 (60-100)	80 (60-120)	77.5 (60-100)	80 (60-90)	80 (60-110)	80 (60-110)
HR (bpm)	65 (44-120)	65 (50-95)	68 (45-110)	70 (45-83)	65 (52-96)	72 (53-90)
LVM (g)	200.8 (71.4-476.6)	133.3 (61.1-272)	133.7 (48.2-295.4)	113.7 (58.4-246.1)	173.9 (77.4-273.8)	141.9(59.1 - 290.5)

*Data summarised as median (Q_1, Q_3); Abbreviations: BSA-body surface area; DBP-diastolic blood pressure; HCM-hypertrophic cardiomyopathy; HR-heart rate; LVM-left ventricular mass; MC-HCM mutation carrier; NC-non-carrier; SBP-systolic blood pressure

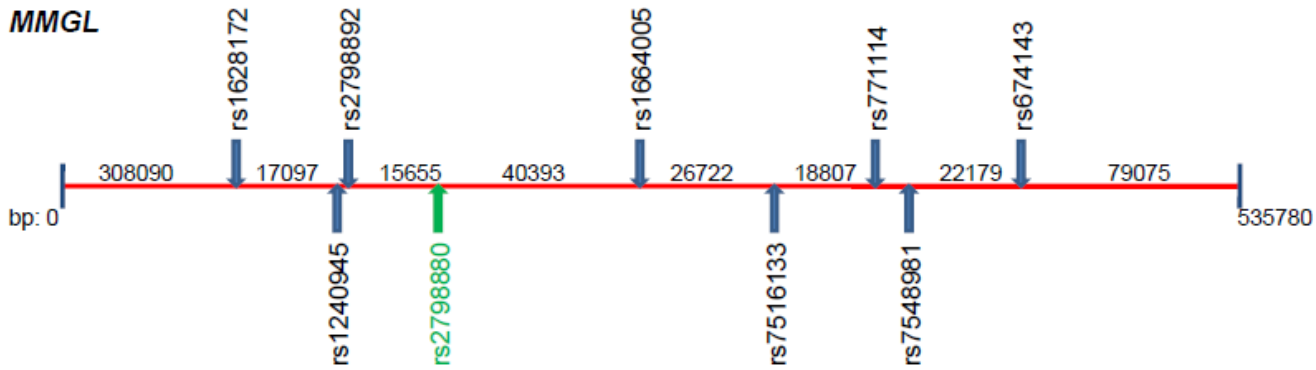

Figure 3.11. Graphical representation of *PDE4DIP* SNPs with a MAF≥0.2 for the CEU or YRI population manually selected to cover the whole gene. SNPs were only considered for selection if validated TaqMan® SNP genotyping assays could be obtained. Rs2798880 (green) was excluded from QTDT analysis due to an insufficient number of informative individuals

Figure 3.12. Graphical representation of *PRKA* SNPs selected to achieve an even spacing of 0.5 LDUs on the metric LD map for the HapMap CEU and YRI populations. SNPs were only considered for selection if validated TaqMan® SNP genotyping assays could be obtained. Rs3923913 was excluded from QTDT analysis due to an insufficient number of informative individuals

Table 3.6. Minor allele frequencies (MAF) of each SNP covered in the present study in the HapMap CEU and YRI population groups

				MAF	
Gene	**Chromosome**	**SNP**	**Nucleotide change**	**CEU**	**YRI**
PDE4DIP	1	rs1628172	a/g	0.22(a)	0.09(a)
		rs12409452	a/g	0.25(a)	0.06(a)
		rs2798892	a/c	0.33(a)	0.41(a)
		rs2798880	a/g	0.5(a/g)	0.5(a/g)
		rs1664005	a/g	0.331(g)	0
		rs7516133	c/t	0.212(c)	0.144(c)
		rs771114	c/t	0	0.358(c)
		rs7548981	c/g	0.237(g)	0.102(g)
		rs674143	a/g	0.237(g)	0.102(g)
PRKAR2A	3	rs3774628	a/g	0.441(g)	0.466(g)
		rs3923913	c/t	0	0.127(t)
		rs9755490	a/c	0.433(a)	0.375(a)
PRKAR1A	7	rs4265886	c/t	0.339(c)	0.2(c)
		rs11651687	a/g	0.228(a)	0.229(a)
		rs3785906	a/g	0.25(g)	0.233(g)
		rs6958	c/g	0.28(c)	0.24(c)

Abbreviations: a - adenine; c - cytosine; g - guanine; *PDE4DIP* - phosphodiesterase 4D-interacting protein; *PRKAR1A* - Protein kinase cAMP-dependant,regulatory, type 1, alpha, *PRKAR2A* - Protein kinase cAMP-dependant,regulatory, type 2, alpha,; SNP - single nucleotide polymorphism; t - thymine

3.6.3. Genotyping via Taqman® allelic discrimination

The Taqman® SNP genotyping PCR amplification runs were all completed successfully and no amplification was observed in the non-template controls, eliminating the possibility of amplification due to contamination. All results from the end-point analyses were exported to a database for statistical analysis. Figure 3.13 shows the genotyping results for the myomegalin SNP rs1628172 as a representation of the allelic discrimination plots obtained with the SDS software during end-point analyses.

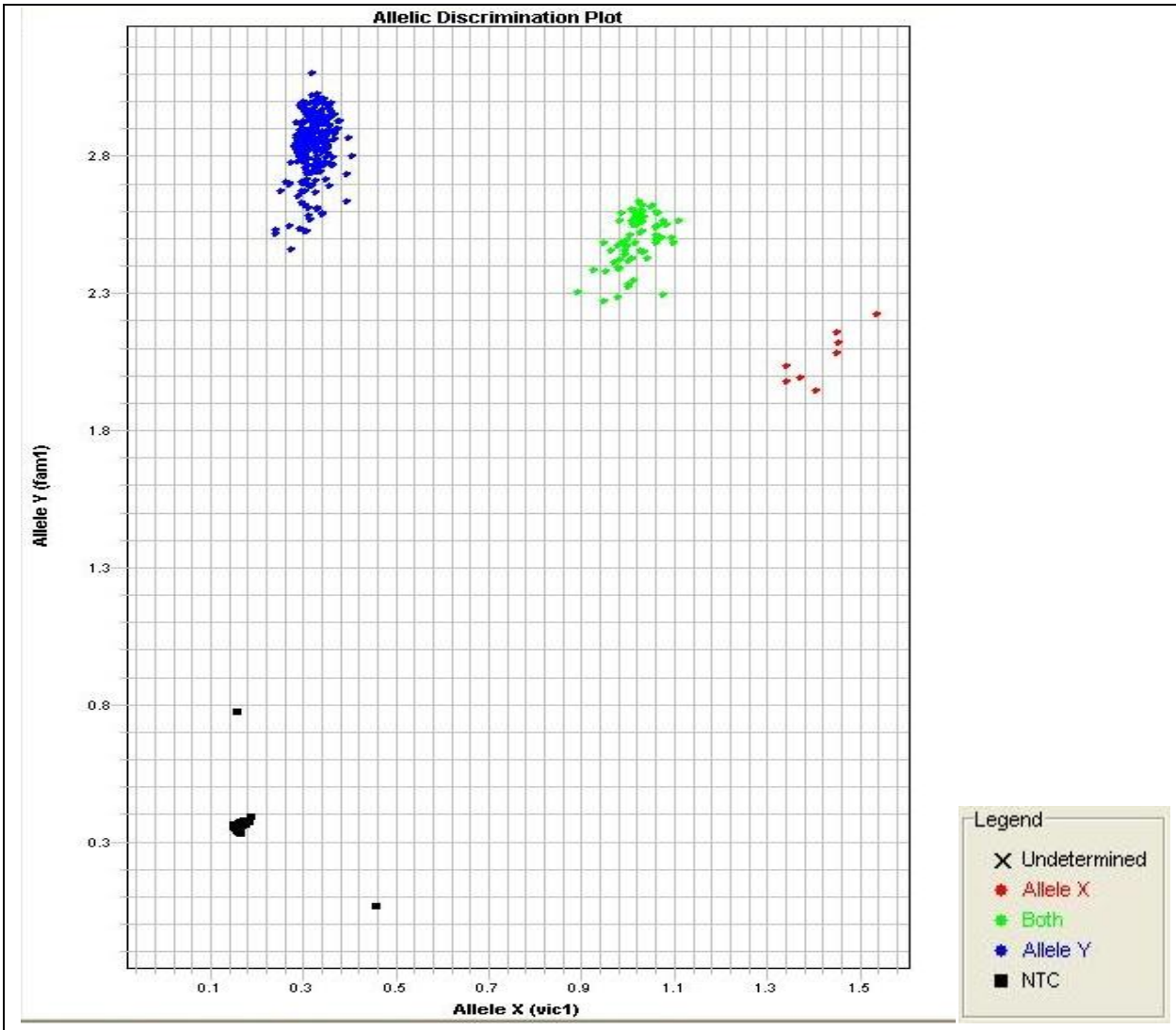

Figure 3.13. Representative genotyping result for TaqMan allelic discrimination. Genotyping results for the rs1628172 SNP as a representation of the allelic discrimination plots obtained with the SDS software during end point analyses. Allele X=a; Allele Y=g

3.6.4. Statistical analyses

3.6.4.1. Descriptive statistics

The statistical program Pedstats was used to determine whether all genotypes were consistent with expected Mendelian inheritance patterns. Genotypes that were inconsistent were resolved by re-genotyping. Table 3.7 shows the exact p-values obtained from an exact Hardy-Weinberg equilibrium (HWE) test among a sample of unrelated individuals as determined with Pedstats. The genotype frequencies for all markers were in agreement with HWE except rs2798880, which was removed and excluded from further analysis due to an insufficient number of informative individuals.

3.6.4.2. Association and population stratification test

An additive model of association was used to assess all the SNP markers. For QTDT, Monte-Carlo permutation tests were used to calculate exact p-values. P-values of 0.05 and lower were considered as significant.

To enable association analysis and in order to run QTDT, at least 30 informative matings are required, i.e. phenotyped individuals with at least one heterozygous parent. One marker (rs2798880) in *PDE4DIP* and another in *PRKAR2A* (rs3774628) had an insufficient number of informative individuals, and hence, could not be assessed for association using QTDT and were thus excluded from further analysis.

To assess whether population stratification existed within the study population, a population stratification test was carried out using QTDT (Table 3.8). This was necessary, to inform a choice of applying either the total or orthogonal model during association analyses. While the total model has more power, it is not robust to population stratification. Conversely, the orthogonal model has less power than the total model, because it performs within-family association, but compensates for population stratification for the same reason.

As can be seen from the table, one SNP variant (rs4265886) in *PRKAR1A* associated with mIVST (p-value of 0.043) showed stratification, and hence, the orthogonal model was used to calculate association for that particular variant. No other population stratification was detected in the samples, and hence, the total model was used for all other variants.

The results of the two QTDT tests can be seen in Table 3.9. Significant association was found between the *PDE4DIP* SNP rs1664005 and all the traits except LVM and mPWT. Significant association was also found with two *PRKAR1A* SNPs (rs11651687 and rs3785906) and the hypertrophy traits mIVST and CWTscore.

The effect sizes of the G-allele of the *PDE4DIP* SNP rs1664005 on untransformed, covariate adjusted traits were an increase of 1.3mm for mIVST, 3.4mm for Maronscore, 8.1mm for CWTscore and 0.5mm for Comp1. For *PRKAR1A*, the effect size for the A-allele of rs11651687 was an increase of 2.1mm for mIVST, whereas for the A-allele of rs3785906, effect sizes were found to be 2.2mm for mIVST and 16.3mm for CWTscore.

Table 3.7. Exact Hardy-Weinberg equilibrium p-values calculated for unrelated individuals

Gene	Chromosome	Marker	HWE exact p-value
PDE4DIP	1	rs1628172	0.2431
		rs12409452	0.3021
		rs2798892	0.0855
		rs2798880	Not determined
		rs1664005	0.7316
		rs7516133	0.0725
		rs771114	0.7082
		rs7548981	0.3121
		rs674143	0.1661
PRKAR2A	3	rs3774628	0.7542
		rs3923913	1.0000
		rs9755490	0.1376
PRKAR1A	7	rs4265886	1.0000
		rs11651687	0.2741
		rs3785906	0.1251
		rs6958	0.7121

Abbreviations: HWE - Hardy-Weinberg equilibrium; *PDE4DIP* - phosphodiesterase 4D-interacting protein; *PRKAR1A* - Protein kinase cAMP-dependant,regulatory, type 1, alpha, *PRKAR2A* - Protein kinase cAMP-dependant,regulatory, type 2, alpha

Table 3.8. Results from the population stratification analysis: p-values for stratification between SNPs in *PDE4DIP*, *PRKAR2A* and *PRKAR1A* and hypertrophy traits. Significant p-values are indicated in bold red

Trait	*PDE4DIP*								*PRKAR2A*		*PRKAR1A*			
	rs1628172	**rs12409452**	**rs2798892**	**rs1664005**	**rs7516133**	**rs771114**	**rs7548981**	**rs674143**	**rs3774628**	**rs9755490**	**rs4265886**	**rs11651687**	**rs3785906**	**rs695843**
LVM	0.549	0.846	0.403	0.872	0.297	0.738	0.672	0.328	0.080	0.750	0.199	0.935	0.989	0.658
mIVST	0.199	0.126	0.305	0.761	0.706	0.942	0.536	0.163	0.460	0.280	**0.043**	0.424	0.345	0.278
mPWT	0.502	0.483	0.476	0.831	0.974	0.564	0.407	0.518	0.337	0.515	0.071	0.436	0.675	0.542
Maronscore	0.171	0.170	0.274	0.966	0.724	0.824	0.112	0.145	0.317	0.383	0.055	0.760	0.862	0.394
CWTscore	0.105	0.319	0.893	0.908	0.966	0.512	0.187	0.077	0.160	0.723	0.137	0.481	0.504	0.585
Comp1	0.157	0.373	0.419	0.723	0.908	0.773	0.169	0.182	0.263	0.450	0.065	0.670	0.637	0.393

Abbreviations: Comp1 - principle component score; CWTscore - cumulative wall thickness score; LVM - left ventricular mass; Maronscore - as defined by Spirito and Maron (1990); mIVST - maximal interventricular septum thickness; *PDE4DIP* - phosphodiesterase 4D-interacting protein; mPWT - maximal posterior wall thickness; *PRKAR1A* - Protein kinase cAMP-dependant,regulatory, type 1, alpha, *PRKAR2A* - Protein kinase cAMP-dependant,regulatory, type 2, alpha

Table 3.9. Results from the association analysis using the total model: p-values for association between SNPs in *PDE4DIP*, *PRKAR2A* and *PRKAR1A* and hypertrophy traits. Significant p-values are indicated in bold red. ***PRKAR1A* SNP rs4265886 analysed using the orthogonal model

Trait	***PDE4DIP***								***PRKAR2A***		***PRKAR1A***			
	rs1628172	**rs12409452**	**rs2798892**	**rs1664005**	**rs7516133**	**rs771114**	**rs7548981**	**rs674143**	**rs3774628**	**rs9755490**	**rs4265886 ** **	**rs11651687**	**rs378590**	**rs695806**
LVM	0.504	0.687	0.148	0.061	0.434	0.124	0.767	0.978	0.308	0.631	0.642	0.252	0.126	0.514
mIVST	0.729	0.737	0.429	**0.038**	0.366	0.334	0.852	0.379	0.585	0.591	0.523	**0.029**	**0.010**	0.438
mPWT	0.752	0.852	0.890	0.248	0.238	0.523	0.933	0.683	0.925	0.534	0.399	0.721	0.605	0.341
Maronscore	0.956	0.584	0.642	**0.022**	0.355	0.177	0.839	0.331	0.151	0.729	0.472	0.191	0.071	0.700
CWTscore	0.917	0.940	0.281	**0.034**	0.531	0.093	0.527	0.172	0.248	0.963	0.857	0.118	**0.042**	0.943
Comp1	0.643	0.917	0.251	**0.028**	0.372	0.212	1.000	0.396	0.356	0.918	0.537	0.174	0.062	0.763

Abbreviations: Comp1 - principle component score; CWTscore - cumulative wall thickness score; LVM - left ventricular mass; Maronscore - as defined by Spirito and Maron (1990); mIVST - maximal interventricular septum thickness; *PDE4DIP* - phosphodiesterase 4D-interacting protein; mPWT - maximal posterior wall thickness; *PRKAR1A* - Protein kinase cAMP-dependant,regulatory, type 1, alpha, *PRKAR2A* - Protein kinase cAMP-dependant,regulatory, type 2, alpha

CHAPTER FOUR: DISCUSSION

INDEX **PAGE**

CHAPTER 4: DISCUSSION

In the study leading to the current one, the functions of the N-terminal domain of cMyBPC were explored by conducting a series of Y2H library screens using constructs mimicking the various phosphorylation states of the C1-C2 region. In two of these screens, using the un- and trisphosphorylated mimic of the C1-C2 region as baits, MMGL isoform 4 was identified as novel ligand of this region of cMyBPC. The interaction between MMGL isoform 4 and the un- and trisphosphorylated mimic of C1-C2 cMyBPC was confirmed by separate, independent methods viz. *in vitro* co-immunoprecipitation and *in vivo* colocalization (A. Ramburan, PhD thesis).

After identifying MMGL as an interactor of PDE4D, Verde *et al.* (2001) described MMGL as a novel structural/scaffolding protein that localizes to the sarcomere in cardiac and skeletal muscle. Moreover, because MMGL is expressed at high levels in the Z region of the sarcomere in cardiac and skeletal muscle cells, together with other cAMP-signal transduction proteins such as adenylyl cyclase, L-channels and PKA regulatory subunits (Gao *et al.*, 1997, Yang *et al.*, 1998), Verde *et al.* speculated that MMGL may act as a scaffolding protein, bringing PDE4D in close proximity to these other proteins so that cAMP signal transduction can take place (Verde *et al.*, 2001). However, the precise function and interactions of MMGL had not been investigated.

Considering the results of the previous study performed in our laboratory, which showed that MMGL isoform 4 interacts with cMyBPC, a known PKA target (Gautel *et al.*, 1995), together with Verde *et al.*'s findings, we hypothesized that MMGL acts not only as scaffolding protein organizing cAMP-signal transduction proteins such as PDE4D, but acts as an anchoring protein for PKA, viz. an AKAP, as well, as it has previously been shown that some adaptor proteins can anchor both PKA and PDE4D (Dodge *et al.*, 2001). Further support for this hypothesis was gained by Fink *et al.*'s (2001) study showing that appropriate second messenger compartmentalization is crucial for normal cardiomyocyte function, because the disruption of AKAP-mediated PKA anchoring to cMyBPC and cTNI had detrimental effects on cardiac contractility following β-adrenergic stimulation.

This study thus set out to investigate the functions of MMGL in the context of the sarcomere. The main finding of the present study is the description of MMGL as a novel AKAP, anchoring PKA, together with PDE4D, to cMyBPC, for the first time delineating a mechanism by which PKA docks to cMyBPC. Not only does MMGL anchor PKA to cMyBPC, but also to at least one other sarcomeric protein whose dynamic phosphorylation is crucial to the regulation of contractility, viz. cTNI. Our findings thus describe a mechanism whereby the precision and speed of second messenger responses in this specialized area of the sarcomere are optimized, which is ultimately key to the regulation of cardiac contractility in response to β-adrenergic signaling.

4.1. MYOMEGALIN ISOFORM 4 BINDS TWO DISTINCT PKA-REGULATORY SUBUNITS

In order for a protein to be classified as an AKAP, it has to show interaction with at least one PKA regulatory isoform and participate in protein-protein or protein-lipid interactions to dictate the subcellular localization of PKA (Colledge and Scott, 1999, Dodge and Scott, 2000). We used Y2H direct protein-protein interaction assays, as described in Section 3.2, to determine whether MMGL isoform 4 interacts with either or both of two distinct PKA regulatory subunits. The two subunits chosen were PRKAR1A, based on its known interaction with MMGL's other known interactor, viz. PDE4D (Dodge *et al.*, 2001), and PRKAR2A, which has a high cardiac expression. The other two regulatory subunits PRKAR1B and PRKAR2B are expressed predominantly in the reproductive and central nervous systems (Cadd *et al.*, 1989, Jahnsen *et al.*, 1985), which rendered them unsuitable for this cardiovascular-focused study.

In the Y2H direct protein-protein interaction assay, both PKA regulatory subunits interacted with MMGL, but PRKAR2A appeared to show a stronger interaction with MMGL than PRKAR1A, based on robustness of activation of nutritional reporter genes by the PKA subunit-MMGL interaction. One of the basic differences between the R1 and R2 subunits is that R1 is found mainly in the cytosol, whereas R2 is particulate bound (Scott 1993); early studies using different types of animal hearts showed that particulate-bound kinase was almost exclusively of the R2 isoform (Corbin *et al.*, 1977). Moreover, independent studies found that different types of hormones activate different PKA regulatory isoforms, e.g. R2 was activated by isoproterenol, an adrenergic agonist, while R1 was activated by prostaglandin E_2, a vasodilator and noradrenalin-release inhibitor (Keely 1977, Keely 1979, Hayes and Brunton, 1982). The R2 subunit also has a higher binding affinity for AKAPs than R1, which facilitates sub-cellular placement of R2 in particulate structures (Carr *et al.*, 1992, Alto *et al.*, 2003). This, together with R2A's high cardiac expression levels, could explain why MMGL showed a stronger interaction with PRKAR2A than PRKAR1A in a Y2H setting. One could speculate that, if MMGL functions as an AKAP binding PKA to cMyBPC, PKA-II would be the predominant kinase responsible for phosphorylating cMyBPC under adrenergic stress. This is supported by McConnell *et. al.*'s finding that cardiomyocyte contractility in response to β-adrenergic stimulation is mediated by anchored pools of PKA, and that mislocalized PKA, due to Ht31-mediated AKAP inactivation, alters the phosphorylation of several key proteins involved in the process of contractility (McConnell *et al.*, 2009, Fink *et al.*, 2001). MMGL, together with other AKAPs involved in the phosphorylation of ryanodine receptors, phospholamban, and L-type calcium channels, could be mediating cardiac contractility by creating such anchored pools of PKA throughout the sarcomere.

Interaction of both PKA regulatory subunits with MMGL isoform 4 was verified in a cellular context and in the absence of GAL4 domains using 3D *in vivo* colocalization and *in vivo* co-immunoprecipitation (pull down) assays. This therefore qualifies MMGL isoform 4 as an AKAP, thereby ascribing a novel function to this protein.

In addition, the ability of MMGL isoform 4 to bind two different PKA regulatory subunits shows not only that it is an AKAP, but that it functions as a dual-specific AKAP (Colledge and Scott, 1999, Wang *et al.*, 2001). The PKA-anchoring domain of most conventional R2-anchoring AKAPs is a conserved amphipathic helix of 14-18 amino acid residues; this region fits into a hydrophobic groove formed by the regulatory subunit dimer (Carr *et al.*, 1992, Hausken and Scott, 1996, Newlon *et al.*, 2001). Single amino acid residues in this conserved region determine the specificity of R1 vs R2-binding, and it has been shown that point mutations in this area abolish dual-specificity of an AKAP, to preferentially binding either R1 or R2. Moreover, some AKAPs, although displaying dual-specificity, prefer interaction with R2, with a weaker binding to R1 (Miki and Eddy, 1999). More recently it has been shown that dual-specific AKAPs contain an additional R1 binding determinant known as the RI Specifier Region (RISR). This region enhances the targeting of PKA-I (Jarnæss *et al.*, 2008). The finding that MMGL isoform 4 displays dual-specificity for PKA regulatory subunits might, amongst other things, contribute to future studies exploring PKA isoform specificity on cMyBPC phosphorylation. This could involve blocking the different PKA subunit binding domains with AKAP inhibiting peptides such as Ht31, which disrupts AKAP-R2A binding, and RI-selective anchoring disrupter peptide (RIAD), which disrupts AKAP-R1A interactions (Carlson *et al.*, 2006, Carr *et al.*, 1992).

4.2. MYOMEGALIN BINDS ADDITIONAL PKA TARGETS

In order to further elucidate the role of MMGL in the sarcomere, and more specifically, the regulation of cardiac contractility, more information about its interacting partners were necessary, and hence a Y2H cardiac cDNA library screen, using MMGL isoform 4 as bait, was conducted. As described in Section 3.3, a total of 1130 clones that were able to activate three reporter genes were screened as putative interactors of MMGL isoform 4. After the selection for activation of additional nutritional and colourimetric reporter genes, heterologous bait mating and bioinformatic analyses, 13 in-frame cDNA clones were prioritized as putative interactors of MMGL isoform 4; these encoded cTNI, CARP, COMMD4, ENO1, ENO3, SNX3, COX5A and a proteosome 26S subunit. One clone, cTNI, was pulled out multiple times by the MMGL bait, which suggests that this interaction is likely to be biologically significant, and less likely to be an artifact of the Y2H system (Parrish *et al.*, 2006).

4.2.1. Preys excluded from further analysis

Many clone inserts had significant DNA matches in the NCBI database (http://www.ncbi.nlm.nih.gov) but were out of the reading frame dictated by the upstream GAL4 domain, and therefore, when translated, had no significant protein matches in the database. This is a common finding when using cDNA libraries derived from oligo dT- primed cDNA, which causes only one out of six of all cloned inserts to be in-frame with the transcription factor activation domain (van Criekinge and Beyaert, 1999). This is indeed a big limitation of any Y2H library screen making use of commercially available libraries. Peptides encoded by such out-of-frame constructs were excluded from further analysis because of their physiological irrelevance.

Previously, MMGL isoform 4 was identified as a ligand of cMyBPC, which is located in the C-zone of the sarcomere, and for the scope of this study, only putative interactors located within the sarcomere were considered for further verification. Therefore COX5A, which encodes part of the terminal enzyme of the respiratory complex localized in the mitochondrion, was excluded; however, it should be noted that proteins in the mitochondria are also PKA targets, which will also require PKA compartementalization by anchoring to various AKAPs, and thus this putative interaction may have physiological relevance and should be investigated. Furthermore, the proteosome 26S subunit, which is part of a multicatalytic proteinase complex and localized throughout eukaryotic cells, was also excluded from further study. SNX3 is a sorting nexin essential for endosome-to-Golgi retrieval of proteins and forms part of a retromer complex for protein trafficking (Verges 2007). MMGL is found in the Golgi area which makes an interaction with SNX3 very plausible, and thus this putative interaction is also plausible and should be investigated in future in order to gain more comprehensive understanding of the role of MMGL in the cell.

An obvious question that arises is why cMyBPC and the two PKA regulatory subunits were not identified as preys in the Y2H library screen? The absence of cMyBPC as a prey is most likely explained by the known absence of cDNAs representing the N-terminals of large proteins in oligo dT-primed libraries. The absence of PRKAR1A and PRKAR2A may relate to the stringency of selection during heterologous bait matings during the Y2H screen. One of the baits provided as control by the manufacturer of the MATCHMAKER Y2H screening system, and used as control in the heterologous bait mating in this study, encodes murine p53, which is a PKA target (Adler *et al.*, 1997). MMGL-PRKA interactions would then have been marked as non-specific, due to observation of p53-PRKA interactions.

Seeing that MMGL is characterized as a PDE4D-interacting protein, one would also expect PDE4D to be identified as Y2H prey. Although it is known that rat myomegalin interacts with the amino terminus of PDE4D in a region corresponding to the upstream conserved region 2 (UCR2) of PDE4D (Verde *et al.*, 2001), it is unknown which MMGL domain specifically interacts with PDE4D. MMGL isoform 4 is the smallest of the five different MMGL isoform in humans and one possible reason for the absence of PDE4D amongst the identified MMGL interactors, is that it might lack the PDE4D binding domain. Future studies should include a direct Y2H protein-protein interaction assay to assess this question more directly.

4.2.2. Preys chosen for further study

The putative MMGL isoform 4 interactors that localize to the sarcomere, according to literature were subjected to further tests to verify these putative interactions in a real cellular environment, and in the absence of the GAL4 domains. *In vivo* 3D co-localization and co-immunoprecipitations verified all interactions between MMGL isoform 4 and CARP, COMMD4, ENO1, ENO3 and cTNI. In addition to cTNI, which is a known PKA target (Mohamed *et al.*, 1998; Patel *et al.*, 2001), the other interactors were also shown to be likely PKA targets

due to the presence of phosphorylatable motifs (www.hrpd.org/PhosphoMotif_finder), supporting our findings of MMGL being an AKAP. A discussion of each interactor will now follow, with proposed mechanisms of function in the particular region of the sarcomere pertaining to cMyBPC and MMGL.

4.2.2.1. Cardiac ankyrin repeat protein (CARP)

CARP, encoded by *ANKRD1*, is expressed in the heart during embryonic and fetal development. It functions as a transcription cofactor, as well as an early differentiation marker of cardiac myogenesis (Jeyaseelan *et al.*, 1997, Zou *et al*., 1997). CARP expression progressively decreases up to adulthood, but is upregulated during end-stage heart failure (Zolk *et al.*, 2002). In hypertrophied hearts of mouse models, increased CARP levels have also been observed (Ihara *et al*., 2002, Baudet *et al*., 2003). This suggests that CARP plays an essential role in cardiac muscle functioning, both in health and disease (Arimura *et al*., 2009).

CARP has been localized to both the nucleus and the sarcoplasm, which suggested that it is shuttled between cellular compartments (Bang *et al*., 2001). In the sarcomere, CARP binds to the N2A domain of titin as well as the N-terminal domain of myopalladin, suggesting that these two proteins act as anchoring proteins for sarcomeric CARP (Bang *et al*., 2001, Miller *et al*., 2003). CARP's interaction with titin is mediated through a unique sequence in titin's N2A domain that is located between the Ig repeats Ig80 and 81. It was found that this region contains a tyrosine residue-rich motif that is highly conserved in human, murine and avian titins; such a region is also present in cMyBPC (Miller *et al*., 2003).

The overproduction of CARP during both heart failure and hypertrophy suggests that CARP-upregulation is a common feature of the adaptive response of the myocardium to stress (Mikhailov and Torrado 2008). *In vivo* studies have focused on *ANKRD1* regulation during various stress conditions including hypertrophy, ischaemia and hemodynamic overload. During the cardiomyocyte stress response, CARP levels are elevated and bind directly to a variety of proteins. These include titin, which is involved in biochemical stress signaling; myopalladin and desmin, both involved in the management of sarcomeric integrity and myofibril orientation; YB-1, involved in the prevention of cell senescence and apoptosis; CASQ2, involved in calcium handling; as well as MuRF1 and MuRF2, which are involved in stretch signal inhibition and protein quality control (Mikhailov and Torrado 2008). All of these CARP-activated pathways lead to an adaptative response of cardiomyocytes to stress.

Arimura *et al.* (2009) found that mutations in *ANKRD1* are associated with HCM. Mutations caused the binding of CARP to titin and myopalladin to increase, and reciprocally, HCM-mutations in titin increases the binding of titin to CARP. This suggests that the reversible binding of sarcomeric CARP to titin and/or myopalladin is involved in the maintenance of cardiac function (Arimura *et al*., 2009). Moreover, Arimura *et al*. (2009) found an abnormal intranuclear accumulation of mutant CARP proteins in mature myofibrils, and hypothesized, based on the fact that the embryonic and fetal gene program of cardiac cytoskeletal proteins is initiated during cardiac

remodeling (Swynghedauw and Baillard 2000, Swynghedauw 1999), that nuclear CARP may cause embryonic/fetal gene expression in mature myofibrils. This abnormal gene expression, together with abnormal recruitment of CARP in cardiomyocytes may be a possible mechanism causing HCM (Arimura *et al*., 2009).

To shed light on the functional relevance of the interaction of CARP, a transcriptional regulator, and MMGL, identified in this study as a novel sarcomeric AKAP, some background on CARP's main interacting partner, viz. titin, is necessary. This giant protein, which spans from the Z-disc all the way to the M-band, connecting the different sarcomeric regions, acts as a bidirectional molecular spring, enabling the sarcomere to have a long-range elasticity (Wang *et al*., 1979, Linke 2008) and determining muscle stiffness. Titin is subjected to rapid turnover and to post-translational modification, which provides a mechanism for tuning the elasticity of titin in response to changes in the physiological environment. Titin stiffness can be tuned by two mechanisms: isoform switching and phosphorylation by PKA and PKG (Kruger and Linke, 2009).

Titin isoform switching occurs before or around birth, when the compliant (long spring) fetal N2BA isoform is replaced by the smaller, less extensible and stiffer N2B isoform (Lahmers *et al*., 2004, Opitz *et al*., 2004). N2B becomes the dominant isoform in humans after birth, so that in general, fetal/neonatal sarcomeres are much more compliant than those in adult myocardium (Warren *et al*., 2004, Opitz *et al*., 2005). This increasing titin stiffness throughout development benefits the heart by allowing for a faster beating frequency, and elevated end-diastolic pressure, stroke volume and LV dimensions (Kruger and Linke, 2009). In adulthood, the four cardiac chambers differ in their N2B:N2BA ratios (Granzier and Labeit, 2004). Titin isoform expression is reversed in patients undergoing progression to end-stage heart failure, where the myofibrils are more compliant (Nagueh *et al*., 2004). This may be an attempt to compensate for the stiffer extracellular matrix that is frequently observed in heart failure due to extensive fibrosis (Nagueh *et al*., 2004, Makarenko *et al*., 2004). Mechanisms of isoform switching include hormonal changes and the activation of the phosphoinositol-3-kinase (PI3K)/PKB pathway (Kruger *et al*., 2008).

A much more acute, possibly beat-to-beat, mechanism of titin isoform stiffness modulation is through phosphorylation, and next to cMyBPC and cTNI, titin is the third major myofilament protein phosphorylated by PKA. This post-translational modification promotes a reduction of passive titin stiffness (Kruger and Linke, 2006, Kruger and Linke, 2009). During the transition to heart failure and in end-stage failing hearts, PKA signaling is severely disturbed. Diastolic function is compromised by elevated titin stiffness due to a phosphorylation deficit. PKG phosphorylation also reduces passive stiffness, but to a lesser degree than achieved by PKA (van Heerebeek *et al*., 2006, Borbely *et al*., 2005). PKA and PKG phosphorylate the same titin domain, viz. the N2B-unique sequence, situated in the elastic segment. PKG, in addition, phosphorylates two additional domains along the spring segment, viz. the Ig-domains I24/25 of the N2B domain, as well as the N2A region (Kruger and Linke, 2006, Kruger *et al*., 2009). Seeing that PKG phosphorylation reduces passive stiffness to a

lesser degree than PKA phosphorylation, it was suggested that these additional PKG sites affect protein-protein interactions with titin, rather than altering titin stiffness directly (Kruger *et al*., 2009).

Interestingly, CARP binds to titin's PKG-phosphorylated N2A domain (Miller *et al*., 2003). If phosphorylation of titin by PKG affects protein-protein interactions rather than altering titin stiffness directly, as suggested (Kruger *et al*., 2009), phosphorylation of N2A may cause CARP to dissociate from N2A and shuttle back to the nucleus to act as a transcriptional regulator (Witt *et al*., 2005), causing the upregulation of the more compliant N2BA isoform required to reduce passive stiffness in periods of mechanical stress. In this way, phosphorylation of N2A indirectly, via CARP transcriptional regulation, could reduce titin passive stiffness.

Experimental evidence exist that CARP is phosphorylated by casein kinase II and PKC (Chu *et al*., 1995, Scurr *et al*., 2008); however, no formal proof exists of CARP being phosphorylated by PKA. However, our results show that MMGL interacts with CARP; by acting as AKAP, MMGL could bring PKA in close proximity to phosphorylate CARP's two putative PKA sites, as predicted by PhosphoMotif Finder (www.hprd.org/Phosphomotif_finder). One of the predicted PKA sites is situated in a coiled-coil domain, which is known to participate in protein-protein interactions. One could speculate that, should this site be phosphorylated by MMGL-bound PKA, the interaction between CARP and the N2A domain of titin might weaken, and along with PKG phosphorylation of N2A itself, cause dissociation of CARP form titin, freeing CARP to shuttle back to the nucleus to upregulate N2BA transcription. This might constitute an additional mechanism of *ANKRD1*-associated HCM, where mutated CARP might lack these phosphorylation sites, thus reducing the ability of CARP to dissociate from N2A to shuttle to the nucleus and cause upregulation of N2BA, and explaining the observed increased binding of mutated CARP to titin (Arimura *et al*., 2009). A mutated PKG site on titin might similarly explain the reciprocal increase of titin binding to CARP (Arimura *et al*., 2009). Of course, the same situation might arise if the MMGL binding site on CARP is mutated, which might cause decreased or delayed PKA phosphorylation and hence, decreased or delayed dissociation from titin. Interestingly, the predicted PKA site is located ten amino acids downstream from a known HCM-causing CARP mutation (Pro52Ala) (Arimura *et al*., 2009), which is situated between a titin-binding domain and the coiled-coil domain. This region may constitute CARP's MMGL-binding domain, and the Pro52Ala mutation might therefore disrupt CARP's ability to interact with MMGL. Without an AKAP in close proximity to the PKA site, spatio-temporal control of phosphorylation in this site would be impaired, preventing CARP from dissociating form titin, as described above. This may constitute a mechanism whereby the Pro52Ala mutation causes HCM. This proposal should be tested in future studies using direct yeast-based protein-protein interaction assays and site-directed mutagenesis.

Rapid phosphorylation and dissociation should be essential in an acute titin stiffness modulation mechanism which is considered to be regulated on a "beat-to-beat" basis. Without an appropriate AKAP, such rapid PKA signaling would not be possible. This implicates the CARP-MMGL complex as a transmitter of mechanical

stress, and implicates MMGL in another HCM-causing mechanism, underscoring the importance of phosphorylation in the regulation of myocardial stress-sensing.

4.2.2.2. α- and β-enolase (ENO1 and ENO3)

In cells with high intermittent energy-requirement levels, such as muscle cells, ATP is primarily derived from glycolysis (Suarez 2003). Enolase is an enzyme involved in one of the terminal steps of glycolysis, catalyzing the conversion of 2-phospho-D-glycerate (2-PGA) to 2-phosphoenolpyruvate (PEP). The enolase dimer is formed by the combination of two of the three enolase subunits (α, β and γ) that is encoded by three separate genes, viz. *ENO1*, *ENO3* and *ENO2,* respectively (Feo *et al*., 1990). During embryonic development, the αα homodimer accounts for all enolase activity. As development progresses, especially in areas with high energy requirements, such as the brain and muscle, the αα isoform is significantly downregulated and replaced by αγ and γγ isoforms in the brain, and by αβ and ββ isoforms in muscle (Comi *et al*., 2001).

Interestingly, it was found that α-enolase was significantly upregulated in hypertrophic left ventricles of spontaneously hypertensive rats (SHR) (Jin *et al*., 2006), but in the normal myocardium of Wistar-Kyoto (WKY) rats, α-enolase levels were very low (Zhu *et al*., 2009). A possible reason for this could be the switch from a relatively hypoxic uterine environment to relatively higher oxygen conditions postnatally, in other words, the myocardium is being exposed to a change in oxygen availability. This is accompanied by a change in substrate selection (Nau *et al*., 2002). In particular, the fetal oxidation of glucose and lactate via glycolysis will shift towards a bigger reliance on fatty acids as the main fuel of the adult heart; this will result in the downregulation of glycolytic α-enolase, and upregulation of fatty acid oxidation enzymes (Zhu *et al*., 2009). However, in order to maintain an energy supply for efficient cardiac function, the hypertrophic heart has an increased demand for oxygen and ATP (Stanley *et al*., 2005, Mizukami *et al*., 2004), and increased levels of α-enolase will therefore accelerate glucose oxidation rates. Upregulated α-enolase therefore seems to play an adaptive role in myocardial hypertrophy (Zhu *et al*., 2009).

β-enolase, which is the primary enolase expressed in muscle postnatally, was identified as a binding partner of MMGL. This enzyme has been shown to localize to the Z-disc and M-line of the sarcomere (Keller *et al*., 2000), and is known to interact with creatine kinase at the M-line (Foucault *et al*., 2000). β-enolase anchors to the M-line via an adaptor protein, FHL2, which binds it to titin (Lange *et al*., 2006). β-enolase has also been identified as an interactor of cMyBPC itself (A.Ramburan, PhD thesis). It has been suggested that the recruitment of metabolic proteins to sarcomeric regions may provide a structural role; this complex therefore might stabilize the particular sarcomeric regions (Clark *et al*., 2002). Importantly, Lange *et al*. (2006) also showed that metabolic enzyme complexes like this β-enolase complex are common throughout the sarcomere in areas of high energy demand. A complex consisting of cMyBPC, MMGL and β-enolase in the C-zone of the sarcomere would therefore be advantageous for two main reasons. Firstly, cMyBPC and MMGL are part of a β-adrenergic

pathway leading to increased contractility during times of increased cardiac demand, in which case it would be advantageous to have β-enolase anchored on site to produce energy via glycolysis. Secondly, the binding between MMGL, an adaptor protein, and β-enolase, a metabolic protein, to cMyBPC might stabilize the C-zone of the sarcomere, which is desirable seeing that it undergoes sudden changes in motion all the time.

Identifying α-enolase as an interactor of MMGL is less easily explained, as α-enolase expression is downregulated to almost negligible levels after birth under normal circumstances and replaced by β- and αβ-enolase in muscle (Comi *et al*., 2001); one would not expect it to be expressed significantly in a normal adult cardiac cDNA library. The levels of β-enolase increase as the energy demand of the muscle fibre type increases, however, this phenomenon is not observed in α-enolase levels (Keller *et al*., 2000). However, a few possibilities exist: Firstly, the explanation for its presence in the library, which was reportedly constructed from cDNA extracted from normal, whole hearts from 3 male Caucasians aged between 28 and 47 years, could be occult hypertension in one or more of the donor subjects. The study by Zhu *et al*. (2009) found upregulation of α-enolase in hypertrophic hearts of spontaneously hypertensive rats. Hypertension is often overlooked, especially in the incipient stages, and does not result in immediate changes in cardiac morphology, hence a donor heart may have appeared normal at time of death, even though molecular changes had already begun to take place. Then, given the presence of α-enolase in the cDNA library, the observed interaction between MMGL and α-enolase may rather reflect a three-way interaction involving the αβ-heterodimer and MMGL (considering that β-enolase is also an interactor of MMGL), rather than the α-enolase homodimer. Alternatively, α- and β-enolase share 83% homology on amino acid level (www.ncbi.nlm.nih.gov/BLASTP), therefore, the MMGL-binding domain on α-enolase might be situated in an area of high β-enolase homology. This might implicate that that α-enolase was only pulled out as a prey because of the high homology across the β-enolase MMGL-binding site. Given other findings in our laboratory, viz. that cMyBPC interacts with β-enolase (A. Ramburan, PhD thesis) and COMMD4, which also interacts with MMGL as well as with cMyBPC, interacts with α-enolase (C. Swanepoel, PhD thesis), the results of MMGL interacting with β-enolase, and possibly with αβ-enolase, suggests a possible complex interaction of the αβ-heterodimer with the ligands MMGL, cMyBPC and COMMD4. MMGL could anchor αβ-enolase to cMyBPC in the sarcomere to provide increased energy via glycolysis for β-adrenergic fight or flight responses, as already described in this section. However, MMGL could also bind αβ-enolase to one of its other ligands identified in this study viz. COMMD4. COMMD4 is implicated in protein trafficking and turnover, and functions as an adaptor protein that stabilizes the interaction between cMyBPC and an E3 ligase. E3 ligase functions by attaching ubiquitin molecules to cMyBPC to mark it for degradation by the ubiquitin proteasome system (UPS), which takes place after cMyBPC has been released from the sarcomere (C. Swanepoel, PhD thesis), as will be discussed in Section 4.2.2.3. This protein degradation process requires energy, which could be provided by glycolysis through αβ-enolase attached to COMMD4 via MMGL.

Both α- and β-enolase contain putative PKA phosphorylation sites, which makes the interaction between these glycolytic enzyme dimers and MMGL, an AKAP, plausible. Phosphorylation of these sites could mediate protein-protein interactions and/or alter the enzyme's catalytic properties. Considering the various proteins that all seem to interact in one multi-protein complex, a means of regulating these interactions is necessary. β-adrenergic stimulation might result in phosphorylation of αβ-/β-enolase via MMGL-anchored PKA, which could facililtate its binding to cMyBPC (which would also be simultaneously phosphorylated by MMGL-bound PKA) to compensate for the increased energy demands required in this part of the sarcomere by anchoring, and activating, an energy-producing enzyme on site. Following the β-adrenergic signal, MMGL-bound PDE4D would then hydrolyze the remaining cAMP, and the reduced PKA levels might cause dissociation and deactivation of αβ-/β-enolase from cMyBPC. αβ-Enolase might bind to COMMD4 in the same phosphorylation-dependent manner, when energy is required for the degradation of cMyBPC by the UPS after it has been released from the sarcomere (see Section 4.2.2.3.).

4.2.2.3. Copper Metabolism Gene *MURR1* Domain 4 (COMMD4)

The COMM (Copper metabolism gene *MURR1*) domain-containing family consists of ten members and is found in all vertebrates. These proteins are characterized by the presence of a highly conserved and unique C-terminal COMM domain and an α-helical rich N-terminal region present in all ten members of the family. The COMM domain functions as a critical interface for protein-protein interactions and defines this family of proteins (Burstein *et al*., 2005). However, since this family has only recently been defined, members, including COMMD4, have not been extensively studied. COMMD1 has been studied to a greater extent, and will be discussed as example to demonstrate the possible functions and roles that COMMD4 plays. COMMD1 functions in two distinct cellular activities viz. regulation of the transcription factor NF-κB and control of copper metabolism (Burstein *et al*., 2005).

NF-κB is a transcription factor and is associated, amongst other things, with cardiac hypertrophy development, cell survival and inflammation. All COMMD family members are capable of inhibiting NF-κB transcriptional activity (de Bie *et al*., 2006, Burstein *et al*., 2005). The termination of the NF-κB response is mediated by COMMD1 by its association with a Cullin 2-containing ubiquitin ligase, and it is predicted that other COMMD proteins will possibly also associate with ubiquitin ligases to play a role in protein turnover and degradation (Burstein *et al*., 2005). To initiate the progression from hypertrophy to heart failure requires signaling pathways that can stimulate NF-κB activation (Li *et al*., 2004, Gupta *et al*., 2008); this makes the inhibition of COMMD-assisted NF-κB inactivation clinically very interesting.

COMMD1 also interacts with the copper transporter ATP7B, responsible for excreting copper in the bile (Burstein *et al*., 2005). There is a well recognized association of copper deficiency with cardiomyopathy as well

as other cardiac diseases (Klevay 2000), and it has been shown that the deterioration in cardiac function and morphology can be reversed upon copper repletion (Elsherif *et al*., 2004).

Sarikas *et al*. showed that truncated cMyBPC proteins resulting from mutations in cMyBPC are degraded by the UPS system, however, truncated mutant cMyBPC impairs the proteolytic capacity of the UPS by forming ubiquinated aggregates, and it was suggested that this impairment could be a mechanism of HCM pathogenesis related to frameshift mutations. However, it was not mechanistically clear how truncated cMyBPC causes impairment of the UPS (Sarikas *et al*., 2005). Interestingly, COMMD4 was identified as a ligand of the monophosphorylated MyBPC motif (A. Ramburan, PhD thesis). Seeing that COMMD proteins associate with ubiquitin ligases, it was speculated that severely truncated cMyBPC, lacking the MyBPC motif, is unable to bind to COMMD4. A study in our laboratory concurrent with the present one suggested that COMMD4 acts as an adaptor protein that stabilizes the interaction between cMyBPC and the E3 ubiquitin ligase (C. Swanepoel, PhD thesis). E3 ligase is essential for the polyubiquitination process by attaching ubiquitin molecules to cMyBPC to mark it as a target protein for recognition and degradation by the UPS. At least four attached ubiquitins are necessary for recognition of the protein for degradation (Mukhopadhyay and Riezman, 2007); therefore, the mutant proteins may pass through the first step of being marked for degradation, but because of the inability of COMMD4, together with E3 ligase, to bind to severely truncated cMyBPC, cannot become polyubiquinated. This will lead to a buildup of truncated protein and subsequent impairment of the UPS (C. Swanepoel, PhD thesis). Other cMyBPC mutations, leading to a less severely truncated protein which still retains the MyBPC motif, did not form ubiquinated aggregates (Sarikas *et al*., 2005). This is congruent with the ability of COMMD4 to bind to the retained MyBPC motif and complete degradation occurring consequently.

The UPS degrades abnormal proteins and therefore serves as an essential quality control system in the cell. Impairment of this system could be detrimental to cardiomyocytes, because the buildup of proteins that should have been removed, such as signaling proteins and transcription regulators could activate transcription and other processes that result in hypertrophy (Powell 2006). COMMD4 levels may also rise due to a lack of substrate, which may result in increased copper clearing, leading to copper depletion, which also has been implicated in cardiomyocyte hypertrophy (Elsherif *et al*., 2004).

COMMD4 was identified as ligand of monophosphorylated cMyBPC. Moreover, in the concurrent study on COMMD4, the protein was shown to interact with Down syndrome critical region 3 protein (DSCR3), F-box and leucine-rich repeat protein 10 (FBXL10) (an E3 ligase subunit) and legumain (LGMN) (C. Swanepoel, PhD thesis). These proteins are involved in protein trafficking and degradation. Moreover, COMMD4 also binds to SNX3 and ENO1, in addition to cMyBPC; thus, COMMD4 shares three interactors with MMGL. The MMGL-COMMD4 interaction therefore strongly suggests that a multiprotein complex consisting out of kinases, phosphodiesterases, glycolytic enzymes and proteins responsible for intracellular trafficking and degradation are anchoring simultaneously to a downstream target viz. cMyBPC. However, it is more likely that this multiprotein

complex assembles when cMyBPC has been released from the sarcomere for turnover by the 26S proteasome complex, and not within the sarcomere. A large multiprotein complex in the confines of the thick and thin filaments might sterically hinder crossbridge formation, especially during β-adrenergic stimulation. MMGL may serve as a scaffold stabilizing this cellular machinery in close proximity to ubiquinated cMyBPC thereby ensuring optimum precision and timing of cellular responses in the proteasome complex.

Assembly of such a multiprotein complex involved in intracellular trafficking and degradation would require a means of regulating which proteins to bind and at which time (i.e. when cMyBPC is released from the sarcomere for turnover). Such regulation could be achieved by phosphorylation. COMMD4 has putative PKA sites, which makes it plausible that MMGL, an AKAP, binds to it to bring PKA in close proximity to its target. Members of the COMMD protein family rely on protein-protein interactions to exert their functions, and these often involve the COMM domain (Burstein *et al*., 2005). Most of these putative PKA sites are situated in the COMM domain of COMMD4, which is used by members of the COMMD protein family to effect protein-protein interactions, by means of which they execute their functions. Thus phosphorylation could alter this domain's interactions with its binding partners and so modulate COMMD4 function. It could be speculated that MMGL might therefore not only play a role in stabilizing this complex, but also ensure that COMMD4 is phosphorylated by PKA, and hence, modulating protein-protein interactions in this complex. Following protein degradation, MMGL-bound PDE4D could hydrolyze the cAMP signal, attenuating PKA phosphorylation. Unphoshorylated COMMD4 might then dissociate from its binding partners, and assembly of the complex may start again upon phosphorylation, to initiate cMyBPC turnover and degradation.

4.2.2.4. Cardiac troponin I (cTNI)

The troponin complex, together with tropomyosin, forms the calcium-sensitive switch on the thin filament that activates contraction. The troponin complex consists of three proteins: the Ca^{2+}-binding subunit, troponin C (TNC), the tropomyosin-binding subunit, troponin T (TNT) and the inhibitory subunit, troponin I (TNI). These subunits are expressed as different isoforms depending on the tissue type, and in the heart, the inhibitory subunit is encoded by *TNNI3* and known as cardiac (c) TNI. In addition to Ca^{2+}, protein-protein interactions in the troponin complex are also modulated by cTNI phosphorylation. Human cTNI has primary phosphorylation sites at Ser23/Ser24, Ser43/Ser45 and Thr144. Ser23/Ser24 are located in a cardiac-specific N-terminal region, and are PKA and PKC substrates, with Ser43/Ser45 and Thr144 being PKC substrates (Noland *et al*., 1989).

Numerous excellent reviews are available on the effects of PKA-induced phosphorylation of cTNI and its physiological roles (Solaro *et al*., 2007, Layland *et al*., 2005, Gomes and Potter, 2004). In short, PKA phosphorylation at Ser23/Ser24 of cTNI results in a change in the cardiac-specific N-terminal interactions between cTNI and cTNC, reducing Ca^{2+} sensitivity of the latter (Solaro *et al*., 2008). In particular, phosphorylation at Ser23/Ser24 weakens the interactions between cTNI and cTNC, which causes the acidic N-

terminal of cTNI to bend. The acidic N-terminal subsequently interacts with the inhibitory region of cTNI, which results in the weakening of the interaction of the inhibitory region with actin, altering crossbridge reactions (Sakthivel *et al*., 2005). In particular, the desensitization of the myofilament due to PKA-induced cTNI phosphorylation, as well as an increase in the rate of Ca^{2+} dissociation from cTnC together causes acceleration of relaxation (Abbott *et al*., 2001, Kentish *et al*., 2001). Because of this, the crossbridge cycling rate increases and unloaded shortening velocity increases, all together contributing to the well-known β-adrenergic-induced lusitropy (Zhang *et al*., 1995, Strang *et al*., 1994, Herron *et al*., 2001).

Animal models are useful in demonstrating the role of PKA-induced cTNI phosphorylation on the lusitropic effect of β-adrenergic stimulation. In transgenic mouse models where cTNI was replaced with skeletal TNI, which lacks the N-terminal with the phosphorylatable Ser residues, β-agonist-induced lusitropy was significantly blunted, PKA-induced increases in unloaded shortening velocity was abolished, and the crossbridge cycling rate was decreased (Fentzke *et al*., 1999, Kentish *et al*., 2001). This suggested that phosphorylation of the N-terminal of cTNI is crucial for these physiological effects to take place. Mice which expressed mutant cTNI where the Ser residues were replaced with non-phosphorylatable alanines, showed decreased myofilament Ca^{2+}-sensitivity after β-adrenergic stimulation, and a reduction in the lusitropic effect (Pi *et al*., 2002, Pi *et al*., 2003). In mice expressing mutant cTNI where the Ser residues were replaced by aspartate residues mimicking a constantly phosphorylated state, enhanced left ventricular relaxation were observed compared to animals expressing normal cTNI, especially noticeable at increased heart rates. Upon isoproterenol treatment, this effect was similar in both groups (Takimoto *et al*., 2004).

Playing such a crucial role in crossbridge kinetics, it is not surprising that mutations in *TNNI3* have been implicated in HCM. Many of the cTNI mutations cause an increase in Ca^{2+}-sensitivity, which could lead to hypercontractility resulting in an increased energy demand. An increase in Ca^{2+}-sensitivity could also have an effect on slowing the rate of relaxation (Gomes and Potter, 2004).

PKA-dependent phosphorylation of Ser23/Ser24 in the cardiac-specific N-terminal of cTNI is thus essential for normal crossbridge cycling. Specificity of second messenger responses due to β-adrenergic signaling acting on cTNI is therefore required for efficient contractility regulation under different stresses, and this is partly achieved by anchoring PKA to cTNI via AKAPs (McConnell *et al*., 2009). However, the specific AKAP/s responsible for this targeting has been unknown until now. McConnell *et al*. have disrupted global PKA-AKAP binding by *in vivo* gene transfer of Ht31, a competing RII-binding peptide, and showed that in order to achieve maximal phosphorylation of PKA substrates upon β-adrenergic signaling, a local pool of PKA is needed in close proximity to its target (McConnell *et al*., 2009). Phosphorylation of cTNI *in vivo*, along with other PKA substrates viz. PLB and RyR_2, was significantly reduced upon isoproterenol stimulation of Ht31-expressing hearts compared with isoproterenol-stimulated controls, leading to increased cardiac contractility (McConnell *et al*., 2009). cTNI is also subjected to increased calpain-dependent proteolysis when Ser23/Ser24 are

dephosphorylated, causing truncation of the cardiac-specific N-terminal (Di Lisa *et al*., 1995). Ht31-mediated disruption of PKA-AKAP interaction resulted in an increase of N-terminal truncation, presumably due to reduced phosphorylation of the N-terminal Ser sites. It could be speculated that upon phosphorylation, conformational changes occur which alters the accessibility of the cleavage site, and therefore protects cTNI against cleavage (McConnell *et al*., 2009).

The present study therefore identified MMGL as an AKAP that is responsible for creating a local pool of PKA close to cTNI, mediating the physiological responses to β-adrenergic signaling as described in this section. It is interesting to note how cTNI and cMyBPC phosphorylation overlaps. Both contain phosphorylation sites in their N-terminals that is cardiac-specific. Upon phosphorylation, cMyBPC and cTNI together causes increased rates of cross-bridge cycling and decreased Ca^{2+} sensitivity of force (Layland *et al*., 2005), and together with altered Ca^{2+}-handling, contribute to increased twitch force, decreased twitch duration as well as increased rates of relaxation (Katz and Lorell, 2000). Separately, cTNI phosphorylation is mainly responsible for reducing Ca^{2+} sensitivity, with cMyBPC phosphorylation playing the dominant role in the PKA-mediated modulation of crossbridge cycling rate and force development (Stelzer *et al*., 2007). Phosphorylation of both cTNI and cMyBPC also protects each protein against proteolytic cleavage, contributing to a cardioprotective effect (McConnell *et al*., 2009, Sadayappan *et al*., 2006). Identifying a single AKAP able to anchor PKA, together with PDE4D, to both these regulatory proteins, both of which have been implicated in HCM when mutated, could therefore be of important clinical relevance for HCM and heart failure in general.

4.3. MYOMEGALIN ISOFORM 4 IS A NOVEL SARCOMERIC AKAP

The current AKAP anchoring model incorporates four important concepts. In order for a protein to be classified as an AKAP, it has to meet these four requirements being 1.) it must interact with the R-subunit of PKA in cells 2.) the unique targeting domains within each AKAP should participate in either protein-protein or protein-lipid interactions, which will determine the subcellular localization of PKA, 3.) it should be able to coordinate multiple signaling pathways by anchoring additional signaling enzymes such as phosphodiesterases, phosphatases and other kinases, and 4.) lastly, it should be able to form larger, multiprotein units by binding additional anchoring and scaffolding proteins (Colledge and Scott, 1999, Dodge and Scott, 2000, Colledge *et al*., 2000, Fraser *et al*., 2000).

MMGL isoform 4 meets all four requirements. It interacts with two distinct R-subunits of PKA (PRKAR1A and PRKAR2A), thereby displaying dual-specifity. By interacting with other PKA targets, such as cTNI and cMyBPC, it demonstrates that the targeting domains contained within MMGL participate in protein-protein interactions. MMGL also meets the criterion for being able to coordinate multiple signaling events by anchoring additional enzymes by interacting with PDE4D (Verde *et al*., 2001) and enolase. Moreover, MMGL meets the final criterion of binding to other adaptor and scaffolding proteins by binding to COMMD4 (C.Swanepoel,

personal communication) and CARP. Our results strongly suggest that MMGL forms part of a larger, multiprotein unit, as Y2H screens have shown that cMyBPC also binds to COMMD4 and ENO3, here shown to be MMGL interactors, while COMMD4 itself also binds to ENO1 and SNX3 (A. Ramburan, PhD thesis, C. Swanepoel, PhD thesis). MMGL isoform 4 may therefore function as a vital link in signaling between upstream activators and numerous downstream targets. It is important to note that some of these interactions certainly occur within the sarcomere, but that not all interactions necessarily occur within the sarcomere, nor do they necessarily all occur concurrently.

By the beginning of 2006, there were no AKAPs known that were responsible for the phosphorylation of sarcomeric proteins (Dodge-Kafka *et al.*, 2006). Currently, several AKAPs have been described in cardiomyocytes, yet there are still very few AKAPs known to be responsible for phosphorylation of sarcomeric proteins. As example, an intermediate filament protein that functions as an AKAP, localized at the Z-disc, has been identified: synemin was speculated to participate in the regulation of myofilament protein phosphorylation (Russell *et al*., 2006). We add to this list by identifying MMGL isoform 4 as a novel dual-specific AKAP that interacts with two sarcomeric PKA targets, viz. cMyBPC and cTNI.

Furthermore, imaging of cardiomyocytes treated with the β-adrenergic agonist isoproterenol showed a higher level of colocalization between MMGL and its two sarcomeric PKA targets, cMyBPC and cTNI. This implies that under adrenergic stress, and consequential increased intracellular cAMP levels, PKA is dynamically recruited by MMGL isoform 4 to distinct sarcomeric locations to mediate cardiac stress responses, leading to increased cardiac contraction.

However, the observed increase in colocalization between MMGL with both cMyBPC and cTNI did not reach statistical significance. This observation is most likely due to the small sample sample size (n=3), resulting in inadequate statistical power, and not due to an inadequate concentration of isoproterenol, shown by McClellan *et al.* (2001) to be an effective concentration to induce β-adrenergic stimulation of cardiomyocytes. An increase in sample size would probably result in statistical significance, and this should be tested by additional experiments.

Moreover, MMGL-bound enolase would also be at the cMyBPC site to provide additional energy via glycolysis for the increased workload. Furthermore, MMGL would also act as AKAP in a different sarcomeric region, viz. titin's N2A domain, to enable PKA phosphorylation of CARP, and thereby regulate part of the myocardial stress-sense response by allowing CARP to dissociate from N2A and shuttle to the nucleus to upregulate the more compliant N2BA titin isoform. Outside the sarcomere, MMGL acts as AKAP by binding to COMMD4, as well as enolase, to facilitate control of efficient PKA phosphorylation of these proteins to mediate protein-protein interactions and enzyme activation in order to effect cMyBPC degradation via the UPS, and to supply this system with glycolytic energy. Lastly, the MMGL-bound PDE4D on these sites will terminate the second

messenger response by degrading cAMP. The lower levels of cAMP may then cause these multiprotein complexes to dissociate again.

4.4. MYOMEGALIN IS AN ESSENTIAL PART OF THE β-ADRENERGIC PATHWAY LEADING TO TRISPHOSPHORYLATED cMYBPC

Our knockdown studies of MMGL isoform 4 (Section 3.5) further suggests that MMGL not only acts as an AKAP at the MyBPC motif, but is an important link in adrenergic signaling and the regulation of cardiac function. In the presence of MMGL, all phosphorylation isoforms of cMyBPC are expressed well in H9C2 cells, and the level of the trisphosphorylated form of cMyBPC increases in such cells when they are treated with $CaCl_2$ and isoproterenol, i.e. under conditions of β-adrenergic stimulation.

However, with knockdown of MMGL under the same conditions of adrenergic stimulation, cMyBPC expression is dramatically reduced. These results can be interpreted as follows: during β-adrenergic stimulation, increased levels of cAMP activate PKA, which is subsequently targeted to the N-terminal of cMyBPC by binding to MMGL isoform 4. This ensures optimum phosphorylation of the MyBPC motif, and hence, enhanced cardiac contraction. When MMGL is not expressed, cMyBPC phosphorylation would be hindered, rendering the protein vulnerable to cleavage by proteases like calpain I (Section 1.2.4) (Decker *et al*., 2005, Sadayappan *et al*., 2009), leading to reduced cMyBPC levels in the cell, as observed in the knockdown experiment under adrenergic conditions. Typically, annulment of the effect of an AKAP is commonly more noticeable on the target protein only after adrenergic stimulation: The study of McConnell *et al.* (2009) showed no significant difference in the level of phosphorylation of cTNI, PLB and RyR_2 between Ht31-transfected versus control rat hearts. However, upon isoproterenol stimulation, dramatically decreased levels of PKA phosphorylation of all three proteins was observed in Ht31-transfected hearts compared to isoproterenol-stimulated hearts not expressing Ht31. Fink *et al.* (2001) also observed that isoproterenol stimulation resulted in significantly reduced PKA-dependent phosphorylation of cTNI and cMyBPC in cardiomyocytes expressing Ht31 compared to controls, and demonstrated that AKAPs regulate phosphorylation of these PKA targets in response to β-adrenergic stimulation, although it has been unknown which AKAP/s are responsible for the phosphorylation of these two proteins up till now. Thus, it appears that MMGL is an essential part in the β-adrenergic pathway leading to trisphosphorylation of cMyBPC and protection of the protein against degradation. The effects of MMGL knockdown on cTNI phosphorylation should also be investigated; however, due to time-constraints this was not attempted in the present study. Like cMyBPC, increased PKA phosphorylation of cTNI renders the protein resistant to N-terminal cleavage by calpain-dependent proteolysis, and it has been shown that disruption of cardiac PKA-AKAP binding under β-adrenergic conditions lead to a decrease in cTNI phosphorylation plus an increase in cTNI N-terminal cleavage, analogous to what was observed for cMyBPC in the present study (McConnell *et al*., 2009). However, in the McConnel *et al.* study the disrupted PKA-AKAP interactions were

mediated by the non-specific RII binding peptide i.e. Ht31, so the AKAP/s involved in this pathway were not identified. MMGL is a good candidate and a study of the effects of MMGL knockdown on cTNI expression and phosphorylation could shed light on these findings.

4.5. A MODEL OF CONTRACTION INCORPORATING MYOMEGALIN AND ITS LIGANDS

The contractile properties of muscle changes in response to phosphorylation of sarcomeric proteins, thus creating a converging point of complex signaling events in the cell (Montgomery *et al*., 2002). Together with its role in maintaining part of the structural arrangement of the sarcomere, cMyBPC phosphorylation plays a crucial role in regulating force by facilitating interaction between the thick and thin filaments (Flashman *et al*., 2004, Tong *et al*., 2008). cMyBPC acts as a link by tethering the myosin heads and the actin filaments, thereby facilitating the activation of crossbridge formation (Colson *et al*., 2008). Phosphorylation of cMyBPC via adrenergic stimulation leads to acceleration of crossbridge recruitment and force generation rates to match the stretch activation response to increases in chronotropy (Stelzer *et al*., 2006).

The C-terminal domains (C8-C10) of cMyBPC interact with the thick filament, by binding to titin and the myosin rod (Freiburg and Gautel, 1996). When cMyBPC is unphosphorylated, the N-terminal (C1-C2) interacts with myosin S2, thereby inhibiting myosin binding to actin, preventing crossbridge formation (Kunst *et al*., 2000, Kulikovskaya *et al*., 2003). In the unphosphorylated state, part of the N-terminal (C1 and the MyBPC motif) also binds to actin (Shaffer *et al*., 2009, Kulikovskaya *et al*., 2003) (Figure 4.1A). In addition, domains C0-C1 bind actin irrespective of the phosphorylation state of the MyBPC motif. The latter interaction allows for tethering of the thick and thin filament, thus cMyBPC structurally couples the thick and thin filaments (Shaffer *et al*., 2009). However, upon maximum phosphorylation of the MyBPC motif by CaMK and PKA, the interaction between the N-terminal of cMyBPC and myosin S2 is abolished (Kunst *et al*., 2000). This frees the myosin heads to make contact with actin, thus initiating force generation. Concurrently, the interaction between the MyBPC motif and actin is also lost.

It has been suggested that the MyBPC motif might block myosin S1 binding to actin, limiting crossbridge formation; upon phosphorylation, the unbinding of the motif from actin could then enable myosin binding and hence crossbridge formation. Alternatively, the unphosphorylated MyBPC motif could be free to bind to other ligands such as thin filament regulatory proteins (Shaffer *et al*., 2009, Razumova *et al*., 2006). Interestingly, in a Y2H library screen conducted in our laboratory, cTNI was found to be one of the most frequent interactors of the C1-C2 region of cMyBPC; this interaction was also shown to be affected by the phosphorylation status of the MyBPC motif. Specifically, binding of cTNI to C1-C2 involved a trisphosphorylated motif, as opposed to myosin S2 and actin that bind to an unphosphorylated motif. This particular study also confirmed the binding of the C1-C2 domains to actin and that it involved the unphosphorylated MyBPC motif. It is therefore likely that the MyBPC motif shuttles between actin and cTNI, depending on the phosphorylation state of the motif.

(A.Ramburan, PhD thesis, Ramburan *et al*., article in preparation). Therefore, the C1-C2 region is able to crosslink thick and thin filaments, possibly by using different surfaces to bind actin, and cTNI vs myosin S2, depending on the phosphorylation state of the motif, and thereby improving contractile efficiency. Figure 4.1B illustrates these changes described in response to phosphorylation.

It is therefore plausible that two PKA targets, i.e. cMyBPC and cTNI, which are both implicated in the regulation of cardiac contractility by increasing crossbridge cycling rates in response to phosphorylation, should have a means of ensuring spatial and temporal control over phosphorylation in response to second messenger signaling. The mechanism of PKA anchoring to these proteins have never been described; the findings of the present study strongly suggest that MMGL isoform 4 acts as AKAP to anchor PKA to these two sarcomeric proteins in response to β-adrenergic signaling, and thereby ensures optimum precision and speed of second messenger responses in this specialized area of contraction.

We, therefore, speculate that the following sequence of events might occur to facilitate cardiac contractility in response to stress: Membrane depolarization will cause a release of a small amount of Ca^{2+} via voltage-gated L-type channels, and this will cause the activation of CaMK, which will phosphorylate the first site (B) of the MyBPC motif (McClellan *et al*., 2001). This in turn will cause the myosin heads to be ordered in a more tight structure along the thick filament backbone. The transient Ca^{2+} concentration, which is not sufficient to directly activate the myofilaments, will subsequently serve as trigger to release Ca^{2+} from the sarcoplasmic reticulum via ryanodine receptors, and this increased level of Ca^{2+} will lead to a greater Ca^{2+} affinity in cTNC. Ca^{2+} activation of cTNC will result in a conformational change of the troponin complex, causing the release of the inhibitory region of cTNI from actin, and enabling crossbrigde formation (Li *et al*., 1999, Dong *et al*., 2003).

Upon β-adrenergic stimulation, the levels of diffusible cAMP will increase, leading to the activation of PKA. This will lead to phosphorylation of a number of sarcomeric and Ca^{2+} handling proteins, such as L-type Ca^{2+} channels, RyR_2, PLB, cMyBPC and cTNI, of which only cMyBPC and cTNI will be described here. Specifically, the binding of adrenaline or noradrenaline to the G-protein-coupled receptor will activate the G-protein, thereby activating adenylyl cyclase to convert ATP to cAMP, which in turn will activate PKA. cAMP-activated, MMGL-bound PKA will phosphorylate the remaining two sites (A and C) on the MyBPC motif, leading to di- and trisphosphorylation of cMyBPC, which then results in greater order of the myosin heads and a looser packing of the myosin backbone (Levine *et al*., 2001).

Although MMGL can bind to the C1-C2 region of cMyBPC irrespective of the phosphorylation state (A.Ramburan, PhD thesis), the increased levels of colocalization of MMGL with cMyBPC (and cTNI) observed upon β-adrenergic stimulation (Section 3.4) suggests that additional MMGL-PKA complexes could be recruited from the cytosol during times of physiological/pathological stress. Interestingly, the AKAP Yotiao, which targets PKA to the K^+ channel responsible for I_{ks} (Section 1.3.5.3), is itself also a substrate for PKA: phosphorylation of

Yotiao increases the functional response of the phosphorylatable cardiac I_{KS} channel to cAMP, whereas channel activation decreased when Yotiao is incapable of being phosphorylated, despite remaining functionally intact as an AKAP (Chen *et al*., 2005). The study by Chen *et al*. thus showed for the first time that an AKAP itself may actively participate in the functional regulation of a target protein, and may play a more important role than merely acting as adaptor (Chen *et al*., 2005). MMGL isoform 4 contains putative phosphorylation sites predicted by Phosphomotif Finder (www.hrpd.org/PhosphoMotif_finder), including PKA and CaMK II sites. Considering the above, the increased levels of colocalization between MMGL and cMyBPC (and cTNI) might be explained by the same principle in that MMGL may first need to be phosphorylated itself in order to recruit PKA to the target site, and/or to bind to the target site, or its ability to do so may be enhanced upon its own phosphorylation.

Therefore, the release of Ca^{2+} upon membrane depolarization will activate CaMK II, which will phosphorylate not only the first site (B) on the MyBPC motif, but may also phosphorylate MMGL. Additionally, phosphorylated MMGL might be able to bind with a higher affinity to cMyBPC (and cTNI) and recruit PKA to phosphorylate the remaining sites on the MyBPC motif (or cTNI). Although binding of PDE4D to isoform 4 of MMGL was not investigated in this study, it would be plausible that MMGL-bound PDE4D may also be on site to hydrolyze the increased amounts of cAMP, eventually attenuating the cAMP signal. This fits with the finding that MMGL interacts with the C1-C2 region of both unphosphorylated and trisphosphorylated cMyBPC: in the unphosphorylated state, MMGL would target PKA to phosphorylate the MyBPC motif, and in the trisphosphorylated state, MMGLwould anchor PDE4D to cMyBPC in order to hydrolyze the excess cAMP and attenuate the signal.

Therefore, in addition to increased levels of Ca^{2+} leading to the activation of the molecular switch of contraction involving the troponin-tropomyosin complex, MMGL-bound PKA trisphosphorylation of cMyBPC would enhance cardiac contractility by initiating the following events: Trisphosphorylation of the MyBPC motif will cause the interaction between the motif and myosin S2 to be abolished, enabling the myosin heads to be free to make contact with actin (Kunst *et al*., 2000). The interaction between the MyBPC motif and actin would concurrently be abolished (Shaffer *et al*., 2009), causing the trisphosphorylated motif to switch to bind to cTNI (Ramburan *et al*., article in preparation) and freeing actin to bind to the myosin heads, thereby accelerating crossbridge recruitment and force generation rates and matching the stretch activation response to the increased heart rate. Additionaly, as described in Section 4.2.2.4, phosphorylation of the N-terminal of cTNI by MMGL-bound PKA would add to the adaptation of cardiac muscle to the increased stress by reducing myofilament sensitivity to Ca^{2+}, as well as increasing the crossbridge cycling rate by reducing the binding affinity of cTNC for Ca^{2+}, all together contributing to β-adrenergic-induced lusitropy (Abbott *et al*., 2001, Kentish *et al*., 2001). Lastly, PDE4D may be anchored by MMGL in close proximity to cMyBPC and cTNI, which will allow for spatio-temporal control of cAMP hydrolysis, thereby attenuating the adrenergic signal. The lower levels of cAMP might then cause dissociation of these complexes (Figure 4.1C).

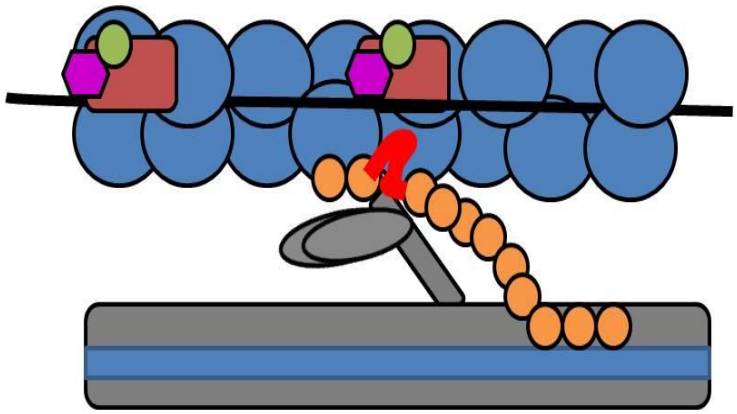

A: cMyBPC = unphosphorylated: MyBPC motif interacts with myosin S2; C0, C1 and MyBPC motif binds actin; crossbridge formation inhibited (see text for details)

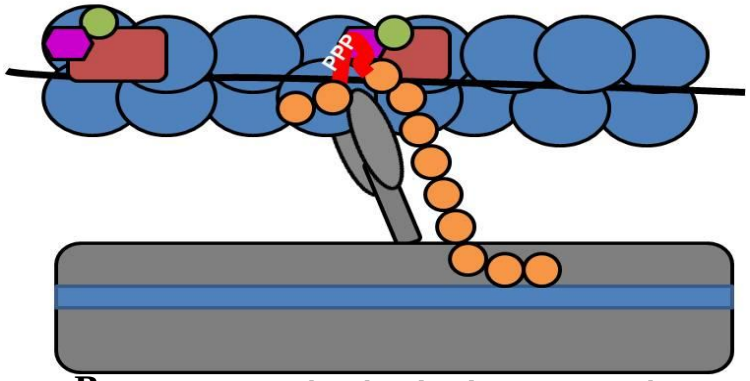

B: cMyBPC = phosphorylated: Interaction between myosin S2 and MyBPC motif abolished; interaction between actin and MyBPC motif is lost; myosin heads free to make contact with actin and initiate force generation; MyBPC motif switches to bind cTNI; C0-C1 binds actin irrespective of phosphorylation state, both these interactions allow structural coupling of thick and thin filaments (see text for details)

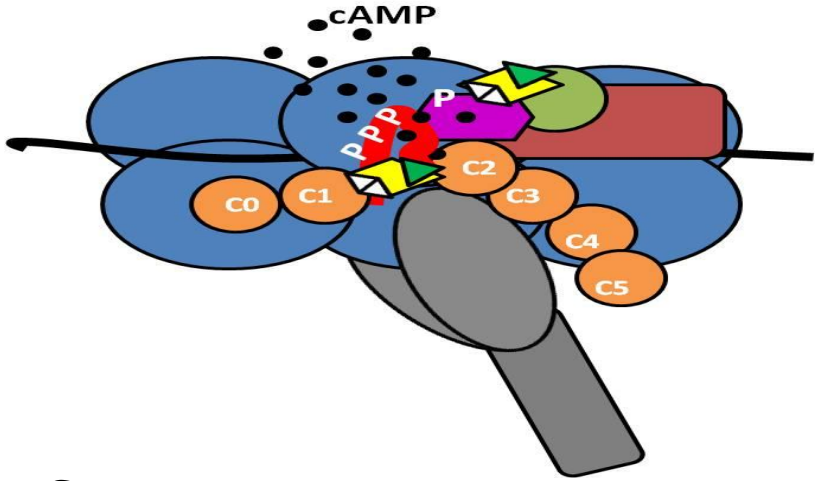

C: Upon β-adrenergic stimulation, cAMP levels increase and activate PKA that is compartmentalized by MMGL in close proximity to its targets, cMyBPC and cTNI. MMGL-bound PKA phosphorylation abolishes binding of myosin S2 and actin with the MyBPC motif, causing the trisphosphorylated motif to switch from actin to cTNI; this renders actin free to bind to myosin heads, resulting in acceleration of crossbridge recruitment and force generating rates. Additionally, MMGL-bound PDE4D hydrolyzes PKA, eventually attenuating the cAMP-derived adrenergic signal (see text for details)

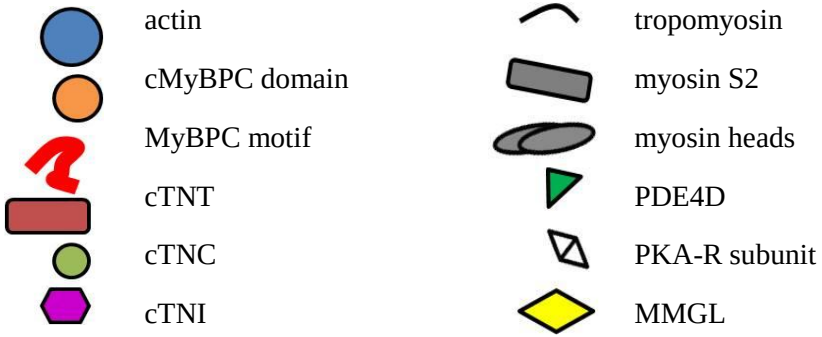

Figure 4.1. A model of contraction. See text for details

In addition, MMGL might act as AKAP at another sarcomeric location by mediating the spatio-temporal control of CARP phosphorylation at the N2A domain of titin. Phosphorylation of CARP might result in weakening of the interaction between CARP's coiled-coil domain with N2A, thereby freeing CARP to shuttle to the nucleus. In the nucleus, CARP would act as a transcription regulator (Kojic *et al*., 2004, Witt *et al*., 2005) and might take part in the upregulating process of N2BA, the more compliant isoform of titin. It could therefore be speculated that MMGL is indirectly involved in facilitating the acute myocardial stress-sensing response via phosphorylation (Section 4.2.2.1).

In this study, both the α- and β-isoforms of enolase were shown to interact with MMGL. In addition, β-enolase was found to interact with cMyBPC (A. Ramburan, PhD thesis) whereas α-enolase was found to interact with COMMD4 (C. Swanepoel, PhD thesis). Given that cMyBPC and COMMD4 also interact with MMGL, we deduce that the αβ-heterodimer of enolase forms a three-way interaction between these three proteins. In the sarcomere, MMGL might act as scaffold and AKAP to enable optimum spatio-temporal control of αβ-enolase phosphorylation by PKA. Phosphorylated αβ-enolase might have an increased binding affinity for cMyBPC; thereby binding to and producing energy required for crossbridge formation through glycolysis in this subcellular space, as discussed in Section 4.2.2.2. Additionally, or alternatively, when cMyBPC is released form the sarcomere for turnover, phosphorylation of αβ-enolase, by MMGL-bound PKA, might increase its binding affinity and/or activate the enzyme to enable glycolysis, providing energy required for the degradation process to the UPS. Simulateously, phosphorylation of COMMD4, also by MMGL-bound PKA, might result in a higher binding affinity of this adaptor protein for its ligands cMyBPC and the E3 ubiquitin ligase. By binding these proteins, COMMD4 will thereby act as adaptor protein bringing the E3 ligase in close proximity to cMyBPC to enable polyubiquination of cMyBPC to mark it for degradation by the UPS (C. Swanepoel, PhD thesis) (Section 4.2.2.3).

4.6. MYOMEGALIN AS A POTENTIAL DRUG TARGET

4.6.1. Current treatments for heart failure

Chronic adrenergic signaling is a compensatory mechanism of the failing heart (Bristow 2000). Increased adrenergic drive will at first support cardiac performance of a failing heart; however, over time, the activation of the sympathetic nervous system causes harmful effects, which are therapeutically typically countered by using β-blockers (Hunt *et al*., 2005, Bristow 2000). Current treatment for chronic heart failure (CHF) consists of an array of drugs, the most commonly used being β-blockers, ACE-inhibitors and angiotensin II receptor antagonists. While there is no cure for CHF, these drugs are available as chronic treatment that aims to postpone further development of heart failure, improve heart function and lead to a general improvement of life quality (Hunt *et al*., 2005). Excellent results are obtained by employing β-adrenergic receptor blockade for CHF, and it is believed to be the only therapy proven to increase survival after myocardial infarction leading to CHF

development, although it is not free of side-effects (Bristow 2000, Lygren and Tasken, 2008). The discovery of new targets in the β-adrenergic signaling pathway could open up a new avenue of pharmacotherapy for CHF: by employing new antagonists capable of inhibiting the effect of cAMP at the level where its acts, rather than reducing total cAMP levels, it may be possible to isolate the favourable effects of β-blockers from its side effects (Lygren and Tasken, 2008).

4.6.2. AKAPs allow for specialized altered cAMP signaling

By altering PKA signaling, a variety of potential applications may arise in clinical settings where abnormal PKA signaling has been observed. By anchoring PKA directly to a target, AKAPs may represent a novel target for drugs that could lead to treatment of numerous diseases. Peptides, such as Ht31, have been designed to compete with full-length AKAPs for binding PKA-RII, and thereby disrupt the PKA-AKAP interaction, and have been successfully used as tools to delineate the specific effects facilitated by PKA isozymes, as described in Section 1.3.4. However, such peptides are non-specific and disrupt all PKARII-AKAP interactions in the cell. Moreover, based on reported X-ray crystal structures, the PKA-AKAP molecular interface is relatively large and covers approximately 30 square nm. This interface is also hydrophobic and flat, with very few grooves, making it difficult to design a small molecular compound capable of disrupting the interaction (Gold *et al*., 2006, Kinderman *et al*., 2006). A possible solution that ensures specificity may therefore be to target the interaction between the AKAP and the PKA substrate, and not the PKA-AKAP interaction itself (Lygren and Tasken, 2008). This, however, requires the identification of the specific AKAP plus its PKA substrate, as well as additional ligands, as was done in the current study.

An example of such identification of a specific AKAP plus its ligands, with the aim of possibly employing it as drug target for heart failure, is AKAP18δ. This AKAP recruits PKA to PLB (Lygren *et al*., 2007). Phosphorylation of PLB alters the interaction between PLB and SR ATP-dependent Ca^{2+} pump sarcoplasmic reticulum Ca^{2+} -ATPase (SERCA) 2, releasing the Ca^{2+} pump from inhibition. This causes rapid entering of Ca^{2+} into the SR, leading to faster cardiac relaxation rates (Bassani *et al*., 1994). AKAP18δ therefore provides a mechanism for precise adrenergic control of Ca^{2+} cycling and hence, regulation of cardiac relaxation. PKA phosphorylation of PLB was reduced upon β-adrenergic stimulation with isoproterenol when a cell-permeable adrenergic disruptor-peptide directed against the AKAP18δ-PLB interaction was introduced in an *in vivo* experiment conducted in cardiomyocytes. This altered Ca^{2+} re-uptake into the SR, and demonstrates that such peptides could block one specific effect of adrenergic signaling (Lygren *et al*., 2007). It is speculated that the targeting of the compartmentalization of this specific cAMP signaling complex with an AKAP18δ antagonist will interfere with adrenergic-induced phosphorylation of PLB, and thereby prevent SERCA2 activation. This will block the adrenaline-induced increase of energy expenditure that induces further damage to the post-infarcted failing heart (Lygren and Tasken, 2008).

In the failing heart, an adrenaline-induced increase in contractility could be detrimental, and validates the use of β-blockers to reduce chronic adrenergic signaling. However, β-blockers reduce cAMP signaling only by about 50%, and are non-specific (Lygren and Tasken, 2008); it would therefore be advantageous to develop antagonists that interferes with cAMP signaling at specific sites. Such compounds could then be used independently or together with β-blockers for a potentially more potent therapeutic effect, with less unwanted effects. By identifying a specific AKAP, such as MMGL, together with its sarcomeric ligands cMyBPC and cTNI, and PDE4D, it is possible to start developing interrupting molecules capable of producing specific alteration of cAMP signaling at a specific subcellular location. Interrupting MMGL-cMyBPC binding may result in reduced levels of trisphosphorylated cMyBPC, and therefore decreased inotropy. Blocking this single effector of the adrenergic pathway might be advantageous in cases of end-stage CHF where adrenergic signaling is constantly elevated and leading to further damage. In the case of cTNI, where phosphorylation leads to an overall increase in β-adrenergic lusitropy, a different effect might be obtained by disrupting MMGL-cTNI binding. This might be advantageous during other stages of heart failure. It would also be interesting to investigate the effect of distruption of both these AKAP bindings simultaneously. By altering cAMP signaling in two different, but still interdependent areas of contraction, different signaling outcomes could be achieved and this could be manipulated until an optimal desired effect is obtained.

On the other hand, disrupting the binding between MMGL and PDE4D could lead to increased phosphorylation of both cMyBPC and cTNI, thereby obtaining the exact opposite pharmacological effect than described above. Different from conventional PDE inhibitors, this would also allow for specificity. PDE inhibitors have been shown to be promising clinical agents for improving cardiac performance under critical conditions such as ischaemic heart attack (Rao and Xi, 2009). Conversely, by lowering PDE4D levels at the specific sarcomeric locations where MMGL binds could improve pathological conditions where increased force of contraction and relaxation rates is required in the long run.

However, our results have shown that MMGL binds additional ligands that are implicated in various cellular mechanisms viz. the degradation of proteins via the UPS (COMMD4), glycolysis (αβ-enolase) and the regulation of myocardial stress-sensing (CARP). This complicates the idea of developing a disrupting peptide that, for instance, is designed to interrupt the binding between MMGL and cMyBPC with the aim of decreasing cMyBPC phosphorylation resulting in reduced cardiac contractility upon β-adrenergic stimulation in patients with CHF. The MMGL domains involved in these interactions are unknown, and because MMGL isoform 4 is such a small protein, the possibility exists that the same domain might be involved in interacting with more than one ligand. If this is the case, blocking such a domain would have multiple effects on the cell, which might be more harmful than beneficial. For example, blocking the binding between MMGL and COMMD4 might result in COMMD4 not being phosphorylated, and therefore unable to anchor cMyBPC and/or E3 ligase, which will lead to the build-up of protein destined for degradation by the UPS. The build-up of truncated cMyBPC, and

subsequent impairment of the UPS, has been implicated in HCM (Sarikas *et al*., 2005). However, if it turns out that different domains are involved in these interactions, specific effects can be obtained that might result in a beneficial effect, as described in this section. Therefore, the next step in determining whether MMGL isoform 4 is a possible drug target would be to identify the specific domains of the protein that interacts with each of its ligands.

In conclusion, it should be remembered that the change in phosphorylation status of different individual PKA substrates can have a beneficial of harmful effect in the failing heart (Movsesian and Bristow, 2005), and therefore it is important to elucidate the effect of manipulating phosphorylation of each individual substrate. The different outcomes can then be combined to enable a mutual advantageous effect depending on the disease. Identifying specific AKAP-PKA substrate complexes will be the starting point toward developing novel drugs targeting AKAPs for the treatment of various human diseases.

4.7. MYOMEGALIN AND PKA AS MODIFIERS OF CONTRACTILITY

Concluding from our results discussed up to this point, we believe that MMGL is directly involved in the phosphorylation of two key regulatory proteins within the sarcomere, and therefore in the regulation of cardiac contractility. By anchoring PKA directly to two proteins implicated in HCM, viz. cMyBPC and cTNI, gene polymorphisms in MMGL and the regulatory subunits of PKA may be considered as potential modifiers of the development of hypertrophy within the context of HCM, as discussed in Section 1.7. According to our knowledge, the role of variants in genes involved with phosphorylation of sarcomeric proteins in cardiac hypertrophy has never been evaluated, and this is the first time a multi-SNP approach has been used to investigate the modulation of hypertrophy in a South African HCM cohort by the genes *PDE4DIP*, *PRKAR1A* and *PRKAR2A*.

4.7.1. SNP selection

The number of SNPs required for an association study depends on the LD pattern in the area of interest (Zhang *et al*., 2004). Only a small number of tag SNPs need to be selected in areas of the genome with high LD regions (Johnson *et al*., 2001, Patil *et al*., 2001), which will reduce genotyping effort without losing power (Zhang *et al*., 2001). *PRKAR1A* and *PRKAR2A* are both in regions of high LD, and SNPs were selected using the SNPbrowser software to achieve an even spacing of 0.5 LDUs on the metric LD map for the HapMap CEU and YRI populations. The LD structure of the CEU and YRI populations were used because previous association studies conducted in our laboratory found that it is the best possible estimation of our own South African population's LD structure, which is still uncharacterized. The metric LD map with additive distances in LDUs was developed by Maniatis *et al*. (2002), who concluded that LDU maps have greater power compared to a centi-Morgan/kb map in context of association mapping (Maniatis *et al*., 2004). The LDU method significantly reduces the number of SNPs required to cover a gene, which lead to the selection of only 4 SNPs in *PRKAR1A* and 3 SNPs

in *PRKAR2A*. However, the LDU method could not be used for SNP selection in *PDE4DIP*, because the gene is in a region of low LD. SNPs were therefore selected manually aiming to cover the gene, with SNPs distributed every 60000kb on average, as described in Section 2.21.2, and lead to the selection of 9 SNPs in *PDE4DIP*.

4.7.2. Genotyping approach

The high-throughput ABI Validated TaqMan® genotyping system used in the present study was much more effective compared to previous PCR-based genotyping approaches (ASREA and SNaPshot® primer extension analysis) conducted in our laboratory for the same cohort. Predesigned and validated TaqMan® assays save time on assay design, testing and optimization. The system also operates at a low concentration of DNA (5-20ng) which spares DNA samples. An automatic liquid handling robot was used to set up 5µl reactions in 384-well plates, which allows for quicker genotyping and reduces human error, while the small reaction volumes involved reduces costs to some extent. This system also eliminates the need for post-PCR transfer and handling.

The SDS software used to assign genotypes post-PCR performs automatic allele-calling based on fluorescence signals, and all genotypes with a confidence level lower than 95% are marked as undetermined. This ensures that doubtful genotypes are not entered into the data analyses. The genotyping results are exported as a text file which allows results to be directly imported to the database, which minimizes human typographical errors. We further monitored genotyping errors by utilizing the program Pedstats to determine whether all genotypes were consistent with expected Mendelian inheritance patterns. Genotypes that were inconsistent were resolved by re-genotyping.

Drawbacks of this system are that the use of commercial systems such as Taqman® is more expensive than conventional PCR-based genotyping approaches, and that validated TaqMan® assays are not yet available for all SNPs. However, it is possible to custom design TaqMan® assays for any SNP, although this will require additional optimization and sequencing to confirm accuracy.

4.7.3. Caveats in association studies

Three situations may give rise to statistical association between an allele and a phenotypic trait. Firstly, the allele itself may be functional and thereby exert a direct effect on the phenotypic expression. Secondly, the allele may be in LD with a functional allele and thirdly, it may be that the association exists due to pure chance. It is therefore crucial to ensure the reproducibility of such a study, yet there are many factors that influence the reproducibility of an association study on complex genetic traits (Cardon and Palmer, 2003).

4.7.3.1. Population stratification

Spurious association may result from undetected population substructure in any association study. Population stratification might confound association between an allele and a disease trait in a population that consists of a

mixture of subpopulations with different allele frequencies and disease risks. This will lead to false positive association between a specific genotype and a disease trait (Colhoun *et al*., 2003). We compensated for this by first testing for population stratification and then using the orthogonal QTDT model for SNPs where stratification was detected. The orthogonal model protects against population stratification by matching each "case-control" pair within a family, making any population-level differences in a given allele frequency irrelevant (Cardon and Palmer, 2003).

4.7.3.2. Phenotypic definition

Phenotypic definition contributes extensively to the reproducibility of any association study and it is therefore important that all measurements taken are relevant to the disease phenotype, and that it is taken with the same precision. Phenotypic expression of HCM varies greatly between individuals, predominantly the extent and distribution of hypertrophy. Hypertrophy in HCM is mainly asymmetrical and patients rarely exhibit uniform concentric hypertrophy, which makes it impossible to quantify the extent of hypertrophy in a whole cohort with a single measurement. To compensate for this problem, composite scores that consist of a number of hypertrophy measurements describing the extent of hypertrophy can be derived. However, there is still no consensus on which composite scores represents the best estimated extent and distribution of hypertrophy in HCM. Alternatively, cardiac magnetic resonance imaging (cMRI) can be used to determine LVM accurately; however cMRI is not as available as the more conventionally used echocardiography. In addition, not all individuals are suited to cMRI investigation (for instance due to implanted pacemakers or ICDs, or due to claustrophobia), reducing the number of individuals who may be phenotyped using this more accurate method; there is thus a play-off between power and accuracy.

These issues were addressed in the present study as follows: A single cardiologist characterized all individuals in the cohort by 2-D and M-mode echocardiography, thereby ensuring that all measurements were taken the same way and with the same precision. A total of 16 wall thickness measurements were taken at three levels of the heart to estimate the distribution of hypertrophy. Left ventricular mass (LVM) was determined by echocardiography as an indication of the extent of hypertrophy, however, due to left ventricular geometry in the presense of HCM-related LVH, a possibility exists that LVM as determined by echocardiography would not be an accurate estimate of hypertrophy. This trait is commonly used in similar studies and was therefore also used in this study as it would be more familiar to researchers in the field. However, to obtain a more comprehensive and possibly less inaccurate indication of the extent of hypertrophy, we made use of a composite score derived by principal component analysis (Comp1), which is the weighted average of the 16 cardiac wall thickness measurements, as well as two additional composite scores (CWT and Spirito-Maron), in addition to LVM.

4.7.3.3. Power

The definition of statistical power in an association study is the probability that a test statistic reflects a true association (or lack thereof) between a genomic variant and a specific disease trait (Gordon and Finch, 2005). The power of an association study therefore relies on the disease allele frequency as well as the sample and effect size (Colhoun *et al.*, 2003, Donahue and Allen, 2005). Genotyping errors and errors in phenotypic classification also significantly impact the power of such a study (Gordon and Finch, 2005).

There is currently no comprehensive method for calculating the power of an association study in extended families such as those used in the present study, and thus no formal calculations were done to estimate the power of the present study. Increasing the number of study subjects was also not possible seeing that every individual that gave consent within these 22 families, including all mutation-carriers, had already been included.

4.7.3.4. Multiple testing

Multiple testing in any cohort may cause an increased probability of obtaining a false positive (type I error). Bonferroni adjustment is a popular solution to this problem, and assumes that all the performed tests are independent and that each p-value is subsequently essentially multiplied by the number of tests performed. In the present study, the traits being evaluated are not truly independent seeing that they are all derived from the same 16 cardiac wall thickness measurements. Furthermore, it is commonly considered that the Bonferroni adjustment is too strict, and may lead to discarding of relevant associations (Perneger 1998).

Bayesian methods for correction are also not applicable seeing that prior knowledge of the probability of involvement are required, which is currently unknown for most genetic variants (Campbell and Rudan, 2002). Therefore, as the current study was conducted as an explorative study, no formal corrections for multiple testing were made, although the probability for type I errors were reduced by determining exact p-values for QTDT analyses with Monte-Carlo permutations, which provides an overall evaluation of significance (McIntyre et al., 2000).

4.7.3.5. Confounding variables

Ensuring that association between a specific variant and a phenotypic trait is due to the effect of the variant and not due to an unrelated covariant or trait is of utmost importance. Blood pressure is an example of a confounding variable in that it has an independent effect on hypertrophy. If these aspects are not accounted for in an association study, one cannot be sure if the variation in hypertrophy is due to variation in the covariant (eg. blood pressure) or the variant. In the current study, all analyses were adjusted for known hypertrophy covariates viz. systolic and diastolic blood pressure, sex, age, body surface area and heart rate, as well as the particular HCM-causing mutation.

4.7.4. Results from the present association study

The present association study forms part of a larger study conducted by our research group, of which the ultimate aim is to identify genes that modify the development of hypertrophy in a South African HCM cohort. Initially viewed as a monogenic disease where a single sarcomeric mutation is sufficient to cause the disease, HCM was used as a model disease to investigate the modifier effect on cardiac hypertrophy in general. However, due to the variable phenotypic expression, it is now accepted that the presentation of HCM is influenced not only by the main causal mutation, but also by additional environmental and genetic modifiers. This study identified a novel AKAP involved in the phosphorylation of cMyBPC, which lead us to believe that SNP variants in *PDE4DIP*, *PRKAR1A* and *PRKAR2A* might contribute to the phenotypic expression of HCM, and possibly also modify cardiac hypertrophy in general.

We found that the G-allele of the *PDE4DIP* SNP rs1664005 was associated with increased hypertrophy. This allele leads to an increase of 1.3mm in mIVST, 3.4mm in Maronscore and 8.1mm in CWTscore in our study population. Comp1 is derived from quantile-normalized data; therefore, the effect size following association analysis of this trait is not interpretable in terms of the original cardiac measurements. We therefore estimated the effect size from an analysis of the mean of the 16 untransformed cardiac wall thickness measurements that was originally used to derive Comp1 and found that the effect size was 0.5mm. This SNP is located in an intronic region of *PDE4DIP*, and therefore does not seem to have any obvious functional role. However, an intronic SNP may influence gene splicing by affecting a splice donor or acceptor site. *In silico* analysis of this SNP variant in two splice site prediction programs viz. Alternative Splice Site Predictor (http://www.es.embnet.org/~mwang/assp.html) and NetGene2 (http://www.cbs.dtu.dk/services/NetGene2/) showed that rs1664005 had no effect on either acceptor or donor splice sites, nor created a cryptic splice site.

It can therefore be speculated that the association found in this study is due to an effect of a functional variant that is in LD with rs1664005, either within *PDE4DIP* itself or with an adjacent gene that is associated with hypertrophy development. Because the LD distribution and and the extent of variation of *PDE4DIP* is unknown in our study population, the LD distribution and genetic variation of the CEU and YRI populations were used as best possible representation of our study population. Non-synonymous (i.e. possible functional) SNPs were found to be in LD with rs1664005 in both the CEU and the YRI populations (http://www.ncbi.nlm.nih.gov/SNP, www.ensembl.org/Homo_sapiens/Transcript/ProtVariations, SNPbrowser™ v 3.0, Haploview 4.2) which could explain the observed association. Rs3010980 is in LD with rs1664005 in the CEU and YRI populations, and results in an amino acid coding for either Ser or Asn. Both these amino acids have uncharged polar side chains, so it is unlikely that a change in the amino acid sequence will have an effect on the tertiary structure of the protein. Rs1324366 is in LD with rs1664005 in the YRI population, and the SNP codes for either Ala or Glu. This will result in either an amino acid with a nonpolar side chain (Ala) or a charged polar side chain (Glu), which may well affect protein tertiary structure, because Ala is hydrophobic and will most likely occur in the

interior of the protein, whereas Glu is hydrophilic and will most likely occur on the outer surface of the protein; therefore subsequent protein-protein interactions could be affected. It is therefore likely that this SNP may have a functional effect. Rs1628172 and rs2762875 are also in LD with rs1664005 in the YRI population. Both SNPs result in either an uncharged polar residue [Cys (rs1628172) or Gln (rs2762875)], or a charged polar residue [Arg (both SNPs)], which may also affect protein tertiary structure and interactions, for the same reasons as described for rs1324366. However, no reports of any studies of these non-synonymous SNPs in hypertrophy development could be found in the literature. Another explanation may be that rs1664005 itself exerts an unknown functional effect, however, to explore this option, additional studies in different and bigger cohorts, as well as functional work, should be conducted.

Two intronic SNPs in *PRKAR1A* were found to have a significant effect on two of the investigated hypertrophy traits. The A-allele of rs11651687 leads to an increase of 2.1mm in mIVST, whereas the A-allele of rs3785906 leads to an increase of 2.2mm in mIVST as well as a 16.3mm increase in CWTscore. It should be noted that although an increase of of 16.3mm in CWTscore seems extravagant, this trait represents the sum of all 16 cardiac wall thickness measurements, and therefore represents an average increase of ~1mm in each of the 16 measurements. *In silico* analyses of these SNPs with splice-site prediction programs (Alternative Splice Site Predictor and NetGene2) predicted no alternative splice-site acceptor or donor sites. These variants are not in LD with any possible functional SNPs known (http://www.ncbi.nlm.nih.gov/SNP, www.ensembl.org/Homo_sapiens/Transcript/ProtVariations, SNPbrowser™ v 3.0, Haploview 4.2). It is possible that this SNP in *PRKAR1A* is in LD with a variant(s) on adjacent gene(s) associated with hypertrophy development, or that these two SNPs themselves exert a currently unknown functional effect. However, this option should be further explored by conducting additional SNP studies in different and bigger cohorts, and by doing functional work.

No association was found between any SNP with mPWT, which is generally more closely associated with LVH than mIVST. Association was, however, found between all three positively associated SNPs with mIVST. This could be explained due to the extreme variability in extent and distribution of LVH in HCM patients, and it could be speculated that in this particular cohort, the distribution of hypertrophy is more localized to the septum than the posterior wall, explaining why association was found between both *PRKAR1A* SNPs, as well as with the *PDE4DIP* SNP, and mIVST, and not with mPWT. However, this should also be further explored by conducting additional SNP studies in different and bigger cohorts.

No association was found between SNPs in *PRKAR2A* and any hypertrophy trait. This was unexpected seeing that the R2A subunit has a high affinity for AKAP binding, and is the predominant PKA subunit expressed in the heart (Section 4.1), and also showed the stronger interaction with MMGL of the two regulatory subunits. However, only two SNPs were suitable for analysis with the genotyping approach followed in this study; it may

be that additional SNP studies should be applied to this gene before it is discarded as a potential modifier of hypertrophy in HCM.

This explorative study therefore identifies MMGL, and, to a lesser extent PRKAR1A, as putative modifiers of cardiac hypertrophy. The interaction work done in this study supports a role for these proteins in regulation of cardiac contractility, and therefore by extension, a role in cardiac morphology (viz. hypertrophy). However, as for any association study, these results need to be verified by independent studies in different populations, with bigger cohort sizes and additional functional work. As genetic modifiers appear sufficient to completely prevent disease expression in some HCM carriers, these two genes may point to new targets for intervention, especially given the interest in PDE4-inhibitors. This finding might lead to an improved understanding of HCM patho-aetiology and may also improve risk profiling. Such understanding may eventually lead to strategies aimed at preventing the development of pathological cardiac hypertrophy in HCM.

4.7.5. *PDE4DIP* as a candidate gene for HCM

The findings of the association of *PDE4DIP* variants with hypertrophy parameters and the functions derived for MMGL by protein interaction as well as knockdown studies, suggest that *PDE4DIP* should also be investigated as a candidate gene for HCM. Variants in *PDE4DIP* could lead to a translated protein with increased or decreased affinity for some of its ligands, perhaps sufficiently so to result in disease. For example, if MMGL is unable to bind cMyBPC, cTNI, the regulatory subunit of PKA, or PDE4D, the regulation of second messenger signaling would be affected. It is quite plausible that a mutant MMGL unable to bind any one of these interactors may have detrimental effects on contractility in general. Many HCM-causing point mutations are found in the C1-C2 region of *MYBPC3* and the N-terminal of cTNI, of which the pathological mechanisms are still unknown. A possible disease mechanism for this may be that MMGL binding is disrupted, and hence PKA cannot be brought close to its target site to mediate second messenger responses. Therefore, the opposite scenario is also likely to result in a similar effect, where MMGL is mutated and unable to bind cMyBPC and/or cTNI.

Moreover, mutations causing the regulatory subunits of PKA to be unable to bind to MMGL will render the protein useless as an AKAP, and this may also lead to hypertrophy development. Although cMyBPC and cTNI are phosphorylated by other kinases as well, only PKA phosphorylation can result in trisphosphorylated cMyBPC which is required for β-adrenergic stress responses, whereas PKA-dependent phosphorylation of Ser23/Ser24 in the N-terminal of cTNI is essential for normal crossbridge cycling. Incomplete phosphorylation of both these proteins will abolish the cardioprotective effect and will lead to increased protease cleavage of both of these sarcomeric proteins. Furthermore, if MMGL isoform 4 interacts with PDE4D, and is mutated in such a way that it cannot target to the sarcomere, it will also lead to insufficient levels of PDE4D in this region, due to lack of appropriate compartmentalization, which will lead to incomplete attenuation of any existing PKA signal. Higher levels of cAMP will activate prolonged PKA signaling, which in turn requires higher consumption of

ATP; such a scenario would fit with the energy depletion hypothesis that proposes that the unifying dysfunction in HCM is an increased energy demand due to increased and inefficient ATP utilizationin the sarcomere (Blair *et al*., 2001, Ashrafian *et al*., 2003). Over-usage of ATP might compromise the capacity of the cell to maintain energy levels in areas where ATP is crucial for normal homeostatic functions such as Ca^{2+} re-uptake and the myosin ATPase. Failure of proper Ca^{2+} re-uptake at the end of each contractile cycle by the SERCA2 pump, which has large energy requirements, will cause a prolonged cytosolic Ca^{2+} transient which will activate downstream mediators and stimulate hypertrophy (Ashrafian *et al*., 2003). Prolonged elevated cytosolic Ca^{2+} is also a trigger for ventricular arrhythmias (Ashrafian *et al*., 2003) which could lead to SCD. Further, if lower levels of ATP are available for the myosin ATPases, some crossbridges might fail to detach, which will result in reduced mechanical efficiency of the crossbridge cycle.

4.8. FUTURE STUDIES

Our understanding of the roles that different AKAPs play in physiological and pathological processes is still in its infancy. Generating animal models that lack individual AKAP genes will be invaluable towards contributing to our current knowledge, as it will not only provide insight into the mechanism of AKAP functioning, but also serve as models for the understanding of diseases.

However, before undertaking such proposed studies, one should first address the obvious questions that resulted from this study, which are the following: Does isoform 4, the smallest isoform of MMGL, of which the full-length isoform is classified as a PDE4D-interacting protein, also interact with PDE4D? To do this, a similar approach can be followed that was used to identify MMGL as a PKA R-subunit ligand, as was done in this study. Secondly, one should investigate the effect on cTNI phosphorylation upon MMGL knockdown, as was done for cMyBPC, to see if what the functional effect of MMGL binding to cTNI. Thirdly, if MMGL is to be considered a potential drug target, one should first identify the specific domains on MMGL that interact with its ligands identified in this study, as described in Section 4.6.

This study identified a novel AKAP involved in the regulation of cardiac contractility, and although it proved to be essential for the normal phosphorylation of its target protein in an *in vivo* RNAi setting, it is not clear what the physiological effects would be in a mammalian organism deficient or defective in MMGL. Generating a MMGL knockout animal model will provide insight into all the speculated roles that it plays in contractility as discussed in this chapter. It may also provide further answers for the pathological mechanisms in HCM, hypertrophy and heart failure. Generating a transgenic expression of different cMyBPC phosphorylation states against a MMGL-null background as well as the expression of wild-type cMyBPC against a MMGL-null background will shed light on the mechanism of how cMyBPC is phosphorylated, and the same approach could be used to better understand the interplay between cTNI, MMGL and cardiac function and structure.

MMGL is also expressed in the Golgi organelles of cells. Considering the fact that the library screen yielded three possible ligands that operate in protein trafficking in the Golgi area viz. SNX3, COMMD4 and the proteasome 26S subunit, the function of MMGL in this area should also be investigated.

Furthermore, MMGL should be considered a candidate HCM-causing gene, and should be assessed by mutation screening of HCM patients.

These proposed studies will be of utmost necessity if MMGL is to be considered as a possible target for pharmacological intervention, which in the end is the ultimate goal of biomedical research.

THESIS REFERENCES

http://cardiogenomics.med.harvard.edu/genes/gene-list

http://circulatory-system.org/muscule/im4.gif

http://www.angis.org.au/Databases/Heart/dbsearch.html

http://www.asecho.org/guidelines.php

http://www.cbs.dtu.dk/services/NetGene2/

http://www.ensembl.org

http://www.es.embnet.org/~mwang/assp.html

http://www.ncbi.nlm.nih.gov/

http://www.ncbi.nlm.nih.gov/BLAST

http://www.ncbi.nlm.nih.gov/Entrez

http://www.ncbi.nlm.nih.gov/gene/9659

www.genecards.org

www.hprd.org/PhosphoMotif_finder

Abbott,M.B., Dong,W.J., Dvoretsky,A., DaGue,B., Caprioli,R.M., Cheung,H.C., and Rosevear,P.R. (2001). Modulation of cardiac troponin C-cardiac troponin I regulatory interactions by the amino-terminus of cardiac troponin I. Biochemistry *40*, 5992-6001.

Abecasis,G.R., Cardon,L.R., and Cookson,W.O. (2000). A general test of association for quantitative traits in nuclear families. Am. J. Hum. Genet. *66*, 279-292.

Abecasis,G.R., Cherny,S.S., Cookson,W.O., and Cardon,L.R. (2002). Merlin--rapid analysis of dense genetic maps using sparse gene flow trees. Nat. Genet. *30*, 97-101.

Adler,V. *et al.* (1997). Conformation-dependent phosphorylation of p53. Proc. Natl. Acad. Sci. U. S. A *94*, 1686-1691.

Ahluwalia,G., Rhoads,A.R., and Lulla,M. (1984). Particulate cyclic 3',5'-nucleotide phosphodiesterase and calmodulin of cardiac muscle. Int. J. Biochem. *16*, 483-488.

Al-Khayat,H.A., Morris,E.P., and Squire,J.M. (2009). The 7-stranded structure of relaxed scallop muscle myosin filaments: support for a common head configuration in myosin-regulated muscles. J. Struct. Biol. *166*, 183-194.

Alcalai,R., Seidman,J.G., and Seidman,C.E. (2008). Genetic basis of hypertrophic cardiomyopathy: from bench to the clinics. J. Cardiovasc. Electrophysiol. *19*, 104-110.

Allison,D.B. (1997). Transmission-disequilibrium tests for quantitative traits. Am. J. Hum. Genet. *60*, 676-690.

Alto,N.M., Soderling,S.H., Hoshi,N., Langeberg,L.K., Fayos,R., Jennings,P.A., and Scott,J.D. (2003). Bioinformatic design of A-kinase anchoring protein-in silico: a potent and selective peptide antagonist of type II protein kinase A anchoring. Proc. Natl. Acad. Sci. U. S. A *100*, 4445-4450.

Angelo,R. and Rubin,C.S. (1998). Molecular characterization of an anchor protein (AKAPCE) that binds the RI subunit (RCE) of type I protein kinase A from Caenorhabditis elegans. J. Biol. Chem. *273*, 14633-14643.

Arimura,T. *et al.* (2009). Cardiac ankyrin repeat protein gene (ANKRD1) mutations in hypertrophic cardiomyopathy. J. Am. Coll. Cardiol. *54*, 334-342.

Ashrafian,H., Redwood,C., Blair,E., and Watkins,H. (2003). Hypertrophic cardiomyopathy:a paradigm for myocardial energy depletion. Trends Genet. *19*, 263-268.

Asirvatham,A.L., Galligan,S.G., Schillace,R.V., Davey,M.P., Vasta,V., Beavo,J.A., and Carr,D.W. (2004). A-kinase anchoring proteins interact with phosphodiesterases in T lymphocyte cell lines. J. Immunol. *173*, 4806-4814.

Baillie,G.S., Sood,A., McPhee,I., Gall,I., Perry,S.J., Lefkowitz,R.J., and Houslay,M.D. (2003). beta-Arrestin-mediated PDE4 cAMP phosphodiesterase recruitment regulates beta-adrenoceptor switching from Gs to Gi. Proc. Natl. Acad. Sci. U. S. A *100*, 940-945.

Baisamy,L., Jurisch,N., and Diviani,D. (2005). Leucine zipper-mediated homo-oligomerization regulates the Rho-GEF activity of AKAP-Lbc. J. Biol. Chem. *280*, 15405-15412.

Bajpai,M., Fiedler,S.E., Huang,Z., Vijayaraghavan,S., Olson,G.E., Livera,G., Conti,M., and Carr,D.W. (2006). AKAP3 selectively binds PDE4A isoforms in bovine spermatozoa. Biol. Reprod. *74*, 109-118.

Bang,M.L., Mudry,R.E., McElhinny,A.S., Trombitas,K., Geach,A.J., Yamasaki,R., Sorimachi,H., Granzier,H., Gregorio,C.C., and Labeit,S. (2001). Myopalladin, a novel 145-kilodalton sarcomeric protein with multiple roles in Z-disc and I-band protein assemblies. J. Cell Biol. *153*, 413-427.

Barefield,D. and Sadayappan,S. (2010). Phosphorylation and function of cardiac myosin binding protein-C in health and disease. J. Mol. Cell Cardiol. *48*, 866-875.

Barrett,J.C., Fry,B., Maller,J., and Daly,M.J. (2005). Haploview: analysis and visualization of LD and haplotype maps. Bioinformatics. *21*, 263-265.

Bartel,S., Stein,B., Eschenhagen,T., Mende,U., Neumann,J., Schmitz,W., Krause,E.G., Karczewski,P., and Scholz,H. (1996). Protein phosphorylation in isolated trabeculae from nonfailing and failing human hearts. Mol. Cell Biochem. *157*, 171-179.

Bassani,J.W., Bassani,R.A., and Bers,D.M. (1994). Relaxation in rabbit and rat cardiac cells: species-dependent differences in cellular mechanisms. J. Physiol *476*, 279-293.

Baudet,S. (2003). Another activity for the cardiac biologist: CARP fishing. Cardiovasc. Res. *59*, 529-531.

Beavo,J.A. (1995). Cyclic nucleotide phosphodiesterases: functional implications of multiple isoforms. Physiol Rev. *75*, 725-748.

Beavo,J.A. and Brunton,L.L. (2002). Cyclic nucleotide research -- still expanding after half a century. Nat. Rev. Mol. Cell Biol. *3*, 710-718.

Beene,D.L. and Scott,J.D. (2007). A-kinase anchoring proteins take shape. Curr. Opin. Cell Biol. *19*, 192-198.

Beltman,J., Sonnenburg,W.K., and Beavo,J.A. (1993). The role of protein phosphorylation in the regulation of cyclic nucleotide phosphodiesterases. Mol. Cell Biochem. *127-128*, 239-253.

Bers,D.M. (2002). Cardiac excitation-contraction coupling. Nature *415*, 198-205.

Bhattacharyya,R.P., Remenyi,A., Yeh,B.J., and Lim,W.A. (2006). Domains, motifs, and scaffolds: the role of modular interactions in the evolution and wiring of cell signaling circuits. Annu. Rev. Biochem. *75*, 655-680.

Blair,E., Redwood,C., Ashrafian,H., Oliveira,M., Broxholme,J., Kerr,B., Salmon,A., Ostman-Smith,I., and Watkins,H. (2001). Mutations in the gamma(2) subunit of AMP-activated protein kinase cause familial hypertrophic cardiomyopathy: evidence for the central role of energy compromise in disease pathogenesis. Hum. Mol. Genet. *10*, 1215-1220.

Bolger,G.B., Erdogan,S., Jones,R.E., Loughney,K., Scotland,G., Hoffmann,R., Wilkinson,I., Farrell,C., and Houslay,M.D. (1997). Characterization of five different proteins produced by alternatively spliced mRNAs from the human cAMP-specific phosphodiesterase PDE4D gene. Biochem. J. *328 (Pt 2)*, 539-548.

Bonne,G. *et al.* (1995). Cardiac myosin binding protein-C gene splice acceptor site mutation is associated with familial hypertrophic cardiomyopathy. Nat. Genet. *11*, 438-440.

Borbely,A., van,d., V, Papp,Z., Bronzwaer,J.G., Edes,I., Stienen,G.J., and Paulus,W.J. (2005). Cardiomyocyte stiffness in diastolic heart failure. Circulation *111*, 774-781.

Bristow,M.R. and Long,C.S. (2002). Cardiotrophin-1 in heart failure. Circulation *106*, 1430-1432.

Burstein,E., Hoberg,J.E., Wilkinson,A.S., Rumble,J.M., Csomos,R.A., Komarck,C.M., Maine,G.N., Wilkinson,J.C., Mayo,M.W., and Duckett,C.S. (2005). COMMD proteins, a novel family of structural and functional homologs of MURR1. J. Biol. Chem. *280*, 22222-22232.

Cadd,G. and McKnight,G.S. (1989). Distinct patterns of cAMP-dependent protein kinase gene expression in mouse brain. Neuron *3*, 71-79.

Campbell,H. and Rudan,I. (2002). Interpretation of genetic association studies in complex disease. Pharmacogenomics. J. *2*, 349-360.

Cardon,L.R. and Palmer,L.J. (2003). Population stratification and spurious allelic association. Lancet *361*, 598-604.

Carlisle Michel,J.J., Dodge,K.L., Wong,W., Mayer,N.C., Langeberg,L.K., and Scott,J.D. (2004). PKA-phosphorylation of PDE4D3 facilitates recruitment of the mAKAP signalling complex. Biochem. J. *381*, 587-592.

Carlson,C.R., Lygren,B., Berge,T., Hoshi,N., Wong,W., Tasken,K., and Scott,J.D. (2006). Delineation of type I protein kinase A-selective signaling events using an RI anchoring disruptor. J. Biol. Chem. *281*, 21535-21545.

Carnegie,G.K., Smith,F.D., McConnachie,G., Langeberg,L.K., and Scott,J.D. (2004). AKAP-Lbc nucleates a protein kinase D activation scaffold. Mol. Cell *15*, 889-899.

Carr,D.W., Stofko-Hahn,R.E., Fraser,I.D., Cone,R.D., and Scott,J.D. (1992). Localization of the cAMP-dependent protein kinase to the postsynaptic densities by A-kinase anchoring proteins. Characterization of AKAP 79. J. Biol. Chem. *267*, 16816-16823.

Carr,D.W., Hausken,Z.E., Fraser,I.D., Stofko-Hahn,R.E., and Scott,J.D. (1992). Association of the type II cAMP-dependent protein kinase with a human thyroid RII-anchoring protein. Cloning and characterization of the RII-binding domain. J. Biol. Chem. *267*, 13376-13382.

Carrier,L. *et al.* (1997). Organization and sequence of human cardiac myosin binding protein C gene (MYBPC3) and identification of mutations predicted to produce truncated proteins in familial hypertrophic cardiomyopathy. Circ. Res. *80*, 427-434.

Chen,L., Kurokawa,J., and Kass,R.S. (2005). Phosphorylation of the A-kinase-anchoring protein Yotiao contributes to protein kinase A regulation of a heart potassium channel. J. Biol. Chem. *280*, 31347-31352.

Chu,W., Burns,D.K., Swerlick,R.A., and Presky,D.H. (1995). Identification and characterization of a novel cytokine-inducible nuclear protein from human endothelial cells. J. Biol. Chem. *270*, 10236-10245.

Chung,M.W., Tsoutsman,T., and Semsarian,C. (2003). Hypertrophic cardiomyopathy: from gene defect to clinical disease. Cell Res. *13*, 9-20.

Clark,K.A., McElhinny,A.S., Beckerle,M.C., and Gregorio,C.C. (2002). Striated muscle cytoarchitecture: an intricate web of form and function. Annu. Rev. Cell Dev. Biol. *18*, 637-706.

Clerk,A. and Sugden,P.H. (2000). Small guanine nucleotide-binding proteins and myocardial hypertrophy. Circ. Res. *86*, 1019-1023.

Coghlan,V.M., Perrino,B.A., Howard,M., Langeberg,L.K., Hicks,J.B., Gallatin,W.M., and Scott,J.D. (1995). Association of protein kinase A and protein phosphatase 2B with a common anchoring protein. Science *267*, 108-111.

Colhoun,H.M., McKeigue,P.M., and Davey,S.G. (2003). Problems of reporting genetic associations with complex outcomes. Lancet *361*, 865-872.

Colledge,M. and Scott,J.D. (1999). AKAPs: from structure to function. Trends Cell Biol. *9*, 216-221.

Colledge,M., Dean,R.A., Scott,G.K., Langeberg,L.K., Huganir,R.L., and Scott,J.D. (2000). Targeting of PKA to glutamate receptors through a MAGUK-AKAP complex. Neuron *27*, 107-119.

Collins,A., Lau,W., and De,L., V (2004). Mapping genes for common diseases: the case for genetic (LD) maps. Hum. Hered. *58*, 2-9.

Colson,B.A., Bekyarova,T., Locher,M.R., Fitzsimons,D.P., Irving,T.C., and Moss,R.L. (2008). Protein kinase A-mediated phosphorylation of cMyBP-C increases proximity of myosin heads to actin in resting myocardium. Circ. Res. *103*, 244-251.

Comi,G.P. *et al.* (2001). Beta-enolase deficiency, a new metabolic myopathy of distal glycolysis. Ann. Neurol. *50*, 202-207.

Conti,M., Nemoz,G., Sette,C., and Vicini,E. (1995). Recent progress in understanding the hormonal regulation of phosphodiesterases. Endocr. Rev. *16*, 370-389.

Corbin,J.D., Sugden,P.H., Lincoln,T.M., and Keely,S.L. (1977). Compartmentalization of adenosine 3':5'-monophosphate and adenosine 3':5'-monophosphate-dependent protein kinase in heart tissue. J. Biol. Chem. *252*, 3854-3861.

Corfield,V.A., Moolman,J.C., Martell,R., and Brink,P.A. (1993). Polymerase chain reaction-based detection of MN blood group-specific sequences in the human genome. Transfusion *33*, 119-124.

Craig,R. and Offer,G. (1976). The location of C-protein in rabbit skeletal muscle. Proc. R. Soc. Lond B Biol. Sci. *192*, 451-461.

Crilley,J.G., Boehm,E.A., Blair,E., Rajagopalan,B., Blamire,A.M., Styles,P., McKenna,W.J., Ostman-Smith,I., Clarke,K., and Watkins,H. (2003). Hypertrophic cardiomyopathy due to sarcomeric gene mutations is characterized by impaired energy metabolism irrespective of the degree of hypertrophy. J. Am. Coll. Cardiol. *41*, 1776-1782.

Davare,M.A., Avdonin,V., Hall,D.D., Peden,E.M., Burette,A., Weinberg,R.J., Horne,M.C., Hoshi,T., and Hell,J.W. (2001). A beta2 adrenergic receptor signaling complex assembled with the Ca2+ channel Cav1.2. Science *293*, 98-101.

Davis,J.S. (1988). Interaction of C-protein with pH 8.0 synthetic thick filaments prepared from the myosin of vertebrate skeletal muscle. J. Muscle Res. Cell Motil. *9*, 174-183.

de,B.P., van de,S.B., Burstein,E., Duran,K.J., Berger,R., Duckett,C.S., Wijmenga,C., and Klomp,L.W. (2006). Characterization of COMMD protein-protein interactions in NF-kappaB signalling. Biochem. J. *398*, 63-71.

De,L., V, Isaac,H.I., and Scafe,C.R. (2006). A tool for selecting SNPs for association studies based on observed linkage disequilibrium patterns. Pac. Symp. Biocomput. 487-498.

De,L., V (2007). Selecting single-nucleotide polymorphisms for association studies with SNPbrowser software. Methods Mol. Biol. *376*, 177-193.

Decker,R.S., Decker,M.L., Kulikovskaya,I., Nakamura,S., Lee,D.C., Harris,K., Klocke,F.J., and Winegrad,S. (2005). Myosin-binding protein C phosphorylation, myofibril structure, and contractile function during low-flow ischemia. Circulation *111*, 906-912.

Dell'Acqua,M.L. and Scott,J.D. (1997). Protein kinase A anchoring. J. Biol. Chem. *272*, 12881-12884.

Di,L.F., De,T.R., Salamino,F., Barbato,R., Melloni,E., Siliprandi,N., Schiaffino,S., and Pontremoli,S. (1995). Specific degradation of troponin T and I by mu-calpain and its modulation by substrate phosphorylation. Biochem. J. *308 (Pt 1)*, 57-61.

Diviani,D., Soderling,J., and Scott,J.D. (2001). AKAP-Lbc anchors protein kinase A and nucleates Galpha 12-selective Rho-mediated stress fiber formation. J. Biol. Chem. *276*, 44247-44257.

Diviani,D., Abuin,L., Cotecchia,S., and Pansier,L. (2004). Anchoring of both PKA and 14-3-3 inhibits the Rho-GEF activity of the AKAP-Lbc signaling complex. EMBO J. *23*, 2811-2820.

Dodge-Kafka,K.L., Soughayer,J., Pare,G.C., Carlisle Michel,J.J., Langeberg,L.K., Kapiloff,M.S., and Scott,J.D. (2005). The protein kinase A anchoring protein mAKAP coordinates two integrated cAMP effector pathways. Nature *437*, 574-578.

Dodge-Kafka,K.L., Langeberg,L., and Scott,J.D. (2006). Compartmentation of cyclic nucleotide signaling in the heart: the role of A-kinase anchoring proteins. Circ. Res. *98*, 993-1001.

Dodge,K. and Scott,J.D. (2000). AKAP79 and the evolution of the AKAP model. FEBS Lett. *476*, 58-61.

Dodge,K.L., Khouangsathiene,S., Kapiloff,M.S., Mouton,R., Hill,E.V., Houslay,M.D., Langeberg,L.K., and Scott,J.D. (2001). mAKAP assembles a protein kinase A/PDE4 phosphodiesterase cAMP signaling module. EMBO J. *20*, 1921-1930.

Donahue,M.P. and Allen,A.S. (2005). Genetic association studies in cardiology. Am. Heart J. *149*, 964-970.

Dong,W.J., Robinson,J.M., Stagg,S., Xing,J., and Cheung,H.C. (2003). Ca2+-induced conformational transition in the inhibitory and regulatory regions of cardiac troponin I. J. Biol. Chem. *278*, 8686-8692.

El-Armouche,A., Pohlmann,L., Schlossarek,S., Starbatty,J., Yeh,Y.H., Nattel,S., Dobrev,D., Eschenhagen,T., and Carrier,L. (2007). Decreased phosphorylation levels of cardiac myosin-binding protein-C in human and experimental heart failure. J. Mol. Cell Cardiol. *43*, 223-229.

Ellerbroek,S.M., Wennerberg,K., and Burridge,K. (2003). Serine phosphorylation negatively regulates RhoA in vivo. J. Biol. Chem. *278*, 19023-19031.

Elsherif,L., Wang,L., Saari,J.T., and Kang,Y.J. (2004). Regression of dietary copper restriction-induced cardiomyopathy by copper repletion in mice. J. Nutr. *134*, 855-860.

Epstein,N.D., Cohn,G.M., Cyran,F., and Fananapazir,L. (1992). Differences in clinical expression of hypertrophic cardiomyopathy associated with two distinct mutations in the beta-myosin heavy chain gene. A 908Leu----Val mutation and a 403Arg----Gln mutation. Circulation *86*, 345-352.

Fananapazir,L. and Epstein,N.D. (1994). Genotype-phenotype correlations in hypertrophic cardiomyopathy. Insights provided by comparisons of kindreds with distinct and identical beta-myosin heavy chain gene mutations. Circulation *89*, 22-32.

Fentzke,R.C., Buck,S.H., Patel,J.R., Lin,H., Wolska,B.M., Stojanovic,M.O., Martin,A.F., Solaro,R.J., Moss,R.L., and Leiden,J.M. (1999). Impaired cardiomyocyte relaxation and diastolic function in transgenic mice expressing slow skeletal troponin I in the heart. J. Physiol *517 (Pt 1)* , 143-157.

Feo,S., Oliva,D., Barbieri,G., Xu,W.M., Fried,M., and Giallongo,A. (1990). The gene for the muscle-specific enolase is on the short arm of human chromosome 17. Genomics *6*, 192-194.

Fink,M.A., Zakhary,D.R., Mackey,J.A., Desnoyer,R.W., pperson-Hansen,C., Damron,D.S., and Bond,M. (2001). AKAP-mediated targeting of protein kinase a regulates contractility in cardiac myocytes. Circ. Res. *88*, 291-297.

Flashman,E., Redwood,C., Moolman-Smook,J., and Watkins,H. (2004). Cardiac myosin binding protein C: its role in physiology and disease. Circ. Res. *94*, 1279-1289.

Flashman,E., Watkins,H., and Redwood,C. (2007). Localization of the binding site of the C-terminal domain of cardiac myosin-binding protein-C on the myosin rod. Biochem. J. *401*, 97-102.

Flashman,E., Korkie,L., Watkins,H., Redwood,C., and Moolman-Smook,J.C. (2008). Support for a trimeric collar of myosin binding protein C in cardiac and fast skeletal muscle, but not in slow skeletal muscle. FEBS Lett. *582*, 434-438.

Flavigny,J., Souchet,M., Sebillon,P., Berrebi-Bertrand,I., Hainque,B., Mallet,A., Bril,A., Schwartz,K., and Carrier,L. (1999). COOH-terminal truncated cardiac myosin-binding protein C mutants resulting from familial hypertrophic cardiomyopathy mutations exhibit altered expression and/or incorporation in fetal rat cardiomyocytes. J. Mol. Biol. *294*, 443-456.

Fodstad,H., Swan,H., Laitinen,P., Piippo,K., Paavonen,K., Viitasalo,M., Toivonen,L., and Kontula,K. (2004). Four potassium channel mutations account for 73% of the genetic spectrum underlying long-QT syndrome (LQTS) and provide evidence for a strong founder effect in Finland. Ann. Med. *36 Suppl 1*, 53-63.

Forissier,J.F. *et al.* (2005). Diagnostic accuracy of a 2D left ventricle hypertrophy score for familial hypertrophic cardiomyopathy. Eur. Heart J. *26*, 1882-1886.

Foucault,G., Vacher,M., Cribier,S., and rrio-Dupont,M. (2000). Interactions between beta-enolase and creatine kinase in the cytosol of skeletal muscle cells. Biochem. J. *346 Pt 1*, 127-131.

Fougier,S., Nemoz,G., Prigent,A.F., Marivet,M., Bourguignon,J.J., Wermuth,C., and Pacheco,H. (1986). Purification of cAMP-specific phosphodiesterase from rat heart by affinity chromatography on immobilized rolipram. Biochem. Biophys. Res. Commun. *138*, 205-214.

Fraser,I.D., Tavalin,S.J., Lester,L.B., Langeberg,L.K., Westphal,A.M., Dean,R.A., Marrion,N.V., and Scott,J.D. (1998). A novel lipid-anchored A-kinase Anchoring Protein facilitates cAMP-responsive membrane events. EMBO J. *17*, 2261-2272.

Fraser,I.D., Cong,M., Kim,J., Rollins,E.N., Daaka,Y., Lefkowitz,R.J., and Scott,J.D. (2000). Assembly of an A kinase-anchoring protein-beta(2)-adrenergic receptor complex facilitates receptor phosphorylation and signaling. Curr. Biol. *10*, 409-412.

Freiburg,A. and Gautel,M. (1996). A molecular map of the interactions between titin and myosin-binding protein C. Implications for sarcomeric assembly in familial hypertrophic cardiomyopathy. Eur. J. Biochem. *235*, 317-323.

Furst,D.O., Vinkemeier,U., and Weber,K. (1992). Mammalian skeletal muscle C-protein: purification from bovine muscle, binding to titin and the characterization of a full-length human cDNA. J. Cell Sci. *102 (Pt 4)*, 769-778.

Gabriel,S.B. *et al.* (2002). The structure of haplotype blocks in the human genome. Science *296*, 2225-2229.

Galinska-Rakoczy,A., Engel,P., Xu,C., Jung,H., Craig,R., Tobacman,L.S., and Lehman,W. (2008). Structural basis for the regulation of muscle contraction by troponin and tropomyosin. J. Mol. Biol. *379*, 929-935.

Gao,T., Yatani,A., Dell'Acqua,M.L., Sako,H., Green,S.A., Dascal,N., Scott,J.D., and Hosey,M.M. (1997). cAMP-dependent regulation of cardiac L-type Ca2+ channels requires membrane targeting of PKA and phosphorylation of channel subunits. Neuron *19*, 185-196.

Gao,T., Puri,T.S., Gerhardstein,B.L., Chien,A.J., Green,R.D., and Hosey,M.M. (1997). Identification and subcellular localization of the subunits of L-type calcium channels and adenylyl cyclase in cardiac myocytes. J. Biol. Chem. *272*, 19401-19407.

Garvey,J.L., Kranias,E.G., and Solaro,R.J. (1988). Phosphorylation of C-protein, troponin I and phospholamban in isolated rabbit hearts. Biochem. J. *249*, 709-714.

Gautel,M., Zuffardi,O., Freiburg,A., and Labeit,S. (1995). Phosphorylation switches specific for the cardiac isoform of myosin binding protein-C: a modulator of cardiac contraction? EMBO J. *14*, 1952-1960.

Gilbert,E.M., Hershberger,R.E., Wiechmann,R.J., Movsesian,M.A., and Bristow,M.R. (1995). Pharmacologic and hemodynamic effects of combined beta-agonist stimulation and phosphodiesterase inhibition in the failing human heart. Chest *108*, 1524-1532.

Gold,M.G., Lygren,B., Dokurno,P., Hoshi,N., McConnachie,G., Tasken,K., Carlson,C.R., Scott,J.D., and Barford,D. (2006). Molecular basis of AKAP specificity for PKA regulatory subunits. Mol. Cell *24*, 383-395.

Gomes,A.V. and Potter,J.D. (2004). Cellular and molecular aspects of familial hypertrophic cardiomyopathy caused by mutations in the cardiac troponin I gene. Mol. Cell Biochem. *263*, 99-114.

Gordon,D. and Finch,S.J. (2005). Factors affecting statistical power in the detection of genetic association. J. Clin. Invest *115*, 1408-1418.

Granzier,H.L. and Labeit,S. (2004). The giant protein titin: a major player in myocardial mechanics, signaling, and disease. Circ. Res. *94*, 284-295.

Gray,P.C., Tibbs,V.C., Catterall,W.A., and Murphy,B.J. (1997). Identification of a 15-kDa cAMP-dependent protein kinase-anchoring protein associated with skeletal muscle L-type calcium channels. J. Biol. Chem. *272*, 6297-6302.

Gruen,M. and Gautel,M. (1999). Mutations in beta-myosin S2 that cause familial hypertrophic cardiomyopathy (FHC) abolish the interaction with the regulatory domain of myosin-binding protein-C. J. Mol. Biol. *286*, 933-949.

Gruen,M., Prinz,H., and Gautel,M. (1999). cAPK-phosphorylation controls the interaction of the regulatory domain of cardiac myosin binding protein C with myosin-S2 in an on-off fashion. FEBS Lett. *453*, 254-259.

Gupta,S., Young,D., Maitra,R.K., Gupta,A., Popovic,Z.B., Yong,S.L., Mahajan,A., Wang,Q., and Sen,S. (2008). Prevention of cardiac hypertrophy and heart failure by silencing of NF-kappaB. J. Mol. Biol. *375* , 637-649.

Harris,S.P., Bartley,C.R., Hacker,T.A., McDonald,K.S., Douglas,P.S., Greaser,M.L., Powers,P.A., and Moss,R.L. (2002). Hypertrophic cardiomyopathy in cardiac myosin binding protein-C knockout mice. Circ. Res. *90*, 594-601.

Harrison,S.A., Reifsnyder,D.H., Gallis,B., Cadd,G.G., and Beavo,J.A. (1986). Isolation and characterization of bovine cardiac muscle cGMP-inhibited phosphodiesterase: a receptor for new cardiotonic drugs. Mol. Pharmacol. *29*, 506-514.

Harshfield,G.A., Grim,C.E., Hwang,C., Savage,D.D., and Anderson,S.J. (1990). Genetic and environmental influences on echocardiographically determined left ventricular mass in black twins. Am. J. Hypertens. *3*, 538-543.

Hartzell,H.C. and Titus,L. (1982). Effects of cholinergic and adrenergic agonists on phosphorylation of a 165,000-dalton myofibrillar protein in intact cardiac muscle. J. Biol. Chem. *257*, 2111-2120.

Hausken,Z.E. and Scott,J.D. (1996). Properties of A-kinase anchoring proteins. Biochem. Soc. Trans. *24*, 986-991.

Haworth,R.S., Cuello,F., Herron,T.J., Franzen,G., Kentish,J.C., Gautel,M., and Avkiran,M. (2004). Protein kinase D is a novel mediator of cardiac troponin I phosphorylation and regulates myofilament function. Circ. Res. *95*, 1091-1099.

Hayes,J.S. and Brunton,L.L. (1982). Functional compartments in cyclic nucleotide action. J. Cyclic. Nucleotide. Res. *8*, 1-16.

Herron,T.J., Korte,F.S., and McDonald,K.S. (2001). Power output is increased after phosphorylation of myofibrillar proteins in rat skinned cardiac myocytes. Circ. Res. *89*, 1184-1190.

Hoffmann,R., Baillie,G.S., MacKenzie,S.J., Yarwood,S.J., and Houslay,M.D. (1999). The MAP kinase ERK2 inhibits the cyclic AMP-specific phosphodiesterase HSPDE4D3 by phosphorylating it at Ser579. EMBO J. *18*, 893-903.

Holzbaur,E.L., Hammarback,J.A., Paschal,B.M., Kravit,N.G., Pfister,K.K., and Vallee,R.B. (1991). Homology of a 150K cytoplasmic dynein-associated polypeptide with the Drosophila gene Glued. Nature *351*, 579-583.

Houslay,M.D. and Adams,D.R. (2003). PDE4 cAMP phosphodiesterases: modular enzymes that orchestrate signalling cross-talk, desensitization and compartmentalization. Biochem. J. *370*, 1-18.

Huang,L.J., Durick,K., Weiner,J.A., Chun,J., and Taylor,S.S. (1997). Identification of a novel protein kinase A anchoring protein that binds both type I and type II regulatory subunits. J. Biol. Chem. *272* , 8057-8064.

Hulme,J.T., Ahn,M., Hauschka,S.D., Scheuer,T., and Catterall,W.A. (2002). A novel leucine zipper targets AKAP15 and cyclic AMP-dependent protein kinase to the C terminus of the skeletal muscle Ca2+ channel and modulates its function. J. Biol. Chem. *277*, 4079-4087.

Hulme,J.T., Lin,T.W., Westenbroek,R.E., Scheuer,T., and Catterall,W.A. (2003). Beta-adrenergic regulation requires direct anchoring of PKA to cardiac CaV1.2 channels via a leucine zipper interaction with A kinase-anchoring protein 15. Proc. Natl. Acad. Sci. U. S. A *100*, 13093-13098.

Hunt,S.A. *et al.* (2005). ACC/AHA 2005 Guideline Update for the Diagnosis and Management of Chronic Heart Failure in the Adult: a report of the American College of Cardiology/American Heart Association Task Force on Practice Guidelines (Writing Committee to Update the 2001 Guidelines for the Evaluation and Management of Heart Failure): developed in collaboration with the American College of Chest Physicians and the International Society for Heart and Lung Transplantation: endorsed by the Heart Rhythm Society. Circulation *112*, e154-e235.

Ihara,Y., Suzuki,Y.J., Kitta,K., Jones,L.R., and Ikeda,T. (2002). Modulation of gene expression in transgenic mouse hearts overexpressing calsequestrin. Cell Calcium *32*, 21-29.

Jacques,A.M., Copeland,O., Messer,A.E., Gallon,C.E., King,K., McKenna,W.J., Tsang,V.T., and Marston,S.B. (2008). Myosin binding protein C phosphorylation in normal, hypertrophic and failing human heart muscle. J. Mol. Cell Cardiol. *45*, 209-216.

Jahnsen,T., Lohmann,S.M., Walter,U., Hedin,L., and Richards,J.S. (1985). Purification and characterization of hormone-regulated isoforms of the regulatory subunit of type II cAMP-dependent protein kinase from rat ovaries. J. Biol. Chem. *260*, 15980-15987.

Jarnaess,E., Ruppelt,A., Stokka,A.J., Lygren,B., Scott,J.D., and Tasken,K. (2008). Dual specificity A-kinase anchoring proteins (AKAPs) contain an additional binding region that enhances targeting of protein kinase A type I. J. Biol. Chem. *283*, 33708-33718.

Jeacocke,S.A. and England,P.J. (1980). Phosphorylation of a myofibrillar protein of Mr 150 000 in perfused rat heart, and the tentative indentification of this as C-protein. FEBS Lett. *122*, 129-132.

Jeyaseelan,R., Poizat,C., Baker,R.K., Abdishoo,S., Isterabadi,L.B., Lyons,G.E., and Kedes,L. (1997). A novel cardiac-restricted target for doxorubicin. CARP, a nuclear modulator of gene expression in cardiac progenitor cells and cardiomyocytes. J. Biol. Chem. *272*, 22800-22808.

Jin,J. *et al.* (2004). Proteomic, functional, and domain-based analysis of in vivo 14-3-3 binding proteins involved in cytoskeletal regulation and cellular organization. Curr. Biol. *14*, 1436-1450.

Jin,S.L., Bushnik,T., Lan,L., and Conti,M. (1998). Subcellular localization of rolipram-sensitive, cAMP-specific phosphodiesterases. Differential targeting and activation of the splicing variants derived from the PDE4D gene. J. Biol. Chem. *273*, 19672-19678.

Jin,X., Xia,L., Wang,L.S., Shi,J.Z., Zheng,Y., Chen,W.L., Zhang,L., Liu,Z.G., Chen,G.Q., and Fang,N.Y. (2006). Differential protein expression in hypertrophic heart with and without hypertension in spontaneously hypertensive rats. Proteomics. *6*, 1948-1956.

Jurevicius,J. and Fischmeister,R. (1996). cAMP compartmentation is responsible for a local activation of cardiac Ca2+ channels by beta-adrenergic agonists. Proc. Natl. Acad. Sci. U. S. A *93*, 295-299.

Kapiloff,M.S., Schillace,R.V., Westphal,A.M., and Scott,J.D. (1999). mAKAP: an A-kinase anchoring protein targeted to the nuclear membrane of differentiated myocytes. J. Cell Sci. *112 (Pt 16)*, 2725-2736.

Kapiloff,M.S., Jackson,N., and Airhart,N. (2001). mAKAP and the ryanodine receptor are part of a multi-component signaling complex on the cardiomyocyte nuclear envelope. J. Cell Sci. *114*, 3167-3176.

Kapiloff,M.S. (2002). Contributions of protein kinase A anchoring proteins to compartmentation of cAMP signaling in the heart. Mol. Pharmacol. *62*, 193-199.

Kass,R.S. and Moss,A.J. (2003). Long QT syndrome: novel insights into the mechanisms of cardiac arrhythmias. J. Clin. Invest *112*, 810-815.

Katano,Y. and Endoh,M. (1992). Effects of a cardiotonic quinolinone derivative Y-20487 on the isoproterenol-induced positive inotropic action and cyclic AMP accumulation in rat ventricular myocardium: comparison with rolipram, Ro 20-1724, milrinone, and isobutylmethylxanthine. J. Cardiovasc. Pharmacol. *20*, 715-722.

Katz,A.M. and Lorell,B.H. (2000). Regulation of cardiac contraction and relaxation. Circulation *102*, IV69-IV74.

Kawasaki,H., Springett,G.M., Mochizuki,N., Toki,S., Nakaya,M., Matsuda,M., Housman,D.E., and Graybiel,A.M. (1998). A family of cAMP-binding proteins that directly activate Rap1. Science *282*, 2275-2279.

Keely,S.L. (1977). Activation of cAMP-dependent protein kinase without a corresponding increase in phosphorylase activity. Res. Commun. Chem. Pathol. Pharmacol. *18*, 283-290.

Keely,S.L. (1979). Prostaglandin E1 activation of heart cAMP-dependent protein kinase: apparent dissociation of protein kinase activation from increases in phosphorylase activity and contractile force. Mol. Pharmacol. *15*, 235-245.

Keller,A., Demeurie,J., Merkulova,T., Geraud,G., Cywiner-Golenzer,C., Lucas,M., and Chatelet,F.P. (2000). Fibre-type distribution and subcellular localisation of alpha and beta enolase in mouse striated muscle. Biol. Cell *92*, 527-535.

Kentish,J.C., McCloskey,D.T., Layland,J., Palmer,S., Leiden,J.M., Martin,A.F., and Solaro,R.J. (2001). Phosphorylation of troponin I by protein kinase A accelerates relaxation and crossbridge cycle kinetics in mouse ventricular muscle. Circ. Res. *88*, 1059-1065.

Kinderman,F.S., Kim,C., von,D.S., Ma,Y., Pham,B.Q., Spraggon,G., Xuong,N.H., Jennings,P.A., and Taylor,S.S. (2006). A dynamic mechanism for AKAP binding to RII isoforms of cAMP-dependent protein kinase. Mol. Cell *24*, 397-408.

Klauck,T.M., Faux,M.C., Labudda,K., Langeberg,L.K., Jaken,S., and Scott,J.D. (1996). Coordination of three signaling enzymes by AKAP79, a mammalian scaffold protein. Science *271*, 1589-1592.

Klevay,L.M. (2000). Cardiovascular disease from copper deficiency--a history. J. Nutr. *130*, 489S-492S.

Kojic,S., Medeot,E., Guccione,E., Krmac,H., Zara,I., Martinelli,V., Valle,G., and Faulkner,G. (2004). The Ankrd2 protein, a link between the sarcomere and the nucleus in skeletal muscle. J. Mol. Biol. *339* , 313-325.

Koretz,J.F. (1979). Effects of C-protein on synthetic myosin filament structure. Biophys. J. *27*, 433-446.

Kostic,M.M., Erdogan,S., Rena,G., Borchert,G., Hoch,B., Bartel,S., Scotland,G., Huston,E., Houslay,M.D., and Krause,E.G. (1997). Altered expression of PDE1 and PDE4 cyclic nucleotide phosphodiesterase isoforms in 7-oxo-prostacyclin-preconditioned rat heart. J. Mol. Cell Cardiol. *29*, 3135-3146.

Kruger,M. and Linke,W.A. (2006). Protein kinase-A phosphorylates titin in human heart muscle and reduces myofibrillar passive tension. J. Muscle Res. Cell Motil. *27*, 435-444.

Kruger,M., Sachse,C., Zimmermann,W.H., Eschenhagen,T., Klede,S., and Linke,W.A. (2008). Thyroid hormone regulates developmental titin isoform transitions via the phosphatidylinositol-3-kinase/ AKT pathway. Circ. Res. *102*, 439-447.

Kruger,M. and Linke,W.A. (2009). Titin-based mechanical signalling in normal and failing myocardium. J. Mol. Cell Cardiol. *46*, 490-498.

Kruger,M., Kotter,S., Grutzner,A., Lang,P., Andresen,C., Redfield,M.M., Butt,E., dos Remedios,C.G., and Linke,W.A. (2009). Protein kinase G modulates human myocardial passive stiffness by phosphorylation of the titin springs. Circ. Res. *104*, 87-94.

Kulikovskaya,I., McClellan,G., Flavigny,J., Carrier,L., and Winegrad,S. (2003). Effect of MyBP-C binding to actin on contractility in heart muscle. J. Gen. Physiol *122*, 761-774.

Kunst,G., Kress,K.R., Gruen,M., Uttenweiler,D., Gautel,M., and Fink,R.H. (2000). Myosin binding protein C, a phosphorylation-dependent force regulator in muscle that controls the attachment of myosin heads by its interaction with myosin S2. Circ. Res. *86*, 51-58.

Kuo,T.Y., Lau,W., and Collins,A.R. (2007). LDMAP: the construction of high-resolution linkage disequilibrium maps of the human genome. Methods Mol. Biol. *376*, 47-57.

Kutyavin,I.V. *et al.* (2000). 3'-minor groove binder-DNA probes increase sequence specificity at PCR extension temperatures. Nucleic Acids Res. *28*, 655-661.

Labeit,S., Gautel,M., Lakey,A., and Trinick,J. (1992). Towards a molecular understanding of titin. EMBO J. *11*, 1711-1716.

Lahmers,S., Wu,Y., Call,D.R., Labeit,S., and Granzier,H. (2004). Developmental control of titin isoform expression and passive stiffness in fetal and neonatal myocardium. Circ. Res. *94*, 505-513.

Lang,P., Gesbert,F., espine-Carmagnat,M., Stancou,R., Pouchelet,M., and Bertoglio,J. (1996). Protein kinase A phosphorylation of RhoA mediates the morphological and functional effects of cyclic AMP in cytotoxic lymphocytes. EMBO J. *15*, 510-519.

Lange,S., Ehler,E., and Gautel,M. (2006). From A to Z and back? Multicompartment proteins in the sarcomere. Trends Cell Biol. *16*, 11-18.

Layland,J., Solaro,R.J., and Shah,A.M. (2005). Regulation of cardiac contractile function by troponin I phosphorylation. Cardiovasc. Res. *66*, 12-21.

Lehnart,S.E., Wehrens,X.H., Reiken,S., Warrier,S., Belevych,A.E., Harvey,R.D., Richter,W., Jin,S.L., Conti,M., and Marks,A.R. (2005). Phosphodiesterase 4D deficiency in the ryanodine-receptor complex promotes heart failure and arrhythmias. Cell *123*, 25-35.

Lester,L.B. and Scott,J.D. (1997). Anchoring and scaffold proteins for kinases and phosphatases. Recent Prog. Horm. Res. *52*, 409-429.

Levine,R., Weisberg,A., Kulikovskaya,I., McClellan,G., and Winegrad,S. (2001). Multiple structures of thick filaments in resting cardiac muscle and their influence on cross-bridge interactions. Biophys. J. *81*, 1070-1082.

Li,M.X., Spyracopoulos,L., and Sykes,B.D. (1999). Binding of cardiac troponin-I147-163 induces a structural opening in human cardiac troponin-C. Biochemistry *38*, 8289-8298.

Li,Y., Ha,T., Gao,X., Kelley,J., Williams,D.L., Browder,I.W., Kao,R.L., and Li,C. (2004). NF-kappaB activation is required for the development of cardiac hypertrophy in vivo. Am. J. Physiol Heart Circ. Physiol *287*, H1712-H1720.

Lim,J., Pahlke,G., and Conti,M. (1999). Activation of the cAMP-specific phosphodiesterase PDE4D3 by phosphorylation. Identification and function of an inhibitory domain. J. Biol. Chem. *274*, 19677-19685.

Lim,M.S. and Walsh,M.P. (1986). Phosphorylation of skeletal and cardiac muscle C-proteins by the catalytic subunit of cAMP-dependent protein kinase. Biochem. Cell Biol. *64*, 622-630.

Linke,W.A. (2008). Sense and stretchability: the role of titin and titin-associated proteins in myocardial stress-sensing and mechanical dysfunction. Cardiovasc. Res. *77*, 637-648.

Liu,H. and Maurice,D.H. (1999). Phosphorylation-mediated activation and translocation of the cyclic AMP-specific phosphodiesterase PDE4D3 by cyclic AMP-dependent protein kinase and mitogen-activated protein kinases. A potential mechanism allowing for the coordinated regulation of PDE4D activity and targeting. J. Biol. Chem. *274*, 10557-10565.

Lugnier,C., Muller,B., Le,B.A., Beaudry,C., and Rousseau,E. (1993). Characterization of indolidan- and rolipram-sensitive cyclic nucleotide phosphodiesterases in canine and human cardiac microsomal fractions. J. Pharmacol. Exp. Ther. *265*, 1142-1151.

Lugnier,C., Keravis,T., Le,B.A., Pauvert,O., Proteau,S., and Rousseau,E. (1999). Characterization of cyclic nucleotide phosphodiesterase isoforms associated to isolated cardiac nuclei. Biochim. Biophys. Acta *1472*, 431-446.

Lygren,B. *et al.* (2007). AKAP complex regulates Ca2+ re-uptake into heart sarcoplasmic reticulum. EMBO Rep. *8*, 1061-1067.

Lygren,B. and Tasken,K. (2008). The potential use of AKAP18delta as a drug target in heart failure patients. Expert. Opin. Biol. Ther. *8*, 1099-1108.

Makarenko,I., Opitz,C.A., Leake,M.C., Neagoe,C., Kulke,M., Gwathmey,J.K., del,M.F., Hajjar,R.J., and Linke,W.A. (2004). Passive stiffness changes caused by upregulation of compliant titin isoforms in human dilated cardiomyopathy hearts. Circ. Res. *95*, 708-716.

Maniatis,N., Collins,A., Xu,C.F., McCarthy,L.C., Hewett,D.R., Tapper,W., Ennis,S., Ke,X., and Morton,N.E. (2002). The first linkage disequilibrium (LD) maps: delineation of hot and cold blocks by diplotype analysis. Proc. Natl. Acad. Sci. U. S. A *99*, 2228-2233.

Maniatis,N., Morton,N.E., Gibson,J., Xu,C.F., Hosking,L.K., and Collins,A. (2005). The optimal measure of linkage disequilibrium reduces error in association mapping of affection status. Hum. Mol. Genet. *14*, 145-153.

Manning,G., Whyte,D.B., Martinez,R., Hunter,T., and Sudarsanam,S. (2002). The protein kinase complement of the human genome. Science *298*, 1912-1934.

Marian,A.J. (2001). On genetic and phenotypic variability of hypertrophic cardiomyopathy: nature versus nurture. J. Am. Coll. Cardiol. *38*, 331-334.

Marian,A.J. (2002). Modifier genes for hypertrophic cardiomyopathy. Curr. Opin. Cardiol. *17*, 242-252.

Maron,B.J., Bonow,R.O., Cannon,R.O., III, Leon,M.B., and Epstein,S.E. (1987). Hypertrophic cardiomyopathy. Interrelations of clinical manifestations, pathophysiology, and therapy (1). N. Engl. J. Med. *316* , 780-789.

Maron,B.J., Gardin,J.M., Flack,J.M., Gidding,S.S., Kurosaki,T.T., and Bild,D.E. (1995). Prevalence of hypertrophic cardiomyopathy in a general population of young adults. Echocardiographic analysis of 4111 subjects in the CARDIA Study. Coronary Artery Risk Development in (Young) Adults. Circulation *92*, 785-789.

Maron,B.J., Shirani,J., Poliac,L.C., Mathenge,R., Roberts,W.C., and Mueller,F.O. (1996). Sudden death in young competitive athletes. Clinical, demographic, and pathological profiles. JAMA *276*, 199-204.

Marston,S., Copeland,O., Jacques,A., Livesey,K., Tsang,V., McKenna,W.J., Jalilzadeh,S., Carballo,S., Redwood,C., and Watkins,H. (2009). Evidence from human myectomy samples that MYBPC3 mutations cause hypertrophic cardiomyopathy through haploinsufficiency. Circ. Res. *105*, 219-222.

Marx,S.O., Reiken,S., Hisamatsu,Y., Jayaraman,T., Burkhoff,D., Rosemblit,N., and Marks,A.R. (2000). PKA phosphorylation dissociates FKBP12.6 from the calcium release channel (ryanodine receptor): defective regulation in failing hearts. Cell *101*, 365-376.

Marx,S.O., Reiken,S., Hisamatsu,Y., Gaburjakova,M., Gaburjakova,J., Yang,Y.M., Rosemblit,N., and Marks,A.R. (2001). Phosphorylation-dependent regulation of ryanodine receptors: a novel role for leucine/isoleucine zippers. J. Cell Biol. *153*, 699-708.

Marx,S.O., Kurokawa,J., Reiken,S., Motoike,H., D'Armiento,J., Marks,A.R., and Kass,R.S. (2002). Requirement of a macromolecular signaling complex for beta adrenergic receptor modulation of the KCNQ1-KCNE1 potassium channel. Science *295*, 496-499.

Matson,S.A., Pare,G.C., and Kapiloff,M.S. (2005). A novel isoform of Cbl-associated protein that binds protein kinase A. Biochim. Biophys. Acta *1727*, 145-149.

McClellan,G., Kulikovskaya,I., and Winegrad,S. (2001). Changes in cardiac contractility related to calcium-mediated changes in phosphorylation of myosin-binding protein C. Biophys. J. *81*, 1083-1092.

McConnachie,G., Langeberg,L.K., and Scott,J.D. (2006). AKAP signaling complexes: getting to the heart of the matter. Trends Mol. Med. *12*, 317-323.

McConnell,B.K. *et al.* (1999). Dilated cardiomyopathy in homozygous myosin-binding protein-C mutant mice. J. Clin. Invest *104*, 1235-1244.

McConnell,B.K., Popovic,Z., Mal,N., Lee,K., Bautista,J., Forudi,F., Schwartzman,R., Jin,J.P., Penn,M., and Bond,M. (2009). Disruption of protein kinase A interaction with A-kinase-anchoring proteins in the heart in vivo: effects on cardiac contractility, protein kinase A phosphorylation, and troponin I proteolysis. J. Biol. Chem. *284*, 1583-1592.

McIntyre,L.M., Martin,E.R., Simonsen,K.L., and Kaplan,N.L. (2000). Circumventing multiple testing: a multilocus Monte Carlo approach to testing for association. Genet. Epidemiol. *19*, 18-29.

Michel,J.J. and Scott,J.D. (2002). AKAP mediated signal transduction. Annu. Rev. Pharmacol. Toxicol. *42*, 235-257.

Mikhailov,A.T. and Torrado,M. (2008). The enigmatic role of the ankyrin repeat domain 1 gene in heart development and disease. Int. J. Dev. Biol. *52*, 811-821.

Miki,K. and Eddy,E.M. (1999). Single amino acids determine specificity of binding of protein kinase A regulatory subunits by protein kinase A anchoring proteins. J. Biol. Chem. *274*, 29057-29062.

Miller,M.K., Bang,M.L., Witt,C.C., Labeit,D., Trombitas,C., Watanabe,K., Granzier,H., McElhinny,A.S., Gregorio,C.C., and Labeit,S. (2003). The muscle ankyrin repeat proteins: CARP, ankrd2/Arpp and DARP as a family of titin filament-based stress response molecules. J. Mol. Biol. *333*, 951-964.

Mizukami,Y., Iwamatsu,A., Aki,T., Kimura,M., Nakamura,K., Nao,T., Okusa,T., Matsuzaki,M., Yoshida,K., and Kobayashi,S. (2004). ERK1/2 regulates intracellular ATP levels through alpha-enolase expression in cardiomyocytes exposed to ischemic hypoxia and reoxygenation. J. Biol. Chem. *279*, 50120-50131.

Mohamed,A.S., Dignam,J.D., and Schlender,K.K. (1998). Cardiac myosin-binding protein C (MyBP-C): identification of protein kinase A and protein kinase C phosphorylation sites. Arch. Biochem. Biophys. *358*, 313-319.

Mongillo,M. *et al.* (2004). Fluorescence resonance energy transfer-based analysis of cAMP dynamics in live neonatal rat cardiac myocytes reveals distinct functions of compartmentalized phosphodiesterases. Circ. Res. *95*, 67-75.

Montgomery,D.E., Wolska,B.M., Pyle,W.G., Roman,B.B., Dowell,J.C., Buttrick,P.M., Koretsky,A.P., Del,N.P., and Solaro,R.J. (2002). alpha-Adrenergic response and myofilament activity in mouse hearts lacking PKC phosphorylation sites on cardiac TnI. Am. J. Physiol Heart Circ. Physiol *282*, H2397-H2405.

Moolman-Smook,J., Flashman,E., de,L.W., Li,Z., Corfield,V., Redwood,C., and Watkins,H. (2002). Identification of novel interactions between domains of Myosin binding protein-C that are modulated by hypertrophic cardiomyopathy missense mutations. Circ. Res. *91*, 704-711.

Moolman-Smook,J.C., De Lange,W.J., Bruwer,E.C., Brink,P.A., and Corfield,V.A. (1999). The origins of hypertrophic cardiomyopathy-causing mutations in two South African subpopulations: a unique profile of both independent and founder events. Am. J. Hum. Genet. *65*, 1308-1320.

Moolman-Smook,J.C., Mayosi,B.M., Brink,P.A., and Corfield,V.A. (2003). Molecular genetics of cardiomyopathy: changing times, shifting paradigms. Cardiovasc. J. S. Afr. *14*, 145-155.

Moolman,J.A. *et al.* (2000). A newly created splice donor site in exon 25 of the MyBP-C gene is responsible for inherited hypertrophic cardiomyopathy with incomplete disease penetrance. Circulation *101*, 1396-1402.

Moolman,J.C., Corfield,V.A., Posen,B., Ngumbela,K., Seidman,C., Brink,P.A., and Watkins,H. (1997). Sudden death due to troponin T mutations. J. Am. Coll. Cardiol. *29*, 549-555.

Moos,C., Offer,G., Starr,R., and Bennett,P. (1975). Interaction of C-protein with myosin, myosin rod and light meromyosin. J. Mol. Biol. *97*, 1-9.

Movsesian,M.A. and Bristow,M.R. (2005). Alterations in cAMP-mediated signaling and their role in the pathophysiology of dilated cardiomyopathy. Curr. Top. Dev. Biol. *68*, 25-48.

Mukhopadhyay,D. and Riezman,H. (2007). Proteasome-independent functions of ubiquitin in endocytosis and signaling. Science *315*, 201-205.

Nagueh,S.F., Shah,G., Wu,Y., Torre-Amione,G., King,N.M., Lahmers,S., Witt,C.C., Becker,K., Labeit,S., and Granzier,H.L. (2004). Altered titin expression, myocardial stiffness, and left ventricular function in patients with dilated cardiomyopathy. Circulation *110*, 155-162.

Nau,P.N., Van,N.T., Ralphe,J.C., Teneyck,C.J., Bedell,K.A., Caldarone,C.A., Segar,J.L., and Scholz,T.D. (2002). Metabolic adaptation of the fetal and postnatal ovine heart: regulatory role of hypoxia-inducible factors and nuclear respiratory factor-1. Pediatr. Res. *52*, 269-278.

Neitzel,H. (1986). A routine method for the establishment of permanent growing lymphoblastoid cell lines. Hum. Genet. *73*, 320-326.

Newlon,M.G., Roy,M., Morikis,D., Carr,D.W., Westphal,R., Scott,J.D., and Jennings,P.A. (2001). A novel mechanism of PKA anchoring revealed by solution structures of anchoring complexes. EMBO J. *20*, 1651-1662.

Niimura,H. *et al.* (1998). Mutations in the gene for cardiac myosin-binding protein C and late-onset familial hypertrophic cardiomyopathy. N. Engl. J. Med. *338*, 1248-1257.

Nikolaev,V.O., Bunemann,M., Schmitteckert,E., Lohse,M.J., and Engelhardt,S. (2006). Cyclic AMP imaging in adult cardiac myocytes reveals far-reaching beta1-adrenergic but locally confined beta2-adrenergic receptor-mediated signaling. Circ. Res. *99*, 1084-1091.

Noland,T.A., Jr., Raynor,R.L., and Kuo,J.F. (1989). Identification of sites phosphorylated in bovine cardiac troponin I and troponin T by protein kinase C and comparative substrate activity of synthetic peptides containing the phosphorylation sites. J. Biol. Chem. *264*, 20778-20785.

Offer,G., Moos,C., and Starr,R. (1973). A new protein of the thick filaments of vertebrate skeletal myofibrils. Extractions, purification and characterization. J. Mol. Biol. *74*, 653-676.

Okagaki,T., Weber,F.E., Fischman,D.A., Vaughan,K.T., Mikawa,T., and Reinach,F.C. (1993). The major myosin-binding domain of skeletal muscle MyBP-C (C protein) resides in the COOH-terminal, immunoglobulin C2 motif. J. Cell Biol. *123*, 619-626.

Okruhlicova,L., Tribulova,N., Eckly,A., Lugnier,C., and Slezak,J. (1996). Cytochemical distribution of cyclic AMP-dependent 3',5'-nucleotide phosphodiesterase in the rat myocardium. Histochem. J. *28*, 165-172.

Oldham,W.M. and Hamm,H.E. (2008). Heterotrimeric G protein activation by G-protein-coupled receptors. Nat. Rev. Mol. Cell Biol. *9*, 60-71.

Opitz,C.A. and Linke,W.A. (2005). Plasticity of cardiac titin/connectin in heart development. J. Muscle Res. Cell Motil. *26*, 333-342.

Osadchii,O.E. (2007). Myocardial phosphodiesterases and regulation of cardiac contractility in health and cardiac disease. Cardiovasc. Drugs Ther. *21*, 171-194.

Pare,G.C., Bauman,A.L., McHenry,M., Michel,J.J., Dodge-Kafka,K.L., and Kapiloff,M.S. (2005). The mAKAP complex participates in the induction of cardiac myocyte hypertrophy by adrenergic receptor signaling. J. Cell Sci. *118*, 5637-5646.

Pare,G.C., Easlick,J.L., Mislow,J.M., McNally,E.M., and Kapiloff,M.S. (2005). Nesprin-1alpha contributes to the targeting of mAKAP to the cardiac myocyte nuclear envelope. Exp. Cell Res. *303*, 388-399.

Parrish,J.R., Gulyas,K.D., and Finley,R.L., Jr. (2006). Yeast two-hybrid contributions to interactome mapping. Curr. Opin. Biotechnol. *17*, 387-393.

Patel,J.R., Fitzsimons,D.P., Buck,S.H., Muthuchamy,M., Wieczorek,D.F., and Moss,R.L. (2001). PKA accelerates rate of force development in murine skinned myocardium expressing alpha- or beta-tropomyosin. Am. J. Physiol Heart Circ. Physiol *280*, H2732-H2739.

Pawson,T. and Scott,J.D. (1997). Signaling through scaffold, anchoring, and adaptor proteins. Science *278*, 2075-2080.

Pawson,T. and Nash,P. (2000). Protein-protein interactions define specificity in signal transduction. Genes Dev. *14*, 1027-1047.

Perneger,T.V. (1998). What's wrong with Bonferroni adjustments. BMJ *316*, 1236-1238.

Perry,S.J. *et al.* (2002). Targeting of cyclic AMP degradation to beta 2-adrenergic receptors by beta-arrestins. Science *298*, 834-836.

Pi,Y., Kemnitz,K.R., Zhang,D., Kranias,E.G., and Walker,J.W. (2002). Phosphorylation of troponin I controls cardiac twitch dynamics: evidence from phosphorylation site mutants expressed on a troponin I-null background in mice. Circ. Res. *90*, 649-656.

Pi,Y., Zhang,D., Kemnitz,K.R., Wang,H., and Walker,J.W. (2003). Protein kinase C and A sites on troponin I regulate myofilament Ca2+ sensitivity and ATPase activity in the mouse myocardium. J. Physiol *552* , 845-857.

Pierre,P., Scheel,J., Rickard,J.E., and Kreis,T.E. (1992). CLIP-170 links endocytic vesicles to microtubules. Cell *70*, 887-900.

Pilia,G. *et al.* (2006). Heritability of cardiovascular and personality traits in 6,148 Sardinians. PLoS. Genet. *2*, e132.

Potet,F., Scott,J.D., Mohammad-Panah,R., Escande,D., and Baro,I. (2001). AKAP proteins anchor cAMP-dependent protein kinase to KvLQT1/IsK channel complex. Am. J. Physiol Heart Circ. Physiol *280*, H2038-H2045.

Powell,S.R. (2006). The ubiquitin-proteasome system in cardiac physiology and pathology. Am. J. Physiol Heart Circ. Physiol *291*, H1-H19.

Pryzwansky,K.B., Kidao,S., and Merricks,E.P. (1998). Compartmentalization of PDE-4 and cAMP-dependent protein kinase in neutrophils and macrophages during phagocytosis. Cell Biochem. Biophys. *28*, 251-275.

Ramburan, A. (2008) Investigation of the N-terminal interactions of cardiac Myosin-Binding Protein C (cMyBPC) under defined phosphorylation states. PhD thesis. University of Stellenbosch.

Ramburan, A., Korkie L.J., Riedemann J., Kinnear C.J., and Moolman-Smook, J.C. (2010). Cardiac troponin I binds to the m-domain of cardiac Myosin binding protein C in a phosphorylation-sensitive manner. Article in preparation.

Rao,Y.J. and Xi,L. (2009). Pivotal effects of phosphodiesterase inhibitors on myocyte contractility and viability in normal and ischemic hearts. Acta Pharmacol. Sin. *30*, 1-24.

Razumova,M.V., Shaffer,J.F., Tu,A.Y., Flint,G.V., Regnier,M., and Harris,S.P. (2006). Effects of the N-terminal domains of myosin binding protein-C in an in vitro motility assay: Evidence for long-lived cross-bridges. J. Biol. Chem. *281*, 35846-35854.

Reeves,M.L., Leigh,B.K., and England,P.J. (1987). The identification of a new cyclic nucleotide phosphodiesterase activity in human and guinea-pig cardiac ventricle. Implications for the mechanism of action of selective phosphodiesterase inhibitors. Biochem. J. *241*, 535-541.

Reinach,F.C., Masaki,T., and Fischman,D.A. (1983). Characterization of the C-protein from posterior latissimus dorsi muscle of the adult chicken: heterogeneity within a single sarcomere. J. Cell Biol. *96*, 297-300.

Rich,T.C., Fagan,K.A., Tse,T.E., Schaack,J., Cooper,D.M., and Karpen,J.W. (2001). A uniform extracellular stimulus triggers distinct cAMP signals in different compartments of a simple cell. Proc. Natl. Acad. Sci. U. S. A *98*, 13049-13054.

Richard,P. *et al.* (2003). Hypertrophic cardiomyopathy: distribution of disease genes, spectrum of mutations, and implications for a molecular diagnosis strategy. Circulation *107*, 2227-2232.

Richter,W., Jin,S.L., and Conti,M. (2005). Splice variants of the cyclic nucleotide phosphodiesterase PDE4D are differentially expressed and regulated in rat tissue. Biochem. J. *388*, 803-811.

Rochais,F., Vandecasteele,G., Lefebvre,F., Lugnier,C., Lum,H., Mazet,J.L., Cooper,D.M., and Fischmeister,R. (2004). Negative feedback exerted by cAMP-dependent protein kinase and cAMP phosphodiesterase on subsarcolemmal cAMP signals in intact cardiac myocytes: an in vivo study using adenovirus-mediated expression of CNG channels. J. Biol. Chem. *279*, 52095-52105.

Rosenmund,C., Carr,D.W., Bergeson,S.E., Nilaver,G., Scott,J.D., and Westbrook,G.L. (1994). Anchoring of protein kinase A is required for modulation of AMPA/kainate receptors on hippocampal neurons. Nature *368*, 853-856.

Rottbauer,W. *et al.* (1997). Novel splice donor site mutation in the cardiac myosin-binding protein-C gene in familial hypertrophic cardiomyopathy. Characterization Of cardiac transcript and protein. J. Clin. Invest *100*, 475-482.

Ruehr,M.L., Russell,M.A., and Bond,M. (2004). A-kinase anchoring protein targeting of protein kinase A in the heart. J. Mol. Cell Cardiol. *37*, 653-665.

Russell,M.A., Lund,L.M., Haber,R., McKeegan,K., Cianciola,N., and Bond,M. (2006). The intermediate filament protein, synemin, is an AKAP in the heart. Arch. Biochem. Biophys. *456*, 204-215.

Sacchetto,R., Damiani,E., and Margreth,A. (2001). Clues to calcineurin function in mammalian fast-twitch muscle. J. Muscle Res. Cell Motil. *22*, 545-559.

Sadayappan,S., Gulick,J., Osinska,H., Martin,L.A., Hahn,H.S., Dorn,G.W., Klevitsky,R., Seidman,C.E., Seidman,J.G., and Robbins,J. (2005). Cardiac myosin-binding protein-C phosphorylation and cardiac function. Circ. Res. *97*, 1156-1163.

Sadayappan,S., Osinska,H., Klevitsky,R., Lorenz,J.N., Sargent,M., Molkentin,J.D., Seidman,C.E., Seidman,J.G., and Robbins,J. (2006). Cardiac myosin binding protein C phosphorylation is cardioprotective. Proc. Natl. Acad. Sci. U. S. A *103*, 16918-16923.

Sakthivel,S., Finley,N.L., Rosevear,P.R., Lorenz,J.N., Gulick,J., Kim,S., VanBuren,P., Martin,L.A., and Robbins,J. (2005). In vivo and in vitro analysis of cardiac troponin I phosphorylation. J. Biol. Chem. *280*, 703-714.

Sarikas,A., Carrier,L., Schenke,C., Doll,D., Flavigny,J., Lindenberg,K.S., Eschenhagen,T., and Zolk,O. (2005). Impairment of the ubiquitin-proteasome system by truncated cardiac myosin binding protein C mutants. Cardiovasc. Res. *66*, 33-44.

Sarkar,D., Erlichman,J., and Rubin,C.S. (1984). Identification of a calmodulin-binding protein that co-purifies with the regulatory subunit of brain protein kinase II. J. Biol. Chem. *259*, 9840-9846.

Sato,N., Kawakami,T., Nakayama,A., Suzuki,H., Kasahara,H., and Obinata,T. (2003). A novel variant of cardiac myosin-binding protein-C that is unable to assemble into sarcomeres is expressed in the aged mouse atrium. Mol. Biol. Cell *14*, 3180-3191.

Schiller,N.B. *et al.* (1989). Recommendations for quantitation of the left ventricle by two-dimensional echocardiography. American Society of Echocardiography Committee on Standards, Subcommittee on Quantitation of Two-Dimensional Echocardiograms. J. Am. Soc. Echocardiogr. *2*, 358-367.

Schlender,K.K., Hegazy,M.G., and Thysseril,T.J. (1987). Dephosphorylation of cardiac myofibril C-protein by protein phosphatase 1 and protein phosphatase 2A. Biochim. Biophys. Acta *928*, 312-319.

Schlender,K.K. and Bean,L.J. (1991). Phosphorylation of chicken cardiac C-protein by calcium/calmodulin-dependent protein kinase II. J. Biol. Chem. *266*, 2811-2817.

Scott,J.D. (1991). Cyclic nucleotide-dependent protein kinases. Pharmacol. Ther. *50*, 123-145.

Scott,J.D. (2003). A-kinase-anchoring proteins and cytoskeletal signalling events. Biochem. Soc. Trans. *31*, 87-89.

Scott,J.D. (2006). Compartmentalized cAMP signalling: a personal perspective. Biochem. Soc. Trans. *34*, 465-467.

Scott,J.D. and Santana,L.F. (2010). A-kinase anchoring proteins: getting to the heart of the matter. Circulation *121*, 1264-1271.

Scurr,L.L. *et al.* (2008). Ankyrin repeat domain 1, ANKRD1, a novel determinant of cisplatin sensitivity expressed in ovarian cancer. Clin. Cancer Res. *14*, 6924-6932.

Seiler,S.H., Fischman,D.A., and Leinwand,L.A. (1996). Modulation of myosin filament organization by C-protein family members. Mol. Biol. Cell *7*, 113-127.

Sette,C. and Conti,M. (1996). Phosphorylation and activation of a cAMP-specific phosphodiesterase by the cAMP-dependent protein kinase. Involvement of serine 54 in the enzyme activation. J. Biol. Chem. *271*, 16526-16534.

Shaffer,J.F., Razumova,M.V., Tu,A.Y., Regnier,M., and Harris,S.P. (2007). Myosin S2 is not required for effects of myosin binding protein-C on motility. FEBS Lett. *581*, 1501-1504.

Shaffer,J.F., Kensler,R.W., and Harris,S.P. (2009). The myosin-binding protein C motif binds to F-actin in a phosphorylation-sensitive manner. J. Biol. Chem. *284*, 12318-12327.

Smith,F.D., Langeberg,L.K., and Scott,J.D. (2006). The where's and when's of kinase anchoring. Trends Biochem. Sci. *31*, 316-323.

Sobel,E., Sengul,H., and Weeks,D.E. (2001). Multipoint estimation of identity-by-descent probabilities at arbitrary positions among marker loci on general pedigrees. Hum. Hered. *52*, 121-131.

Soejima,H. *et al.* (2001). Isolation of novel heart-specific genes using the BodyMap database. Genomics *74*, 115-120.

Solaro,R.J., Rosevear,P., and Kobayashi,T. (2008). The unique functions of cardiac troponin I in the control of cardiac muscle contraction and relaxation. Biochem. Biophys. Res. Commun. *369*, 82-87.

Solomon,S.D., Wolff,S., Watkins,H., Ridker,P.M., Come,P., McKenna,W.J., Seidman,C.E., and Lee,R.T. (1993). Left ventricular hypertrophy and morphology in familial hypertrophic cardiomyopathy associated with mutations of the beta-myosin heavy chain gene. J. Am. Coll. Cardiol. *22*, 498-505.

Spirito,P. and Maron,B.J. (1990). Relation between extent of left ventricular hypertrophy and diastolic filling abnormalities in hypertrophic cardiomyopathy. J. Am. Coll. Cardiol. *15*, 808-813.

Squire,J.M., Luther,P.K., and Knupp,C. (2003). Structural evidence for the interaction of C-protein (MyBP-C) with actin and sequence identification of a possible actin-binding domain. J. Mol. Biol. *331*, 713-724.

Stanley,W.C., Recchia,F.A., and Lopaschuk,G.D. (2005). Myocardial substrate metabolism in the normal and failing heart. Physiol Rev. *85*, 1093-1129.

Starr,R. and Offer,G. (1978). The interaction of C-protein with heavy meromyosin and subfragment-2. Biochem. J. *171*, 813-816.

Stelzer,J.E., Patel,J.R., and Moss,R.L. (2006). Protein kinase A-mediated acceleration of the stretch activation response in murine skinned myocardium is eliminated by ablation of cMyBP-C. Circ. Res. *99*, 884-890.

Stelzer,J.E., Patel,J.R., Walker,J.W., and Moss,R.L. (2007). Differential roles of cardiac myosin-binding protein C and cardiac troponin I in the myofibrillar force responses to protein kinase A phosphorylation. Circ. Res. *101*, 503-511.

Strang,K.T., Sweitzer,N.K., Greaser,M.L., and Moss,R.L. (1994). Beta-adrenergic receptor stimulation increases unloaded shortening velocity of skinned single ventricular myocytes from rats. Circ. Res. *74*, 542-549.

Suarez,R.K. (2003). Shaken and stirred: muscle structure and metabolism. J. Exp. Biol. *206*, 2021-2029.

Swanepoel C. Investigating ligands of cardiac myosin binding protein C (cMyBPC) as potential regulators of contractility and modifiers of hypertrophy. (2010). PhD thesis. University of Stellenbosch.

Swynghedauw,B. (1999). Molecular mechanisms of myocardial remodeling. Physiol Rev. *79*, 215-262.

Swynghedauw,B. and Baillard,C. (2000). Biology of hypertensive cardiopathy. Curr. Opin. Cardiol. *15*, 247-253.

Takimoto,E., Soergel,D.G., Janssen,P.M., Stull,L.B., Kass,D.A., and Murphy,A.M. (2004). Frequency- and afterload-dependent cardiac modulation in vivo by troponin I with constitutively active protein kinase A phosphorylation sites. Circ. Res. *94*, 496-504.

Tao,J., Wang,H.Y., and Malbon,C.C. (2003). Protein kinase A regulates AKAP250 (gravin) scaffold binding to the beta2-adrenergic receptor. EMBO J. *22*, 6419-6429.

Tasken,K. and Aandahl,E.M. (2004). Localized effects of cAMP mediated by distinct routes of protein kinase A. Physiol Rev. *84*, 137-167.

Tasken,K.A., Collas,P., Kemmner,W.A., Witczak,O., Conti,M., and Tasken,K. (2001). Phosphodiesterase 4D and protein kinase a type II constitute a signaling unit in the centrosomal area. J. Biol. Chem. *276*, 21999-22002.

Theurkauf,W.E. and Vallee,R.B. (1982). Molecular characterization of the cAMP-dependent protein kinase bound to microtubule-associated protein 2. J. Biol. Chem. *257*, 3284-3290.

Thierfelder,L., Watkins,H., MacRae,C., Lamas,R., McKenna,W., Vosberg,H.P., Seidman,J.G., and Seidman,C.E. (1994). Alpha-tropomyosin and cardiac troponin T mutations cause familial hypertrophic cardiomyopathy: a disease of the sarcomere. Cell *77*, 701-712.

Tong,C.W., Stelzer,J.E., Greaser,M.L., Powers,P.A., and Moss,R.L. (2008). Acceleration of crossbridge kinetics by protein kinase A phosphorylation of cardiac myosin binding protein C modulates cardiac function. Circ. Res. *103*, 974-982.

Trinick,J. (1996). Titin as a scaffold and spring. Cytoskeleton. Curr. Biol. *6*, 258-260.

Vander A, Sherman J, Luciano D. Molecular mechanisms of contraction. In: Vander A, Sherman J and Luciano D. Human physiology: The mechanisms of body function. New York, Pa: McGraw-Hill; 2001:295-300

van Dijk,S.J. *et al.* (2009). Cardiac myosin-binding protein C mutations and hypertrophic cardiomyopathy: haploinsufficiency, deranged phosphorylation, and cardiomyocyte dysfunction. Circulation *119*, 1473-1483.

Van Driest,S.L., Ommen,S.R., Tajik,A.J., Gersh,B.J., and Ackerman,M.J. (2005). Yield of genetic testing in hypertrophic cardiomyopathy. Mayo Clin. Proc. *80*, 739-744.

Van,C.W. and Beyaert,R. (1999). Yeast Two-Hybrid: State of the Art. Biol. Proced. Online. *2*, 1-38.

van,H.L., Borbely,A., Niessen,H.W., Bronzwaer,J.G., van,d., V, Stienen,G.J., Linke,W.A., Laarman,G.J., and Paulus,W.J. (2006). Myocardial structure and function differ in systolic and diastolic heart failure. Circulation *113*, 1966-1973.

Venema,R.C. and Kuo,J.F. (1993). Protein kinase C-mediated phosphorylation of troponin I and C-protein in isolated myocardial cells is associated with inhibition of myofibrillar actomyosin MgATPase. J. Biol. Chem. *268*, 2705-2711.

Verde,I., Pahlke,G., Salanova,M., Zhang,G., Wang,S., Coletti,D., Onuffer,J., Jin,S.L., and Conti,M. (2001). Myomegalin is a novel protein of the golgi/centrosome that interacts with a cyclic nucleotide phosphodiesterase. J. Biol. Chem. *276*, 11189-11198.

Verges,M. (2007). Retromer and sorting nexins in development. Front Biosci. *12*, 3825-3851.

Wang,K., McClure,J., and Tu,A. (1979). Titin: major myofibrillar components of striated muscle. Proc. Natl. Acad. Sci. U. S. A *76*, 3698-3702.

Wang,L., Sunahara,R.K., Krumins,A., Perkins,G., Crochiere,M.L., Mackey,M., Bell,S., Ellisman,M.H., and Taylor,S.S. (2001). Cloning and mitochondrial localization of full-length D-AKAP2, a protein kinase A anchoring protein. Proc. Natl. Acad. Sci. U. S. A *98*, 3220-3225.

Watanabe,A., Nakamura,K., Morita,H., Kusano,K.F., and Ohe,T. (2005). [Long QT syndrome]. Nippon Rinsho *63*, 1171-1177.

Watkins,H., Conner,D., Thierfelder,L., Jarcho,J.A., MacRae,C., McKenna,W.J., Maron,B.J., Seidman,J.G., and Seidman,C.E. (1995). Mutations in the cardiac myosin binding protein-C gene on chromosome 11 cause familial hypertrophic cardiomyopathy. Nat. Genet. *11*, 434-437.

Weber,F.E., Vaughan,K.T., Reinach,F.C., and Fischman,D.A. (1993). Complete sequence of human fast-type and slow-type muscle myosin-binding-protein C (MyBP-C). Differential expression, conserved domain structure and chromosome assignment. Eur. J. Biochem. *216*, 661-669.

Weisberg,A. and Winegrad,S. (1996). Alteration of myosin cross bridges by phosphorylation of myosin-binding protein C in cardiac muscle. Proc. Natl. Acad. Sci. U. S. A *93*, 8999-9003.

Welikson,R.E. and Fischman,D.A. (2002). The C-terminal IgI domains of myosin-binding proteins C and H (MyBP-C and MyBP-H) are both necessary and sufficient for the intracellular crosslinking of sarcomeric myosin in transfected non-muscle cells. J. Cell Sci. *115*, 3517-3526.

Westphal,R.S., Tavalin,S.J., Lin,J.W., Alto,N.M., Fraser,I.D., Langeberg,L.K., Sheng,M., and Scott,J.D. (1999). Regulation of NMDA receptors by an associated phosphatase-kinase signaling complex. Science *285*, 93-96.

Wigle,E.D., Sasson,Z., Henderson,M.A., Ruddy,T.D., Fulop,J., Rakowski,H., and Williams,W.G. (1985). Hypertrophic cardiomyopathy. The importance of the site and the extent of hypertrophy. A review. Prog. Cardiovasc. Dis. *28*, 1-83.

Winegrad,S. (1999). Cardiac myosin binding protein C. Circ. Res. *84*, 1117-1126.

Witt,S.H., Labeit,D., Granzier,H., Labeit,S., and Witt,C.C. (2005). Dimerization of the cardiac ankyrin protein CARP: implications for MARP titin-based signaling. J. Muscle Res. Cell Motil. *26*, 401-408.

Wolska,B.M., Arteaga,G.M., Pena,J.R., Nowak,G., Phillips,R.M., Sahai,S., de Tombe,P.P., Martin,A.F., Kranias,E.G., and Solaro,R.J. (2002). Expression of slow skeletal troponin I in hearts of phospholamban knockout mice alters the relaxant effect of beta-adrenergic stimulation. Circ. Res. *90*, 882-888.

Wong,W. and Scott,J.D. (2004). AKAP signalling complexes: focal points in space and time. Nat. Rev. Mol. Cell Biol. *5*, 959-970.

Wynne,J. (2001). The clinical meaning of the third heart sound. Am. J. Med. *111*, 157-158.

Yang,J., Drazba,J.A., Ferguson,D.G., and Bond,M. (1998). A-kinase anchoring protein 100 (AKAP100) is localized in multiple subcellular compartments in the adult rat heart. J. Cell Biol. *142*, 511-522.

Yasuda,M., Koshida,S., Sato,N., and Obinata,T. (1995). Complete primary structure of chicken cardiac C-protein (MyBP-C) and its expression in developing striated muscles. J. Mol. Cell Cardiol. *27*, 2275-2286.

Zaccolo,M. and Pozzan,T. (2002). Discrete microdomains with high concentration of cAMP in stimulated rat neonatal cardiac myocytes. Science *295*, 1711-1715.

Zakhary,D.R., Fink,M.A., Ruehr,M.L., and Bond,M. (2000). Selectivity and regulation of A-kinase anchoring proteins in the heart. The role of autophosphorylation of the type II regulatory subunit of cAMP-dependent protein kinase. J. Biol. Chem. *275*, 41389-41395.

Zakhary,D.R., Moravec,C.S., and Bond,M. (2000). Regulation of PKA binding to AKAPs in the heart: alterations in human heart failure. Circulation *101*, 1459-1464.

Zhang,J., Ma,Y., Taylor,S.S., and Tsien,R.Y. (2001). Genetically encoded reporters of protein kinase A activity reveal impact of substrate tethering. Proc. Natl. Acad. Sci. U. S. A *98*, 14997-15002.

Zhang,J., Hupfeld,C.J., Taylor,S.S., Olefsky,J.M., and Tsien,R.Y. (2005). Insulin disrupts beta-adrenergic signalling to protein kinase A in adipocytes. Nature *437*, 569-573.

Zhang,K., Qin,Z.S., Liu,J.S., Chen,T., Waterman,M.S., and Sun,F. (2004). Haplotype block partitioning and tag SNP selection using genotype data and their applications to association studies. Genome Res. *14*, 908-916.

Zhang,Q., Skepper,J.N., Yang,F., Davies,J.D., Hegyi,L., Roberts,R.G., Weissberg,P.L., Ellis,J.A., and Shanahan,C.M. (2001). Nesprins: a novel family of spectrin-repeat-containing proteins that localize to the nuclear membrane in multiple tissues. J. Cell Sci. *114*, 4485-4498.

Zhu,L.A., Fang,N.Y., Gao,P.J., Jin,X., and Wang,H.Y. (2009). Differential expression of alpha-enolase in the normal and pathological cardiac growth. Exp. Mol. Pathol. *87*, 27-31.

Zoghbi,M.E., Woodhead,J.L., Moss,R.L., and Craig,R. (2008). Three-dimensional structure of vertebrate cardiac muscle myosin filaments. Proc. Natl. Acad. Sci. U. S. A *105*, 2386-2390.

Zolk,O., Frohme,M., Maurer,A., Kluxen,F.W., Hentsch,B., Zubakov,D., Hoheisel,J.D., Zucker,I.H., Pepe,S., and Eschenhagen,T. (2002). Cardiac ankyrin repeat protein, a negative regulator of cardiac gene expression, is augmented in human heart failure. Biochem. Biophys. Res. Commun. *293* , 1377-1382.

Zou,Y., Evans,S., Chen,J., Kuo,H.C., Harvey,R.P., and Chien,K.R. (1997). CARP, a cardiac ankyrin repeat protein, is downstream in the Nkx2-5 homeobox gene pathway. Development *124*, 793-804

APPENDIX I

1. YEAST TRANSFORMATION REAGENTS

1M LiAc

LiAC	5.1g

Make up to 50ml with sterile water

100mM LiAc

1M LiAc	5ml

Make up to 50ml with sterile water

50% PEG 4000

PEG 4000	25g

Make up to 50ml with sterile water

2. YEAST PLASMID PURIFICATION SOLUTIONS

Yeast Lysis Buffer

SDS	1%
Triton X-100	2%
NaCl	100mM
Tris, pH 8	10mM
EDTA, pH 8	1mM

3. ELECTROPHORESIS STOCK SOLUTIONS

10% Ammonium Persulphate

Ammonium Persulphate	10g
Sterile water	10ml

Mix well and store at 4°C

20X SB Stock Solution

di-Sodium tetraborate decahydrate	38.14g

Sterile water to a final volume of 1litre

1X SB Solution

20X SB solution	50ml

Sterile water to final volume of 1 litre

SDS-PAGE Resolving Gel Buffer (4X)

Tris base	109.2g

ddH_2O	330ml
10% SDS	24ml

pH to 8.8 using 1M HCl. Make up to 600ml using ddH_2O

SDS-PAGE Stacking Gel Buffer (4X)

Tris base	36.3g
ddH_2O	330ml
10% SDS	24ml

pH to 6.8 using 1M HCl. Make up to 600ml using ddH_2O

10X SDS-PAGE Running Buffer

Tris base	30g
Glycine	144g
10% SDS	100ml

Add ddH_2O to a final volume of 1litre

1X SDS-PAGE Running Buffer

10X SDS-PAGE running buffer	100ml

Sterile water to a final volume of 1litre

4. GELS

1% Agarose gel

Agarose	1g
SB Buffer (1X)	100ml

Microwave for 1min on maximum power and add 5µl ethidium bromide (10mg/ml) when temperature of ±55°C is reached

2% Agarose gel

Agarose	2g
SB Buffer (1X)	100ml

Microwave for 1min on maximum power and add 5µl ethidium bromide (10mg/ml) when temperature of ±55°C is reached

15% SDS-PAGE Stacking Gel

Sterile water	2.56ml
10% SDS	40µl
SDS-PAGE stacking gel buffer (4X)	1ml
Acrylamide (40%)	390µl

APS (10%)	30µl
TEMED	6µl

Makes two gels for the Bio-Rad Mini gel apparatus system (Bio-Rad Laboratories, Hercules, CA, USA)

15% SDS-PAGE Resolving Gel

Sterile water	4.82ml
10% SDS	100µl
SDS-PAGE resolving gel buffer(4X)	1.25ml
Acrylamide (40%)	3.75ml
APS (10%)	80µl
TEMED	6µl

Makes two gels for the Bio-Rad Mini gel apparatus system (Bio-Rad Laboratories, Hercules, CA,USA)

5. LOADING DYES

Ethidium Bromide Stock (10mg/ml)

Ethidium bromide	500mg
Sterile water	50ml

Stir well on magnetic stirrer for 4h and store in dark container at 4°C

Bromophenol Blue Loading Dye

Bromophenol Blue	0.1% (w/v)

Sterile water to a final volume of 100ml. Store at 4°C

SDS Loading Dye

1M Tris-HCl (pH6.8)	50mM
DTT	100mM
SDS	2%
Bromophenol Blue	0.1%
Glycerol	10%

6. CO-IP REAGENTS

Co-IP Buffer

1M Tris (pH 7.5)	400µl
5M NaCl	60µl
1M DTT	20µl
2ng/ml Aprotinin	50µl
50mM PMSF	200µl

Tween 20	20µl

Make up to 20ml using sterile water

Pre-washed Protein G Agarose

A volume of Co-IP buffer (double the volume of protein G agarose) was used to wash the protein G agarose (10µl/reaction) by centrifugation for 30sec. Following centrifugation, the supernatant was discarded and the pellet resuspended (double the volume of Co-IP buffer) before another round of centrifugation. This was repeated five times. After the final centrifugation step, the pellet was resuspended in a volume of Co-IP buffer representing the initial volume of protein G aliquoted.

TBST (pH 7.6)

NaCl	8g
1M Tris-HCl (pH7.6)	20ml
Tween 20	1ml

Make up to 1litre using sterile water

7. SOLUTIONS USED FOR THE ESTABLISHMENT OF BACTERIAL COMPETENT CELLS

CAP-Buffer

$CaCl_2$	2.21g
Glycerol	37.5ml
PIPES	0.76g

Sterile water to a final volume of 250ml. Adjust pH to 7.0 and store at 4°C

8. BACTERIAL MEDIA

LB media

Bacto tryptone	5g
Yeast extract	2.5g
NaCl	5g

Sterile water to final volume of 500ml. Autoclave and add appropriate antibiotic (Ampicillin 25mg/l, Kanamycin 5mg/l or Zeocin™ 10mg/l to media when temperature of ±55°C is reached

LB agar plates

Bacto tryptone	5g
Yeast extract	2.5g
NaCl	5g
Bacto agar	8g

Sterile water to final volume of 500ml. Autoclave and add appropriate antibiotic (Ampicillin 25mg/l, Kanamycin 5mg/l or Zeocin™ 10mg/l to media when temperature of ±55°C is reached, prior to pouring

~20, 90mm plates. These plates were then allowed to set for 2-5 hours and stored at room temperature for up to three weeks

9. YEAST MEDIA

YPDA media

Difco peptone	10g
Yeast extract	10g
Glucose	10g
L-adenine hemisulphate (0.2%stock solution)	7.5ml

Add sterile water to a final volume of 500ml. Autoclave at 121°C for 15min

YPDA agar plates

Difco peptone	10g
Yeast extract	10g
Glucose	10g
L-adenine hemisulphate (0.2%stock solution)	7.5ml
Bacto agar	10g

Add sterile water to a final volume of 500ml. Autoclave at 121°C for 15min. Allow to cool to a temperature of ±55°C, before pouring ~20, 90mm plates. These plates were then allowed to set for 2-5 hours and stored at room temperature for up to three weeks

SD^{-W} media

Glucose	12g
Yeast nitrogen base without amino acids	4g
SD^{-W} amino acid supplement	0.4g

Add sterile water to a final volume of 600ml. Adjust pH to 5.8 and autoclave at 121°C for 15min

SD^{-W} agar plates

Glucose	12g
Yeast nitrogen base without amino acids	4g
SD^{-W} amino acid supplement	0.4g
Bacto agar	12g

Add sterile water to a final volume of 600ml. Adjust pH to 5.8 and autoclave at 121°C for 15min. Allow to cool to temperature of ±55°C, before pouring ~20, 90mm plates. Plates were allowed to set for 2-5h and stored at room temperature for up to 3 weeks

SD^{-L} media

Glucose	12g

Yeast nitrogen base without amino acids	4g
SD^{-L} amino acid supplement	0.4g

Add sterile water to a final volume of 600ml. Adjust pH to 5.8 and autoclave at 121°C for 15min

SD^{-L} agar plates

Glucose	12g
Yeast nitrogen base without amino acids	4g
SD^{-L} amino acid supplement	0.4g
Bacto agar	12g

Add sterile water to a final volume of 600ml. Adjust pH to 5.8 and autoclave at 121°C for 15min. Allow to cool to temperature of ±55°C, before pouring ~20, 90mm plates. Plates were allowed to set for 2-5h and stored at room temperature for up to 3 weeks

SD^{-L-W} media

Glucose	12g
Yeast nitrogen base without amino acids	4g
SD^{-L-W} amino acid supplement	0.4g

Add sterile water to a final volume of 600ml. Adjust pH to 5.8 and autoclave at 121°C for 15min

SD^{-L-W} agar plates

Glucose	12g
Yeast nitrogen base without amino acids	4g
SD^{-L-W} amino acid supplement	0.4g
Bacto agar	12g

Add sterile water to a final volume of 600ml. Adjust pH to 5.8 and autoclave at 121°C for 15min. Allow to cool to temperature of ±55°C, before pouring ~20, 90mm plates. Plates were allowed to set for 2-5h and stored at room temperature for up to 3 weeks

TDO media

Glucose	12g
Yeast nitrogen base without amino acids	4g
SD^{-L-W-H} amino acid supplement	0.4g

Add sterile water to a final volume of 600ml. Adjust pH to 5.8 and autoclave at 121°C for 15min

TDO agar plates

Glucose	12g
Yeast nitrogen base without amino acids	4g
SD^{-L-W-H} amino acid supplement	0.4g

Bacto agar	12g

Add sterile water to a final volume of 600ml. Adjust pH to 5.8 and autoclave at 121°C for 15min. Allow to cool to temperature of ±55°C, before pouring ~20, 90mm plates. Plates were allowed to set for 2-5h and stored at room temperature for up to 3 weeks

QDO media

Glucose	12g
Yeast nitrogen base without amino acids	4g
$SD^{-L-W-H-Ade}$ amino acid supplement	0.4g

Add sterile water to a final volume of 600ml. Adjust pH to 5.8 and autoclave at 121°C for 15min

QDO agar plates

Glucose	12g
Yeast nitrogen base without amino acids	4g
$SD^{-L-W-H-Ade}$ amino acid supplement	0.4g
Bacto agar	12g

Add sterile water to a final volume of 600ml. Adjust pH to 5.8 and autoclave at 121°C for 15min. Allow to cool to temperature of ±55°C, before pouring ~20, 90mm plates. Plates were allowed to set for 2-5h and stored at room temperature for up to 3 weeks

X-α-Galactosidase Solution (5mg/ml)

X-α-Galactosidase	25mg
Dimethylformamide	1ml

Make a 25mg/ml stock. Dilute with dimethylformamide to a 5mg/ml working solution

10. EUKARYOTIC CELL CULTURE MEDIA

Complete Growth Media

DMEM (4.5g/L glucose, with L-glutamine)	178ml
Foetal calf serum	20ml
Penstrep	2ml

Pre-warm to 37°C before use

Serum-free Media

DMEM (4.5g/L glucose, with L-glutamine)	100ml

Pre-warm to 37°C before use

Differentiating Growth Media

DMEM (4.5g/L glucose, with L-glutamine)	196ml

Horse serum	2ml
Penstrep	2ml

Pre-warm to 37°C before use

10X Isoproterenol

Isoproterenol	2.48mg

Add 100ml sterile water for 1000X stock. Dilute further 1:100 with sterile water for 10X working solution. Make up as required as it cannot be stored in solution

65mM $CaCl_2$

Calcium chloride	478mg

Add 50ml sterile water for a 10X working solution

11. WESTERN BLOT REAGENTS

Bradford solution

Coomassie Brilliant Blue	100mg
Phosphoric acid	100ml
95% ethanol	50ml

Dilute Coomassie Brilliant Blue in phosphoric acid, add ethanol. Make up to 1litre with ddH_2O, stir. Filter 2-5X until solution has light brown colour. Store at room temperature in lightproof container

Phosphate Buffered Saline (PBS)

PBS tablet (Sigma)	one tablet
ddH_2O	200ml

Dissolve tablet in ddH_2O. Store solution at 0-5°C

Passive Lysis Buffer

EDTA	0.5M
$NaVO_4$	1M
Nappi	1M
HEPES	1M
NaCl	5M
Triton-X-100	1%

Add ddH_2O to final volume required. Store at 4°C. Prior to use, add 1mM PMSF and dissolve protein inhibitor tablet (Roche) (1 tablet/20ml working solution)

Transfer Buffer

Tris Base (25mM)	3.03g

Glycine (192mM)	14.4g
Methanol	200ml

Add sterile water to a volume of 1L

12. DNA EXTRACTION SOLUTIONS

Cell lysis buffer

Sucrose	0.32M
Triton-X-100	1%
$MgCl_2$	5mM
Tris-HCl	10mM
H_2O	1L

3M NaAc

$NaAc.3H_2O$	40.18g
ddH_2O	50ml

Adjust pH to 5.2 with glacial acetic acid and adjust volume to 100ml with ddH_2O

DNA Extraction Buffer

NaCl	0.1M
Tris-HCl	0.01M
EDTA (pH 8)	0.025M
SDS	0.5%
Proteinase K	0.1mg/ml

TBE Buffer (10X Stock)

Tris-HCl	0.89M
Boric Acid	0.89M
Na_2EDTA (pH 8)	20mM

APPENDIX II

CALCULATING YEAST MATING EFFICIENCIES (Calculations based on Clontech Manual)

Count number of colonies on all plates with 30-300 colonies after 4 days

#colony forming units (cfu)/ml = cfu x 1000µl/ml / volume plated (µl) x dilution factor

1. Number of cfu/ml on SD^{-L} plates = viability of prey partner
2. Number of cfu/ml on SD^{-W} plates = viability of bait partner
3. Number of cfu/ml on SD^{-L-W} plates = viability of diploids
4. Lowest number of cfu/ml of SD^{-L} or SD^{-W} plates indicate limiting partner
5. Mating efficiency = #cfu/ml of diploids x 100 / #cfu/ml of limiting partner

Library titer

Count number of colonies on all plates with 30-300 colonies after 4 days

cfu/ml = #colonies / plating volume (ml) x dilution factor

colonies clones screened = #cfu/ml x final resuspension volume

Haemocytometric cell count

A Neubauer haemocytometer (Superior, Berlin, Germany) was used to perform haemocytometric cell counts to determine the titer of the bait culture used in the library mating experiment. A glass coverslip was placed over the counting surface before aliquoting the sample onto the haemocytometer. About 50µl of a 1 in 10 dilution of bait culture was then pipetted into one of the haemocytometer's V-shaped wells. This allowed for the area under the coverslip to fill up with the sample through capillary action. The counting chamber was then placed under a microscope (Nikon TMS, Nikon Instruments, New York, USA) and the counting area was brought into focus under low magnification. The number of cells in the large central quadrant of the haemocytometer was counted and this value was used to calculate the number of cells per milliliter using the following formula:

number of cells/ml = number of cells x dilution factor x 10^4 (a constant used because the depth of the haemocytometer is 0.1 mm)

APPENDIX III

BACTERIAL STRAIN PHENOTYPES

E. coli strain DH5α

Φ 80d *lacZ*Δ*M15* recA1, *end*A1, *Gry* A96 *thi*-1, *hsd*R17 *sup*E44, *rel*A1, *deoR* Δ(*lac*ZYA *argF*)u169

YEAST STRAIN PHENOTYPES

Yeast strain AH109

*MAT*a, *trp1-901, leu2-3, ura3-5, his3-200, gal4*Δ, *gal80*Δ, *LYS::GAL1*$_{uas}$*-GAL1*$_{TATA}$*-HIS3, GAL2*$_{UAS}$*-GAL2*$_{TATA}$*-ADE2, URA3::MEL1*$_{UAS}$*-MEL1*$_{TATA}$*-lacZ* (James *et al*., 1996)

Yeast strain Y187

*MATα, ura3-52, his3-200, ade2-101, trp1-901, leu2-3, 112, gal4*Δ, *met*$^{-}$, *gal80*Δ, *URA3::GAL1*$_{UAS}$*-GAL1*$_{TATA}$*-lacZ* (Harper *et al.*, 1993)

APPENDIX IV

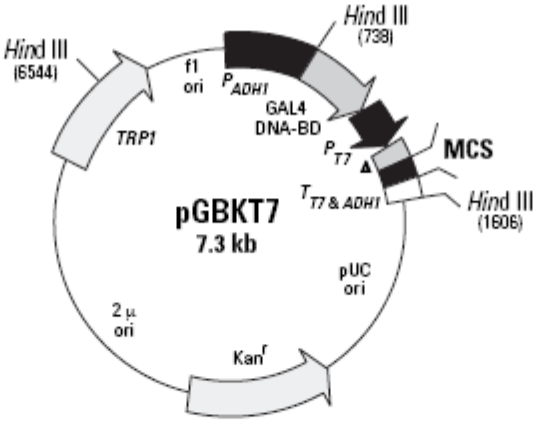

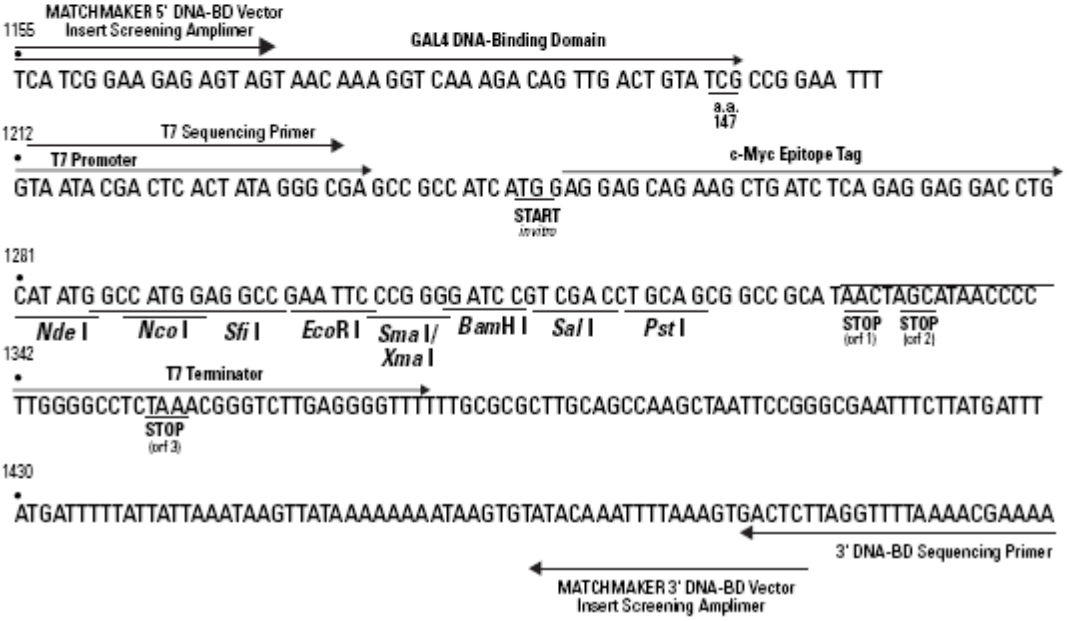

Restriction map and multiple cloning site (MCS) of pGBKT7 Y2H bait vector a) The positions of the kanamycin resistance gene (*Kan*), TRP1 and GAL4-BD coding sequences, f1 bacteriophage and pUC plasmid origins of replication, the truncated *S. cerevisiae* ADH1 promoter sequence (P_{ADH1}), the T7 RNA polymerase promoter, the T7 and c-Myc epitope tag are indicated on the map. b) Nucleotide sequence of the pGBKT7 MCS. The positions of all unique restriction enzyme recognition sequences, stop codons in the T7 terminator sequence, the GAL4-BD coding sequence, the T7 promoter sequence, c-Myc epitope tag and the positions of pGBKT7-F and pGBKT7-R screening primers are indicated on the sequence (Taken from Clontech MATCHMAKER™ vectors handbook).

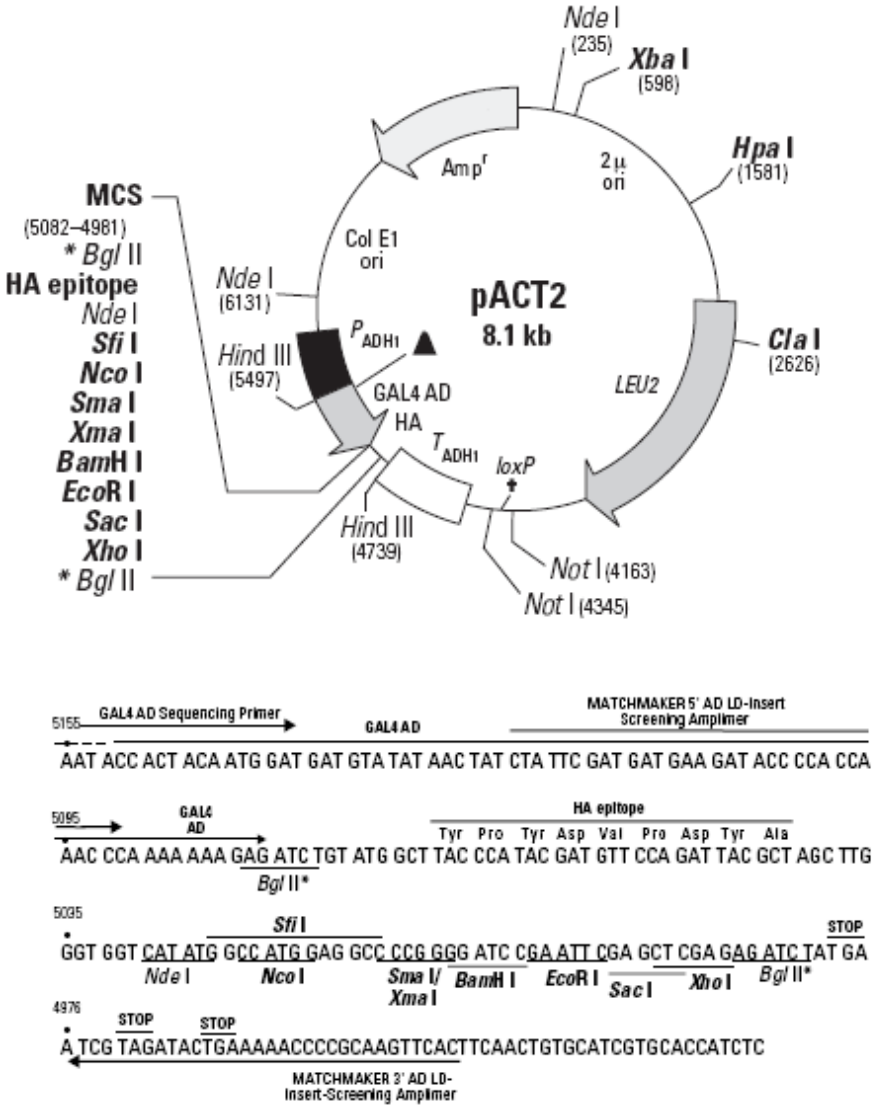

Restriction map and multiple cloning site (MCS) of pACT2 Y2H prey vector a) The positions of unique restriction sites are indicated in bold. The position of the ampicillin resistance gene (*Amp*^{r}), LEU2 and GAL4-AD coding sequences, and pBR322 plasmid origins, the S. cerevisiae ADH1 termination sequences, Lox sites (Lox 1 and Lox 2), the Haemagglutinin (HA) epitope tag and the MCS are indicated on the map. b) Nucleotide sequence of the pACT2 MCS. The positions of all unique restriction sites, stop codons, the position of the final codon of GAL4-AD coding sequence, the positions of the pACT2-F and pACT2-R primers and the HA epitope tags are all indicated on the map (Taken from Clontech MATCHMAKER™ vectors handbook).

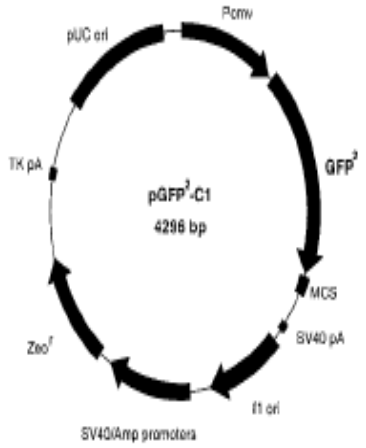

P_{CMV}	1 - 583
SV40 early poly (A) signal	1561 - 1611
GFP^2 gene	606 - 1322
TK poly (A) signal	3222 - 3285
Multiple cloning site (MCS)	1342 - 1418
P_{SV40}/P_{amp}	2175 - 2589
Zeo^R	2626 - 3000
f1 origin	1661 - 2113
pUC sequences (ori)	3571 - 4214

Codon humanized pGFP^2-C1 Vector

TAC AAG TCC GGA CTC AGA TCT CGG CGA GCT CTC GAG AAT TCT CAC GCG
GFP^2 BspEI BglII * SacI EcoRI XhoI

TCT GCA GGA TAT CAA GCT TGC GGT ACC GCG GGC CCG GGA TCC ACC GGA
PstI EcoRV HindIII KpnI ApaI BamHI SacII

Stop Stop Stop
TCT AGA TAA CTG ATC A
XbaI

* Frame changes characterizing pGFP^2-C1, C2 and C3 vectors occur after this site.

Restriction map and multiple cloning site (MCS) of pGFP^2-C1 vector a) The positions of the zeocin resistance gene (*Zeo^r*), GFP^2 coding sequence, f1 bacteriophage and pUC plasmid origins of replication, the truncated P_{CMV} promoter sequence, the multiple cloning site, the TK poly (A) signal and the SV40 early poly (A) signal are indicated on the map. b) Nucleotide sequence of the pGFP^2-C1 MCS. The positions of all unique restriction enzyme sequences as well as stop codons are indicated on the sequence (Taken from BioSignal Packard BRET^2 ™ technical data sheet).

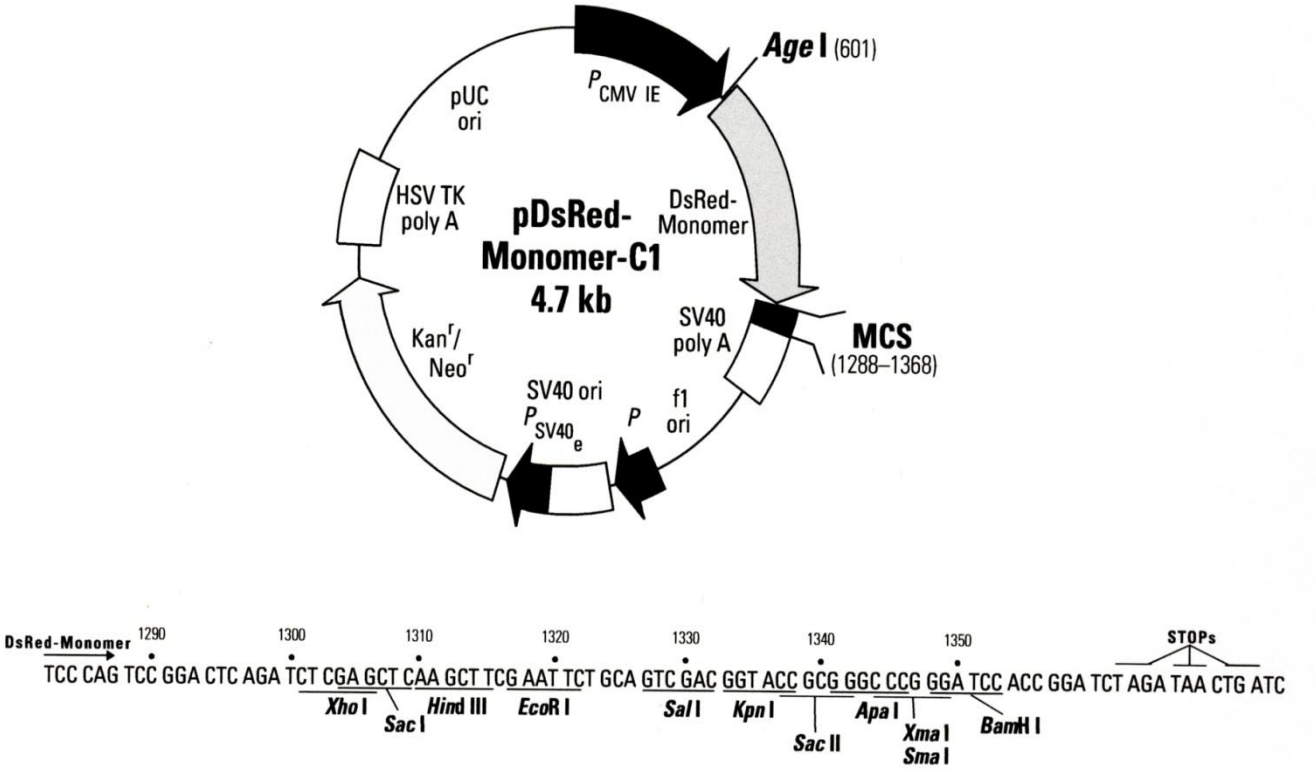

Restriction map and multiple cloning site (MCS) of pDsRed-Monomer-C1 vector a) pDsRed-Monomer-C1 is a mammalian expression vector that encodes DsRed-Monomer, a monomeric mutant derived from the tetrameric *Discosoma* sp. red fluorescent protein DsRed. The multiple cloning site (MCS) is positioned between the DsRed-Monomer coding sequence and the SV40 polyadenylation signal (SV40 poly A). The position of the f1 ori, P_{CMV} early promoter, *Kan/Neo resistance* genes, SV40 origin of replication, pUC plasmid replication origin and the Herpes simplex virus (HSV) thymidine kinase (TK) are indicated on the map. b) Nucleotide sequence of the pDsRed-Monomer-C1 MCS. The positions of all unique restriction enzyme sequences as well as stop codons are indicated on the sequence (Taken from Clontech MATCHMAKER™ vectors handbook).

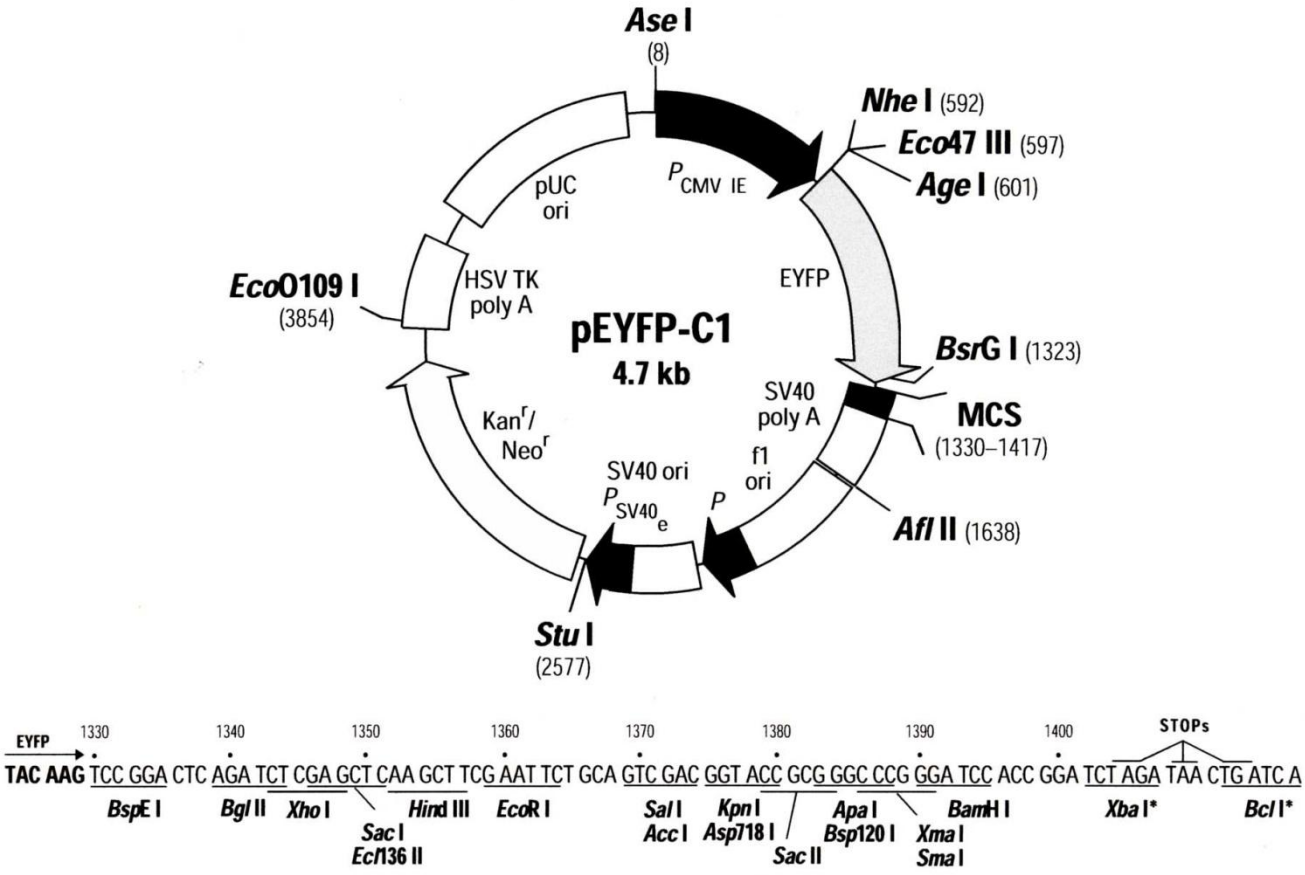

Restriction map and multiple cloning site (MCS) of pdEYFP-C1 vector a) The position of the EYFP tag, *chloramphenicol resistance* gene, *ccdA* gene, *ccdB* gene, SV40 early poly A signal, P_{CMV} early promoter, *Kan resistance* gene, SV40 origin of replication, pUC plasmid replication origin, attR1 and attR2 recombination sites are indicated on the map. b) Nucleotide sequence of the pdEYFP-C1 MCS. The positions of all unique restriction enzyme sequences as well as stop codons are indicated on the sequence (Taken from Clontech MATCHMAKER™ vectors handbook).

APPENDIX V

Articles submitted to peer reviewed journals using data generated in the present study

Myomegalin is a novel A-kinase anchoring protein involved in the phosphorylation of cardiac myosin binding protein C (Under review in BMC Cell Biology)

Regular Research Article

Gerrida M Uys[1], Amsha Ramburan[1], Benjamin Loos[2], Craig J Kinnear[1], Lundi J Korkie[1], Johann Riedemann[1] and Johanna C Moolman-Smook[1*]

[1]US/MRC Centre for Molecular and Cellular Biology, Department of Biomedical Sciences, University of Stellenbosch, South Africa

[2]Central Analytical Facility, Department of Physiology, University of Stellenbosch, South Africa

*Corresponding author

Email addresses:

GMU: grietjie@sun.ac.za

AR: amshar@sun.ac.za

BL: bloos@sun.ac.za

CJK: gkin@sun.ac.za

LJK: lji@sun.ac.za

JR: 12172073@sun.ac.za

JCM-S: hm@sun.ac.za

Abstract

Background

Cardiac contractility is regulated by dynamic phosphorylation of sarcomeric proteins by kinases such as cAMP-activated protein kinase A (PKA). Efficient phosphorylation requires that PKA be anchored close to its targets by A-kinase anchoring proteins (AKAPs). Cardiac Myosin Binding Protein-C (cMyBPC) and cardiac troponin I (cTNI) are hypertrophic cardiomyopathy (HCM)-causing sarcomeric proteins which regulate contractility in response to PKA phosphorylation.

Results

During a yeast 2-hybrid (Y2H) library screen using a trisphosphorylation mimic of the C1-C2 region of cMyBPC, we identified isoform 4 of myomegalin (MMGL) as an interactor of this N-terminal cMyBPC region. As MMGL has previously been shown to interact with phosphodiesterase 4D, we speculated that it may be a PKA-anchoring protein (AKAP).

To investigate this possibility, we assessed the ability of MMGL isoform 4 to interact with PKA regulatory subunits R1A and R2A using Y2H-based direct protein-protein interaction assays. Additionally, to further elucidate the function of MMGL, we used it as bait to screen a cardiac cDNA library. Other PKA targets, viz. CARP, COMMD4, ENO1, ENO3 and cTNI were identified as putative interactors, with cTNI being the most frequent interactor.

We further assessed and confirmed these interactions by fluorescent 3D-colocalization in differentiated H9C2 cells as well as by *in vivo* co-immunoprecipitation. We also showed that quantitatively more interaction occurs between MMGL and cTNI under β-adrenergic stress. Moreover, siRNA-mediated knockdown of MMGL leads to reduction of cMyBPC levels under conditions of adrenergic stress, indicating that MMGL-assisted phosphorylation is requisite for protection of cMyBPC against proteolytic cleavage.

Conclusions

This study ascribes a novel function to MMGL isoform 4: it meets all criteria for classification as an AKAP, and we show that is involved in the phosphorylation of cMyBPC as well as cTNI, hence MMGL is an important regulator of cardiac contractility. This has further implications for understanding the patho-aetiology of HCM-causing mutations in the genes encoding cMyBPC and cTNI, and raises the question of whether MMGL might itself be considered a candidate HCM-causing or modifying factor.

Key Words: AKAPs, cMyBPC, HCM, phosphorylation, PKA, regulation of contractility

Background

Cardiac contractility is significantly enhanced by the dynamic phosphorylation of a number of sarcomeric proteins, including cardiac myosin binding protein C (cMyBPC) [1,2]. This highly modular protein, found in the C-zone of the sarcomere, is encoded by a gene which is frequently implicated in hypertrophic cardiomyopathy (HCM) [3], a common inherited cardiac disease characterised by hypertrophy of the ventricular muscle [4]. There are multiple isoforms of this protein; the cardiac isoform differs from its skeletal counterparts by containing an extra immunoglobulin–like (IgI) domain (C0) at the amino terminal, a charged residue-rich insertion in domain C5 and three phosphorylation sites in a motif between the second and third IgI domains (C1-C2), known as the MyBPC motif or m-domain. Originally thought to have only a structural role, cMyBPC has been shown to play an important role in the regulation of cardiac contractility [1], for which the N-terminal region of the protein appears to be crucial. Upon β-adrenergic stimulation, three sites within the MyBPC motif are phosphorylated by protein kinase A (PKA) and calcium/calmodulin-activated protein kinase (CaMK), the phosphorylation of this region of MyBPC then leads to rearrangement of the myosin crossbridges and thick filament structure [1,5,6] such that cardiac contractility is increased [7].

However, since these kinases regulate a broad range of cellular responses, their compartmentalization in close proximity to their sarcomeric targets is required to facilitate control over which proteins are phosphorylated in response to second messenger signalling [8,9]. At the same time, co-compartmentalization of enzymes or proteins that generate or terminate these second messenger metabolites, such as the phosphodiesterases (PDEs) which degrade cAMP and cGMP, with the relevant responsive kinases helps to optimise the precision and speed of response to second messenger signaling [10]. Compartmentalization of kinases in general is achieved by either direct docking of the kinase on the target protein, or by anchoring of the kinase to, or close to, the target via an adaptor protein, named A-kinase anchoring proteins or AKAPs in the case of PKA [11]. Although a CaMK has been found to co-purify with cMyBPC [1,12], the mechanism of co-compartmentalization of cMyBPC and PKA has never been described and very little is knowns about sarcomeric AKAPs in general.

In this study we identified myomegalin (MMGL) isoform 4, a PDE4D-interacting protein [13], as a binding partner of PKA, the cMyBPC N-terminal region, as well as other PKA-targets, and show that MMGL meets all the requirements for classification as a novel sarcomeric AKAP, with important implications for regulation of cardiac contractility during adrenergic stimulation.

Results

Interaction of trisphospho-cMyBPC with MMGL

As the interactions of the N-terminal region of cMyBPC under its various phosphorylation states appear to be integral to the regulatory role of cMyBPC in contracility, we aimed to gain further insight into the interactions of the trisphosphorylated form of the N-terminal region of cMyBPC. Thus, we used a construct of C1-C2 in which

the serines in the three phosphorylation sites of the MyBPC motif had been replaced by glutamic acids (PPP), mimicking the trisphosphorylated state, as bait in a Y2H cardiac library screen.

During successive rounds of nutritional and colorimetric selection, 19 putative interactors of PPP were identified, which were able to activate the *HIS3*, *ADE2* and *MEL1* reporter genes in the presence of the PPP bait, but not in the presence of heterologous baits (Table 1). Of these, three in-frame prey plasmids encoded isoform 4 of PDE4D-interacting protein, also known as myomegalin (MMGL) (Table 1). This putative interaction between MMGL and the N-terminal of cMyBPC was intriguing, as the former protein is known to anchor PDE4D to particulate structures; PDE4D, in turn, is known to hydrolyze cAMP and thus to attenuate PKA-driven phosphorylation [13]. Furthermore, it has been shown that some adaptor proteins can anchor both PKA and PDE4D [14], raising the possibility that MMGL may be anchoring PKA to at least cMyBPC in the sarcomere as an AKAP; hence this interaction was prioritized for further investigation.

3D-fluorescence microscopy indicated that cMyBPC and MMGL isoform 4 colocalize in the cytoplasmic (encompassing the sarcomeric) region of differentiated rat cardiac H9C2 cells. Exposure of the cells to the adrenergic agonist isoproterenol led to an increase in colocalization of the two proteins, as evidenced by the increased yellow staining during fluorescence microscopy of such cells (Fig. 1A, B).

Furthermore, in order to verify that it is the C1-C2 region of cMyBPC that interacts with MMGL isoform 4, specifically, and does so in the absence of the GAL4 regions of the Y2H bait protein, we used *in vitro* co-immunoprecipitation assays. We also used these assays to assess whether trisphosphorylation of the MyBPC motif within this region was crucial to the putative interaction. Both the native C1-C2 and a trisphospho-mimic of the C1-C2 region interacted with MMGL isoform 4 in the absence of the Y2H GAL4 domains (Fig. 1C), suggesting that the interaction can take place whether or not the MyBPC-motif is phosphorylated.

MMGL binds to PKA regulatory subunits

As the primary characteristic of an AKAP is the ability to bind at least one PKA regulatory subunit, we investigated the possibility that MMGL functions as an AKAP by using Y2H-based direct protein-protein interaction assays to determine binding between MMGL and the two cardiac-expressed regulatory subunits of PKA. Both regulatory subunits (PRKAR1A and PRKAR2A) interacted with MMGL, as assessed by growth and light colour of the colonies on quadruple dropout nutritional selection medium, compared to relevant controls (Fig. 2A).

Further support for this finding was garnered by co-localization studies using 3D-fluorescence microscopy: we demonstrated that MMGL isoform 4 occurs in the same 3D-subcellular region as the two PKA regulatory isoforms in H9C2 cardiomyocytes (Fig. 2B).

To further verify physical interaction between MMGL and these PKA isoforms in a cellular context and in the absence of GAL4 domains, we performed pull-down assays in diffentiated H9C2 cardiomyocytes. As commercial antibodies against MMGL/PDE4DIP are not able to detect isoform 4, the smallest isoform of this protein (results not shown), we used an antibody directed against dsRed to detect a dsRed-tagged version of MMGL isoform 4 in these assays. In this way, endogenous PRKAR1A and PRKAR2A were shown to immunoprecipitate dsRed-MMGL, and *vice versa* (Fig. 2C), indicating physical interaction of MMGL with these two PKA regulatory isoforms.

MMGL binds to additional PKA targets

We further investigated the function of MMGL isoform 4 by using it as Y2H bait to screen a cardiac cDNA library in order to identify its additional binding partners. Thirteen in-frame putative MMGL-interactors were identified that activated all three nutritional reporter genes in the presence of the MMGL bait, but not in the presence of heterologous baits (Table 2). As we were primarily interested in the possibility of MMGL acting as a sarcomeric AKAP, proteins with defined vesicular localizations were not considered of primary interest for follow-up in this study; these included the mitochondrial protein COX5A, the proteosome 26S subunit and the endosomal protein SNX3. Of the remaining ten putative MMGL interactors, six encoded cardiac troponin I (cTNI) (Table 2).

Further support for the validity of these interactions was provided by finding that MMGL occurs in the same 3D-subcellular region as all five of the putative interactors identified in the Y2H library screen, viz. cardiac ankyrin repeat protein (CARP), copper metabolism gene *MURR1* domain 4 (COMMD4), α-enolase (ENO1), β-enolase (ENO3) (Fig. 3), and cardiac troponin I (cTNI) (Fig. 4A), in differentiated cardiomyocytes.

cTNI is a known PKA target [15], while the remaining four putative interactors were shown to be likely targets using Phosphomotif Finder (www.hprd.org/PhosphoMotif_finder); we therefore investigated the effect of isoproterenol stimulation of the H9C2 cells on colocalization, using the most frequent, and sarcomeric-located, putative interactor, cTNI, as example. Treating H9C2 cells transfected with dsRed-MMGL/GFP-cTNI with isoproterenol resulted in significantly more 3D colocalization between these two proteins, as shown in Fig. 4, compared to non-treated cells.

Moreover, in pull-down assays, exogenous, fluorescently-tagged MMGL and endogenous ENO1, ENO3, CARP and cTNI reciprocally co-precipitated each other (Fig. 5i-iv). As COMMD4 had a similar mobility to antibody light chains, which interfered with detection of these proteins in Western blots, a GFP-tagged fusion of this protein was expressed in H9C2 cells for pull-down assays. In these assays, exogenous GFP-COMMD4 immunoprecipiated exogenous dsRed-MMGL, and *vice versa* (Fig. 5v). Thus, Western blot analysis data supported the proposed interaction of MMGL with ENO1, ENO3, CARP, cTNI and COMMD4.

Thus, our results strongly suggest that MMGL interacts with both PKA regulatory isoforms, as well as with each of the prioritized five putative prey interactors identified in the Y2H screen, in a cellular milieu, and in the absence of the GAL4 domains.

Effect of MMGL knockdown

In order to evaluate the role of MMGL in cMyBPC phosphorylation, we assessed the expression of the different phosphorylation isoforms of cMyBPC, in the context of siRNA-mediated MMGL knockdown. Typically, interference with AKAP-functioning is commonly more noticeable on the target protein only after adrenergic stimulation [16], thus we also tested the effect of MMGL knockdown in the presence of adrenergic stimulation. Of four siRNAs tested, Rn_RGD:708410_3_HP siRNA (MMGL 3) (Qiagen) was found to provide optimal knockdown of MMGL (80%) in H9C2 cells (Fig. 6A); thus MMGL 3 siRNA was used in subsequent experiments to silence MMGL gene expression.

Using Western blots of 2-dimensional IEF gels, we found that similar amounts of the mono- and diphosphorylated forms of cMyBPC were expressed in untreated H9C2 cells, while lesser amounts of the un- and trisphosphorylated forms, relative to the other isoforms, were present (Fig. 6Bi, Ci). When these cells were exposed to increased $CaCl_2$ and isoproterenol, to activate CaMK and PKA such that maximum phosphorylation of the MyBPC-motif is likely [7], the relative amount of the trisphosphorylated form increases markedly, while the relative amount of unphosphorylated cMyBPC decreased (Fig 6Bii, Cii). However, adrenergic stimulation in the presence of MMGL knockdown resulted in very low expression of all isoforms (Fig. 6Biii, Ciii). This finding is compatible with previous findings of an inverse relationship between phosphorylation of cMyBPC and its proteolytic degradation, suggesting that phosphorylated cMyBPC is protected against proteolytic cleavage, whereas absence of phosphorylation results in increased degradation of the protein and reduced levels of cMyBPC in the cell [17,18].

Discussion

Myomegalin has been characterized as a protein with the properties of a scaffold or structural protein that is expressed at high levels in skeletal and cardiac tissue, suggesting an important function in muscle, and which interacts with a cAMP-specific phosphodiesterase [13]. However, the precise function and interactions of this protein, and its five isoforms, have been largely unknown. We here describe how the smallest MMGL isoform, isoform 4, binds to known and predicted PKA targets in the cardiac myocyte, including some sarcomeric proteins, viz. cMyBPC, cTNI, ENO1, ENO3, CARP and COMMD4 (Tables 1 and 2). Moreover, we show that MMGL isoform 4 interacts with two regulatory subunits of PKA (Fig. 2). Together these results describe MMGL isoform 4 as a novel sarcomeric AKAP, which, like mAKAP [14], is involved in assembling a PKA/PDE cAMP signalling module.

In addition to interacting with both types of regulatory subunits, viz. RI and RII, which qualifies MMGL isoform 4 as a dual-specific AKAP [11,19], MMGL also meets the three other criteria for classification as an AKAP: By verifying its interaction with its proposed binding partners, we demonstrate that the targeting domains contained within the proposed AKAP participates in protein-protein interactions [11]. Further, it has previously been shown that MMGL is a phosphodiesterase 4D-interacting protein [13], thus it meets the criterion for being able to coordinate multiple signaling pathways by anchoring additional signaling enzymes [11,20]. Lastly, we have shown in other Y2H screens that cMyBPC also binds to COMMD4 (unpublished results), here shown to be a MMGL interactor, while COMMD4 itself also binds to ENO1 and SNX3 (unpublished results). This strongly suggests that MMGL is part of a larger, multiprotein unit [11,20], and that MMGL isoform 4 may function as a vital link in signaling between upstream activators and numerous downstream targets [21].

Co-compartmentalization of both PKA and PDE4D is crucial for maintaining specificity of adrenergic signaling, and for maintaining contractility in cardiac cells [16]. We here established an important and novel link between PKA and PDE4D co-compartmentalization at the sarcomere level, and cMyBPC phosphorylation, and hence, regulation of cardiac contraction. The mechanism of docking of PKA to cMyBPC for phosphorylation of the MyBPC motif has previously not been elucidated; this study strongly suggests that MMGL isoform 4 anchors PKA to the N-terminal region, viz. C1-C2, of cMyBPC. The interaction between MMGL isoform 4, PKA, PDE4D and the N-terminal region of cMyBPC therefore sheds light on how second messenger responses are regulated in this particular part of the sarcomere.

We also found that β-adrenergic stimulation led to greater colocalization of myomegalin with both cMyBPC and cTNI in live cardiomyocytes, as evidenced by the increase in yellow staining during fluorescence microscopy in Figs. 1 & 4. This implies that under adrenergic stimulation, and consequential increased intracellular levels of cAMP, PKA is dynamically recruited by MMGL isoform 4 to distinct sarcomeric locations. This translocation of MMGL to the sarcomeric region is therefore compatible with a mechanism that would lead to increased phosphorylation of cMyBPC and cTNI, which is known to form part of the cardiac cellular stress response that leads to increased cardiac contraction [22]. Furthermore, given MMGL's known interaction with PDE4D [13], the mechanism for termination of the second messenger response, by degrading cAMP, would also be on site; lower levels of cAMP may then cause this multiprotein complex to dissociate again.

The knockdown studies of MMGL further suggests that MMGL not only acts as an AKAP at the MyBPC motif, but by implication plays a role in cardioprotection during adrenergic signaling. Although, in the presence of MMGL, all phosphorylation isoforms of cMyBPC are expressed well in H9C2 cells, and the level of the trisphosphorylated cMyBPC is increased in such cells under conditions of β-adrenergic stimulation as is to be expected, knockdown of MMGL under the same conditions dramatically reduced cMyBPC expression (Fig. 5). The latter finding suggests that when MMGL expression is reduced, cMyBPC phosphorylation is hindered, rendering the protein vulnerable to cleavage by proteases and reducing cMyBPC protein levels in the cell, as

described by others [17,18,23]. Thus, it appears that MMGL is an essential part in the β-adrenergic pathway leading to trisphosphorylation of cMyBPC and protection of the protein against degradation, which in turn is essential for normal sarcomeric integrity and cardiac function, as well as cardioprotection during ischemia-reperfusion injury.[24]

The subcellular localization and functions of some of the putative PKA targets identified via the Y2H library screen suggest that MMGL may act as AKAP in regions outside the sarcomere as well. Although some of the identified interactions, such as those with cMyBPC and cTNI, certainly occur within the sarcomere, associations with the other identified interactors (Table 2) do not necessarily occur within the sarcomere, nor do they necessarily all occur concurrently. In fact, a multiprotein subunit in the sarcomere consisting simultaneously of all identified MMGL-ligands would most likely sterically hinder crossbridge formation, and is therefore improbable. However, interaction of MMGL with proteins such as COMMD4, CARP, ENO1 and ENO3 may facilitate control of efficient PKA phosphorylation of these proteins; the protein-protein interactions and/or activation of these proteins may thus be regulated.

Although this study prioritized investigation of the interaction between the N-terminal of cMyBPC and MMGL, the other putative interactions of this region of cMyBPC should be further explored. The absence of cMyBPC as a prey in the MMGL Y2H library screen is most likely explained by the known absence of cDNAs representing the N-terminals of large proteins in oligo dT-primed libraries, while the absence of PRKAR1A and PRKAR2A may relate to the stringency of selection during heterologous bait-matings during this Y2H screen [25].

Interaction between myomegalin, PKA and cMyBPC or cTNI is also relevant to understanding of HCM patho-aetiology, as both of the latter proteins cause HCM when defective. It is known that point mutations in the C1-C2 region and in the MyBPC motif lead to HCM [3,26]; a potential mechanism for this may be involve disruption of binding between MMGL and cMyBPC. Such disruption would have consequences for PKA-phosphorylation of the cMyBPC motif (with implications for regulation of cardiac contractility), implying a poison-peptide mechanism underlying disease, as well as maintenance of sufficient cMyBPC levels within the sarcomere, particularly under conditions of adrenergic stress, implying a haplo-insufficiency mechanism. Point mutations in cTNI may have a similar patho-aetiology. It could be further speculated that, mutations in MMGL could similarly lead to inadequate binding of PKA and/or its sarcomeric partners, which might affect cMyBPC or cTNI phosphorylation and hence affect adaptation of cardiac contractility to adrenergic stimulation. Future studies could therefore consider MMGL as either a candidate causal gene or a potential modifier gene for HCM.

Conclusions

This study shows that myomegalin isoform 4 is a novel sarcomeric AKAP, which forms part of a multiprotein complex that functions in cAMP signalling. It is particularly relevant to phosphorylation of cMyBPC and cTNI, and therefore, is of significance in the regulation of cardiac contractility in both health and disease.

Methods

Plasmid constructs

Y2H constructs

The region of MYBPC3 encoding domains C1-C2 was PCR-amplified from a MYBPC3 cDNA clone (kind gift of Prof Hugh Watkins, Oxford University). PCR-based site-directed mutagenesis, as previously described by Elliott *et al*.[27], was then used to generate a PCR fragment representing domains C1-C2 in which the codons for serines within all three phosphorylation sites of the cMyBPC motif were mutated to encode glutamic acids to mimic the trisphosphorylated state (PPP). The full-length cDNA from MMGL isoform 4 was amplified from a commercial construct, in vector pdEYFP-C1 (imaGenes GmbH). These fragments were individually cloned into the *Nde*I and *Eco*RI restriction sites in-frame with *GAL4*BD in the Y2H bait yeast expression vector pGBKT7 (Clontech) for use in the respective Y2H library screens or in Y2H-based direct protein-protein experiments.

The cDNA of the two PKA regulatory isoforms (*PRKAR1A* and *PRKAR2A*) were PCR amplified from a cardiac cDNA library (Clontech). These fragments were cloned into the *Bam*HI and *Xho*I restriction sites or the *Nco*I and *Bam*HI sites, respectively, of the Y2H prey vector pACT2 (Clontech).

Integrity of insert sequences, reading frame and cloning sites were verified by means of bi-directional sequencing, after which pGBKT7-PPP and pGBKT7-MMGL were transformed into *S. cerevisiae* strain AH109, and pACT2-R1A and pACT2-R2A into strain Y187 (Clontech).

Constructs used for verification analyses

The cDNAs from the putative interactors of MMGL isoform 4 identified in the Y2H library screen viz. *TNNI3*, *CARP*, *COMMD4*, *ENO1* and, *ENO3*, as well as *PRKAR1A* and *PRKAR2A*, were PCR amplified and cloned into the pGFP2-C1 fluorescent vector (BD Bioscience). *MMGL* was further subcloned from the pGBKT7-MMGL construct into the pDs-Red-C1 vector (dsRed-MMGL) (BD Bioscience). The integrity of the cloning sites, reading frames and all interactor sequences were verified by bi-directional sequencing. These constructs were subsequently used in 3D *in vivo* colocalization and *in vivo* co-immunoprecipitation analyses.

Y2H library screening

A *S.cerevisciae* Y187 pre-transformed human MATCHMAKER™ cardiac cDNA library constructed in pACT2 (BD Bioscience) was mated with the AH109 strain transformed with pGBKT7-PPP and the library screen performed according to manufacturer's instructions. Clones that expressed all three reporter genes, *HIS3*, *ADE2*, and *MEL1*, were further analyzed. An interaction-specificity test was used to identify preys that did not activate reporter genes in the presence of the following heterologous baits: pGBKT7-C5 (encoding Igl domain C5 of cMyBPC), pGBKT7-53 (encoding murine p53) and unrecombined pGBKT7. Prey plasmids interacting

specifically with PPP were sequenced using a vector specific primer, and in-frame ORF sequences analyzed via BLASTN and BLASTP (http://ncbi.nlm.nih.gov/blast) to assign identity. Literature and public database searches were used to prioritize putative ligands according to function and subcellular localization. A Y2H library screen with pGBKT7-MMGL was subsequently similarly performed.

Direct Y2H protein-protein interaction assay

pGBKT7-MMGL in yeast strain AH109 was mated individually with pACT2-R1A and pACT2-R2A in yeast strain Y187 to determine whether the PKA regulatory subunits interacts directly with MMGL. A single colony of pGBKT7-MMGL in AH109 was taken from appropriate selection plates and suspended with a single colony of pACT2-R1A or -R2A in YPDA media overnight. Mating mixes were plated onto solid growth medium lacking leucine (Leu) and tryptophan (Trp). Following an incubation period of four days, the colonies on each plate were transferred to medium lacking Leu, Trp and histidine (His), and incubated five days. Surviving colonies were finally transferred to medium lacking Leu, Trp, His and adenine (Ade) and growth was assessed on day 4 and 7. Control matings were included those of pGBKT7-MMGL with pACT2-cTNI(+), pACT2-TUSC4(-) and empty pACT2(-).

Antibodies

Anti-HA, anti-Myc and anti-CARP antibodies were purchased from Santa Cruz Biotechnology. Living colours™ anti-dsRed and -JL-8 antibodies were purchased from Clontech and anti-β-actin antibody from Cell Signaling Technology. Anti-ENO1, -ENO3, -PRKAR1A, -PRKAR2A and -cTNI antibodies were purchased from Abnova.

Cell culture and transfection

H9C2 cells were maintained at 37°C and 5% CO2 in Dulbecco's modified Eagle's medium, supplemented with 10% fetal bovine serum, 100µg/ml penicillin and 100µg/ml streptomycin. For *in vivo* co-immunoprecipitation, approximately 4 million H9C2 cells were seeded per 135mm petri dish, and were transfected once 70-80% confluency was reached. Genejuice® (Novagen) was used for transfections according to manufacturer's instructions. For 3D *in vivo* colocalization, approximately 20 000 – 30 000 H9C2 cells were seeded per well in 8-well borosilicate coverglass chambers (Nunc), and transfected after 70-80% confluency have been reached using Lipofectamine™ (Invitrogen) according to manufacturer's recommendations. Cells were differentiated into myotubes 24h after transfection by changing the growth media to differentiation media (Dulbecco's modified Eagle's medium, 1% horse serum, 100µg/ml penicillin and 100µg/ml streptomycin). Fresh differentiation media was added every 48h until cells were fully differentiated.

Three-dimensional *in vivo* co-localization

Prior to image acquisition, the differentiation media was removed from the co-transfected, differentiated H9C2 cells and replaced with culture media containing a 1:200 dilution of Hoechst H-33342 nucleic acid stain (Sigma). Cells in three wells co-transfected with GFP-MyBPC/dsRed-MMGL were photographed using an Olympus IX 81 motorised inverted microscope (Olympus); after photography, cells were treated with 0.1μM isoproterenol in order to stimulate phosphorylation of the MyBPC motif [7] and the same cells photographed again, to monitor changes in colocalization upon adrenergic stimulation. CellR software was used to perform image analysis. Z-stacks were done in order to co-localize the tagged proteins in three dimensions. Double-labeled images, utilizing the co-transfected samples, were obtained at different focal planes which were processed by the CellR software to determine colocalization. A 60X oil immersion objective was used to collect image stacks at 0.26μm intervals in the plane. Subsequently, each co-localized image was created from the average of 25 frames. Changes in colocalization of MMGL isoform 4 and cTNI were obtained in a similar manner.

***In vitro* protein transcription and translation**

The cDNA encoding the native as well as the trisphosphorylated mimic of the C1-C2 region of cMyBPC and the full-length MMGL isoform 4 cDNA were PCR amplified to generate fragments that incorporates the T7 promoter and Myc- or HA-epitope tags, respectively. The TnT Quick Coupled Transcription/Translation System (Promega) was then used to transcribe and translate these PCR products into Met-35S-radiolabelled proteins, according to manufacturer's instructions.

***In vitro* co-immunoprecipitation**

Five microlitres of the respective 35S-labelled HA-MMGL and Myc-C1-C2 were mixed and incubated for 1h at room temperature. One microlitre of anti-HA or anti-Myc antibody (5μg/ml) was added followed by incubation of 1h. Ten microlitres of pre-washed protein G agarose (Kirkegaard & Perry Laboratories) were subsequently added, together with 135μl Co-IP buffer [5mM phosphate-buffered saline (PBS), 5μg/ml aprotinin, 0.5mM PMSF, 100mM DTT, 1% Tween-20]. Incubation of 1h at 4°C followed on a rotating device. Centrifugation followed for 30s at 3000*g*, after which the pellet was washed five times with Tris-buffered saline with Tween-20 [20mM Tris-HCl, pH7.5, 150mM NaCl, 1% Tween-20]. Samples were electrophoresed on a 20% SDS-polyacrylamide gel, and protein bands were detected by autoradiography.

***In vivo* co-immunoprecipitation**

H9C2 cells transfected with the appropriate constructs were harvested 48h following transfection, centrifuged at 3000rpm for 3min and the pellet washed with PBS. Two hundred microlitres of passive lysis buffer (PLB) [0.5M EDTA, 1M NaVO4, 10mM Nappi, 1M HEPES, 5M NaCl, 1% TritonX, protease inhibitors and phenylmethylsulfonyl fluoride (PMSF)] was added to each sample. Samples were then incubated on ice for 30min followed by centrifugation at 14000rpm and the supernatants collected. Lysate concentration was determined via a Bradford assay, and the volumes equalized to 200µl by adding PLB containing protease inhibitors and PMSF with a final concentration of 200µg/µl. Lysates were pre-cleared by adding 20µl Protein G agarose beads (KPL) and incubating samples at 4°C for 2h on a rotating device. Fluorescent-tagged or endogenous proteins were immunoprecipitated from lysates using 1-2µg of the appropriate antibody, as indicated in Fig. 2c and 5. Following overnight incubation, 60µl of protein G agarose beads was added to each sample, and incubated at 4°C for 2h on a rotating device. Afterwards, immunoprecipitates were washed 5X in cold PLB containing protease inhibitors and PMSF, followed by resuspension in SDS loading buffer, and boiling prior to SDS-PAGE and subsequent Western blotting**.**

RNA interference

The effect of siRNA transfection on myomegalin mRNA expression using different *PDE4DIP* siRNAs (Qiagen) was determined and optimized by a 2-step Q-RT-PCR using the Corbett Rotorgene system as follows: Approximately $4x10^4$ H9C2 cells were seeded per well of an 8-well chamber slide, and siRNA transfected when cells reached 50-60% confluency, using HiPerFect transfection reagent (Qiagen) as per manufacturer's instructions. Total RNA extraction followed after 24 hours using the RNeasy Plus Mini kit (Qiagen) as per manufacturer's instructions. cDNA was subsequently transcribed using the Quantitect Reverse Transcription kit (Qiagen) as per manufacturer's instructions. The Quantifast SYBR green PCR kit (Qiagen) was then used to perform a real-time quantification of cDNA transcribed from the extracted RNA with or without non-silencing control (NSC) or PDE4DIP siRNAs. PDE4DIP levels were quantified with reference to three rodent reference genes (transferring receptor – *TRFR*, glyceraldehydes-3-phosphate dehydrogenase – *GAPDH* and heat shock protein 1β - *Hsp1β*) selected from a panel of 6 commonly used housekeeping genes.

The Genomewide designed non-validated Rn_RGD:708410_3_HP siRNA (Qiagen) resulted in the lowest MMGL gene expression quantification levels, and was used in subsequent experiments. Confluent H9C2 cells were transfected with GFP-tagged cMyBPC using Genejuice® (Novagen). These cells were then transfected after 24h with 10nM *PDE4DIP* Rn_RGD:708410_3_HP siRNA using HiPerFect Transfection Reagent (Qiagen); control cells were not transfected with siRNA. For adrenergic stimulated cells, cells were treated with 65mM CaCl2 for 10min at 24h post-transfection, followed by a 0.1µM isoproterenol treatment for another 10min. All cells were then lysed (as done for *in vivo* co-immunoprecipitation) and concentrations determined via

Bradford assays, and all volumes equalized to 200µl by adding PLB containing protease inhibitors and PMSF with a final concentration of 200µg/µl. A non-denaturing immunoprecipitation of GFP-cMyBPC from the lysate followed using 1µg of the JL-8 antibody with the Dynabeads® Protein G and DynaMag™-2 system (Invitrogen) as per manufacturer's instructions. Isoelectric focusing of the GFP-cMyBPC immunoprecipitates followed to separate the four possible phosphorylation isoforms of cMyBPC.

Isoelectric focusing

For the first dimension separation, the GFP-tagged cMyBPC immunoprecipitates were suspended in ReadyPrep 2-D Rehydration buffer 1 (Bio-Rad) containing Bio-lite pH 3-10 buffer (Bio-Rad) to a final volume of 200µl. The protein/rehydration buffer mix was then applied to a pH 4-7 (11cm) immobilized pH gradient (IPG) strip (Bio-Rad). Rehydration of the strip followed for 12 hours at room temperature. Afterwards, IEF was done under the following conditions: 8000V for 20min, 8000V for 2 hours and 8000V for 40 000 V hours at 21°C (Protean IEF Cell, Bio-Rad). Strips were stored at -80°C after IEF until required.

For 2-dimensional gel electrophoresis (2-DE), IPG strips were equilibrated by incubating the strips in equilibration buffer (0.375M tris-HCl, 6M urea, 20% glycerol, 2%, SDS) containing DTT (Sigma-Aldrich) for 15min and then in equilibration buffer containing iodoacetamide (Sigma-Aldrich) for 15min shaking at room temperature. Following equilibration, the IPG strips were placed on top of a Criterion XT 12% bis-tris precast gel (Bio-Rad) and sealed with 0.5% agarose (Bio-Rad). Electrophoresis of the second dimension separation was done under constant voltage (200V) for 1-2 hours in 5% XT-MOPS running buffer (Bio-Rad). Gels were then transferred to a nitrocellulose membrane and subsequently western blotted with the JL-8 antibody.

Authors' contributions

GMU carried out the MMGL Y2H direct protein-protein interactions and library screen, cell culture, 3D *in vivo* co-localization assays, *in vivo* co-immunoprecipitations, RNA interference and isoelectric focusing, and drafted the manuscript. AR carried out the cMyBPC-PPP Y2H library screen and *in vitro* co-immunoprecipitations. BL assisted with operating the Olympus IX 81 inverted microscope and CellR software. CJK assisted with interpretation of data and technical assistance. LJK carried out cell culture and optimized siRNA transfections and MMGL knockdown. JR assisted with siRNA and western blot optimization. JCM-S conceived of the study, acquired funding, participated in its design, coordination and interpretation of data, and revised and approved the final manuscript.

Acknowledgements

This work was funded by the Wellcome Trust (International Senior Research Fellowship fellowship GR073610MA to JCM-S)

References

1. Gautel M, Zuffardi O, Freiburg A, Labeit S: **Phosphorylation switches specific for the cardiac isoform of myosin binding protein-C: a modulator of cardiac contraction?** *EMBO J* 1995, **14:** 1952-1960.

2. Garvey JL, Kranias EG, Solaro RJ: **Phosphorylation of C-protein, troponin I and phospholamban in isolated rabbit hearts.** *Biochem J* 1988, **249:** 709-714.

3. Richard P, Charron P, Carrier L, Ledeuil C, Cheav T, Pichereau C *et al*.: **Hypertrophic cardiomyopathy: distribution of disease genes, spectrum of mutations, and implications for a molecular diagnosis strategy.** *Circulation* 2003, **107:** 2227-2232.

4. Maron BJ, Gardin JM, Flack JM, Gidding SS, Kurosaki TT, Bild DE: **Prevalence of hypertrophic cardiomyopathy in a general population of young adults. Echocardiographic analysis of 4111 subjects in the CARDIA Study. Coronary Artery Risk Development in (Young) Adults.** *Circulation* 1995, **92:** 785-789.

5. Weisberg A, Winegrad S: **Alteration of myosin cross bridges by phosphorylation of myosin-binding protein C in cardiac muscle.** *Proc Natl Acad Sci U S A* 1996, **93:** 8999-9003.

6. Levine R, Weisberg A, Kulikovskaya I, McClellan G, Winegrad S: **Multiple structures of thick filaments in resting cardiac muscle and their influence on cross-bridge interactions.** *Biophys J* 2001, **81:** 1070-1082.

7. McClellan G, Kulikovskaya I, Winegrad S: **Changes in cardiac contractility related to calcium-mediated changes in phosphorylation of myosin-binding protein C.** *Biophys J* 2001, **81:** 1083-1092.

8. Pawson T, Scott JD: **Signaling through scaffold, anchoring, and adaptor proteins.** *Science* 1997, **278:** 2075-2080.

9. Wong W, Scott JD: **AKAP signalling complexes: focal points in space and time.** *Nat Rev Mol Cell Biol* 2004, **5:** 959-970.

10. Pawson T, Nash P: **Protein-protein interactions define specificity in signal transduction.** *Genes Dev* 2000, **14:** 1027-1047.

11. Colledge M, Scott JD: **AKAPs: from structure to function.** *Trends Cell Biol* 1999, **9:** 216-221.

12. Schlender KK, Bean LJ: **Phosphorylation of chicken cardiac C-protein by calcium/calmodulin-dependent protein kinase II.** *J Biol Chem* 1991, **266:** 2811-2817.

13. Verde I, Pahlke G, Salanova M, Zhang G, Wang S, Coletti D *et al.*: **Myomegalin is a novel protein of the golgi/centrosome that interacts with a cyclic nucleotide phosphodiesterase.** *J Biol Chem* 2001, **276:** 11189-11198.

14. Dodge KL, Khouangsathiene S, Kapiloff MS, Mouton R, Hill EV, Houslay MD *et al.*: **mAKAP assembles a protein kinase A/PDE4 phosphodiesterase cAMP signaling module.** *EMBO J* 2001, **20:** 1921-1930.

15. Patel JR, Fitzsimons DP, Buck SH, Muthuchamy M, Wieczorek DF, Moss RL: **PKA accelerates rate of force development in murine skinned myocardium expressing alpha- or beta-tropomyosin.** *Am J Physiol Heart Circ Physiol* 2001, **280:** H2732-H2739.

16. Fink MA, Zakhary DR, Mackey JA, Desnoyer RW, pperson-Hansen C, Damron DS *et al.*: **AKAP-mediated targeting of protein kinase a regulates contractility in cardiac myocytes.** *Circ Res* 2001, **88:** 291-297.

17. Decker RS, Decker ML, Kulikovskaya I, Nakamura S, Lee DC, Harris K *et al.*: **Myosin-binding protein C phosphorylation, myofibril structure, and contractile function during low-flow ischemia.** *Circulation* 2005, **111:** 906-912.

18. Sadayappan S, Osinska H, Klevitsky R, Lorenz JN, Sargent M, Molkentin JD *et al.*: **Cardiac myosin binding protein C phosphorylation is cardioprotective.** *Proc Natl Acad Sci U S A* 2006, **103:** 16918-16923.

19. Wang L, Sunahara RK, Krumins A, Perkins G, Crochiere ML, Mackey M *et al.*: **Cloning and mitochondrial localization of full-length D-AKAP2, a protein kinase A anchoring protein.** *Proc Natl Acad Sci U S A* 2001, **98:** 3220-3225.

20. Dodge K, Scott JD: **AKAP79 and the evolution of the AKAP model.** *FEBS Lett* 2000, **476:** 58-61.

21. Dodge-Kafka KL, Langeberg L, Scott JD: **Compartmentation of cyclic nucleotide signaling in the heart: the role of A-kinase anchoring proteins.** *Circ Res* 2006, **98:** 993-1001.

22. Chandra M, Dong WJ, Pan BS, Cheung HC, Solaro RJ: **Effects of protein kinase A phosphorylation on signaling between cardiac troponin I and the N-terminal domain of cardiac troponin C.** *Biochemistry* 1997, **36:** 13305-13311.

23. Sadayappan S, Gulick J, Klevitsky R, Lorenz JN, Sargent M, Molkentin JD *et al*.: **Cardiac myosin binding protein-C phosphorylation in a {beta}-myosin heavy chain background.** *Circulation* 2009, **119:** 1253-1262.

24. Barefield D, Sadayappan S: **Phosphorylation and function of cardiac myosin binding protein-C in health and disease.** *J Mol Cell Cardiol* 2010, **48:** 866-875.

25. Adler V, Pincus MR, Minamoto T, Fuchs SY, Bluth MJ, Brandt-Rauf PW *et al*.: **Conformation-dependent phosphorylation of p53.** *Proc Natl Acad Sci U S A* 1997, **94:** 1686-1691.

26. Erdmann J, Daehmlow S, Wischke S, Senyuva M, Werner U, Raible J *et al*.: **Mutation spectrum in a large cohort of unrelated consecutive patients with hypertrophic cardiomyopathy.** *Clin Genet* 2003, **64:** 339-349.

27. Elliott RJ, Bennet AJ, Braun CA, MacLeod AM, Borgford TJ: **Active-site variants of Streptomyces griseus protease B with peptide-ligation activity.** *Chem Biol* 2000, **7:** 163-171.

Tables

Table 1 - Interactors of the C1-C2 region of cMyBPC in the trisphospho-mimic state as identified by yeast 2-hybrid library screening

Clone #	Genomic Hit, Accession no (E-value)	In-frame ORF Protein Hit, Accession no (E-value)	Subcellular localization
P205, P272, P403	PDE4DIP, transcript 4 NM_001002810 (0.0)	Homo sapiens phosphodiesterase 4D interacting protein (myomegalin) NP_055459.3 (1e-70)	Cytoplasm, Cytoskeleton
P182, P286, P267	ACTC1 NM_005159 (0.0)	Homo sapiens actin, alpha, cardiac muscle 1 NP_005150 (1e-89)	Thin filament sarcomere
P259	ACTCB NM_001101 (0.0)	Homo sapiens actin, beta AAH23548.1 (8e-34)	Cytoplasm, cytoskeleton
P62, P213, P319	MYBPC3 NM_000256 (0.0)	Homo sapiens cardiac myosin binding protein C, NP_000247.2 (2e-26)	Thick filament; Sarcomere
P2,P81	Gcom1 transcript 12 NM_001018100 (0.0)	Homo sapiens GRINL1A combined protein NP_001018100.1, (2e-65)	Unknown
P80	FLNC NM_001458.2 (0.0)	Homo sapiens filamin C, gamma NP_001449.3(2e-91)	Myofibrillar z-disks; actin cytoskeleton

Clone #	Genomic Hit, Accession no (E-value)	In-frame ORF Protein Hit, Accession no (E-value)	Subcellular localization
P175, P465	CNN1 NM_001299.4 (0.0)	Homo sapiens calponin 1, basic, smooth muscle NP_001290.2 (1e-104)	Cytoplasm, cytoskeleton
P11	PARD3 NM_019619.2 (3e-121)	Homo sapiens par-3 partitioning defective 3 homolog NP_062565.2 (1e-24)	Plasma membrane; tight junctions
P223	CCT7 NM_001009570.1 (0.0)	Homo sapiens chaperonin containing TCP1, subunit 7 (eta) NP_001009570.1 (1e-83)	Cytoplasm
P238	SVIL NM_021738.1 (0.0)	Homo sapiens supervillin NP_003165.1 (1e-15)	Actin cytoskeleton, plasma membrane, nucleus
P398	FLJ21347 NM_022827.2 (0.0)	FLJ21347 NP_073738.2 (4e-101)	Unknown

Table 2 - Interactors of MMGL isoform 4 identified by yeast 2-hybrid library screening

Clone #	**Genomic Hit, Accession no & E-value**	**In-frame ORF Protein Hit, Accession no & E-value**	**Subcellular localization**
128, 137, 148, 149, 160, 200	TNNI3 NM 000363, 0.0	*Homo sapiens* troponin I type 3 (cardiac) NP 000354.3, 2e-82	Thin filament
192	CARP NM 014391, 0.0	*Homo sapiens* Cardiac ankyrin repeat protein NP 055206, 2e-121	Cytosol, nucleus
715	COMMD4 NM 017828, 0.0	*Homo sapiens* COMM domain containing 4 NP 060298.2, 3e-97	Cytoplasm
130	ENO1 NM 001428, 0.0	*Homo sapiens* Enolase 1 (alpha) NP 001419, 4e-116	Cytoplasm
203	ENO3 NM 053013, 0.0	*Homo sapiens* Enolase 3 (beta, muscle) NP 001967.1, 000.1	Cytoplasm

Figures

Figure 1 - MMGL isoform 4 interacts with the C1-C2 region of cMyBPC

A: Live cell fluorescence imaging showing that colocalization of MMGL isoform 4 and cMyBPC increases under adrenergic stress. Each panel represents a single frame of the 25 images that were captured for the Z-stack. Each of the first three columns shows a single colour channel, while the image in the last column shows an overlay of the four colour channels used. Column iii shows colocalization (yellow fluorescence) between dsRed-MMGL and GFP-cMyBPC in the absence (-isopro) and presence (+isopro) of the beta-adrenergic agonist, isoproterenol. As evidenced by the increased yellow staining, co-localization levels between MMGL and cMyBPC increased ten minutes after the addition of isoproterenol. **B:** Quantification of colocalization shown in A demonstrates the noticeable increase in co-localization, although the increase does not reach statistical significance. **C:** *In vitro* co-immunoprecipitation showing that MMGL interacts with the native as well as the trisphospho-mimic of C1-C2 in the absence of Y2H GAL4 domains. *Abbreviations:* isopro-isoproterenol

Figure 2 – MMGL acts as a dual-specific AKAP by anchoring PKA regulatory isoforms R1A and R2A

A: Activation of nutritional reporter genes by PKA-MMGL interaction during direct protein-protein interaction assays. Small-scale Y2H matings between pGBKT7-MMGL and pACT2-PRKAR1A (i) and pACT2-PRKAR2A (ii) on solid medium lacking Leu, Trp, His and Ade. Growth of yeast yells indicate interaction of MMGL with PRKAR1A as well as PRKAR2A **B:** Live cell fluorescence imaging of co-localization of MMGL with PRKAR1A and PRKAR2A in differentiated H9C2 cardiomyocytes. (i) GFP-tagged PRKAR1A and PRKAR2A is seen in the cytosol as green fluorescence. (ii) dsRed-tagged MMGL expression is seen as red fluorescence. (iii) Yellow fluorescence indicates the co-localization of PRKAR1A and PRKAR2A with MMGL. (iv) Overlay of images A-C with Hoechst H-33342 labeling of the nuclei (blue fluorescence), for orientation purposes. **C:** Western blots of *in vivo* co-immunoprecipitations of PKA regulatory subunits and MMGL. (i) Endogenous PRKAR1A and PRKAR2A immunoprecipitated exogenous dsRed-MMGL in lysates of dsRed-MMGL-transfected, differentiated H9C2 cardiomyocytes. Conversely, (ii) PRKAR1A and (iii) PRKAR2A also immunoprecipitated exogenous dsRed-MMGL in these lysates. The clear protein G control lanes showed that these precipitations are not spurious, but are the result of physical association between the relevant proteins. *Abbreviations:* IP-immunoprecipitate; Prot G-protein G control; R1A-PRKAR1A; R2A-PRKAR2A WB-western blot

Figure 3 – 3D co-localization of MMGL and its respective preys identified in the Y2H library screen

Live cell fluorescence imaging of co-localization of MMGL and the putative interactors identified in the Y2H library screen in differentiated H9C2 cardiac myocytes. (i) Individual GFP-tagged putative library screen interactors are seen as green fluorescence, as indicated by labels to the left of the row. (ii) dsRed-tagged MMGL expression in the same cell(s) are shown are red fluorescence. (iii) Co-localization of interactors and MMGL

within these cell(s), generated from 3D Z-stack images, are shown as yellow fluorescence. (iv) Overlay of images A-C with Hoechst H-33342 labelling of the nuclei (blue) for orientation purposes. The presence of yellow staining in each of the images in (iii) indicates that each of the respective preys colocalize with MMGL in differentiated H9C2 cardiomyocytes.

Figure 4 – Co-localization increases between MMGL and PKA target upon β-adrenergic stimulation

A: Live cell fluorescence imaging showing that co-localization of MMGL isoform 4 and cTNI increases under adrenergic stress. Each panel represents a single frame of the 25 images that were captured for the Z-stack. Each of the first three columns shows a single colour channel, while the image in the last column shows an overlay of the four colour channels used. Column iii shows colocalization (yellow fluorescence) between dsRed-MMGL and GFP-cTNI in the absence (-isopro) and presence (+isopro) of the beta-adrenergic agonist, isoproterenol. The increase in intensity of yellow fluorescence in the second row demonstrates that co-localization levels of MMGL and cTNI had increased ten minutes after the addition of isoproterenol. **B:** Quantification of co-localization shown in A shows that co-localization increased noticeably, although the increase does not reach statistical significance. *Abbreviations:* isopro-isoproterenol

Figure 5 – Western blots of *in vivo* co-immunoprecipitations of MMGL and putative interactors

A: Western blots showing that endogenous CARP (i), ENO1 (ii), ENO3 (iii) and cTNI (iv) immunoprecipitated exogenous dsRed-/YFP-MMGL *in vivo* in lysates of ds-Red-/YFP-MMGL transfected, differentiated H9C2 cardiomyocytes. (v) Western blot showing that GFP-COMMD4 immunoprecipitates dsRed-MMGL in differentiated H9C2 cardiomyocytes transfected with both GFP-COMMD4 and dsRed-MMGL **B:** Western blots of reciprocal immunoprecipitations indicated that dsRed-/YFP-MMGL immunoprecipitated endogenous CARP (i), ENO1 (ii), ENO3 (iii) and cTNI (iv) in lysates of ds-Red-/YFP-MMGL transfected, differentiated H9C2 cardiomyocytes. (v) Western blot indicating that dsRed-MMGL immunoprecipitates GFP-COMMD4. The dsRed antibody is directed against the dsRed-MMGL fusion protein, while the JL-8 antibody is directed against the YFP/GFP fusion proteins. The clear protein G control lanes show that these precipitations are not spurious, but are the result of physical association between the relevant proteins. Abbreviations: IP-immunoprecipitate; Prot G-protein G control; WB-western blot

Figure 6 - siRNA-mediated knockdown of MMGL leads to reduced levels of cMyBPC phosphorylation under adrenergic stimulation.

A: Graph demonstrating that real-time quantification of *MMGL* cDNA transcribed from RNA extracted from cells transfected with either a non-silencing control or a particular *MMGL* siRNA. *Pde4dip* Rn_RGD:708410_3_HP (MMGL 3) resulted in optimal knockdown of *MMGL* (80%). **B:** Western blots of 2-dimensional IEF gels showing the expression of the four phosphorylation isoforms of GFP-cMyBPC in H9C2

cells (i) under non-stimulated conditions; (ii) under adrenergic stimulation, and (iii) under adrenergic stimulation in the absence of MMGL (i.e. with MMGL knock-down). **C:** Quantification of cMyBPC isoforms in the autoradiographs of the 2-dimensional IEF gels shown in (B), graphing the levels of the four phosphorylation isoforms (0=unphosphorylated; 1=monophosphorylated, 2=diphosphorylated, 3=trisphosphorylated). B and C(i) show that under non-stimulated conditions, levels of the mono- and diphosphorylated forms are similar and increased compared to the trisphosphorylated form. B and C(ii) show that under adrenergic stimulation, there is a relative increase in the trisphosphorylated form of cMyBPC and reduction of the non-phosphorylated form. B and C(iii) show that, upon MMGL knock-down, adrenergic stress leads to a reduction in the levels of all cMyBPC phosphorylation forms.

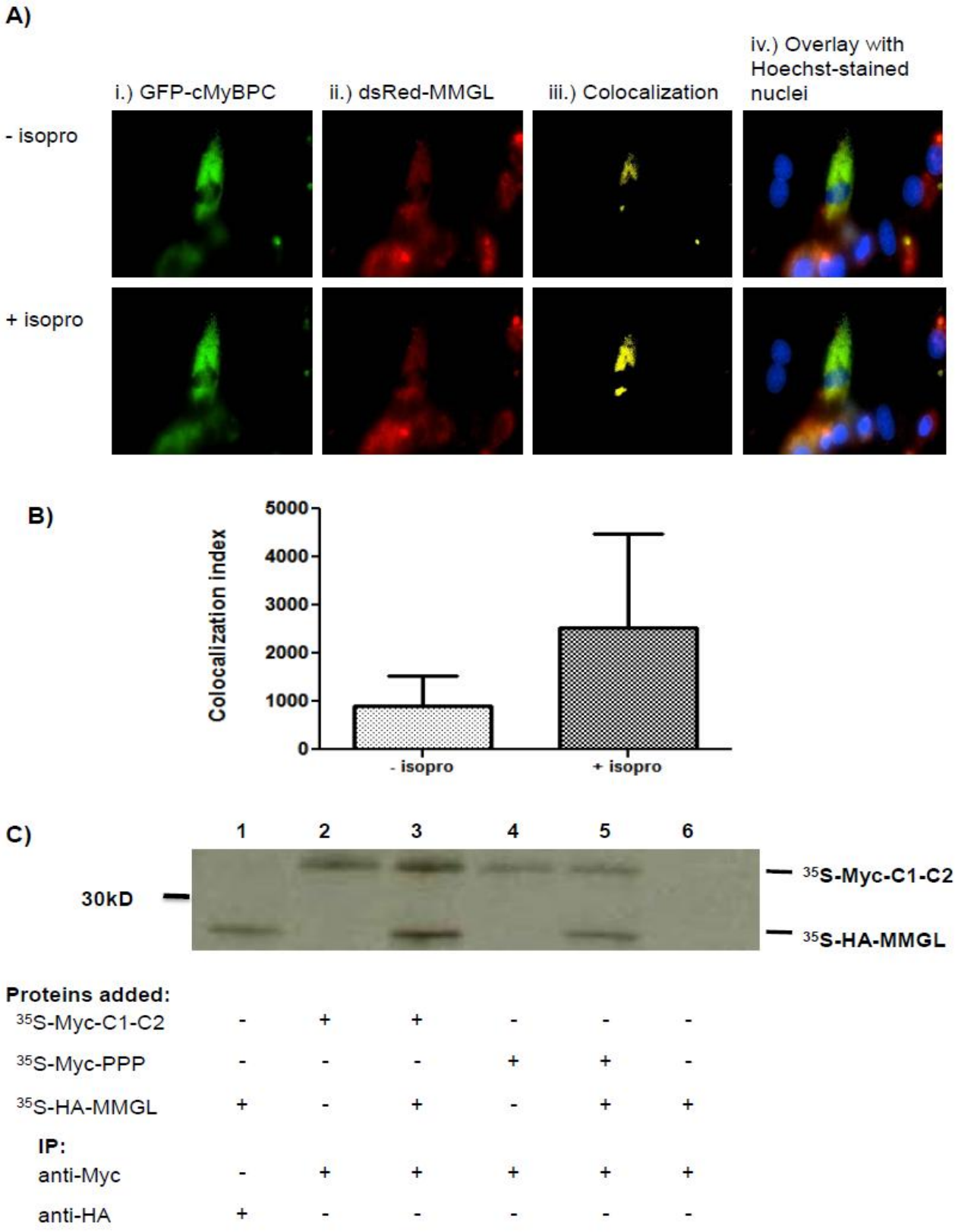
A)
i.) GFP-cMyBPC
ii.) dsRed-MMGL
iii.) Colocalization
iv.) Overlay with Hoechst-stained nuclei
- isopro
+ isopro
B)
Colocalization index
5000
4000
3000
2000
1000
0
- isopro
+ isopro
C)
1
2
3
4
5
6
30kD
35S-Myc-C1-C2
35S-HA-MMGL
Proteins added:
35S-Myc-C1-C2 - + + - - -
35S-Myc-PPP - - - + + -
35S-HA-MMGL + - + - + +
IP:
anti-Myc - + + + + +
anti-HA + - - - - -

Figure 1

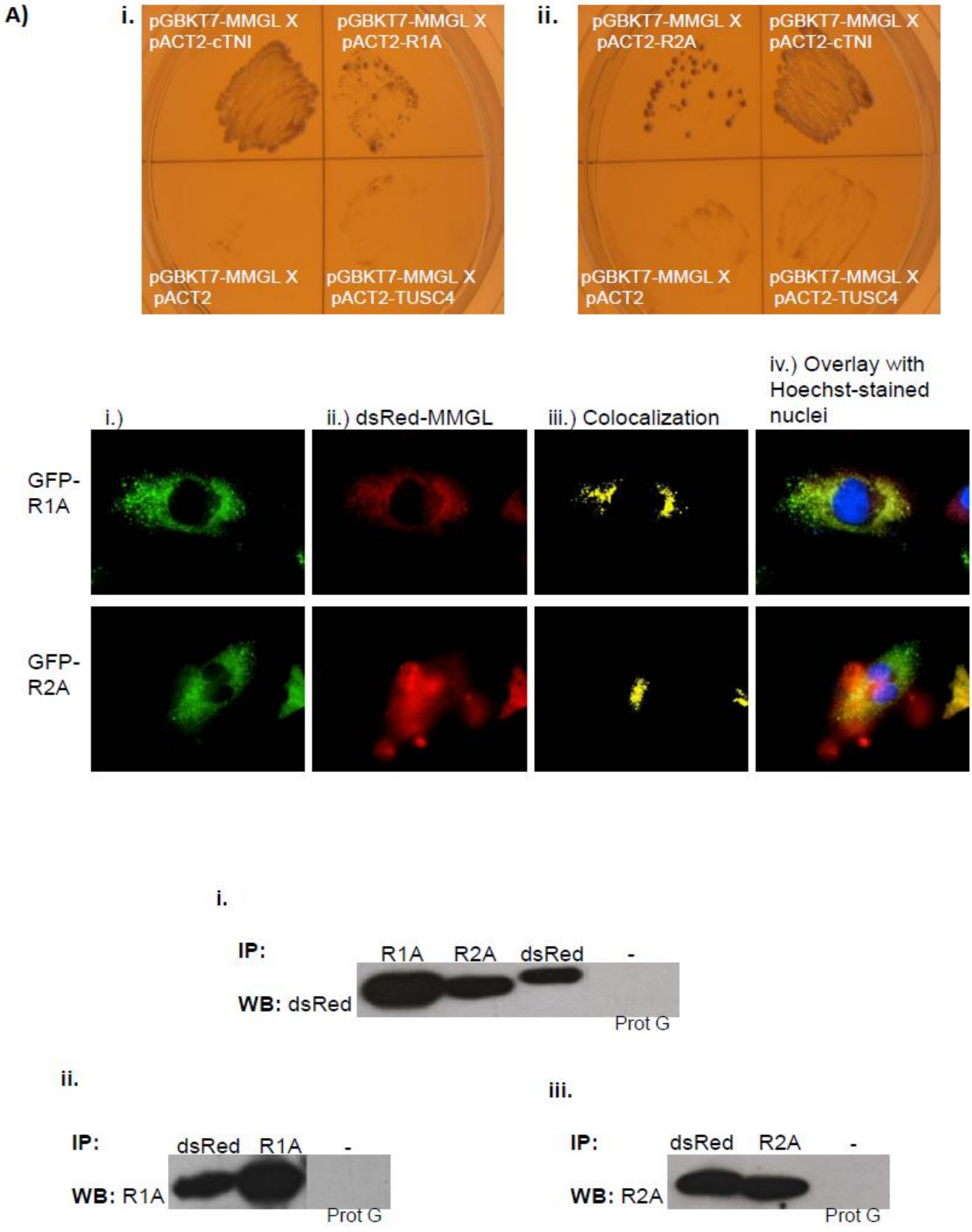
A)
i.
pGBKT7-MMGL X pACT2-cTNI
pGBKT7-MMGL X pACT2-R1A
pGBKT7-MMGL X pACT2
pGBKT7-MMGL X pACT2-TUSC4
ii.
pGBKT7-MMGL X pACT2-R2A
pGBKT7-MMGL X pACT2-cTNI
pGBKT7-MMGL X pACT2
pGBKT7-MMGL X pACT2-TUSC4
i.)
ii.) dsRed-MMGL
iii.) Colocalization
iv.) Overlay with Hoechst-stained nuclei
GFP-R1A
GFP-R2A
i.
IP:
R1A R2A dsRed -
WB: dsRed
Prot G
ii.
IP:
dsRed R1A -
WB: R1A
Prot G
iii.
IP:
dsRed R2A -
WB: R2A
Prot G

Figure 2

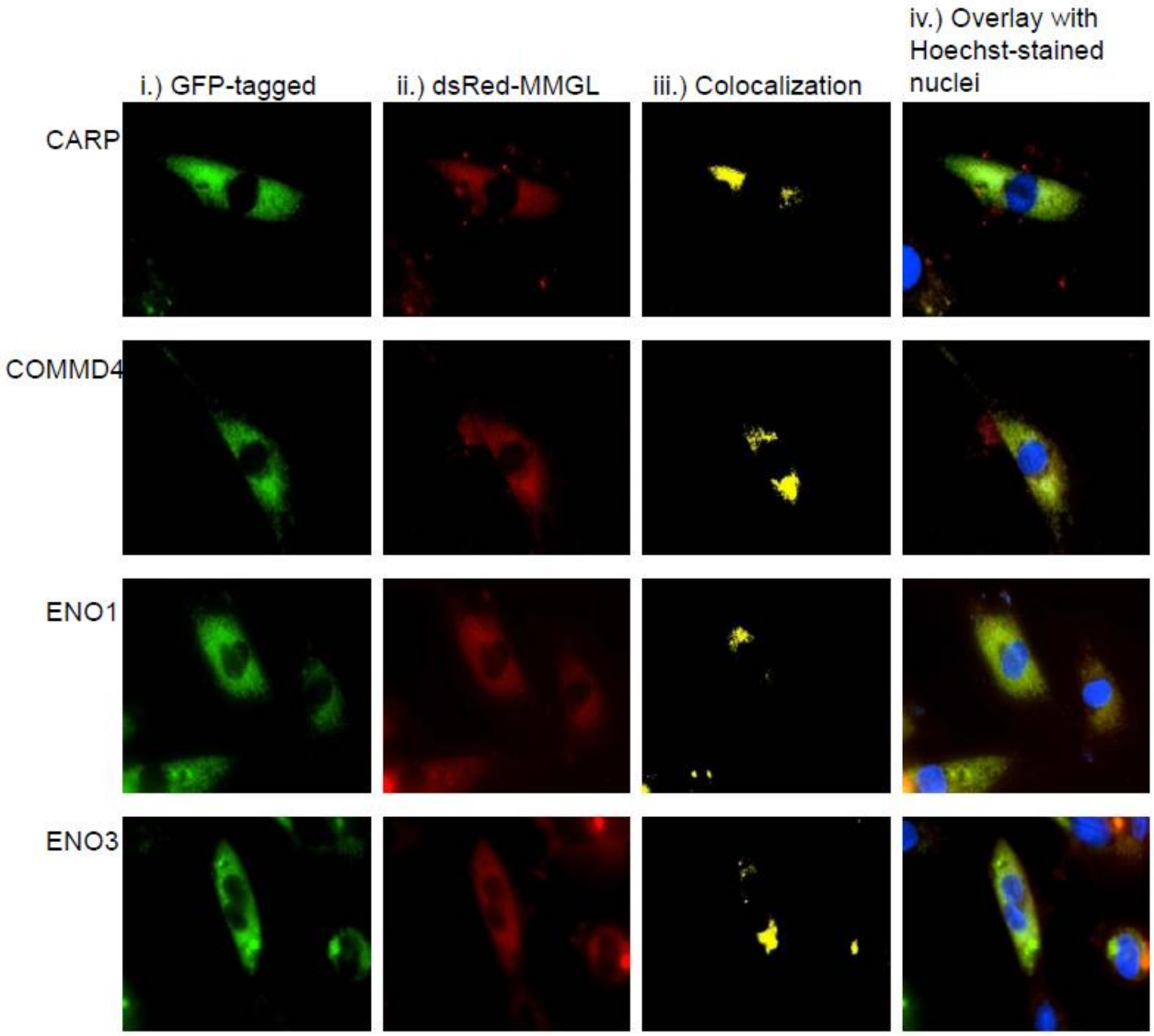
i.) GFP-tagged
ii.) dsRed-MMGL
iii.) Colocalization
iv.) Overlay with Hoechst-stained nuclei
CARP
COMMD4
ENO1
ENO3

Figure 3

A)

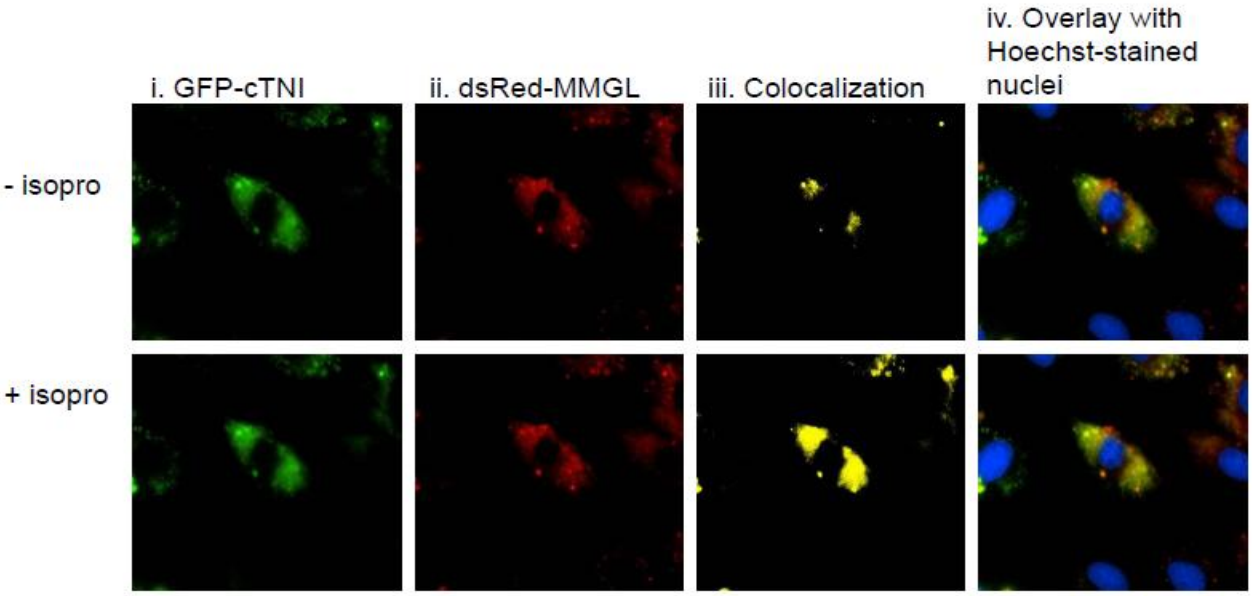
i. GFP-cTNI
ii. dsRed-MMGL
iii. Colocalization
iv. Overlay with Hoechst-stained nuclei
- isopro
+ isopro

B)

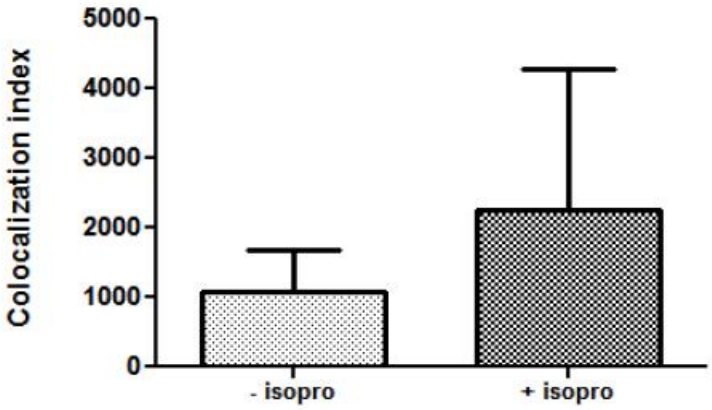
Colocalization index
5000
4000
3000
2000
1000
0
- isopro
+ isopro

Figure 4

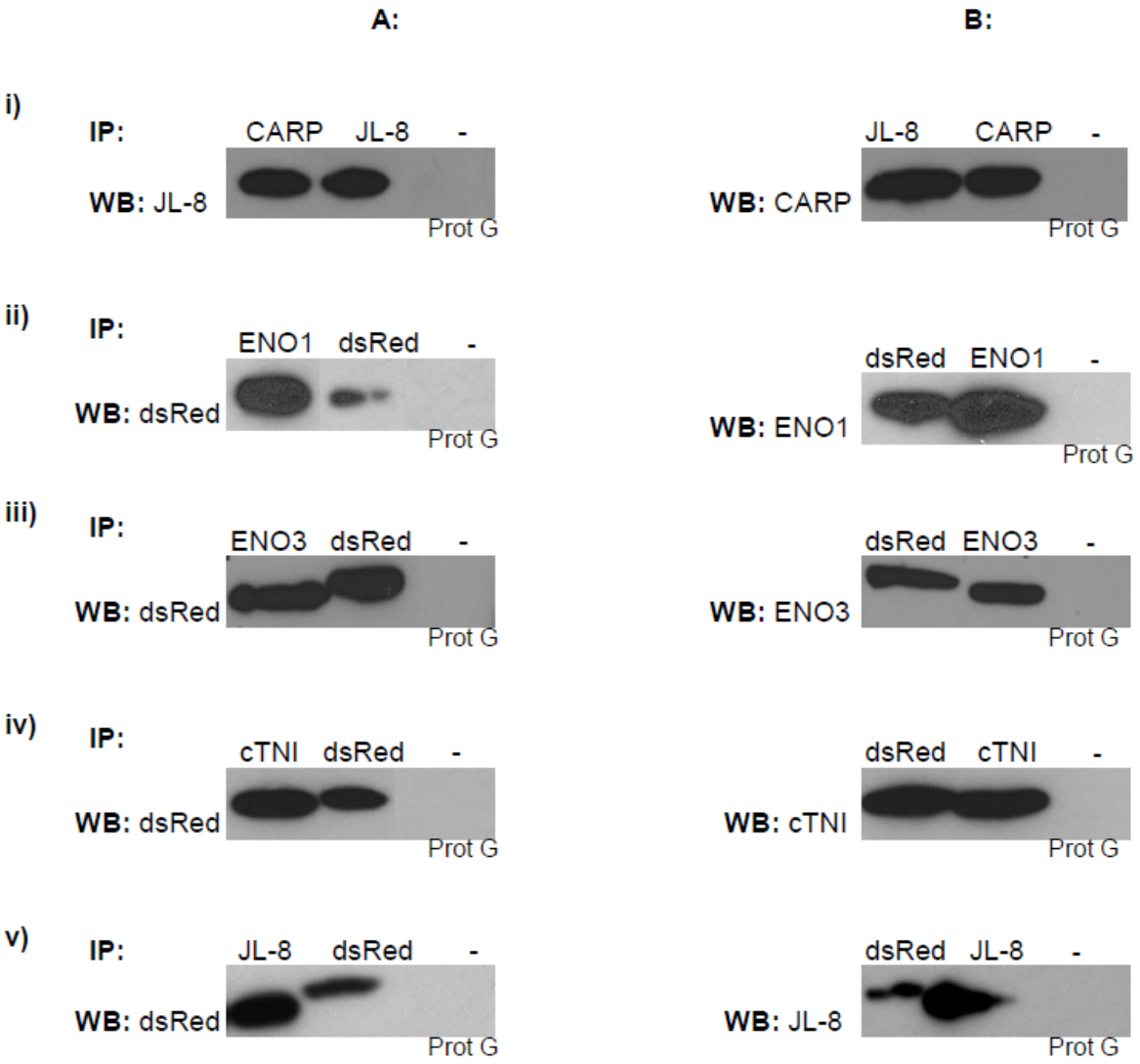
A:
B:
i)
IP:
CARP JL-8 -
WB: JL-8
Prot G
JL-8 CARP -
WB: CARP
Prot G
ii)
IP:
ENO1 dsRed -
WB: dsRed
Prot G
dsRed ENO1 -
WB: ENO1
Prot G
iii)
IP:
ENO3 dsRed -
WB: dsRed
Prot G
dsRed ENO3 -
WB: ENO3
Prot G
iv)
IP:
cTNI dsRed -
WB: dsRed
Prot G
dsRed cTNI -
WB: cTNI
Prot G
v)
IP:
JL-8 dsRed -
WB: dsRed
Prot G
dsRed JL-8 -
WB: JL-8
Prot G

Figure 5

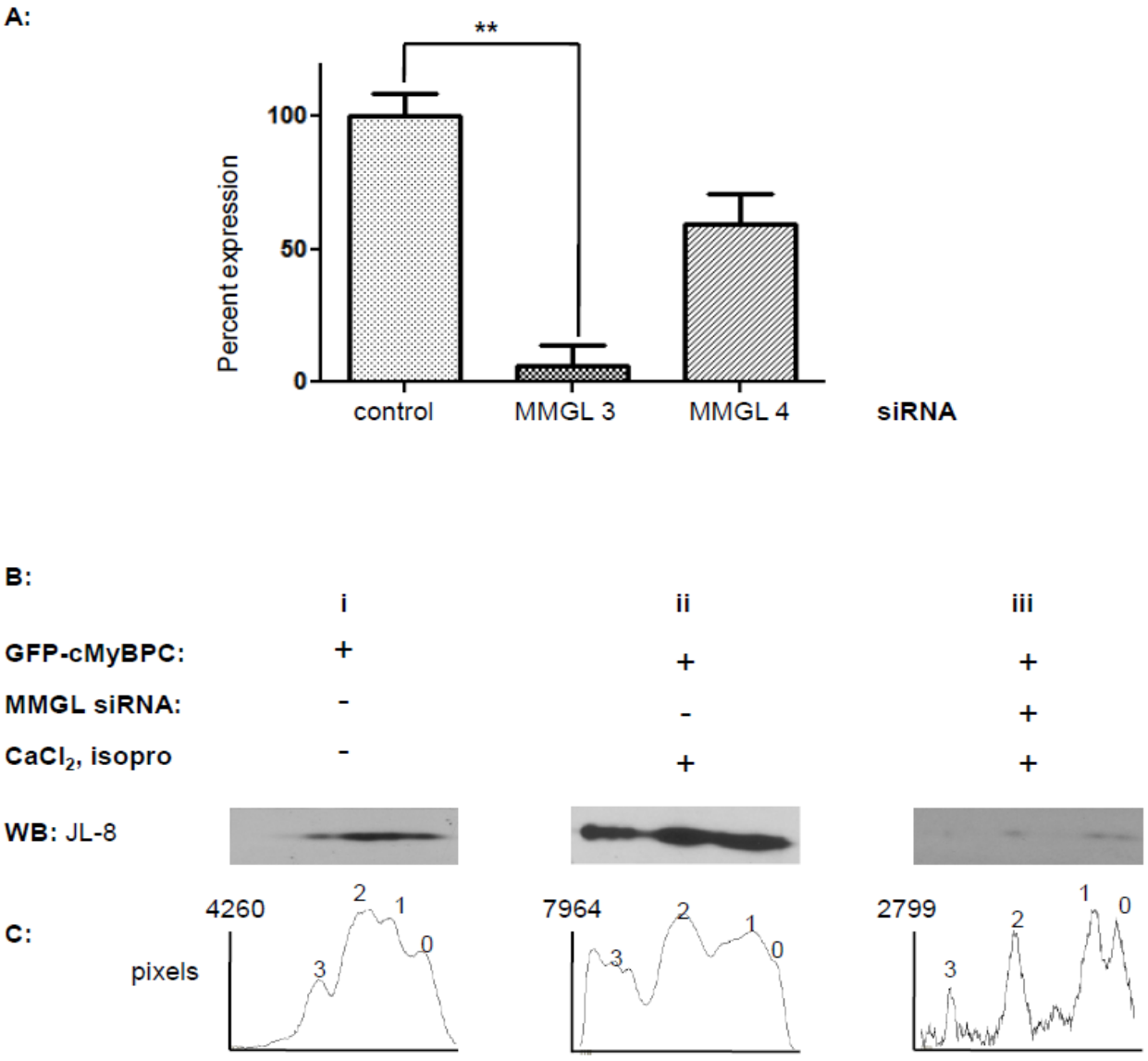
A:
**
100
50
0
Percent expression
control
MMGL 3
MMGL 4
siRNA
B:
i
ii
iii
GFP-cMyBPC:
+
+
+
MMGL siRNA:
-
-
+
CaCl2, isopro
-
+
+
WB: JL-8
C:
pixels
4260
7964
2799
0
1
2
3

Figure 6